ADVANCES IN PHYSICS, 1999, VOL. 48, NO. 2, 167–293

Mixed-valence manganites

J. M. D. COEY, M. VIRET†
Physics Department, Trinity College, Dublin 2, Ireland

and S. VON MOLNÁR,
MARTECH, Florida State University, Tallahassee, FL 32306, USA

[Accepted 11 December 1997]

Abstract

Mixed-valence manganese oxides $(R_{1-x}A_x)MnO_3$ (R = rare-earth cation, A = alkali or alkaline earth cation), with a structure similar to that of perovskite $CaTiO_3$, exhibit a rich variety of crystallographic, electronic and magnetic phases. Historically they led to the formulation of new physical concepts such as double exchange and the Jahn–Teller polaron. More recent work on thin films has revealed new phenomena, including colossal magnetoresistance near the Curie temperature, dense granular magnetoresistance and optically-induced magnetic phase transitions. This review gives an account of the literature on mixed-valence manganites, placing new results in the context of established knowledge of these materials, and other magnetic semiconductors. Issues addressed include the nature of the electronic ground states, the metal-insulator transition as a function of temperature, pressure and applied magnetic field, the electronic transport mechanisms, dielectric and magnetic polaron formation, magnetic localization, the role of cation disorder and the Jahn–Teller effect. Sample preparation, and the properties of related ferromagnetic oxides are also discussed.

Contents

† Present address: Service de Physique de l'Etat Condensée, Commissariat de l'Energie Atomique Saclay, 91191 Gif sur Yvette, France.

1. Introduction

Mixed valence manganites with the perovskite† structure have been studied for almost 50 years. The system offers a degree of chemical flexibility which permits the relation between the oxides' structure, electronic and magnetic properties to be examined in a systematic way. Research on the manganites has revealed new phenomena such as colossal [1] and dense granular magnetoresistance [2], and has led to the formulation of important physical concepts such as double exchange [3, 4] and the Jahn–Teller polaron [5, 6]. Early research was motivated by a need to develop insulating ferromagnets with a large magnetization for high-frequency applications. More recent work has been driven by a desire to understand and exploit the large negative magnetoresistance effects which appear near and below the Curie temperature. The manganites also have potential as solid electrolytes, catalysts, sensors and novel electronic materials. Their rich electronic phase diagrams reflect the fine balance of interactions which determine the electronic ground state. These compounds represent, in microcosm, the interplay of experiment, theory and application which is at the heart of solid state physics.

The broad features of the mixed-valence manganese perovskites were described for polycrystalline ceramic samples by Jonker and van Santen [7], van Santen and Jonker [8] and Jonker [9] working at Philips in the late 1940s. They discussed the preparation, crystal structure and magnetic properties of the $(La_{1-x}Ca_x)MnO_3$ series [7] and gave a short account of the electrical resistivity [8]. Similar results were found for the $(La_{1-x}Sr_x)MnO_3$ and $(La_{1-x}Ba_x)MnO_3$ series, but the range of solid solution was limited to $x < 0.7$ or $x < 0.5$ respectively. Magnetoresistance and other transport properties were first described in 1954 by Volger [10] who showed that the magnetoresistance of $(La_{0.8}Sr_{0.2})MnO_3$ is negative with a peak near the Curie temperature (figure 1).

An extensive study of flux-grown single crystals of $(La_{1-x}Pb_x)MnO_3$ with $0.2 < x < 0.44$ was carried out by Searle and Wang [11, 12], Morrish *et al.* [13] and Leung *et al.* [14] in 1969 and 1970. They found metallic conductivity below the Curie point T_C and a large negative magnetoresistance effect of about 20% at 1 T in the vicinity of T_C, similar to that in polycrystalline $(La_{1-x}Sr_x)MnO_3$. The value of the magnetization suggested that a fully spin-polarized d band is involved in the ferromagnetic ordering process.

Interest in the mixed-valence manganites revived in the 1990s following the preparation of high-quality thin films with large magnetoresistance by von Helmholt *et al.* [15] and Chahara *et al.* [16] using a method employed for high-temperature superconductors, to which the manganites are structurally related. Optimized films show remarkable magnetoresistance effects near T_C which were epitomized by Jin *et al.* as the 'colossal magnetoresistance' (CMR) [1]. The Curie point coincides with a metal–insulator transition, and there are associated anomalies in various physical properties. Films may be used as sensors, and there are prospects for developing spin electronic devices based on thin-film heterostructures.

The mixed-valence oxides can be regarded as solid solutions between end members such as $LaMnO_3$ and $CaMnO_3$ with formal valence states $La^{3+}Mn^{3+}O_3^{2-}$ and $Ca^{2+}Mn^{4+}O_3^{2-}$, leading to mixed-valence compounds such as $(La^{3+}_{1-x}Ca^{2+}_x)(Mn^{3+}_{1-x}Mn^{4+}_x)O_3$. The nominal electronic configurations of Mn^{3+} and Mn^{4+} are

† The eponymous mineral $CaTiO_3$ is named after a village in Russia.

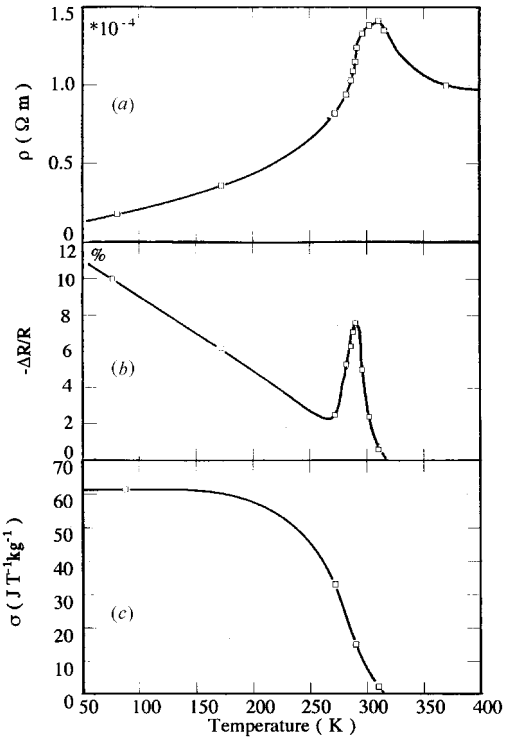

Figure 1. (*a*) Resistivity, (*b*) magnetoresistance in 0.3 T and (*c*) magnetization of a $(La_{0.8}Sr_{0.2})MnO_3$ ceramic. [Reprinted from *Physica*, Volume 20, J. Volger, page 49, © 1954 [10], with permission from Elsevier Science.]

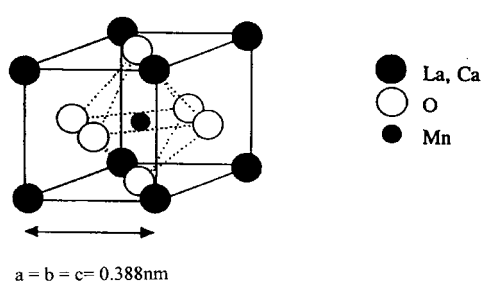

Figure 2. The ideal, cubic perovskite structure, ABO_3. A is a large cation, similar in size to O^{2-}; B is a small cation such as Mn^{3+} or Mn^{4+}, octahedrally-coordinated by oxygen.

$3d^4$ and $3d^3$ respectively. Each of the end members is antiferromagnetic and insulating, but the solid solutions with $x \approx 0.3$ are ferromagnetic and conducting. For instance, $(La_{0.7}Ca_{0.3})MnO_3$ has a Curie temperature $T_C = 220$ K, and a low-temperature resistivity $\rho_0 \approx 10^{-5}\ \Omega$ m.

Chemically, the system is characterized by the wide range of cations which can occupy the A site in the perovskite structure, which may be set at the body-centre or the cube corner (figure 2). A good way to regard the structure is as a cubic close-packed array formed of O^{2-} anions and large A cations, with the small B cations in the octahedral interstitial sites. As discussed in section 4.1.1, the ideal cubic structure

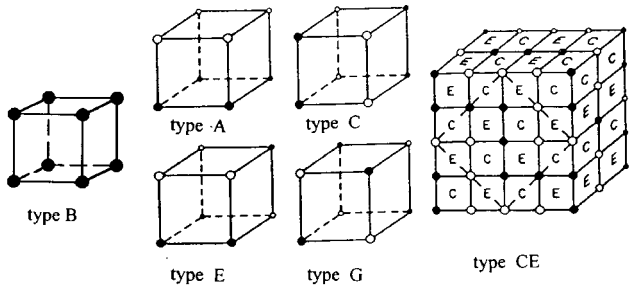

Figure 3. Some possible magnetic modes for the B-site cations in the perovskite structure (solid and open circles represent the two antiferromagnetic sublattices).

is distorted by cation size mismatch and the *Jahn–Teller effect*, whereby a distortion of the oxygen octahedron surrounding the B site cation splits the energy levels of a 3d ion such as Mn^{3+}, thus lowering the energy. The distorted structures are frequently orthorhombic. Divalent cations which can occupy the body-centre A site include calcium, barium, strontium and lead; trivalent cations include yttrium, lanthanum, praseodymium, neodymium and some other rare earths (R). Besides manganese, many perovskite-structure oxides form with aluminium, gallium or another 3d element such as chromium, iron, cobalt or nickel on the B sites. The rare-earth orthoferrites $RFeO_3$ are one example of a series of perovskite-structure oxides. There are many others. Any of the trivalent 3d cations can substitute partially for manganese. An exhaustive compilation of data on perovskite-structure compounds by Goodenough and Longho [17] was published in a 1970 Landoldt-Börnstein volume.

The main effects of the various substitutions are to vary the number of electrons in the 3d band and to alter the interatomic distances and bond angles. Whenever different ions of the same 3d element with different numbers of electrons occupy crystallographically equivalent B sites, say B_1 and B_2, there is a partly-filled d band with a tendency towards metallic conduction. The configurations $3d^n(B_1)$–$3d^{n+1}(B_2)$ and $3d^{n+1}(B_1)$–$3d^n(B_2)$ are degenerate provided that there is no charge ordering. The idea that mixed valence can lead to metallic conduction is due to Verwey and de Boer [18]. It was developed with particular reference to magnetite (Fe_3O_4) [19] in The Netherlands in the 1930s. The occupancy of the B sites in the spinel structure of magnetite by a mixture of Fe^{3+} ($3d^5$) and Fe^{2+} ($3d^6$) leads to electrical conduction and ferromagnetic B–B exchange interactions. The idea of mixed-valence ferromagnetism was then applied to oxides with the perovskite structure.

The mixed-valence manganites can exhibit magnetic order, charge order and orbital order. Examples of charge and orbital order are given later in figure 6. Some of the simplest magnetic modes for the B sites in the perovskite structure are illustrated in figure 3. Mode B is ferromagnetic, but all the others are antiferromagnetic and entail an enlarged magnetic unit cell. Modes A, C and G consist of oppositely aligned ferromagnetic planes of the type {001}, {110} and {111} respectively. Mode G, where each B-site cation is oriented antiparallel to its six neighbours will be favoured by negative B–O–B superexchange interactions. Modes C and E each have four antiparallel and two parallel neighbours, whereas mode A has four parallel and two antiparallel neighbours. A composite CE mode is composed of a chequerboard of alternating C and E blocks. The magnetic axis is usually indicated by a suffix x, y or z. Modes may be combined, so that A_xB_z for

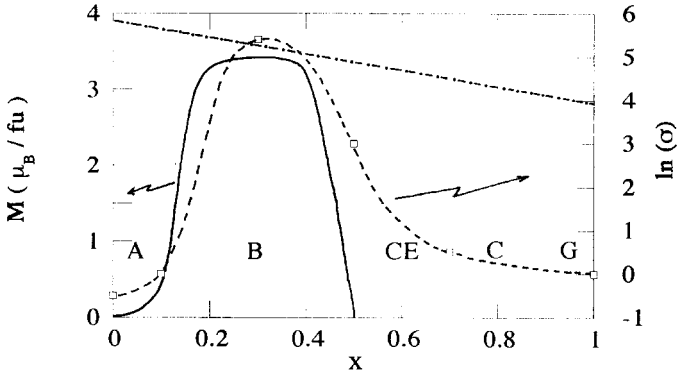

Figure 4. Low-temperature magnetic modes (letters) and ferromagnetic moment for the $(La_{1-x}Ca_x)MnO_3$ series compared with the electrical conductivity at 80 K (- - -): (- ' -), the spin-only moment for a mixture of Mn^{3+} and Mn^{4+} (fu, formula unit). (After [20, 25].) [Derived by permission of the American Physical Society from page 545 of *Physical Review*, Volume 100, 1955, and the authors E. O. Wollan and W. C. Koehler, © 1955 by the American Physical Society; page 564 of *Physical Review*, Volume 100, 1955, and the author J. B. Goodenough, © 1955 by the American Physical Society.]

example represents a canted antiferromagnet with the antiferromagnetic axis along x ($\equiv a$) but with the net ferromagnetic moment along z ($\equiv c$).

The crystallographic and magnetic structures for the $(La_{1-x}Ca_x)MnO_3$ compounds were determined in 1955 by Wollan and Koehler [20] in a remarkably complete neutron and X-ray diffraction study as a function of Mn^{4+} content. In particular, the neutron data revealed a very rich magnetic phase diagram where, for different doping levels, antiferromagnetism can take different configurations (A, C, CE and G types) and can even coexist with ferromagnetism (B type). The magnetic structures are indicated on figure 4. There are three main regions: for small amounts of Mn^{4+} the compounds have essentially antiferromagnetic properties. For x around 0.3, they become ferromagnetic but, for $x > 0.5$, they revert to antiferromagnetism up to the end-member $CaMnO_3$. From magnetization and susceptibility results, Jonker [9] concluded that the exchange is weakly positive (ferromagnetic) between two $3d^4$ Mn^{3+} ions, negative (antiferromagnetic) between two $3d^3$ Mn^{4+} ions and positive between a $3d^4$ Mn^{3+} and a $3d^3$ Mn^{4+} ion. These measurements provided the first clear evidence for a ferromagnetic exchange interaction in an oxide. Resistivity measurements also revealed a strong correlation between electron transport and magnetic properties. The resistivity is lowest for the $x \approx 0.3$ composition corresponding to the best ferromagnetism, whereas high resistivities are associated with the antiferromagnetic compositions.

Zener [3] offered an explanation of this behaviour in 1951 in terms of his theory of indirect magnetic exchange between 3d atoms. He considered that the intra-atomic Hund rule exchange was strong and that the carriers do not change their spin orientation when hopping from one ion to the next, so they can only hop if the spins of the two ions are parallel. On minimizing the total free energy of the system, Zener found that ferromagnetic interactions are favoured when the magnetic atoms are fairly well separated and conduction electrons are present. The theory was applied to the manganese perovskites [4] with the aim of explaining the strong correlation

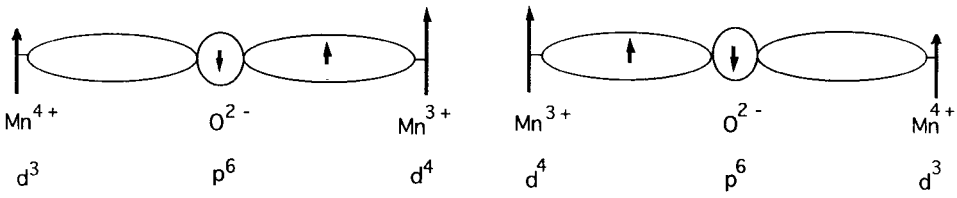

Figure 5. Schematic diagram of the double-exchange mechanism. The two states Mn^{3+}–Mn^{4+} and Mn^{4+}–Mn^{3+} are degenerate if the manganese spins are parallel.

between conductivity and ferromagnetism, and the value of the zero-temperature saturation magnetization which corresponds to the sum of all the unpaired electron spins. Starting from the insulating antiferromagnetic $LaMnO_3$ end member where electrons are localized on the atomic orbitals, Zener showed how the system should gradually become more ferromagnetic upon hole doping (introduction of Mn^{4+}). He considered the problem of the exchange between Mn^{3+} and Mn^{4+} ions via an oxygen ion and introduced the concept of simultaneous transfer of an electron from the Mn^{3+} to the oxygen and from the oxygen to the neighbouring Mn^{4+} (figure 5). Such a transfer was called *double exchange*. In the case of magnetic atoms, the configurations Mn^{3+}–O^{2-}–Mn^{4+} and Mn^{4+}–O^{2-}–Mn^{3+} are degenerate if the spins of the two d shells are parallel, and the lowest energy of the system at low temperature corresponds to parallel alignment of the spins of the two adjacent cations. Double exchange is always ferromagnetic, unlike superexchange which involves virtual electron transfer and is frequently antiferromagnetic. If the manganese spins are not parallel or if the Mn–O–Mn bond is bent, the electron transfer becomes more difficult and the mobility decreases. It follows that there is a direct connection between conductivity and ferromagnetism and a quantitative relation with Curie temperature was proposed: $\sigma = (xe^2/ah)(T_C/T)$, where x is the doping and a is the Mn–Mn distance, which agreed with the available experimental results of Jonker and van Santen in the limited region $0.2 < x < 0.4$.

Anderson and Hasegawa [21] generalized the double exchange mechanism by considering interactions between a pair of magnetic ions with general spin directions. They calculated the transfer integral t to be

$$t = t_0 \cos\left(\frac{\theta}{2}\right), \tag{1.1}$$

where t_0 is the normal transfer integral which depends on the spatial wavefunctions and the term $\cos(\theta/2)$ is due to the spin wavefunction; θ is the angle between the two spin directions. This is quite unlike superexchange where the coupling is proportional to $\cos\theta$. They also considered the problem of the high-temperature paramagnetic state of the manganites where the exchange energy will be much larger than the transfer integral and predicted that the susceptibility χ should be Curie like, with $1/\chi$ intercepting the axis at zero, which contradicted the experimental results showing Curie–Weiss behaviour. This point was corrected by deGennes [22] who pointed out that the prediction is erroneous when the carrier bandwidth is large with respect to kT. Double exchange therefore leads to normal Curie–Weiss behaviour of the susceptibility, $1/\chi = C/(T - \theta_p)$ with $\theta_p > 0$.

DeGennes [22] studied the case of low doping of the end member $LaMnO_3$ in more detail and showed in general that mobile electrons in an antiferromagnetic

lattice produce some canting of the spin arrangment. Taking as a starting point the well established A-type planar antiferromagnetic order and a transfer (hopping) integral depending on the angle between two neighbouring spins varying as $\cos(\theta/2)$, as demonstrated by Anderson, DeGennes found that the stable magnetic configuration at low doping should be an AB canted state. He calculated the fixed angle between the magnetizations of adjacent planes to be proportional to the carrier concentration x. Although this conclusion has been questioned recently, he successfully explained the values of the saturation magnetization and the non-zero magnetic susceptibility at high fields and a canted structure was in accord with the neutron diffraction data. DeGennes also considered the case when the carriers were not completely mobile but localized in the vicinity of a divalent A-site ion. The bound hole interacting with spins on the eight B sites neighbouring the impurity produces a local ferromagnetic distortion of the spin system; this is the concept of the bound *magnetic polaron*.

Charge ordering, also known as Wigner crystallization, is driven by interatomic Coulomb interactions. The mobile d electrons can be localized on certain manganese ions to form a regular lattice for particular occupancies of the d band provided that the interelectronic Coulomb interaction is comparable with the conduction-electron bandwidth W [23]. The effect is accentuated by small displacements of the oxygen atoms to accommodate the ordered cation lattice. Charge ordering is most likely when the temperature is low and x is a rational fraction, especially $x = \frac{1}{8}, \frac{1}{2}$ or $\frac{3}{4}$. The extra fourth d electrons may then be localized on alternate manganese sites in a plane, as shown in figure 6(*a*).

Kanamori [24] pointed out that the carriers in mixed-valence manganites may be strongly coupled to local lattice distortions. Orbital ordering can occur at certain

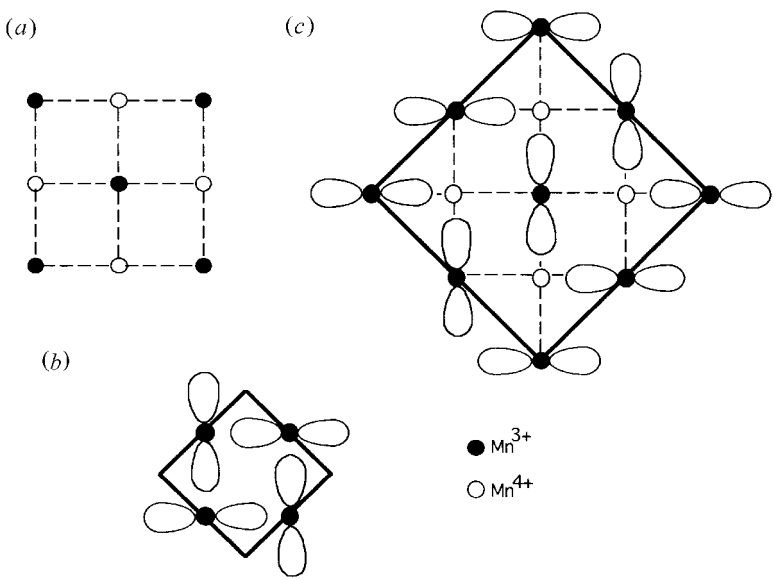

Figure 6. (*a*) Charge ordering of Mn^{3+} and Mn^{4+} in a mixed crystal with $x = \frac{1}{2}$. (*b*) Orbital ordering of the d_{z^2} orbitals of Mn^{3+} when $x = 0$. (*c*) Combined charge and orbital ordering when $x = \frac{1}{2}$.

carrier concentrations when the d electrons occupy an asymmetric orbital, as shown in figure 6(*b*). The driving force is partly direct electrostatic repulsion of the charge clouds, but coupled Jahn–Teller distortions of adjacent octahedra stabilize the effect. Finally, figure 1.6(*c*) illustrates the coupled charge and orbital order expected when $x = \frac{1}{2}$.

Goodenough [25] rationalized the magnetic phase diagram obtained by Wollen and Koehler in terms of indirect exchange between manganese ions. Postulating that the hybridization of the Mn^{3+} d orbitals with O^{2-} p orbitals is square and coplanar and that Mn^{4+} and O^{2-} hybridize octahedral orbitals, he reviewed the indirect exchange mechanisms between the different manganese ions and estimated the sign of the magnetic interactions. Then, depending on the ratio of Mn^{3+} to Mn^{4+}, the charge and orbital ordering of bonds determines both the crystallographic and the magnetic configuration. The compounds exhibit different kinds of antiferromagnetism: the $x = 0$ end member is a planar antiferromagnet where the ordering is ferromagnetic in plane but antiferromagnetic out-of-plane (type A). The other end member ($x = 1$) is a pure near-neighbour antiferromagnet where each manganese atom is antiparallel to its nearest neighbour (type G). For intermediate concentration ranges (near $x = 0.75$) the compounds are chain antiferromagnets where the coupling is ferromagnetic along one-dimensional chains which are ordered antiferromagnetically. In view of the strong Hund coupling in these materials and Zener's double exchange, the largest mobility is found in the ferromagnetic domain around $x = 0.3$. The negative sign of the Mn^{4+}–Mn^{4+} exchange interactions deduced from the paramagnetic Curie temperature of $CaMnO_3$ [9] is explained by the Goodenough–Kanamori rule for d^3–d^3 overlap. The Mn^{3+}–Mn^{3+} interaction is mostly ferromagnetic, although the magnetic order in $LaMnO_3$ is A-type antiferromagnetic. The interaction is ferromagnetic for overlap of d_{z^2} orbitals in the plane, and antiferromagnetic along the perpendicular axis [25].

To justify equation (1.1), and to deduce the double exchange Hamiltonian which is the basis of much recent theoretical modelling, we let J_H be the Hund rule coupling between either of two ion cores, $S = S_{1,2} = \frac{3}{2}$, and the mobile electron, $s = \frac{1}{2}$. The Hamiltonian matrix H for the system of two ions and the electron is written in block form

$$\begin{array}{c} \\ \mathrm{I} \\ \mathrm{II} \end{array} \begin{array}{c} \begin{array}{cc} \mathrm{I} & \mathrm{II} \end{array} \\ \begin{bmatrix} -J_H \mathbf{S}_1 \cdot \mathbf{s} & t_0 \mathsf{I} \\ t_0 \mathsf{I} & -J_H \mathbf{S}_2 \cdot \mathbf{s} \end{bmatrix} \end{array},$$

where the 2×2 diagonal blocks I–I and II–II correspond to energy states of the electron and a Mn^{4+} ion core at sites 1 and 2 respectively, and the off-diagonal blocks represent electron transfer between them, where I is the 2×2 unit matrix. Diagonalization of the Hamiltonian can be done in two steps; first the terms I–I and II–II are expressed in their respective diagonal representations, and then the I–II and II–I terms have to be modified to connect the two representations. To diagonalize I–I or II–II, let $\mathbf{S}_1' = \mathbf{S}_1 + \mathbf{s}$; $\mathbf{S}_0 = \mathbf{S}_1' + \mathbf{S}_2$ and $S' = |\mathbf{S}_1'| = |\mathbf{S}_2'| = 2$ for Mn^{3+}. In the representation where $\mathbf{S}_1'$ is diagonal the eigenvalues of $-J_H \mathbf{S}_1 \cdot \mathbf{s}$, which correspond to the electron $\uparrow$ or $\downarrow$ with respect to the core spin, are evaluated from the identity $\mathbf{S}_1'^2 = \mathbf{S}_1^2 + \mathbf{s}^2 + 2\mathbf{S}_1 \cdot \mathbf{s}$ as $-J_H S/2$ for $S_1' = S_1 + \frac{1}{2}$ and $J_H(S+1)/2$ for $S_1' = S_1 - \frac{1}{2}$. Hence each of the blocks can be written

$$\begin{bmatrix} -\frac{J_H S}{2} & 0 \\ 0 & \frac{J_H(S+1)}{2} \end{bmatrix}. \tag{1.2}$$

The two diagonal representations of these blocks are inclined at an angle θ, corresponding to the classical angle between the two Mn^{4+} core spins. The I–II and II–I blocks are modified to express the rotation of the electron spin between these two representations, by replacing the unit matrix by the rotation matrix for angle θ, $\mathbf{R}_\theta(\mathbf{I}) = \exp(\mathrm{i}\theta I_x)$ where I_x is the angular momentum operator for spin $\frac{1}{2}$ about the x-axis. This may be written [26]

$$\begin{bmatrix} \cos\left(\frac{\theta}{2}\right) & -\sin\left(\frac{\theta}{2}\right) \\ \sin\left(\frac{\theta}{2}\right) & \cos\left(\frac{\theta}{2}\right) \end{bmatrix}.$$

The total Hamiltonian expressed in terms of the basis states $S_1' = S_1 \pm \frac{1}{2}$ and $S_2' = S_2 \pm \frac{1}{2}$ is

$$\begin{bmatrix} -\frac{J_H \mathrm{S}}{2} & 0 & t_0 \cos\left(\frac{\theta}{2}\right) & t_0 \sin\left(\frac{\theta}{2}\right) \\ 0 & \frac{J_H(S+1)}{2} & -t_0 \sin\left(\frac{\theta}{2}\right) & t_0 \cos\left(\frac{\theta}{2}\right) \\ t_0 \cos\left(\frac{\theta}{2}\right) & -t_0 \sin\left(\frac{\theta}{2}\right) & -\frac{J_H S}{2} & 0 \\ t_0 \sin\left(\frac{\theta}{2}\right) & t_0 \cos\left(\frac{\theta}{2}\right) & 0 & \frac{J_H(S+1)}{2} \end{bmatrix}.$$

The quantity $\cos(\theta/2)$ can be written $(S_0 + \frac{1}{2})/(2S+1)$. Solving the secular equation $|\mathbf{H} - E_i| = 0$ leads to the four eigenvalues of the system. In the case where $J_H \gg t_0$ there are two low-energy solutions

$$E = -\frac{J_H S}{2} \pm t_0 \cos\left(\frac{\theta}{2}\right). \tag{1.3}$$

These eigenstates correspond to the symmetric and antisymmetric combinations of the localized orbitals with the electron spin parallel to the first or second Mn^{4+} ion core. The physical implication is that the effective transfer integral is reduced by $\cos(\theta/2)$, as indicated in equation (1.1).

The double exchange Hamiltonian for the whole solid is therefore taken as

$$H = \sum_{\langle ij \rangle} t_0 \cos\left(\frac{\theta_{ij}}{2}\right) c_i^\dagger c_j - J_H \sum_i \mathbf{S}_i \cdot \mathbf{s}_i, \tag{1.4}$$

where $c_i^\dagger$ (c_i) creates (annihilates) an electron on the site i with spin parallel to the ionic core.

This review gives an account of the literature on mixed-valence manganites published up to mid-1997, with a few later references. Emphasis is on experimental data and physical models. Another review with a more theoretical approach has been

written by Nagaev [27], and there is a short review by Ramirez [28] that focuses on experimental aspects of CMR. Since the field has recently become very active, there is a need to set new work in the context of what was already known about these materials and other model magnetic semiconductors. The structural, magnetic, transport and other properties of mixed-valence manganites are discussed in detail in section 4. Some emphasis is placed on compounds with $x \approx 0.3$ which usually show a ferromagnetic ground state with metallic conductivity and large negative magnetoresistance near T_C. Issues to be addressed include the nature of the electronic ground states, the metal–insulator transitions observed as a function of temperature or applied field, the electronic transport mechanisms, magnetic localization, dielectric and magnetic polaron formation, the role of structure, cation disorder and the Jahn–Teller effect. Sample preparation is treated in section 3, and applications in section 6. A summary of results on related 3d oxides is given in section 5. Our understanding of magnetotransport in transition-metal compounds owes much to studies of the rare-earth magnetic semiconductors which were studied intensively in the 1960s and 1970s. We therefore begin our review in section 2 with a discussion of these model systems.

2. Model magnetic semiconductors

The mixed-valence manganites are examples of a larger class of magnetic semiconductors. These include the rare earth chalcogenides, the rare-earth thorium phosphide structure compounds and the chromium chalcogen spinels, among others. They also include diluted magnetic systems, such as $(Cd_{1-x}Mn_x)Te$, where the magnetic manganese atoms are randomly distributed throughout the cadmium sublattice. In their simplest form, magnetic semiconductors are semiconductors containing magnetic ion cores which interact with one another via mobile carriers. The latter are introduced in an insulating end member by doping, in the same way that silicon is an elemental semiconductor having a large bandgap which does not conduct well unless impurities are introduced. Carrier concentrations in magnetic semiconductors are typically much higher than in silicon, and at a critical carrier concentration the materials undergo a semiconductor-metal transition.

In the following, we review features of the rare earth model compounds EuX (X = O, S, Se or Te) and $Gd_{3-x}\square_xS_4$ (where $\square$ = vacancy) which are salient to a discussion of the physical properties of the magnetic perovskites. Here we encounter phenomena such as a magnetically-driven metal–insulator transition at the Curie point, huge negative magnetoresistance, magnetic polaron transport and the effects of local potential fluctuations on carriers in narrow bands in a context where the localized (4f) and itinerant (5d–6s) electron systems are quite distinct. The potential fluctuations, created by disorder of both chemical and magnetic origin, can lead in three dimensions to a threshold in the density of states known as the *mobility edge*, separating extended from localized electron states. We also remark on various experiments in these systems which have provided evidence for net spin polarization of electrons in the conduction band. The ideas developed here carry over to the manganites, where the localized and itinerant-electron systems are both 3d, but they occupy distinctly different bands.

2.1. *EuX* (*X* = *O, S, Se or Te*)

2.1.1. *Influence of carriers on the magnetic properties*

The rare earths are chemically very similar and, consequently there is the possibility of making complete series of solid solutions between, for example, europium and gadolinium chalcogenides or europium and lanthanum chalcogenides. The monochalcogenides [29] are the simplest magnetic semiconductors. They crystallize in the fcc NaCl structure. Furthermore, the electrons responsible for the magnetism are in tightly bound 4f states, whose radial extent is much smaller than the extended states responsible for the bonding and for transport. Thus, europium has an electronic configuration $4f^7 5d^0 6s^2$ and that of gadolinium is $4f^7 5d^1 6s^2$. In both cases, therefore, the $4f^7$ core, through the Hund rule coupling, adopts a $^8S_{7/2}$ ground state which makes it possible to view the materials as having a $\frac{7}{2}$ spin located at each cation site in the lattice. EuO was, in fact, the first insulating rare-earth ferromagnet ($T_C \approx 69$ K) ever discovered.

The magnetic properties of all the europium chalcogenides were first studied in the absence of conduction electrons by McGuire *et al.* [30] and later refined by Passell *et al.* [31]. They are considered to be good Heisenberg magnets and their magnetic transition temperatures are given in table 1. The magnetic order and transition temperatures reflect the competition between the exchange interactions J_1 and J_2, coupling first and second neighbours in the NaCl structure. These interactions are of opposite sign, and their ratio varies as $1/a_0$, where a_0 is the lattice parameter [32].

The ferromagnetic exchange interaction J_1 between nearest-neighbour Eu ions is of interest, especially since the wavefunctions do not overlap sufficiently in the monochalcogenide for the 4f electrons to interact directly. The microscopic theory, given by Kasuya [33], involves intersite electron transfer of a 4f electron to an empty (6s, 5d) state of an adjacent cation where it couples to the 4f core via the Hund rule. This suggests that, if the (6s, 5d) band states are partially filled, the magnetism should be affected. Direct evidence for this was obtained by Holtzberg *et al.* [34] who successfully doped the europium monochalcogenides with gadolinium or lanthanum, each of which brings one electron to a (6s, 5d) state Their early results are given in figure 7. Curves a are for gadolinium substituted EuSe. The Gd^{3+} ion has the same $4f^7$ configuration with spin $S = \frac{7}{2}$ as Eu^{2+}. Electron doping initially doubles the paramagnetic Curie temperature to approximately 45 K before it starts to decrease again, crossing zero where the net sum of the ferromagnetic and antiferromagnetic exchange interactions cancel at about 60 at.% Gd. Thereafter, the material remains antiferromagnetic up to the GdSe end member with ever-increasing antiferromagnetic Néel temperature. More recent investigations show that the peak in θ_p is reached at 1 at.% Gd. Curves b, on the other hand, show the effect of lanthanum doping. Lanthanum is non-magnetic ($4f^0$). Its (6s, 5d) conduction electrons increase

Table 1. Magnetic properties of Eu chalcogenides [29].

	Ordering temperature (K)	Magnetic order
EuO	69.4	Ferromagnetic
EuS	16.5	Ferromagnetic
EuSe	4.6; 2.8	Antiferromagnetic; Ferromagnetic
EuTe	7.8 to 11	Antiferromagnetic

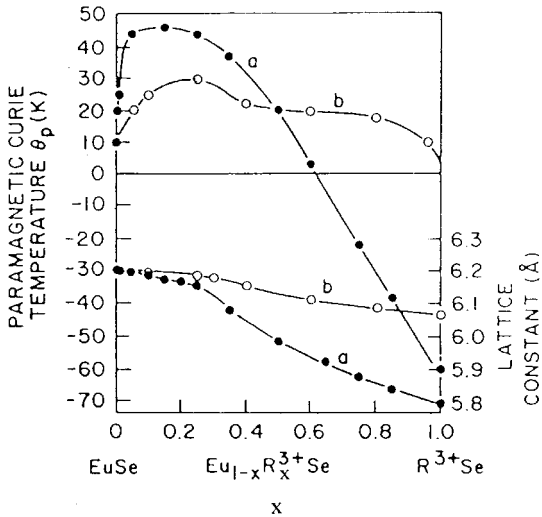

Figure 7. Paramagnetic Curie temperature and lattice constant for $Eu_{1-x}Gd_xSe$ (●, curves a) and $Eu_{1-x}La_xSe$ (○, curves b) against x [34]. [Reprinted by kind permission of the American Physical Society from page 18 of *Physical Review Letters*, Volume 13, 1964, and the authors, F. Holtzberg, T. R. McGuire, S. Methfessel and J. C. Suits, © 1964 by the American Physical Society.]

the magnetic interaction between europium spins slightly but, because it dilutes the magnetic lattice, it has a much weaker effect and never produces antiferromagnetism. More recent phase diagrams include a spin glass region with a complicated magnetic structure. The fundamental observation is that band electrons in an otherwise insulating system can strongly affect the magnetic properties. In the perovskite manganites, hole doping transforms an antiferromagnetic insulator into a ferromagnetic metal.

2.1.2. *Transport and related phenomena*

Of particular relevance here are the transport and magnetotransport properties of the europium chalcogenides. The magnetic state of the system has an enormous influence on the resistivity. An early example of a large variation in transport properties with magnetic field is given in figure 8 [35]. This curve depicts a change in resistivity of more than four orders of magnitude in an applied magnetic field of approximately 1 T for EuSe nominally doped with 1 at.% of Gd. The data were taken at 4.2 K, well below the magnetic ordering temperature $T_C \approx 10$ K.

The physical reasons given for these large negative magnetoresistance effects were twofold. Firstly, there is spin disorder scattering, initially described by deGennes and Friedel [36] and later elaborated by Fisher and Langer [37], which applies to both metals and degenerate semiconductors. These workers pointed out that the largest effects will occur near the ordering temperature of the ferromagnetic or antiferromagnetic material. In fact, the scattering amplitude depends on the correlation length of the spin fluctuations relative to the Fermi wavelength of the electrons. This critical scattering has been observed in the europium chalcogenides [38]. It was found, however, that for low carrier concentrations the theory of spin disorder scattering could not explain the size of the resistivity peak (figure 9).

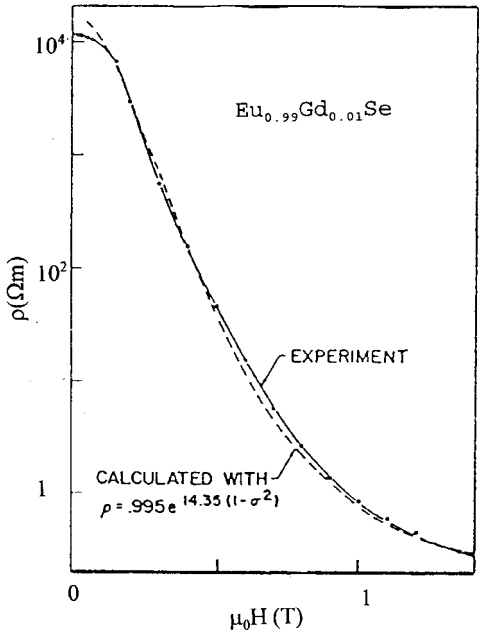

Figure 8. Resistivity ρ of single-crystal $Eu_{0.99}Gd_{0.01}Se$ as a function of applied field at 4.2 K [64]. [Reprinted by kind permission of the American Physical Society from page 852 of *Physical Review Letters*, Volume 19, 1967, and the authors, L. Esaki, P. J. Stiles and S. von Molnár, © 1967 by the American Physical Society.]

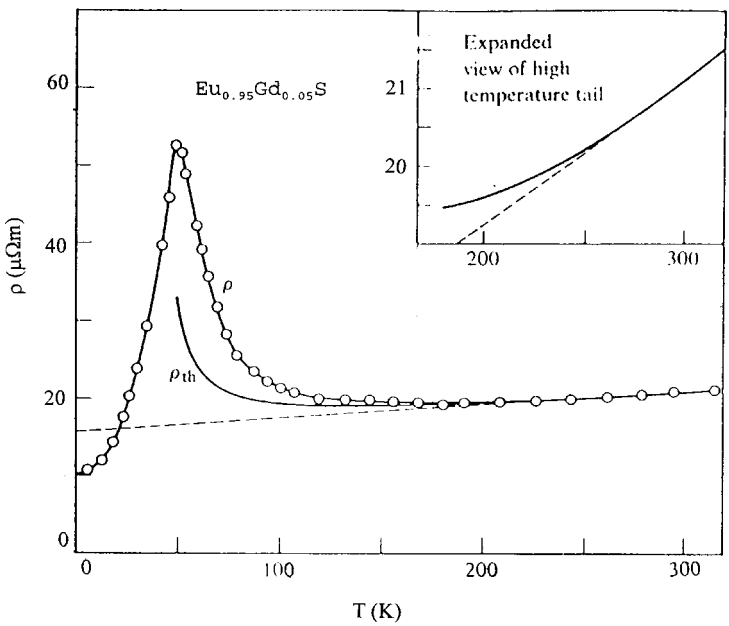

Figure 9. Temperature dependence of the resistivity ρ in $Eu_{0.95}Gd_{0.05}Se$. ρ_{th} is calculated using the theory of deGennes and Friedel [38]. [Reprinted by kind permission of the American Physical Society from page 1757 of *Physical Review Letters*, Volume 21, 1968, and the authors, S. von Molnár and T. Kasuya, © 1968 by the American Physical Society.]

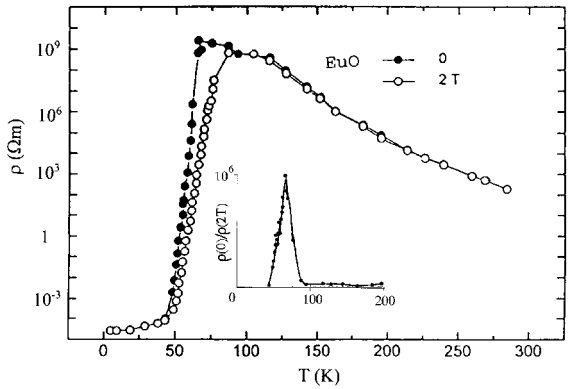

Figure 10. Resistivity of non-stoichiometric (europium-rich) EuO against temperature: (- - -) the magnetoresistance ratio defined as $\rho(0)/\rho(2T)$ [46]. [Reprinted by kind permission of the American Physical Society from page 3669 of *Physical Review* B, Volume 5, 1972, and the authors, T. Penney, M. W. Shafer and J. B. Torrance, © 1972 by the American Physical Society.]

The large magnetoresistive effects (see figure 8) characteristic of non-degenerate Eu chalcogenides clearly require a model that goes beyond magnetic scattering theory in metals. Magnetic polarons, magnetically ordered clusters due to exchange between bound carriers and localized spins, could account for the discrepancy. The effects of magnetism on the band structure have been studied in seminal papers by Kasuya and co-workers [33, 39–41]. Nagaev [42, 43] independently discussed magnetic polarons in these and related systems. We consider magnetic polarons in more detail in section 2.2.

An outstanding example of band structure effects on giant magnetoresistance (GMR) is non-stoichiometric EuO [44–47]. Figure 10 shows the change in the resistivity near the magnetic transition temperature of an oxygen-deficient sample where the resistivity falls by 14 orders of magnitude.

The inset of figure 10 shows the negative magnetoresistance, defined as the ratio $\rho(0)/\rho(2T)$. The effect is impressive, of order 10^6. Oliver *et al.* [44] suggested that the electronic phase transition occurs because deep impurity levels, whose energy is only weakly affected by magnetic order, empty into a conduction band which is split at T_C by the effective internal magnetic field. In other words, the explanation for the 14 order-of-magnitude resistivity change lies in the giant band splitting experienced by a concentrated magnetic semiconductor in the presence of the effective field developed in the ordered state of the material. As can be seen from figure 11, the band simply sweeps over the localized impurity electrons, first reducing the activation energy for transport and then ending up with impurity states lying within the extended states of the conduction band above the mobility edge. Penney *et al.* [46] were able to show that the change in activation energy for the transport evaluated point by point along the metal–insulator phase boundary could be mapped directly onto the magnetization of the sample, thereby demonstrating that the origin of the effect is purely magnetic in nature.

All these observations may be explained in terms of the extra energy term in magnetic semiconductors which is absent in ordinary semiconducting materials. We may write the Zeeman energy in the presence of an externally applied magnetic field

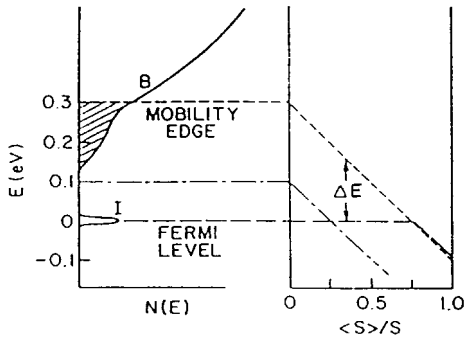

Figure 11. Schematic density of states and its position relative to the localized states I as a function of long-range magnetic order $\langle S \rangle$. (After [46].) [Reprinted by kind permission of the American Physical Society from page 3669 of *Physical Review* B, Volume 5, 1972, and the authors, T. Penney, M. W. Shafer and J. B. Torrance, © 1972 by the American Physical Society.]

as the sum of two terms

$$E_Z = -g^* \mu_B \mu_0 H - J_{sf} \mathbf{s} \cdot \langle \mathbf{S} \rangle_\alpha, \tag{2.1}$$

where the first term represents the ordinary splitting of conduction electrons in the presence of the externally applied field $\mathbf{H}$ and the second term expresses the splitting provided by the average value of the sublattice magnetization $\langle \mathbf{S} \rangle_\alpha$ interacting with the spin $\mathbf{s}$ of the electron in question, with a coupling constant J_{sf}, which corresponds to J_H in manganites. $\langle \mathbf{S} \rangle$ is equal to the value of the spin, $\mathbf{S}$ averaged over a region occupied by the electron with spin $\mathbf{s}$. In general, especially for the concentrated magnetic semiconductors described here, the second term in equation (2.1) is much larger than the first and dominates the energy splitting. It produces the giant band splitting just mentioned for EuO. It can, however, also lead to local effects. If the region occupied by the electron in question is not extended, as in a band state, but rather has a localization radius of order one nanometre characteristic of dopants in semiconductors, then the appropriate picture is a magnetic polaron, an island of local ferromagnetic order in a paramagnetic or antiferromagnetic host.

2.2. *Magnetic polarons*

2.2.1. *General description*

The concept of spin-dependent electron transfer was first formulated in order to explain the conductivity-induced ferromagnetism in $LaMnO_3$ by the double-exchange mechanism [4, 21], and spin polarons were already suggested in the work of deGennes [22]. Here we present here arguments for the stability of a simple spherical spin polaron of radius R first given by Kasuya [48] and von Molnar and Kasuya [49]. Suppose that a single electron or hole is introduced into an otherwise antiferromagnetic or paramagnetic lattice. If no defects or impurities are present and the s–f interaction is weak, then the incremental free energy ΔF of a polarized cluster in this background may be expressed as the sum of kinetic and magnetic energy terms:

$$\Delta F = \frac{E_0}{\gamma^2} - \frac{J_{sf}^2 \chi}{2\gamma^3} \tag{2.2}$$

where $E_0 = \pi^2 h^2 / 2ma^2$. Here $\gamma = R/a$ where a is defined by the equation $4\pi a^3/3 = 1/N$. N is the density of magnetic cations and χ is the magnetic susceptibility. Since the susceptibility in ferromagnets is high only near T_C, it is expected that polarons will only have substantial binding energy near the ordering temperature. However, minimizing this free energy with respect to the polaron radius results in a solution that is only stable at infinity or R approaching zero. An additional energy term is needed to stabilize the polaron. This may be the Coulomb attraction E_C/γ of the electron to an oppositely charged centre, where $E_c = e^2/4\pi\epsilon_0 a$, a situation frequently encountered in practice since the magnetic semiconductors are insulators until they are doped, and the dopant acts as an attractive center, just as in any ordinary semiconductor. Instead of equation (2.2), we have

$$\Delta F = \frac{E_0}{\gamma^2} - \frac{J_{sf}^2 \chi}{2\gamma^3} - \frac{E_C}{\gamma}. \tag{2.3}$$

There is now a minimum in $\Delta F(\gamma)$ and a stable configuration may be obtained for some value of R. Kasuya referred to this as the *bound magnetic polaron* or magnetic impurity state. A strong s–f interaction will lead to a constant second term $-J_{sf}S$, but in an antiferromagnetic matrix there will be a positive term $(\frac{4}{3})\pi J_{af}\gamma^3$ due to the broken bonds which again gives a minimum [50]. Below the Néel temperature of an antiferromagnet, the polarons will not easily move in the presence of an electric field, since they have to drag their magnetic polarization cloud along, which leads to localization or to a large effective mass for diffusive motion. The polaron tends to become delocalized below the Curie temperature of a ferromagnet. Thus it becomes clear how an applied magnetic field can produce an insulator–metal transition. The magnetic contributions to the localization come from the energy difference between the paramagnetic disorder or antiferromagnetic order of the host and the ferromagnetic order of the polaron. In a magnetic field, the host sublattice develops a magnetization, which, when saturated, has the same magnetic structure as the polaron cluster and the carrier becomes unbound. If defects such as that producing the Coulomb potential are present, then this polaron, which ordinarily might be described as a very heavy but band-like particle moving diffusively [41] will typically be bound to the defects. Thus, transport under these conditions can only occur via *hopping,* where thermal activation takes the bound polaron from one localized trapping centre to the next.

2.2.2. *Disorder, the mobility edge and transport*

This section describes the physical properties of materials where the electrons are localized by Coulombic disorder and extends these ideas to magnetic materials. In particular, paramagnetic $(Ce_{3-x}\square_x)S_4$ studied by Cutler and Mott [51] is discussed, and its relation to the magnetic semiconductor, $(Gd_{3-x}\square_x)S_4$ developed [52, 53]. Such a comparison is helpful in describing the anomalous properties of the magnetic solid in terms of the concepts of the band tail and mobility edge, well established for semiconductors [50, 54]. The second part of the discussion deals with magnetotransport in $(Gd_{3-x}\square_x)S_4$ [55, 56]. It will be shown that the magnetic semiconductor exhibits a metal–insulator phase transition at a characteristic magnetic field. On the

insulator side, localization occurs with the formation of bound magnetic polarons, small regions of ferromagnetic gadolinium spin alignment in an antiferromagnetic host, in which the conduction electron spin is trapped. On the metal side, where the host spins are canted or aligned in the applied field directions, the electrons undergo anomalous diffusive motion. These physical considerations are equally relevant in the doped manganites.

$(Ce_{3-x}\square_x)S_4$ crystallizes in the Th_3P_4 structure [57]. Zachariasen predicted that up to a third of the cation sites per unit cell could be vacant and therefore the structure should exist over a single-phase region extending from Ce_2S_3 to Ce_3S_4. The existence of randomly placed vacancies in these crystalline materials produces the random potential fluctuations and concomitant energy band tails so familiar in amorphous and highly doped semiconductors. Cutler and Mott [51] demonstrated the applicability of the concepts of Anderson localization [58] in a band tail and the mobility edge to this class of crystalline materials.

The existence of a rigid band tail in Th_3P_4 structure compounds is a fair assumption as long as the donor concentration is small relative to the total number of vacancies (about $2.1 \times 10^{27}\,m^{-3}$ in $(Ce_{3-x}\square_x)S_4$). Cutler and Mott [51] argued that, when $E_F(0)$, the low-temperature Fermi energy, lies below $E\mu$, (position E_a in figure 12(*a*), conduction is thermally activated and approaches 0 as $T \rightarrow 0$. When $E_F(0)$ is above E, conduction occurs in extended states and remains finite as T approaches 0 (see figure 12(*b*)). $E_F(0)$ is a function of the number of vacancies occupied by the rare earth atoms cerium or gadolinium. In the case of $(Ce_{3-x}\square_x)S_4$, Cutler and Mott [51] found experimentally that $E_F(0) = E\mu$ for a critical concentration $n_c = 8 \times 10^{25}\,m^{-3}$. In fact, a major conclusion of their work was the existence of n_c, which has formed the basis for all subsequent analyses of the metal–insulator transition in three dimensions.

In magnetic $(Gd_{3-x}\square_x)S_4$, it has been shown [56] that $|E\mu - E_F|$ is not only a function of concentration (and temperature) but also of magnetization. Gd_2S_3, the $x = \frac{1}{3}$ compound, is an antiferromagnetic insulator whereas, with increasing n,

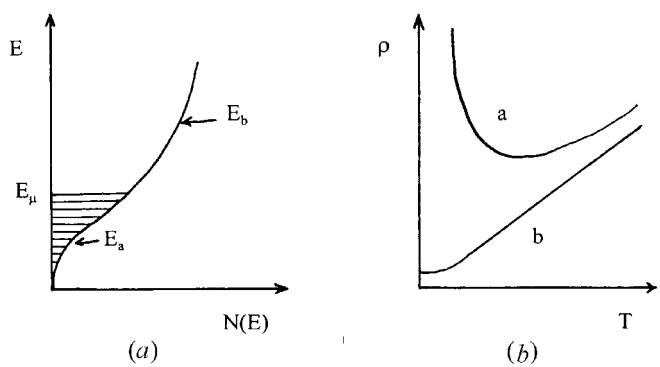

Figure 12. (*a*) Schematic density of states $N(E)$. The shaded region represents localized states, $E\mu$ is the mobility edge, and E_a and E_b give the positions of the low-temperature Fermi energy, E_F, for small and large electron concentration, respectively. (*b*) Schematic plots of resistivity against temperature for $E_F = E_a$ and $E_F = E_b$, respectively. (After [51].) [Reprinted by kind permission of the American Physical Society from page 1336 of *Physical Review*, Volume 181, 1969, and the authors, M. Cutler and N. F. Mott, © 1969 by the American Physical Society.]

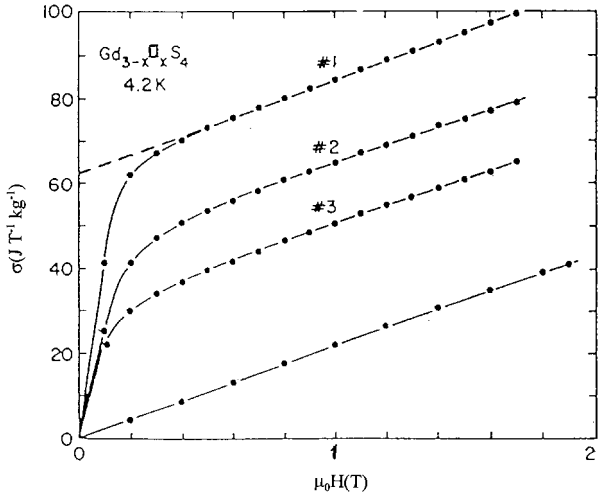

Figure 13. Magnetization M against applied field H for samples 1, 2 and 3 (carrier concentration $n_1 > n_2 > n_3$) together with the pure antiferromagnetic insulator: (- - -) extrapolation to M_0. (After [53].) [Reprinted by kind permission of the American Physical Society from page 908 of *AIP Conference Proceedings*, Volume 18, 1974, and the authors, T. Penney, F. Holtzberg, L. J. Tao and S. von Molnár, © 1974 by the American Physical Society.]

(increasing gadolinium), the compound becomes a ferromagnetic metal [34, 52, 53]. These magnetic structures and their variation with carrier concentration suggest the presence of localized magnetic polarons. An alternative interpretation has been suggested by Kamijo *et al.* [59], involving Wigner localization. For the present purposes, the important features of the magnetic data are a pronounced field dependence which shows the coexistence of both ferromagntic and antiferromagnetic order (figure 13)

For the doped materials there is, at low fields, a rapid rise similar to domain rotation in a ferromagnet. At higher fields, the data are described by $M = M_0 + \chi_L H$, where χ_L is nearly the same for all samples and is, therefore, characteristic of the antiferromagnetic background. The M_0 value is the magnetization of the ferromagnetic polarons and increases with increasing carrier concentration n.

The concepts of the mobility edge and the magnetic polaron together explain the transport in figure 14 including the metal–insulator transitions. Sample 3 is non-metallic because the Fermi energy lies below the mobility edge at $T \rightarrow 0$ (see figure 14). At low temperatures, the slopes of $\ln \rho$ against $1/T$ are constant because χ_L and therefore the magnetic contribution to the binding energy in equation (2.1) are nearly temperature independent. With increasing temperature, however, χ_L and the binding energy decrease, and the resistivity drops more dramatically. The change in sign of the slope at the highest measuring temperatures reflects the fact that $\Delta E = |E_F(T) - E_\mu| \approx kT$.

Sample 2 has similar features, but, most importantly, it has undergone the metal–insulator transition by 3.2 T. In zero field, the electron concentration of this sample is slightly below the critical concentration n_c, for which $E_F(0) = E_\mu$. The transition in field may be understood in terms of the motion of E_c with respect to E_F such that

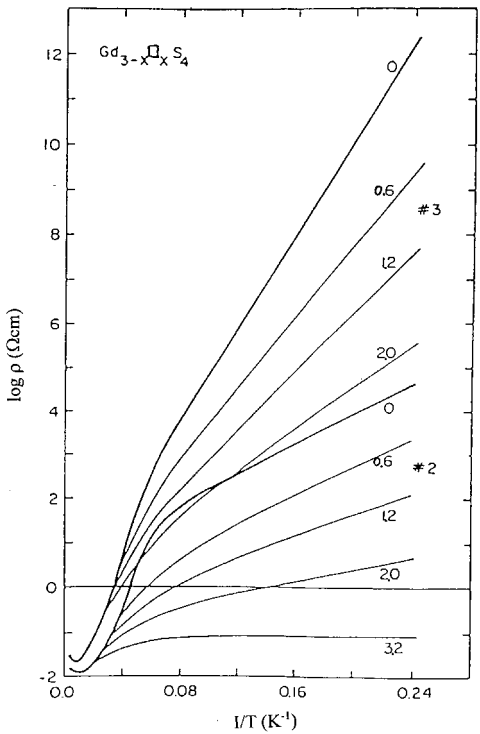

Figure 14. Logarithm of the resistivity against reciprocal temperature for sample 2 ($n = 1.6 \times 10^{26}\,m^{-3}$) and sample 3 ($n = 8.7 \times 10^{25}\,m^{-3}$) in applied fields of 0, 0.6, 1.2, 2.0 and 3.2 T. (After [53].) [Reprinted by kind permission of the American Physical Society from page 908 of *AIP Conference Proceedings*, Volume 18, 1974, and the authors, T. Penney, F. Holtzberg, L. J. Tao and S. von Molnár, © 1974 by the American Physical Society.]

$E_F(0) - E_\mu > 0$ for large fields and, therefore, large sublattice magnetization [60] In the most extreme case, with no applied field, the electron is bound as a magnetic polaron and can only move by hopping from occupied to unoccupied donor sites. The material behaves like an insulator. With the application of a high magnetic field, the host spins align and the electron becomes free to move diffusively through the lattice. It behaves like a metal. It will be shown that the manganites also often experience a similar insulator–metal transition which is magnetic in origin. Magnetic polarons may offer a plausible explanation for this effect.

2.3. *Spin polarization*

The conjecture that conduction electrons in ferromagnetic systems have a net spin polarization has found indirect experimental support throughout much of the history of magnetic research. Early evidence was the famous Slater [61]–Pauling [62] curve which showed that the magnetic moment peaked and then disappeared depending on the electron concentration of 3d transition metal alloys. Indirect evidence that such polarization must exist in magnetic semiconductors came from the early optical studies by Busch and Wachter [63] on europium chalcogenides. These researchers showed that the internal fields created by the magnetically ordered

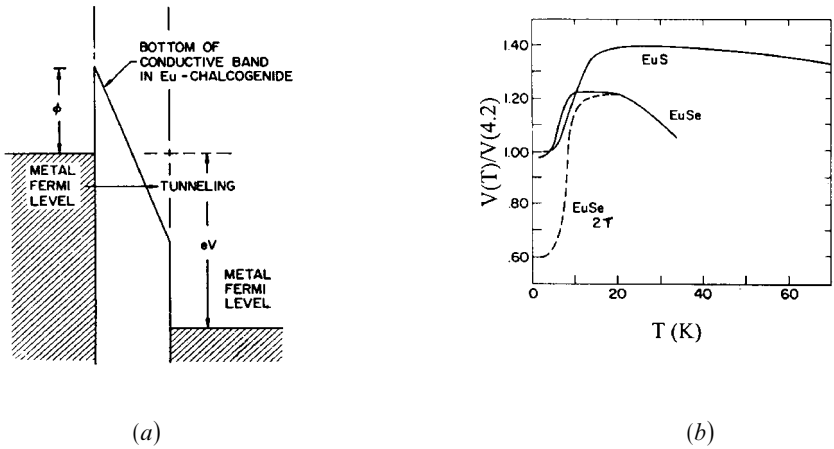

(*a*) (*b*)

Figure 15. (*a*) The potential barrier of an EuX tunnel junction where X = S, Se, at an applied voltage V. ϕ is the barrier height. (*b*) $V_T/V_{4.2K}$, the voltage at a given current level (normalized to its value at 4.2K), against temperature, for EuSe at 0 and 2 T and for EuS at zero field [64]. [Reprinted by kind permission of the American Physical Society from page 852 of *Physical Review Letters*, Volume 19, 1967, and the authors, L. Esaki, P. J. Stiles and S. von Molnár, © 1967 by the American Physical Society.]

rare earth ions in, for example, insulating EuS, split the empty conduction bands by large fractions of an electronvolt. The first evidence for band splitting and, consequently, spin polarization in transport was provided by Esaki *et al.* [64], who produced tunnelling structures of two conductors separated by insulating EuS or EuSe, in which the thickness of the insulating barrier was large enough for the probability of tunnelling at very small biases to be negligible. The tunnel current, which was strongly dependent on the magnetization of the insulator, was interpreted as Fowler–Nordheim tunnelling from the metal into the (empty) conduction band of the insulating EuSe (figure 15).

It is obvious that these tunnelling structures ought to be excellent spin filters. Furthermore, the model in which the band is split into two spin polarized subbands, suggested doped Eu chalcogenides as good sources of spin polarized electrons [65]. For example, EuS doped with a number of electrons such that $E_F \leqslant g\mu_B B_W$, where g is the g factor equal to 2 for electrons, μ_B is the Bohr magneton and B_w is the Weiss molecular field acting on them, should achieve almost 100% polarization at 4.2 K. Low temperature field emission experiments on W–EuS junctions, in which the EuS insulator is supposed to act as spin filter, were not able to verify this prediction [66], but more recent experiments [67, 68] have demonstrated that polarization in excess of 85% is possible. Spin-polarized tunnelling has been reviewed by Meservey and Tedrow [69].

A source of spin-polarized carriers is essential for the development of spin electronics [70]. Transistors based on the distinction between spin-up and spin-down electrons were suggested as early as 1968 [71, 72]. The carriers in doped magnetic perovskites are expected to be spin polarized below T_C, which may be above room temperature and, consequently, the manganites could become important elements in a developing new technology.

In this section, we have outlined the concepts of carrier–local spin interactions, their effect on the magnetism of solids and concomitantly the effect of the magnetic

state on the properties of the carriers. In concentrated magnetic semiconductors, electron scattering, electron localization and the position of the mobility edge are all intimately coupled to the magnetic properties. It will be shown in the ensuing sections that many of these ideas also apply to (and in some cases were originally developed for) the mixed-valence manganites.

3. Materials preparation

The mixed-valence manganites have been prepared as polycrystalline ceramics, single crystals and thin films. The methods used for preparing magnetic oxides have been discussed in some detail in a book by Valenzuela [73], with particular reference to ferrites. The methods for making manganites, on which there is much less literature, are summarized here.

3.1. *Ceramics*

Polycrystalline ceramics are relatively easy to prepare, although some care is needed to achieve a composition with a specific oxygen stoichiometry. The standard ceramic method involves repeated grinding, compaction and firing of component oxides until a single-phase material is achieved [73]. To make $(La_{1-x}Ca_x)MnO_3$, for example, a mixture of La_2O_3, CaO and MnO_2 may be ground together, pelletted and fired at 1200°C in air for several hours, and the process repeated as often as necessary to obtain a uniform single phase. The final firings may be at a higher temperature, in a controlled atmosphere to achieve a desired stoichiometry. The method depends on solid-state interdiffusion between the oxide powders, and so it is necessary to use fine, well-compacted powder. The temperature for the solid-state reaction should be high enough for the diffusion length $(2Dt)^{1/2}$ to exceed the particle size, where D is the diffusion constant for the fast-diffusing species, and t is the firing time [73].

A standard variant of the method uses precursors which decompose into ultrafine-grained oxides on a first heating (calcining), yielding a highly reactive powder. Commonly used precursors are carbonates and oxalates such as $MnCO_3$, $CaCO_3$ and $MnC_2O_4{\cdot}2H_2O$. In their original work, Jonker and van Santen [7] used mixtures of oxides and carbonates to make the mixed-valence manganites. A typical procedure for $(La_{1-x}Ca_x)MnO_3$ involves grinding, compacting and firing La_2O_3, $CaCO_3$ and $MnCO_3$ several times in air at 1250°C for 5 h, followed by similar treatments at 1380°C for 12 h and at 1390°C for 20 h [74].

Wet chemical methods which produce a precursor gel of intimately mixed and poorly crystallized hydrated oxides by co-precipitation are also suitable for preparing polycrystalline oxides. There are many instances of the use of these methods for making bulk ceramics of the present materials [7, 75–79]. For example, $(La_{0.60}Y_{0.07}Ca_{0.33})MnO_3$ was prepared from a citrate gel by dissolving La_2O_3, Y_2O_3, $CaCO_3$ and $MnCO_3$ in nitric acid, adding citric acid and ethylene glycol. The solution was dried, yielding a gel which was calcined in air at 900°C, ground, pressed and sintered at 1000°C and finally reground and sintered at 1300°C [78].

3.2. *Crystals*

Single crystals of the manganites have been grown in several ways. The lead-doped series $(La_{1-x}Pb_x)MnO_3$ with $0.25 < x < 0.45$ has been grown by a flux method, which involves cooling a 100 cm^3 charge of the oxide with a $PbO–PbF_2$ flux closed in a platinum crucible extremely slowly through the liquidus. The charge

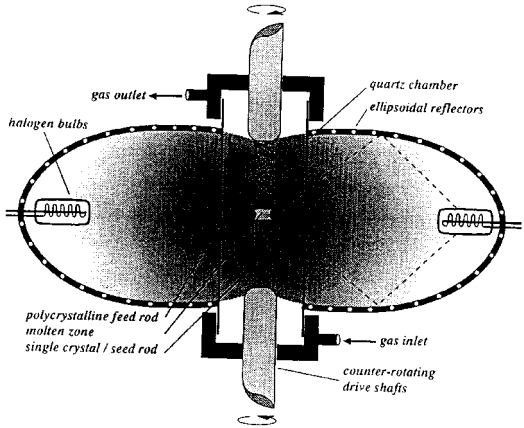

Figure 16. Crystal growth in an infrared image furnace. (By courtesy of G. Balakrishnan.)

was held near 1200°C for 24 h and then cooled at a rate of $1^{\circ}C\,h^{-1}$ from 1200 to 980°C. This yielded crystals a few millimetres in size [13]. A similar method has been used for $(Nd_{0.5}Pb_{0.5})MnO_3$ [80, 81] and other lead-containing compositions [82].

A more generally applicable growth method is from a molten zone, produced in an infrared image furnace [83] shown in figure 16. Heat from the source is focused onto a region in a polycrystalline rod to form a molten zone which passes through the boule, as the rod is lowered in the furnace. The crystal growth rate is carefully controlled by monitoring the diameter of the boule continuously with a video camera. Furthermore, the atmosphere in the image furnace can be controlled to provide the required composition [84]. Crystals grown in this way include $LaMnO_3$, $(La_{1-x}Ca_x)MnO_3$ with $0 < x < 0.25$ [305], $(La_{1-x}Sr_x)MnO_3$ with $0 < x < 0.6$ [84–87], $(Pr_{0.5}Sr_{0.5})MnO_3$ [88], $(Pr_{0.7}Ca_{0.3})MnO_3$ [89], [90] and $(La_{0.7}Pb_{0.3})MnO_3$ [91]. Some examples are shown in figure 17.

3.3. *Thin films*

Thin films of the manganites have mainly been produced by sputtering or pulsed laser deposition (PLD) from sintered ceramic targets. The laser method had been extensively developed for cuprate superconductors, and it was readily adapted for manganites. A beam from a pulsed laser, typically an excimer laser operating in the ultraviolet at $\lambda = 248$ nm with KrF is focused onto a ceramic target with the required cation composition. A frequency-tripled or quadrupled neodymium-doped yttrium aluminium garnet (Nd:YAG) laser may also be used. The energy per pulse is about $2\,J\,cm^{-2}$. It creates a plasma which takes the form of a plume several centimetres long, emerging normal to the surface of the target (figure 18). The high-energy species in the plasma are collected onto a substrate and the thin film is built up. For PLD, as for sputtering, both the atmosphere in the chamber and the substrate temperature are critical variables. By using an oxygen pressure of 10–50 Pa, and a substrate of MgO, $LaAlO_3$ or $SrTiO_3$ heated at 600–800°C, it is possible to achieve good-quality oriented films. Compounds prepared in this way include $(La_{1-x}Ca_x)MnO_3$ [92, 93], $(La_{0.7}Sr_{0.3})MnO_3$ [601] and $(La_{0.67}Bd_{0.33})MnO_3$ [599] on MgO, $(La_{0.67}Ba_{0.33})MnO_3$ [15, 94], $(La_{1-x}Sr_x)MnO_3$ [95] and $(Sm_{1-x}Sr_x)MnO_3$ [96] on $SrTiO_3$ [95] and $(La_{0.67}Ca_{0.33})MnO_3$ [97, 98], $(La_{0.7}Ca_{0.3})MnO_3$ [99], $(La_{0.67}Sr_{0.33})MnO_3$ [598], $(La_{0.6}Pb_{0.4})MnO_3$ [95, 100] and $(Nd_{0.7}Sr_{0.3})MnO_3$ [101]

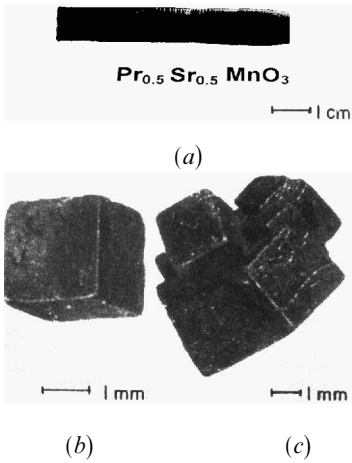

Figure 17. Single crystals of (*a*) $(Pr_{0.5}Sr_{0.5})MnO_3$ from within an infrared image furnace (courtesy of G. Balakrishnan) and $(La_{0.68}Pb_{0.32})MnO_3$ grown by the flux method; (*b*) a typical cube-shaped crystal with 100 faces; (*c*) a multitwinned crystal. [Reprinted from page 2691 of *Canadian Journal of Physics*, Volume 47, by A. H. Morrish, B. J. Evans, J. A. Eaton and L. K. Leung, © 1969 [13], by kind permission of NRC Research Press.]

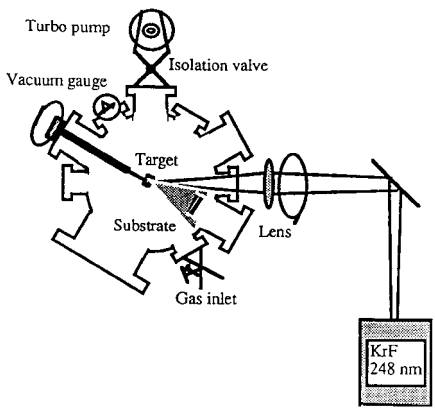

Figure 18. Schematic arrangement for preparing thin films by PLD.

on $LaAlO_3$. Films of the lanthanum-deficient compounds La_xMnO_3 have been produced on $SrTiO_3$ at 700°C, using a frequency-tripled Nd:YAG laser ($\lambda = 355$ nm) [102]. Lawler *et al.* [93] described PLD for the $(La_{1-x}Ca_x)MnO_3$ system in some detail. The Curie temperature of '$(La_{0.7}Ca_{0.3})MnO_3$' can vary from 150 to 290 K according to the substrate temperature [103]. As with oxide superconductors, post-deposition annealing of the films can lead to significant modification of the oxygen stoichiometry, and very large values of the magnetoresistance [1, 95, 98, 99]. Manganites can be grown on silicon, with [104–106] or without [107, 108] a buffer or template layer. Films with monovalent cation doping have also been grown by PLD [109].

A persistent problem with PLD is the tendency for the films to be splattered with 'blobs' or 'particulates' (submicron droplets ejected from the target). A solution is to

work close to the energy threshold for ablation with a dense target and raster or rotate the target in the beam. An off-axis deposition geometry is also advantageous [15]. Other solutions involve mechanical or magnetic filters. This difficulty does not arise with sputtering, which is better suited to making large-area thin films and multilayer structures [110–112]. Films produced by PLD [113] or sputtering [114] can have compositions which turn out to be significantly different from that of the target. Dc [115, 116], rf [110, 111, 117] and ion beam sputtering [112] have all been used to make manganites. Single-crystal films of $(La_{1-x}Ca_x)MnO_3$ with $x = 0.25$ and 0.33 are obtained on $NdGaO_3(110)$ at 600°C by the dc method [116]. The thicknesses of films produced by PLD or sputtering are typically of order 100 nm, but it is possible to produce much thinner films, if required. Manganite films grown by PLD on $SrTiO_3$ are often strained by lattice match with the substrate. Those grown on MgO, where the larger lattice mismatch prevents perfect epitaxy, are generally unstrained.

High-quality manganite films may be prepared by single-source metal–organic chemical vapour deposition (MOCVD). Vapours from a mixture of volatile organometallic compounds, either liquid or solid, are transported to the deposition chamber by a carrier gas (helium or nitrogen). Highly-oriented $(La_{0.8}Ca_{0.2})MnO_3$ (001) films [118] and single-crystal $(La_{1-x}Sr_x)MnO_3$ with $x = 0.24$ and 0.30 [119, 120] were obtained on $LaAlO_3$ substrates at temperatures between 600 and 750°C. In contrast with physical vapour deposition methods, the MOCVD process does not require ultrahigh-vacuum conditions and therefore allows deposition at much higher partial pressures of O_2. Hence films can be of sufficiently high quality to exhibit good magnetoresistance properties without the need for post-deposition annealing. For example, the *in-situ* grown $(La_{0.74}Sr_{0.26})MnO_3$ gives a magnetoresistance value of 70% at 6 T at 270 K, and $(La_{0.7}Sr_{0.3})MnO_3$ gives 60% at 290 K in the same field [120, 121]. Post-annealed MOCVD films on $LaAlO_3$ substrates with composition $(La_{0.67}(Sr, Ca)_{0.33})MnO_3$ gave a maximum magnetoresistance value $\Delta R/R(H)$ of 250% for the calcium-doped film and 25% for the strontium-doped film [122, 123]. Film quality is improved by repeated annealing [124].

The highest-quality films are those prepared by molecular-beam epitaxy (MBE) [125–128]. Rocking curves of width 0.07° are reported for $(La_{0.58}Ca_{0.33})MnO_3$ produced by ozone-assisted MBE on $SrTiO_3$ [126]. Oriented tetragonal films of $(La_{0.7}Ca_{0.3})MnO_3$ and $(La_{0.7}Sr_{0.3})MnO_3$ have been grown by MBE on $SrTiO_3$ {001} [129–130].

Manganite films may also be obtained by electrochemistry. Growth of films of $LaMnO_3$ on $SrTiO_3$ from a 1 M solution of lanthanum and manganese nitrate under ultraviolet illumination has been described [131]. Amorphous films of $LaMnO_3$ [132] and $(La_{1-x}Sr_x)MnO_3$ [133] a few microns thick have been electrochemically deposited onto platinum electrodes and crystallized by subsequent heat treatment at about 800°C. A method of electroless deposition of $LaMnO_3$ onto yttria-stabilized zirconia, where the manganite is suitable as an air electrode in solid oxide fuel cells on account of its high-temperature stability has been reported [134]. The substrate for electroless deposition does not have to be conducting. Lithium can be introduced into cation-deficient manganites by electrochemical methods [135].

Other possible methods of making manganite films include spray pyrolysis and sol–gel dip coating. Thick films (> 10 μm) can be prepared by screen printing onto Al_2O_3 or ZrO_2 substrates and sintered at about 1400°C [136].

3.4. *Non-stoichiometry and defects*

It must be emphasized that manganites of nominally identical compositions produced by different methods in different laboratories can show very different physical properties. Figure 19 is a compendium of Curie temperature data for the $(La_{1-x}Ca_x)MnO_3$ and $(La_{1-x}Sr_x)MnO_3$ systems. The variations presumably reflect differencs in the composition, stoichiometry and defect structure of the oxides, rather than instrumental errors in the measurement of T_C. Agreement is achieved between the results from different laboratories when preparation conditions are well controlled, as in the growth of single crystals by the floating zone method.

While it is convenient to fire ceramics in air at an oxygen partial pressure of 2×10^4 Pa (the oxygen partial pressure in the ambient atmosphere), this does not necessarily generate a stoichiometric oxide. The oxygen partial pressure has a critical influence on the physical properties [137]. For example, $LaMnO_{3+\delta'}$ produced by firing in air is ferromagnetic, whereas if it is fired in nitrogen it is antiferromagnetic [138, 139]. Work by Kuo *et al.* [140] has established the equilibrium composition of $LaMnO_{3+\delta'}$ and $(La_{1-x}Sr_x)MnO_{3+\delta'}$ over a range of temperatures and oxygen pressures (figure 20). At 1000°C, $LaMnO_3$ is in equilibrium at an oxygen pressure of 0.25 Pa. At 1200°C, the oxide forms stoichiometrically for 10^{-5} Pa $< P_{O_2} <$ 1 Pa, but the equilibrium at 2×10^4 Pa is oxygen-rich: $\delta' = 0.06$. In fact, the oxygen content can be as high as $LaMnO_{3.20}$, which corresponds to 40% Mn^{4+}, when the material is fired at 600°C at an oxygen pressure of 13 MPa [141]. At the other extreme, the perovskite structure can tolerate oxygen deficiency at very low oxygen partial pressure [142]. Oxygen-deficient compositions can be produced by reduction in the presence of a getter. The defects there are best considered as clusters of an oxygen vacancy with two Mn^{2+} ions [143]. Diffusion of these oxygen vacancies gives rise to ionic conduction [144, 145], and absorption of water by oxygen-deficient material may lead to proton conduction [146]. $LaMnO_3$ is found to decompose at 1200°C when the oxygen pressure is less than $10^{-6.9}$ Pa [140, 147]. The defects then tend to order into extended arrays as in $La_8Mn_8O_{23}$ and $La_4Mn_4O_{11}$ [148]. Extreme oxygen deficiency while retaining the perovskite structure was achieved by heating $SrMnO_3$ at 1450°C in the presence of zirconium to yield $Sr_2Mn_2O_5$ [149]. Defects can also be introduced by argon ion implantation [150, 151].

For the standand ceramic method consisting of calcining a mixture of oxides in air, the defects associated with excess oxygen take the form of *cation vacancies* on A

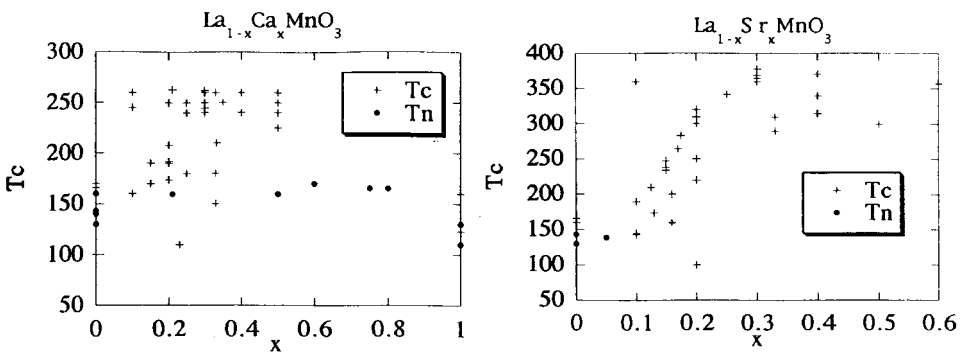

Figure 19. Compilation of measured Curie temperatures in nominal $(La_{1-x}Ca_x)MnO_3$ and $(La_{1-x}Sr_x)MnO_3$ compounds.

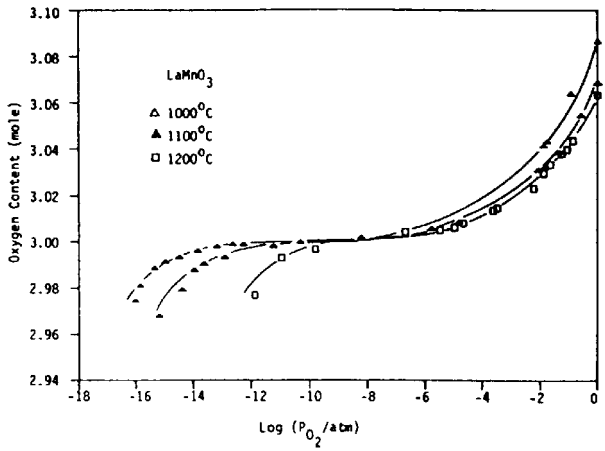

Figure 20. Equilibrium oxygen content in $LaMnO_{3+\delta}$ as a function of oxygen pressure at different temperatures [140]. [Reprinted from page 212 of *Journal of Solid-state Chemistry*, Volume 83, 1989, [140], authored by J. H. Kuo, H. Andersen and D. Sparlin, with kind permission of the authors and Academic Press.]

and B sites [76, 139–141, 152] as there is no straightforward way of accommodating any extra oxygen in the close-packed structure of perovskite. The compound can be prepared with either lanthanum or manganese deficiency, or both [153]. The formula of the oxygen-excess 1:1 compound is more properly written $(LaMn)_{1-\delta}O_3$. Assuming that the oxygen is O^{2-}, this formula may be rewritten in the form

$$(La^{3+}_{1-\delta}\square_{\delta})(Mn^{3+}_{1-7\delta}Mn^{4+}_{6\delta}\square_{\delta})O_3, \tag{3.1}$$

where $\delta \approx \delta'/3$. The fraction of total manganese as Mn^{4+} is therefore $6\delta/(1-\delta) = 6\delta'/(3-\delta')$, so that $\delta = 0.04$ corresponds to 25% Mn^{4+}. The near-stoichiometric oxide can be prepared by firing in a reduced pressure of oxygen such as 10^{-3} Pa [154], in a nitrogen [7, 139] or argon [84, 155] atmosphere, or by reduction in hydrogen [156]. More cation-deficient material can be obtained by electrochemical oxidation [76].

Another type of non-stoichiometry which converts Mn^{3+} into Mn^{4+} is lanthanum deficiency. The formula $La_{1-z}MnO_3$ may be written as

$$(La^{3+}_{1-z}\square_{z})(Mn^{3+}_{1-3z}Mn^{4+}_{3z})O_3, \tag{3.2}$$

so that there is no Mn^{3+} at all in the limit $z = 0.33$. Lanthanum-deficient samples tend to be ferromagnetic and metallic [102, 157, 158].

In $(La_{1-x}Sr_x)MnO_3$, as the lanthanum is substituted by divalent strontium, the equilibrium is shifted to higher oxygen pressures; when $x = 0.2$, the range is approximately 10^{-2} Pa < P_{O_2} < 10^3 Pa [140]. Firing the compositions with $x = 0.3$ in air at 1400°C is therefore likely to yield near-stoichiometric oxides. In some cases the stoichiometry has been determined directly by refining the site occupancies from neutron diffraction data; δ' is found to be zero when $x \approx 0.3$ [159]. A similar conclusion has been drawn from density measurements for several other divalent substitutions [160].

4. Physical properties of manganites

4.1. *Crystal and electronic structure*

Considering the perovskite structure of figure 2 as a cubic close-packed array formed of O^{2-} anions and A^{2+} or A^{3+} cations with small B cations in octahedral interstitial sites, the ideal cation radii r_A and r_B can be deduced. The former must be the same as that of oxygen, $r_O = 0.140$ nm, while the latter is $(2^{1/2} - 1)r_O = 0.058$ nm. Goldschmidt [161] defined a tolerance factor

$$t' = \frac{(r_A + r_O)}{2^{1/2}(r_B + r_O)}, \tag{4.1}$$

which is unity for ideally sized ions. Relevant ionic radii are listed in table 2. The A-site cation radii are for twelve-fold oxygen coordination, whereas the B site radii are for six-fold oxygen coordination. In fact the perovskite structure may form in oxides for which $0.89 < t' < 1.02$. Stability limits will be slightly different if other ionic radii, such as Goldschmidt's original set based on $r_O = 0.132$ nm, are used or if radii appropriate for a different coordination number are chosen.

A rough estimate of the number of electrons in the d bands may be made from the Mn^{3+} to Mn^{4+} ratio based on the stoichiometric formula, assuming that A-site cations and O^{2-} ($2p^6$), make no contribution. This number is $4 - x$ for divalent substitutions and $4 - 2x$ for monovalent substitutions. Oxide stoichiometry may be determined by refinement of site occupancies by neutron diffraction or appropriate chemical analysis for Mn^{3+} and Mn^{4+} [163], which often gives smaller d-band occupancy (more holes or a larger effective x) because of the non-stoichiometry discussed above [20, 164]. Indications of the true manganese charge state are provided by electron-energy-loss spectroscopy [165], measurement of the X-ray absorption near-edge structure [166, 167] and photoelectron spectroscopy [168].

4.1.1. *Crystal structure*

Although all the manganites considered here have structures derived from the elementary cubic perovskite cell of figure 2 where the lattice parameter a_0 is 0.39 nm and the elementary cell contains one formula unit ($Z = 1$), few of them have precisely this structure because the atoms are displaced from their ideal positions

Table 2. Ionic radii for ions in perovskite-structure oxides (nm) [162].

Ti^{4+}	0.0605	Y^{3+}	0.119	Ca^{2+}	0.134	Na^{+}	0.139
Mn^{4+}	0.053	La^{3+}	0.136	Sr^{2+}	0.144	K^{+}	0.164
Mn^{3+}	0.0645	Pr^{3+}	0.129	Cd^{2+}	0.131	Rb^{+}	0.172
Mn^{2+}	0.083	Nd^{3+}	0.127	Sn^{2+}	0.130		
Fe^{3+}	0.0645	Sm^{3+}	0.124	Ba^{2+}	0.161		
Co^{3+}	0.061, 0.0545 (ls)	Gd^{3+}	0.122	Pb^{2+}	0.149		
Ni^{3+}	0.069	Bi^{3+}	0.096				
Ga^{3+}	0.062						
Al^{3+}	0.0535						
						O^{2-}	0.140

ls = low spin.

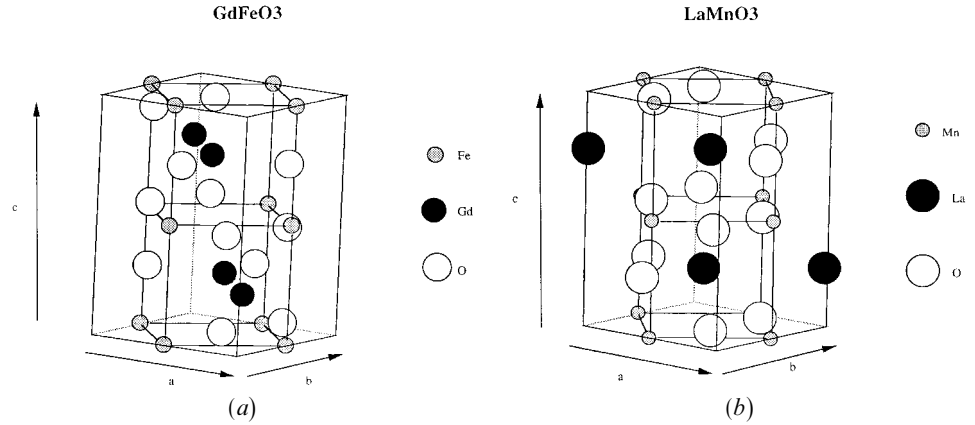

Figure 21. (*a*) The O-type orthorhombic $GdFeO_3$ structure which is a distorted version of the ideal perovskite structure of figure 2 with a buckling of the oxygen octahedra to accommodate a smaller than ideal A cation. (*b*) The O′-type orthorhombic $LaMnO_3$ structure, which incorporates a Jahn–Teller distortion of the oxygen octahedra.

when $t' \neq 1$. The perovskite structure accommodates misfit in the ionic sizes and electronically induced deformations by various kinds of distortion to larger cells with lower symmetry. If t' is close to unity, there may be a slight rhombohedral distortion involving cooperative rotation of the BO_6 octahedra in the structure of figure 2 about a 111 axis. When the misfit is larger, there is a buckling of the network of octahedra corresponding to cooperative rotation about a 110 axis which may lead to the O-type orthorhombic $GdFeO_3$ structure shown in figure 21(*a*). This compound has $t' = 0.91$ and $a = 0.5346\,\text{nm}$, $b = 0.5616\,\text{nm}$ and $c = 0.7668\,\text{nm}$; the B–O–B bond angle, which is sensitive to the size of the A cation, is reduced from 180° to 161°. It is typical of the O-type structure that $a < c/2^{1/2} < b$. A different, O′-type, orthorhombic structure adopted by $RMnO_3$ (R = La–Dy) is shown in figure 21(*b*). It is a variant with more severely-distorted octahedral environments where $c/2^{1/2} < a < b$. The reason for the severe distortion is the Jahn–Teller effect of Mn^{3+} [169], which causes the octahedra to extend in one direction in the *a*–*b* plane.

Besides the orthorhombic O and O′ structures with $Z = 4$, there is a bewildering variety of cubic, tetragonal, rhombohedral, hexagonal, orthorhombic and monoclinic cells to which the manganite structures are referred in the literature. These unit cells are closely related, and rhombohedral or monoclinic angles are very near the ideal values $\alpha = 60°$ or 90°, $\beta = 90°$.

Figure 22 sketches the relation between the various cells. The doubled cubic cell with $a \approx a_0$ contains eight formula units ($Z = 8$). The rhombohedral cell with $a \approx 2a_0$ and $\alpha \approx 90.4°$ is a deformed version, slightly flattened along a 111 direction. A smaller rhombohedral cell with $a \approx 2^{1/2}a_0$ and $\alpha \approx 61°$ is similarly deformed but has $Z = 2$. As usual for rhombohedral structures, it is more convenient to index them on an hexagonal cell. The orthorhombic cells with $a \approx 2^{1/2}a_0$, $b \approx 2^{1/2}a_0$, $c \approx 2a_0$ have $Z = 4$. A closely-related tetragonal cell has $a = b \approx 2^{1/2}a_0$, $c \approx 2a_0$. Finally, the monoclinic cells are slightly-deformed versions of the small cubic cell ($Z = 1$) or the orthorhombic cells ($Z = 4$). In the case where $a = b$, the monoclinic cell is equivalent to a larger orthorhombic cell.

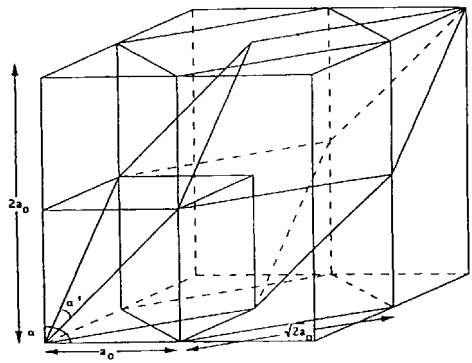

Figure 22. Relation between the unit cells used to describe manganese perovskites.

Table 3. Structure of $LaMnO_3$ at 1.5 K [170] space group, *Pbnm*, $Z = 4$; $a = 0.553\,33$ nm, $b = 0.574\,61$ nm and $c = 0.766\,37$ nm).

	x	*y*	*z*
La (4c)	−0.0095	0.0513	$\frac{1}{4}$
Mn (4b)	$\frac{1}{2}$	0	0
O(1) (4c)	0.0777	0.4849	$\frac{1}{4}$
O(2) (8d)	0.7227	0.3085	0.0408

4.1.1.1. *$LaMnO_3$*. A near-stoichiometric crystal grown in argon by Urushibara *et al.* [84] has the O′-type orthorhombic structure (space group *Pbnm*†) with $a = 0.554$ nm, $b = 0.575$ nm and $c = 0.770$ nm. The Mn–O–Mn bond angles are about 155°. The MnO_6 octahedron is Jahn–Teller distorted in such a way that the long and short Mn–O bonds lie in the a–b plane, giving the pattern of orbital order illustrated in figure 6(*b*). Mn–O bond lengths are 0.218 nm and 0.191 nm in plane and 0.196 nm along the *c* axis. The in-plane Mn–Mn distance is 0.399 nm, but the interplane separation along the *c* axis which corresponds to the intermediate Mn–O distance is a little shorter, 0.385 nm. A similar structural refinement was obtained at 1.5 K by Moussa *et al.* [170] (table 3). At a temperature of about 1020 K, the orthorhombic distortion disappears and the compound becomes rhombohedral (quasicubic) with the R-type $LaAlO_3$ structure [157, 171, 172]. There is also an $O' \rightarrow O$ orthorhombic transition at 940 K. Similar transitions occur in $PrMnO_3$ at 945 K [5], and at 820 K [173]. These can be regarded as order–disorder ('lattice → liquid') transitions where the local Jahn–Teller distortions become spatially uncorrelated but do not disappear [174]. Alternatively, they have been identified with the temperature where the electron hopping frequency exceeds that of the optical phonon corresponding to the Jahn–Teller distortion [5].

† This is equivalent to *Pnma*, with a different choice of axes. *a*, *b*, *c* in *Pbnm* become *c*, *a*, *b* in *Pnma*.

Table 4. Structure and stoichiometry of $LaMnO_3$ and $CaMnO_3$.

Compound	δ	Structure	Lattice parameters: *a* (nm), *b* (nm, *c* (nm)	β (degrees)	T_N (K)	T_C (K)	Reference
$(LaMn)_{1-\delta}O_3$	0.003	O′	0.554, 0.575, 0.770		143		[84]
	0.00	M	0.397, 0.397, 0.383	92.0			[9]
	0.05	R	0.547; 60.7				[152]
	0.00	M	0.7973, 0.7973, 0.7693	91.1			[178]
	0.02		0.7891, 0.7891, 0.7737	91.1			
	0.03		0.7809, 0.7809, 0.7782	90.2			
	0.01	O′	0.554, 0.573, 0.773		120		[156]
	0.05	C	0.781			125	
	0.02	O	0.5514, 0.5499, 0.7885				[76]
	0.04	R	0.5480; 60.56				
	0.05	C	0.7788				
	0.00	O′	0.55378, 0.57385, 0.77024		138		[139]
	0.05	O	0.55355, 0.54954, 0.77854		140		
		M	0.55241, 0.54660, 0.77616	90.909	131		
		H (R)	0.55259, 1.133240				
$NdMnO_3$		C	0.7557		85		[17]
$GdMnO_3$		C	0.7432		21		[17]
$YMnO_3$		H	1.141, 0.6125		80		[17]
$CaMnO_3$		O	0.5270, 0.5275, 0.7464		123		[179]
		C	0.7465		130		[178]

The La end member has an extended homogeneity range [175]. As discussed in section 3, the standard ceramic method of preparation which involves calcining a mixture of oxide and repeated firing and regrinding in air yields an off-stoichiometric product with composition $(LaMn)_{1-\delta}O_3$ where $\delta \approx 0.03$. The fraction of total manganese as Mn^{4+} is therefore 19% . This compound is typically rhombohedral or orthorhombic with an O-type structure. The more-stoichiometric oxide has the O′-type structure. Table 4 summarizes lattice parameters reported for a number of samples. Hervieu *et al.* [76], who have carried out a Rietvelt analysis of powder X-ray diffraction patterns as well as high-resolution transmission electron microscopy describe three structures, an orthorhombic structure for $\delta = 0.02$, a rhombohedral structure for $\delta = 0.04$ and a cubic structure for $\delta = 0.05$. Cheetham *et al.* [176] also describe a rhombohedral structure for $\delta = 0.04$. The oxygen octahedra are highly distorted in the orthorhombic phase. Töpfer and Goodenough [175] also find the O′ structure for $\delta \leqslant 0.02$, separated by a two-phase region from the R structure, stable for $x \geqslant 0.03$, but they find no cubic structure up to $\delta = 0.06$. The O → R transition falls precipitously with increasing δ, reaching 200 K at $\delta = 0.045$. Huang *et al.* [139] used neutron diffraction to describe orthorhombic O-type, monoclinic and rhombohedral phases, as well as a new O′-type structure. The Mn–O–Mn bond angle varies from 155° to 164° according to stoichiometry. The magnetic and electrical properties are strongly influenced by the stoichiometry, as discussed in section 4.2 below. Oxides with $\delta < 0.03$ are antiferromagnetic, whereas those with $\delta > 0.03$ are ferromagnetic. When $\delta > 0.05$, there is a metal–insulator transition. A monoclinic ferromagnetic phase has a lanthanum-to-manganese ratio of 0.9 [177].

4.1.1.2. *Solid solutions.* The monovalent A^+ cations listed in table 2 have a narrow range of solid solubility in the rare earth manganites, up to about $x = 0.2$ [180]. The divalent A^{2+} cations will substitute to a greater extent for the rare earth. The calculated energies of solution are lowest for strontium and calcium [181], and these ions most frequently form an extended or complete range of solid solution. With increasing divalent A-site substitution (i.e. increasing Mn^{4+} content) a sequence of crystallographic and magnetic phases ensues. These are summarized for $(La_{1-x}Ca_x)MnO_3$ in figure 23 for $(La_{1-x}Sr_x)MnO_3$ and $(Pr_{1-x}Sr_x)MnO_3$ in figure 24 and for $(Pr_{1-x}Ca_x)MnO_3$ in figure 34 later. A more detailed discussion of the structures of these solid solutions is given in section 4.2.1. Substitution of trivalent A^{3+} cations for lanthanum does not alter the manganese valence, but bismuth, yttrium or a heavier rare earth reduces t', and increases the distortion of the perovskite lattice.

The sequence of phases, $O' \rightarrow O \rightarrow R, C$, found on increasing the Mn^{4+} content by A-site substitution in these solid solutions is similar to that found by cation vacancies in $(LaMn)_{1-\delta}O_3$. The same sequence from distorted to less distorted phases may be seen on increasing temperature, or changing the oxygen stoichiometry [182, 183].

In addition to the Mn–O distance, the other important structural parameter in solid solutions is the M–O–Mn bond angle [184], which is related to the A-site cation radius and the tolerance factor t'. Variations from 156° to 168° are reported for $(R^{3+}_{0.7}A^{2+}_{0.3})MnO_3$ with different cations [185, 186], and from 155° to 164° in non-stoichiometric $LaMnO_3$ [139]. Substitution of different rare earth combinations in $((R_{1-y}R'_y)_{0.67}Ca_{0.33})MnO_3$, for example, allow for variation in the Mn–O–Mn bond angle without changing the Mn–O distances [186–188].

A structural study of a $(La_{0.7}Sr_{0.3})MnO_3$ crystal as a function of temperature shows it to be rhombohedral above and below T_C (378 K) with $a = 0.3876$ nm and $\alpha = 90.46°$ at room temperature. There is little change in the distortion of the MnO_6 octahedra or the Mn–O–Mn bond angle at T_C [189]. However, in other compounds

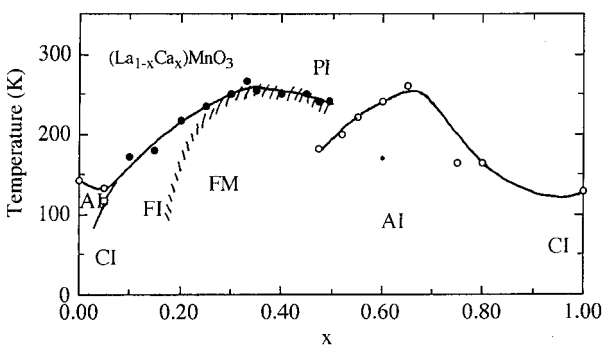

Figure 23. Magnetic phases in $(La_{1-x}Ca_x)MnO_3$. The shaded line represents the insulator-metal transition. The regions indicated are as follows: AI, antiferromagnetic insulator; CI, canted antiferromagnetic insulator; FI, ferromagnetic insulator; FM, ferromagnetic metal; PI paramagnetic insulator (After [20], [74].) [Adapted by kind permission of the American Physical Society from page 545 of *Physical Review*, Volume 100, 1955, and the authors, E. O. Wollan and W. C. Koehler, © 1955 by the American Physical Society; and page 3336 of *Physical Review Letters*, Volume 75, 1995, and the authors, P. Schiffer, A. P. Ramirez, W. Bao and S.-W. Cheong, © 1995 by the American Physical Society.]

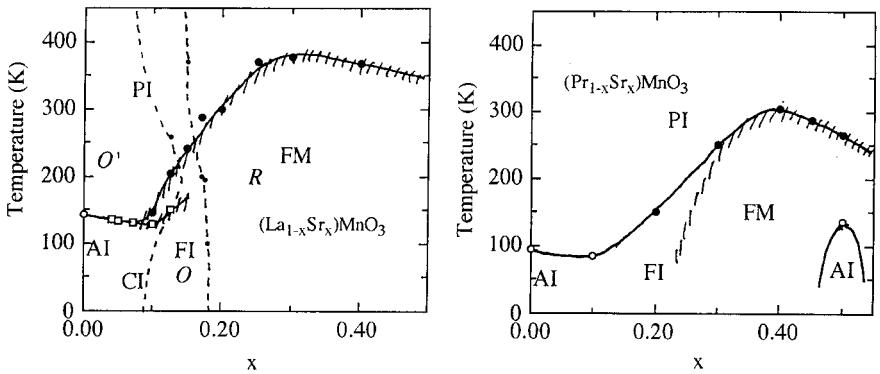

Figure 24. Crystallographic and magnetic phases in $(La_{1-x}Sr_x)MnO_3$ and $(Pr_{1-x}Sr_x)MnO_3$. (After [84, 191, 249, 320].) The symbols have the same meanings as in figure 23 except that the regions labelled O', O and R separated by broken curves refer to the crystal structures. [Adapted by kind permission of the American Physical Society from page 545 of *Physical Review* B, Volume 51, 1995, and the authors A. Urushibara, Y. Moritomo, T. Arima, A. Asamitsu, G. Kido and Y. Tokura, © 1995 by the American Physical Society; page 904 of *Physical Review Letters*, Volume 77, 1996, and the authors Y. Yamada, O. Hino, S. Nohdo, R. Kanao, T. Inami and S. Katano, © 1996 by the American Physical Society; page 14 709 of *Physical Review* B, Volume 53, 1996, and the authors H. Kawano, R. Kajimoto, M. Kubota and H. Yoshizawa, © 1996 by the American Physical Society; and page 1716 of *Physical Review* B, Volume 54, 1996, and the authors A. Asamitsu, Y. Moritomo, R. Kumai, Y. Tomioka and Y. Tokura, © 1996 by the American Physical Society.]

with $x \approx 0.3$ which have an orthorhombic structure and show a large resistivity peak there is a more significant change in the distortion of the MnO_6 octahedron near T_C [190].

Superstructures associated with charge ordering occur in $(La_{1-x}Sr_x)MnO_3$ at $x = \frac{1}{8}$ [191] and $\frac{1}{2}$. They are found in $(Pr_{1-x}Ca_x)MnO_3$ between $x = 0.3$ and 0.8 [192, 193], and in $(La_{1-x}Ca_x)MnO_3$ [194, 554, 596] at $\frac{1}{2}$, $\frac{2}{3}$, $\frac{3}{4}$ and $\frac{4}{5}$. The charge order includes pairs of Mn^{3+} stripes separated by rows of Mn^{4+} ions in $(Pr_{1-x}Sr_x)MnO_3$ [88] and $(Nd_{1-x}Sr_x)MnO_3$ [195–197] around $x = \frac{1}{2}$.

In summary, three broad trends evident in the crystal and electronic structures of manganite solid solutions are firstly passage from static to dynamic Jahn–Teller distortion of the oxygen octahedra surrounding the Mn^{3+} on increasing x or T ($O' \rightarrow O$, R transition), secondly passage from charge-ordered states at certain values of x to charge-disordered states on increasing T or changing x and thirdly passage from localized to delocalized electronic states in the vicinity of $x \approx 0.3$ on decreasing the temperature below the Curie point.

4.1.2. *Crystal field*

The crystal field at the cation sites in the perovskite structure has a far-reaching influence on the electronic and magnetic properties of the oxides. In the ideal structure, both sites have cubic point symmetry $m3m$. However, in the real distorted structures, the point symmetry is much lower.

4.1.2.1. *A site.* The crystal field at the A site in the perovskite structure is conveniently investigated in compounds with a non-magnetic trivalent B-site ion

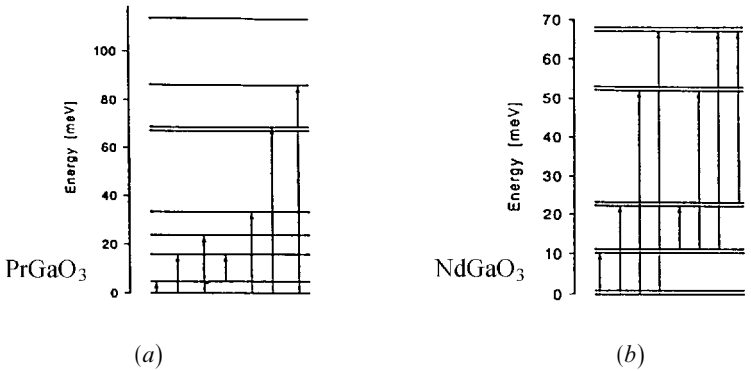

Figure 25. Crystal-field energy levels in (*a*) $PrGaO_3$ and (*b*) $NdGaO_3$ determined by inelastic neutron scattering. [Reproduced from the *Journal of Physics: Condensed Matter*, Volume 6, page 4099, © 1994 [198] and Volume 5, page 8973, © 1993 [199], by kind permission of the authors and IOP Publishing Limited.]

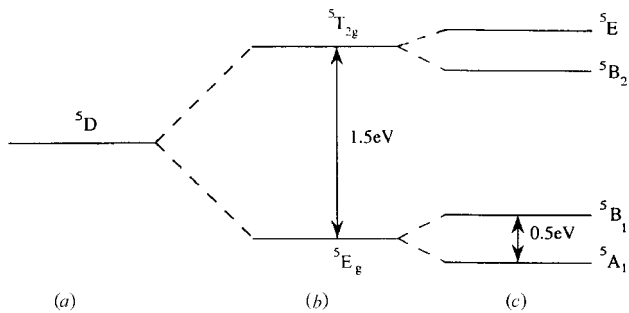

Figure 26. Optical transitions for Mn^{3+} in (*a*) a free ion, (*b*) an octahedral site and (*c*) a uniaxially distorted octahedral site.

such as Al^{3+} or Ga^{3+}. The rare-earth energy levels in crystals of $PrGaO_3$ [198] and $NdGaO_3$ [199] have been investigated by inelastic neutron scattering. These compounds are both orthorhombic, with space group *Pbnm* and $Pbn2_1$ respectively. The environment of the rare earth is considerably distorted with a low point symmetry: *m* in $PrGaO_3$ and C_2 in $NdGaO_3$. The ninefold degeneracy of the ground state Pr^{3+} J multiplet $^3H_4$ is entirely lifted by the crystal field, whereas the $^4I_{9/2}$ multiplet of Nd^{3+} is split into five Kramers doublets, as shown in figure 25. The ground state has mainly $|\pm\frac{1}{2}\rangle$ character, giving rise to *x*–*y*-type easy-plane anisotropy [200]. The reduced higher-order crystal field parameters A_n^0, $n = 4$, 6, are similar for aluminates and gallates of praseodymium and neodymium. There is no magnetic order down to about 1 K in these oxides; $NdGaO_3$, for example, orders magnetically at 0.97 K [200].

4.1.2.2. *B site.* The crystal field here has predominantly cubic character. Insofar as the delocalization of manganese electrons can be neglected, which is certainly the case for the end members, $x = 0$ and $x = 1$, the strong intra-atomic interactions mean that the energy of the Mn^{3+} or Mn^{4+} ions can be represented by a crystal-field energy level arising from the spectroscopic term. For Mn^{3+} in octahedral

coordination the ground state is ^5E_g, issuing from ^5D (figure 26). In purely cubic symmetry the ground state is a magnetic singlet [201]. For Mn^{4+} it is $^4A_{2g}$, issuing from ^4F. The transition from the ^5E_g ground state to the $^5T_{2g}$ excited state of Mn^{3+} in $RMnO_3$, which corresponds to promoting an electron from a t_{2g} to an e_g orbital, was found from optical spectra to be at about 2.1 eV for light rare earths and at 2.3 eV for heavy rare earths [202]. In $LaMnO_3$ films, two absorption bands appear, namely a strong band at 1.8 eV and a weaker band at 2.3 eV; the splitting has been attributed to the Jahn–Teller effect [92]. The d^4 ^5E_g ion in octahedral coordination $t_{2g}^3e_g^1$ is a strong Jahn–Teller ion because it lowers its energy in proportion to the splitting of the e_g levels by a uniaxial distortion. This was first discussed by Kanamori [24]. Comparison with spectra of Mn^{3+} in other distorted octahedral environments [203] leads to an estimate of $\Delta_{cf} = 10Dq \approx 1.5$ eV and $2\delta_{JT} \approx 1.0$ eV. The Jahn–Teller stabilization energy is therefore δ_{JT}, which was independently estimated from optical phonon frequencies [204] to be about 0.6 eV [174].

The one-electron energy levels are discussed further in the following section.

4.1.3. *Electronic structure*

The perovskite-structure oxides with a closed-shell ion on B sites are transparent insulators. Examples are $CaTiO_3$, $SrTiO_3$, $LaAlO_3$, $LaScO_3$ and $LaGaO_3$. The Ti^{4+} and Sc^{3+} cations have a d^0 configuration, whereas that of Ga^{3+} is d^{10}. In $LaAlO_3$ there is a gap of 5.6 eV between the top of the valence band which is derived from the filled oxygen 2p orbitals of O^{2-} and the bottom of the empty conduction bands which are derived from the unoccupied 5d–6s orbitals of the La^{3+} or 3s orbitals of the Al^{3+}. Empty d^0 levels usually lie near the top of this 2p–*n*s gap, whereas filled $3d^{10}$ levels lie below the top of the 2p band (see figure 68 later). The d levels fall at progressively lower energy on passing along the 3d series because of the increasing nuclear charge. $LaScO_3$ is a transparent insulator with a gap of about 6 eV between the oxygen 2p valence band and the bottom of the empty 3d conduction band [205]; the gap in $CaTiO_3$ or $SrTiO_3$ is less, about 3 eV.

For $3d^n$ cations, the Fermi level falls in the narrow d band, and very interesting physics arises because of the strong electron correlations in this band. The traditional approach has been to regard transition-metal oxides as ionic compounds with well defined 3d configurations incorporating an integral number of localized electrons per ion. This approach has been successful in accounting for many aspects of their behaviour, including magnetic moment formation. The model has considerable predictive power, and it is possible to relate the parameters in the model to spectroscopic measurements. However electron transfer and orbital admixtures are more properly treated in a band model. Band structure determinations involve extensive computations, and it is more difficult to build up an intuitive understanding of the relation between electron number and physical properties. Recent developments, particularly the local spin density approximation [206], offer access to magnetic ground-state properties via a workstation and provide insight into the extent of orbital mixing which is considerable in all transition-metal oxides. Most difficult to treat accurately are the interatomic correlations.

Transition-metal oxides are materials whose electronic properties are determined by an interplay of several interactions of comparable magnitude, all of order 1 eV. Schematically, these are as follows:

Table 5. Estimates of characteristic energies in $LaMnO_3$.

U_{dd}	4.0 eV	$J_H = U_{ex}/2$	1.0 eV
U_{pd}	4.5 eV	Δ_{cf}	1.8 eV
		δ_{JT}	0.6 eV
$W = 12t$	1.0 eV	$\lvert J_{ij}\rvert$	0.001 eV

(i) the Mott–Hubbard interaction U_{dd}, which is the cost of creating a $d^{n+1}d^{n-1}$ charge excitation in an array of d^n ions;
(ii) the charge-transfer interaction U_{pd}, which is the cost of transferring an oxygen p electron to the neighbouring d ion to create a p^5d^{n+1} charge excitation from p^6d^n;
(iii) the transfer integral t which determines the d-electron bandwidth W;
(iv) the Hund rule on-site exchange interaction U_{ex} which is the energy required to flip a d-electron spin;
(v) the crystal-field interactions Δ_{cf} and δ_{JT}.

Besides the classical Bloch–Wilson insulators where the Fermi level falls in a gap in the one-electron density of states, transition-metal oxides may be Mott–Hubbard or charge-transfer insulators when the electron correlations are such that $U_{dd} > W$ or $U_{pd} > W$ respectively [207, 208]. Most oxides of the early 3d transition metals are Mott–Hubbard insulators and many oxides of the late 3d transition metals are charge-transfer insulators. At the end of the 3d series, the charge transfer gap may go to zero, and the oxides then become metals. In the middle of the series where $U_{dd} \approx U_{dp}$ the nature of the gap is less clear cut. A summary of the magnitudes of these interactions in $LaMnO_3$ is given in table 5.

4.1.3.1. *Ionic model.* We consider further the electronic structure of manganese ions in B sites of the perovskite structure, where they are coordinated by an octahedron of oxygen neighbours, assuming for the moment that there is an integral number of d electrons per site. It is useful to focus here on the one-electron energy levels rather than on the multiple-electron states of section 4.1.2, although they are closely related for the d^4 ion Mn^{3+}. The interelectronic correlations which give rise to the Hund rules for the free ion are perturbed by the crystalline electrostatic field due to the oxygen anions. The five d orbitals, each of which can accommodate one electron of each spin, are split by the octahedral crystal field into a group of three t_{2g} ($\equiv d\epsilon$)–d_{xy}:d_{yz}:d_{zx} orbitals which have their lobes oriented between the oxygen neighbours and a group of two e_g ($\equiv d_\gamma$)–$d_{x^2-y^2}$, d_{z^2} orbitals which are directed towards the oxygen neighbours. The former obviously have a lower energy because of the electrostatic repulsion of electrons on neighbouring sites, and the crystal field splitting Δ_{cf} ($\equiv 10Dq$) between the t_{2g} and e_g orbitals is of the order 1.5 eV. The intra-atomic correlations which give rise to the Hund first rule (maximum S) is represented on a one-electron energy diagram by introducing an energy splitting U_{ex} of $\uparrow$ and $\downarrow$ orbitals, which is greater than Δ_{cf}. Good evidence that U_{ex} and Δ_{cf} are quite similar in magnitude in the perovskite-structure oxides is provided by the trivalent cobalt in $LaCoO_3$ which does not follow the Hund first rule; it is in a low-spin state, $3d^6$, t_{2g}^6 with $S = 0$. Trivalent nickel in nickel-substituted manganites is also of a low-spin nature [17]. Manganese ions

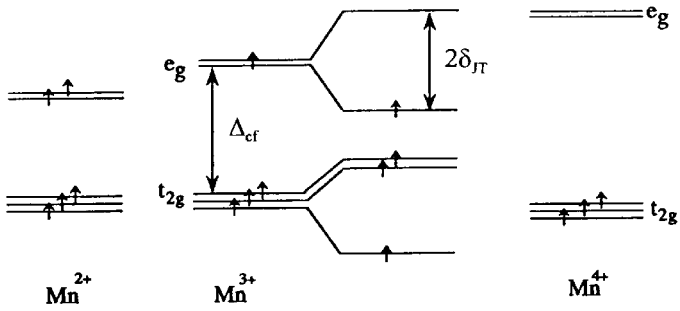

Figure 27. Occupancy of one-electron energy levels for Mn^{4+}, Mn^{3+} and Mn^{2+} in octahedral coordination. The effect of a tetragonal distortion is to lower the energy of Mn^{3+} by δ_{JT}, but it leaves the others unchanged.

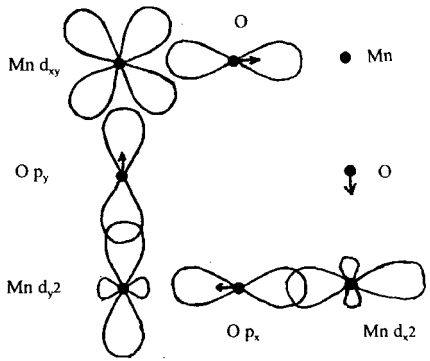

Figure 28. Illustration of the orbital overlap in a plane of the perovskite structure. The d_{xy} orbital (a t_{2g} orbital) has little overlap with the 2p orbitals of the oxygen neighbours, whereas the d_{x^2} and d_{y^2} orbitals (e_g orbitals) overlap strongly with the oxygen p_x or p_y orbitals to form a σ^* band. Displacements of the oxygen atoms in the plane are indicated by arrows.

generally have a high spin; the divalent ion Mn^{2+} has a very stable $3d^5$ configuration, a half-filled shell $t_{2g}^{3\uparrow}e_g^{2\uparrow}$ with $S=\frac{5}{2}$ and a spherically symmetric electron density. Trivalent manganese is $3d^4$, $t_{2g}^{3\uparrow}e_g^{\uparrow}$ with $S=2$, whereas quadrivalent manganese is $3d^3$, $t_{2g}^{3\uparrow}$ with $S=\frac{3}{2}$. The spin-only moments of these ions are $5\mu_B$, $4\mu_B$ and $3\mu_B$ respectively.

A distortion of the oxygen octahedron lowers the symmetry of the cubic crystal field in such a way that the centre of gravity of the t_{2g} levels and the centre of gravity of the e_g levels is unchanged. There is therefore nothing to be gained by Mn^{2+} or Mn^{4+} from such a distortion, but Mn^{3+} can lower its energy in proportion to the distortion, and the corresponding penalty in elastic energy will scale as the distortion squared, hence we have the marked tendency of d^4 ions to distort their octahedral environment in order to lower their energy. This is the Jahn–Teller effect. For example, the tetragonal elongation of the octahedron found in the O′-type structure will stabilize the d_{z^2} orbital relative to the $d_{x^2-y^2}$ orbital, as shown in figure 27.

The t_{2g} orbitals overlap relatively little with the orbitals of nearby oxygen or lanthanum ions (figure 28) so these electrons tend to form a localized $t_{2g}^{3\uparrow}$ ion core.

However the e_g orbitals overlap directly with the p orbitals of the oxygen neighbours, so they tend to form a σ^* antibonding band.

The end-member compounds such as $LaMnO_3$ have a distorted perovskite structure where the Fermi level falls in a gap between the two Jahn–Teller split e_g bands. However, intermediate compositions such as $(La_{1-x}Ca_x)MnO_3$ with a cubic structure have a partly-filled σ^* band, extending in three dimensions. These band electrons, which we refer to as the Zener electrons, hop from one manganese site to another with spin memory. They are both conduction electrons and mediators of the ferromagnetic exchange (see figure 65 later). Direct overlap of the t_{2g} core electrons of adjacent manganese ions leads to antiparallel exchange coupling, since only the $\downarrow$ orbitals are empty [169].

The energies involved in the ionic model can be deduced from spectroscopic measurements. The octahedral crystal field splitting Δ_{cf} decreases with increasing Mn–O distance. Typical values for Mn^{4+}, Mn^{3+} and Mn^{2+} in oxides are 2.5 eV, 1.8 eV and 1.0 eV respectively [203]. Estimates for manganese perovskites from soft X-ray spectroscopy are 2.4 eV for Mn^{4+} and 1.5 eV for Mn^{3+} [209]. Actually Mn^{3+} has a tendency to disproportionate into a mixture of Mn^{2+} and Mn^{4+}, for instance in aqueous solution, but the ion can be stabilized in octahedral sites by the Jahn–Teller distortion. The Jahn–Teller splitting of the e_g levels is in the range $2\delta_{JT} = 0.5$–1.5 eV in various Mn^{3+} minerals [203].

In $LaMnO_3$, attribution of the broad feature in the optical absorption spectrum near 2 eV to the $^5E_g \rightarrow {}^5T_{2g}$ transition of Mn^{3+} gives a value of Δ_{cf} which is consistent with other estimates; the absorption edge at 3.1 eV is ascribed to $2p \rightarrow 3d$ charge transfer [92]. This then places the t_{2g} levels above the top of the oxygen 2p band, in accord with molecular orbital calculations for the $(MnO_6)^{9-}$ cluster [210]. X-ray photoemission studies, optical conductivity and electron-energy-loss spectroscopy, however, place the t_{2g} levels below the top of the 2p band [211, 558].

The Hund rule exchange splitting U_{ex} between the states with total spin 2 and 1 is evaluated from equation (1.2) taking $s = \frac{1}{2}$ and $S = \frac{3}{2}$ as the spins of the e_g electrons and the t_{2g}^3 ion core. The result $U_{ex} = J_H(S + \frac{1}{2})$ gives $2J_H$ as the splitting. The value of U_{ex} is found from optical conductivity data to be 2.0 eV [204] which is slightly greater than Δ_{cf}, as expected. Hence $J_H = 1.0$ eV. A somewhat larger value was inferred from scanning tunnelling spectroscopy [212].

Values of U_{dd} and U_{pd} for $LaMnO_3$ obtained from electron spectroscopy are 4.0 eV and 5.0 eV respectively [75] and 3.5 eV and 4.5 eV, respectively [213]. Other estimates are $U_{dd} = 7.8$ eV and $U_{pd} = 4.5$ eV [168, 214] and $U_{dd} \approx U_{pd}$ [209]. $LaMnO_3$ has consequently been identified either as a charge-transfer insulator [168, 205, 211, 214], or as a Mott–Hubbard insulator [75, 213]. It is a borderline case†. Most likely, the holes in mixed-valence oxides such as $(La_{0.7}Ca_{0.3})MnO_3$ have mixed 2p–3d character [75, 168, 209, 213]. Saitoh *et al.* found that the ground state electronic configuration of $LaMnO_3$ consists of a mixture of about 50% of $3d^42p^6$, about 40% of $3d^52p^5$ and about 10% of $3d^62p^5$ where the ligand holes are spin polarized. Although we normally refer to Mn^{3+} and Mn^{4+} as d^4 and d^3 respectively, the likelihood that there are significant numbers of 2p holes has important consequences for the analysis of the exchange interactions and transport properties [27, 211].

† Or it may be neither; band calculations show a small gap at E_F due to Jahn–Teller splitting of the e_g band; so $LaMnO_3$ is actually a Bloch–Wilson insulator.

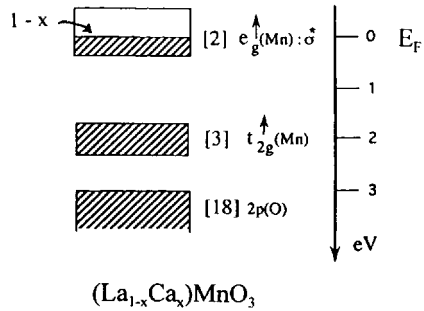

Figure 29. Schematic energy band structure of $(La_{1-x}Ca_x)MnO_3$.

Estimates of U_{dd} and U_{pd} for $CaMnO_3$ are 5.2 eV and 3.0 eV [213]. It might be a charge-transfer insulator, but band calculations (figure 31 later) show a gap of 0.4 eV at E_F.

The effective exchange parameters J_{ij} ($= J_1, J_2$) for neighbouring manganese ions in the Heisenberg Hamiltonian $-2J_{ij}\mathbf{S}_i \cdot \mathbf{S}_j$ are of order t^2/U, where t is the transfer integral which gives rise to the bandwidth W.

4.1.3.2. *Band model.* Unlike the ionic 4f levels, which are little broadened by overlap and hybridization, the 3d ionic levels acquire a substantial bandwidth, of order 1 eV, from overlap with the neighbouring orbitals. The bandwidth $W = 2Zt$, where t is the transfer integral and Z is the number of manganese nearest neighbours. This is indicated in the modified one-electron energy levels of figure 29. The e_g bandwidth W is sensitive to Mn–O distances and Mn–O–Mn bond angles [187]. In the double-exchange model it also depends on magnetic order, via equation (1.1). Band structure calculations take account of intra-atomic correlations in an averaged way and they reproduce the one-electron energy level splittings of the crystal-field theory by admixture of p and d electron orbitals. One method that has proven quite successful in reproducing the density of states, the ordered magnetic structures and even the magnetocrystalline anisotropy of 3d metals and alloys is the local spin density approximation (LSDA). Sarma *et al.* [206], Pickett and Singh [215, 216], Satpathy *et al.* [217, 218] and Solovyev *et al.* [219] have applied the LSDA method to $LaMnO_3$ and related oxides such as $LaBO_3$, where B = Fe, Co or Ni. Both the linear augmented plane wave [220, 221], and linear muffin-tin orbital-atomic sphere approximation give nearly identical results [206]. The unrestricted Hartree–Fock method has also been successfully applied to the perovskite oxides [222, 223] and there have been calculations using the Korringa–Kohn–Rostoker method [224].

Before discussing the electronic structure of materials which exhibit large negative magnetoresistance, it is appropriate to consider first the end members. With this method, it is possible to take different crystallographic unit cells (orthorhombic or cubic) and different magnetic arrangements (ferromagnetic, antiferromagnetic or paramagnetic) in order to calculate the free energy associated with each of them and thereby to evaluate which is the ground state. For each case, an electronic density of states is obtained and the character of the wavefunctions (s, p, d) can be evaluated. The different calculations agree very well on the main features. Sarma *et al.* [206] were able to predict the most stable magnetic arrangements for the four oxides that they studied, namely $LaCoO_3$, $LaFeO_3$,

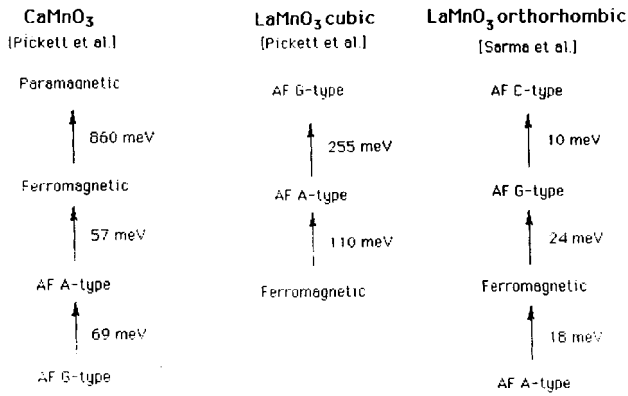

Figure 30. Energy differences between the possible magnetic states of the end members.

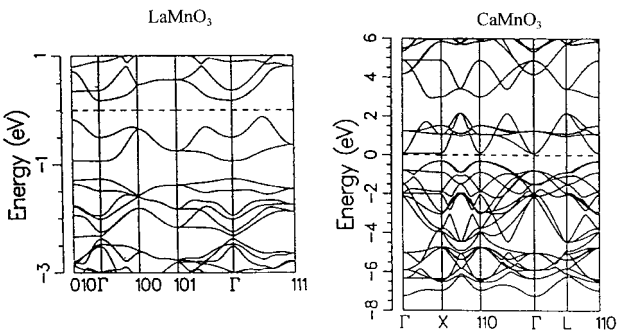

Figure 31. Energy bands for $LaMnO_3$ (A-type antiferromagnet; *Pnma*) and $CaMnO_3$ (G-type antiferromagnet) calculated by Pickett and Singh [216]. In each case there is a small gap at E_F, which is indirect for $LaMnO_3$. [Reprinted by kind permission of the American Physical Society from page 1146 of *Physical Review* B, Volume 53, 1996, and the authors, W. E. Pickett and D. J. Singh, © 1996 by the American Physical Society.]

$LaNiO_3$ and $LaMnO_3$. The importance of the crystal structure is demonstrated by the result that, without the Jahn–Teller distortion (i.e. for a cubic cell), $LaMnO_3$ would be a ferromagnetic metal rather than an A-type antiferromagnetic insulator [206, 215–217, 219]. The same conclusion had been drawn from susceptibility measurements above 750 K by Jonker [9]. The Jahn–Teller effect responsible for the O′ orthorhombic distortion also leads to the stabilization of the A type antiferromagnetism (figure 30). The splitting of the e_g bands, due to the Jahn–Teller distortion, leads to a small indirect gap of order 0.1 eV between the e_{g1} ($\approx d_{z^2}$) and e_{g2} ($\approx d_{x^2-y^2}$) bands, each about 1 eV wide.

The other end member, $CaMnO_3$, is cubic with the G-type antiferromagnetic structure, as observed experimentally (figure 30) without any splitting of the e_g bands. The exchange splitting $U_{ex} = 3.0$ eV and a 0.42 eV gap opens between the $t_{2g}^{\uparrow}$ and a band of mixed $t_{2g}^{\downarrow}$ and $e_g^{\uparrow}$ character [216]. Calculated energy bands near E_F for $LaMnO_3$ and $CaMnO_3$ are shown in figure 31.

For both end-member compounds, Satpathy *et al.* found that the ionic descriptions $La^{3+}Mn^{3+}O_3^{2-}$ and $Ca^{2+}Mn^{4+}O_3^{2-}$ are good approximations to reality.

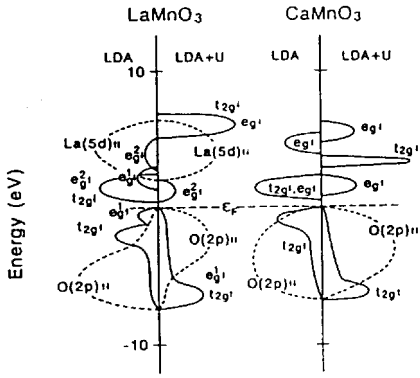

Figure 32. Band structure for the end members in the LSDA and LSDA+ U calculations. [Reprinted by kind permission of the American Physical Society from page 960 of *Physical Review Letters*, Volume 76, 1996, [217] and the authors, S. Satpathy, Z. S. Popovic and F. R. Vukajlovic, © 1996 by the American Physical Society.]

In order to account for the difficulty where two electrons occupy the same manganese ion, a strong on-site Coulomb interaction U_{dd} can be introduced into the LSDA calculation [217, 225]. The valence band is originally composed of the Mn 3d and O 2p bands with the Mn 3d band centre above the O 2p band centre. The effect of the large Hubbard U is to swap those two as depicted in figure 32. In this case, the density of states near the Fermi level would become mainly of O 2p character.

The calculated magnetic moments for $LaMnO_3$ are in quite good agreement with the experimental values of $(3.7–3.9)\mu_B$. [170, 226].

For their Hartree–Fock calculations, Mizokawa and Fujimori [222, 223] take realistic values $U_{dd} = 5.5$ eV and $U_{pd} = 4.0$ eV from photoemission spectroscopy and show how the antiferromagnetic order in $LaMnO_3$ is related to orbital order and the Jahn–Teller distortion.

For mixed La–Ca compositions, for example, or in a real end member which does not have perfect stoichiometry, there is not an integral number of d electrons per atom and the bands are not completely filled. (This is also true of an unsubstituted compound which does not have the ideal stoichiometry.) One may therefore expect the compounds to become metallic in the absence of a distortion which creates distinct Mn^{3+} and Mn^{4+} sites. Pickett and Singh [215, 216] modelled the $x = 0.33$ system by an ordered triple cell of general formula $La_2CaMn_3O_9$ incorporating layers of cations (La–Ca–La). The compound is found to be ferromagnetic with an average moment of $3.51\mu_B$ per formula unit. Two distinct manganese sites appear in such a cell where some manganese atoms have an A-site cation environment with lanthanum neighbours only (Mn_{La-La}) and the others have one plane of lanthanum and one plane of calcium surrounding them (Mn_{La-Ca}). The moments for the two manganese sites are very close and the system should be viewed more in terms of hybridized spin-polarized Mn 3d–O 2p bands rather than strong mixed valence. It was also found that a metastable ferrimagnetic configuration exists consisting of Mn_{La-La} aligned antiparallel to the Mn_{La-Ca} sites which have an energy only 70 meV higher than that of the purely ferromagnetic ground state. This emphasizes the importance of local environment effects on the magnetic order connected with the relative number of 2+ or 3+ A-site cations

surrounding the Mn. Also, in both ferromagnetic and ferrimagnetic configurations, the local densities of states are quite distinct for the two manganese sites. Near E_F, Mn_{La-Ca} bands constitute a nearly 'half metallic' pair (i.e. the d states are fully spin polarized) whereas Mn_{La-La} bands have an equal number of spin-up and spin-down states. The minority spin occupation is therefore determined by shifts in potential arising from nearby cation charges (La^{3+} neighbours create a more favourable environment for an electron). The precise electronic structure is then expected to depend sensitively on local environment effects such as the cation disorder, deviations from stoichiometry and local strain. Pickett and Singh [216] also suggested that charge disorder could lead to localization of *minority* states (in fact Mn_{La-La} states) which would generate purely half metallic conduction when the majority carriers are not localized. Above T_C, the absence of a net moment forces charge carriers to go through differently oriented regions which, owing to minority state localization, would induce very poor conductivity (thermally activated behaviour).

These calculations, and others [227], suggest that *disorder* plays a crucial role in the electronic state of the manganites. This feature had already been emphasized by the group from Bariloche [228] and they later studied the problem in more detail [229]. In order to account for the possibility of non-equivalence of the sites in $(La_{1-x}Sr_x)MnO_3$, a random diagonal (on-site) energy was introduced. Their Hamiltonian is composed of four terms: a ferromagnetic coupling energy J_H, between localized and itinerant electrons the on-site Coulomb repulsion U, the hopping parameter t and the random on-site energy E_i. In their first paper, only two different sites were considered corresponding to Mn^{3+} and Mn^{4+}. The main consequence of that choice was a possible splitting of the bands in the paramagnetic state if the diagonal energies are taken to be very different. The gap that could be opened above T_C is reduced in the ferromagnetic state. The effect could be so large as to close the gap and turn the system metallic with a fully polarized band at E_F. The possibility of Anderson localization was analysed in the second paper. The first important result concerns the case where no diagonal distribution is considered ($E_i = E$). Depending on the ratio J_H/t, the density of states can be split into two bands with weights and widths proportional to the number of states of each spin, that is the magnetization M. When M increases, the gap decreases and the material becomes more conducting. With the introduction of a Lorentzian distribution of diagonal energies, Anderson localization occurs and a mobility edge appears. The important result here is that, although its exact position depends on the criterion chosen for its definition, the mobility edge shifts with magnetization M (figure 33) and can be swept through the Fermi level. Allub and Alascio [230] also predicted that the Curie temperature is reduced when the disorder increases, through the width of the Lorentzian distribution, and they drew phase diagrams which correspond well with experiment.

The above band structure calculations emphasize the importance of disorder in differentiating the manganese sites. This can lead to Anderson localization with a determinant role of the magnetization [231, 232], discussed in section 4.3.4. In the partly ferromagnetic state, the homogeneous compounds have mixed electronic spin character at the Fermi level. However, the interesting idea of preferential localization of carriers in the minority spin subband provides support for the full spin polarization of mobile charge carriers: half-metallic ferromagnetism.

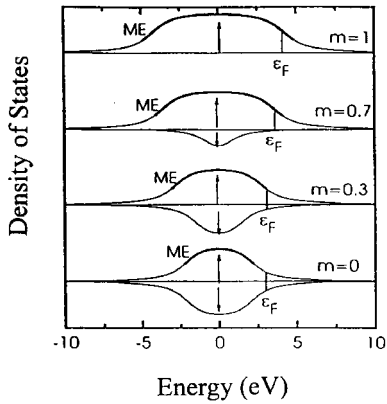

Figure 33. Positions of the Fermi level and mobility edge (ME) as functions of the reduced magnetization. [Reprinted from *Solid State Communications*, Volume 99, page 613, by R. Allub and B. Alascio [229], © 1996, with permission from Elsevier Science.]

Experimentally, there is good evidence of electron localization by potential fluctuations. $(LaMn)_{1-\delta}O_3$ compounds with $\delta = 0.01$ and 0.05 are both insulators, although they exhibit a large linear term in the heat capacity which suggests a high density of states. The Fermi level therefore lies below the mobility edge [233]. It is also apparent from the conductivity of cation-deficient and doped $LaMnO_3$ that B site vacancies are more effective than A-site vacancies or A-site cation disorder at localizing the electronic states.

4.2. *Magnetic properties*

4.2.1. *Magnetic structures*

Two characteristic distortions of the perovskite structure influence the magnetic order of the manganites. The first is a consequence of the small size relative to oxygen of the A-site cations (tolerance factor $t' < 1$) and consists of a cooperative tilting of MnO_6 octahedra. The second is connected to the Jahn–Teller distortion of octahedra which contain a Mn^{3+} at their centre and their cooperative ordering. The critical temperatures at which these two distortions set in are different. The former produces a double tilting of the octahedra (buckling) below about 1250 K which may extend over the entire range of concentrations, leading to the orthorhombic O-type structure with a relatively small lattice deformation (figure 21). At lower temperatures (dependent on the amount of Mn^{3+}), cooperative Jahn–Teller ordering may take place. The other determining feature for magnetic structure is the composition and distribution of Mn^{3+} and Mn^{4+} ions in the lattice.

4.2.1.1. *$LaMnO_3$*. The stoichiometric $LaMnO_3$ end member contains only Mn^{3+} magnetic ions which arrange themselves in the A_y-type planar antiferromagnetic structure (figure 3) with a Néel temperature $T_N = 140$ K. The arrangement in the *a–b* plane is ferromagnetic (spins in plane with the moments parallel to the orthorhombic *b* axis in the *Pbnm* space group (*a* axis in *Pnma*)) but successive planes are coupled antiferromagnetically [20, 226]. The moment in the A_y mode is $3.87\mu_B$; in-plane and intraplane exchange parameters have been determined by inelastic neutron scattering [170] (section 4.2.3). There may be a weak moment

along the c axis [154, 568, 569], attributed in the stoichiometric compound to the Dzyaloshinsky [234]–Moriya [235] interaction. Precise measurements on untwinned single crystals at 20 K have shown that there is a moment of 0.18 μ_B/Mn along the c axis but no moment was measured along the a or b axes. A narrow peak in the susceptibility at T_N is characteristic of a canted antiferromagnet [569].

Cation-deficient lanthanum manganites $(LaMn)_{1-\delta}O_3$ are antiferromagnetic, orthorhombic and insulating when $\delta < 0.03$, but compounds with $\delta > 0.03$ are ferromagnetic with a spin-only moment of up to $3.8\mu_B$ per manganese atom [156, 184, 236]. A sample with $\delta = 0.4$ has a canted spin structure with the moments at 45° to the rhombohedral (001) axis [176]. The $\delta \leqslant 0.04$ compounds remain insulating to low temperatures but the $\delta \geqslant 0.05$ compounds exhibit a metal–insulator transition at T_C. A tentative δ–T phase diagram has been proposed by Töpfer and Goodenough [175]. When the cation deficiency is on only one sublattice, the oxide tends to order ferromagnetically [237].

Lanthanum can be replaced by a magnetic rare earth ion such as praseodymium or neodymium. The pure end members $RMnO_3$ can be classified in two groups: those where the rare earth has an ionic radius larger than holmium which crystallize in the orthorhombic *Pbnm* space group and the others which are hexagonal and belong to the $P6_3cm$ group with six molecules per cell. Although the manganese ions order antiferromagnetically with Néel temperatures ranging from 30 K to 91 K, the rare-earth sublattice was not found to order above 1.5 K [238]. The Néel temperature of $PrMnO_3$, for example, is 91 K and the magnetic order is of the A_y type.

4.2.1.2. $(La_{1-x}Ca_x)MnO_3$. Magnetic structures in the mixed-valence manganites were first determined from neutron diffraction measurements carried out by Wollan and Koehler [20] in 1955 on the $(La_{1-x}Ca_x)MnO_3$ system. The sequence of magnetic phases shown in figures 4 and 23 was deduced from a study of neutron peak intensities where both ferromagnetic and antiferromagnetic moments were obtained as functions of manganese mixed valency. As first established from magnetization measurements [7], the compounds are ferromagnetic around $x = 0.3$ where moments are close to the expected spin-only value. The sublattice moments for the pure antiferromagnetic phases at $x = 0$ and $x = 1$ are also close to the spin-only values. The different magnetic ordering found as the proportion of Mn^{3+} to Mn^{4+} is varied depends primarily on the charge ordering in the perovskite lattice. A simple set of rules can be inferred by comparing the magnetic and charge order; exchange coupling is ferromagnetic between Mn^{3+} and Mn^{4+} ions, antiferromagnetic between two Mn^{4+} ions, and ferromagnetic or antiferromagnetic between two Mn^{3+} ions. The ferromagnetic bond between the ions in different valence states is also the shortest.

At low Mn^{4+} contents ($x \gtrsim 0$ in $(La_{1-x}Ca_x)MnO_3$), a ferromagnetic component B_z along the c axis appears in the neutron diffraction patterns which grows for increasing x up to $x = 0.3$ where the samples are entirely ferromagnetic [20, 226]. The coexistence of A_y and B_z modes is consistent with spin canting or microscale phase segregation. The variation in the ^{55}Mn hyperfine frequencies in an applied field favours the latter interpretation [239]. The existence of narrow magnetic Bragg peaks associated with the B_z mode indicates some underlying long-range ferromagnetic order in the $0 < x < 0.3$ compounds [226] but weak magnetic satellites around the Bragg peaks in a crystal with $x = 0.08$ have been attributed to correlated ferromagnetic density fluctuations on the scale of 1.7 nm with an average separation

of 3.5 nm [570]. Curie temperatures in this concentration range reach 250 K with a saturation magnetization slightly less than the expected spin only value of $3.7\mu_B$ per manganese atom. The cubic structure obtained in this region reflects the absence of charge ordering. At Mn^{4+} concentrations above 0.35, a different mixture of ferromagnetism and antiferromagnetism is found. The new antiferromagnetic phase consists of a regular stacking of the C and E types, called the CE type by Wollan and Koehler. It is the result of charge ordering near a Mn^{4+} to Mn^{3+} ratio of unity ($x = 0.5$; figure 6). On heating the $x = 0.5$ compound, the antiferromagnetic order turns ferromagnetic at $T_N = 170$ K before becoming paramagnetic at $T_C = 225$ K [240]. The antiferromagnetic → ferromagnetic transition is accompanied by a change from commensurate to incommensurate charge order [194]. As x increases, the CE structure progressively transforms itself to the C-type structure corresponding to another charge ordering obtained for a Mn^{4+} to Mn^{3+} ratio of 3 ($x = 0.75$). The magnetic configuration is then one of ferromagnetic chains ordered antiferromagnetically. Both C and CE structures present tetragonal distortions from the ideal cubic phase with $c < a$ (the ferromagnetic bond again being shorter than the antiferromagnetic bond). As the proportion of Mn^{4+} increases further, they replace Mn^{3+} ions at random creating more antiferromagnetic bonds in the structure. The end member $CaMnO_3$ indeed contains only Mn^{4+} and is fully antiferromagnetic, with the nearest-neighbour G-type antiferromagnetic structure. The crystallographic cell for the latter is almost cubic since Mn^{4+} ($3d^3$), unlike Mn^{3+} ($3d^4$), does not tend to deform its octahedral environment.

4.2.1.3. $(Pr_{1-x}Ca_x)MnO_3$. Extensive neutron measurements have also been carried out on the $(Pr_{1-x}A_x)MnO_3$ systems (A = Ca, Ba, Sr, Na or K) by a Czech group [5, 192, 241–243]. The full range of solid solutions exists only for A = Ca but when A = Sr or Ba, solid solubility extends to $x = 0.5$ or $x = 0.4$ respectively [242]. Their work on the $(Pr_{1-x}Ca_x)MnO_3$ system extended the early study of Wollan and Koehler on the $(La_{1-x}Ca_x)MnO_3$ system to higher temperatures which allowed them to examine the charge ordering transitions. Salient features of crystallographic and magnetic structures are presented on figure 34.

The low-temperature phases in $(Pr_{1-x}Ca_x)MnO_3$ can be divided into four compositional regions, depending on the ordering of the Mn^{3+} ions and their d_{z^2} orbitals.

(1) *Orthorhombic O′ type for* $0 < x < 0.3$ where the cooperative Jahn–Teller effect sets in below a first-order transition temperature of 945 K for the end member which decreases rapidly when x increases (fewer Mn^{3+} ions). Above this transition temperature, electron hopping dominates the crystallographic properties. The hopping frequency of electrons at high temperature may exceed the vibrational frequency of the Jahn–Teller distortion so that the local deformations do not have time to establish themselves, which accounts for the quasicubic symmetry. A similar O–O′ phase boundary is found for other $(R_{1-x}A_x)MnO_3$ systems [17]. It is known both from susceptibility measurements [9] and electronic structure calculations [206, 215, 219] that, if cubic $LaMnO_3$ existed at low temperatures, it would be ferromagnetic. It is interesting to note that a pure cooperative Jahn–Teller distortion would lead to a tetragonal cell. The orthorhombic O′-type structure is obtained because of the ever-present influence of buckling, which leads

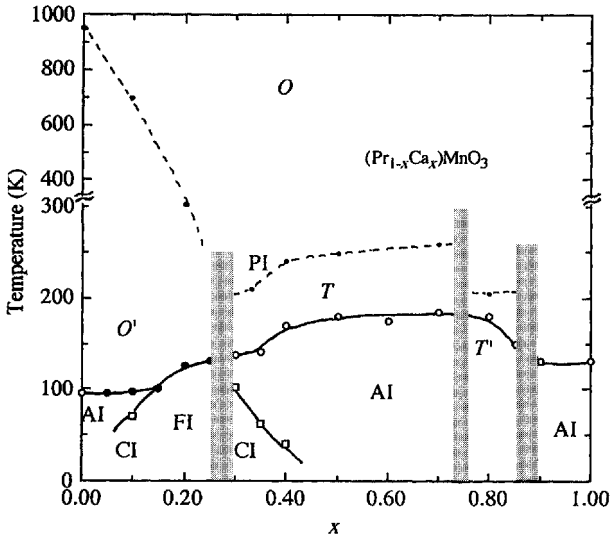

Figure 34. Crystallographic and magnetic order in the $(Pr_{1-x}Ca_x)MnO_3$ system [5, 89, 192]: (○), T_N; (●), T_C; (•), T_{CO}; (×), T_s; (□), T_1. The letters have the same meaning as in figure 23. Grey denotes a two-phase region. [Reprinted from the *Journal of Magnetism and Magnetic Materials*, Volume 53, page 153, by Z. Jirak, S. Krupicka, Z. Simsa, M. Dlouha and S. Vratislav [192], © 1985, with permission from Elsevier Science.]

to different Mn–Mn distances in plane and along the *c* axis, allowing the establishment of A-type planar antiferromagnetic order. In-plane charge ordering of the CE type appears in the orthorhombic phase at $x \approx 0.3$ [192].

(2) *Pseudotetragonal compressed type T for* $0.3 < x < 0.75$. This is imposed by the CE-type charge order. The transition temperatures are around room temperature (250 K for the $x = 0.5$ phase).

(3) *Pseudotetragonal elongated type T′ for* $0.75 < x < 0.9$. The charge ordering below T = 200 K for the $x = 0.75$ prototype proposed by the Czech group is different from that suggested by Wollan and Koehler. A base-centred orthorhombic structure of the crystallographic type *Amm2* is better able to fit the neutron diffraction pattern [192] (figure 35).

(4) *Pseudocubic O type for* $0.9 < x < 1$. This arises where the preponderance of Mn^{4+} ions imposes a nearly cubic lattice.

The magnetic order associated with the four compositional regions in the $(Pr_{1-x}Ca_x)MnO_3$ system exhibits characteristic features which confirm theoretical expectations regarding the magnetic structures [22, 25]. These are summarized below.

(*a*) $0 < x < 0.2$. Antiferromagnetism of type A for the end member occurs where moments in the (010) direction gradually cant as holes are added (x increasing). For $x = 0.1$, at 4.2 K, the moments are along the (110) directions. Above a transition temperature of 70 K, the compound becomes ferromagnetic with its easy axis along the (010) direction. This transition, predicted by deGennes, was observed for the first time in this system. The

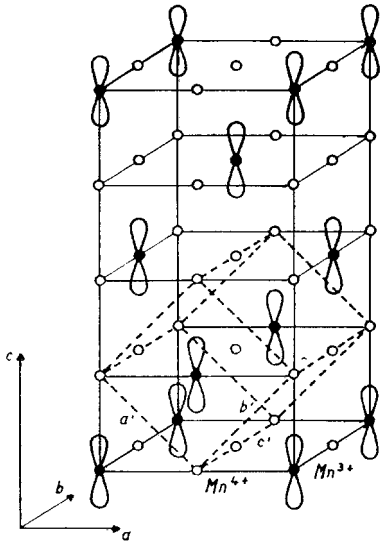

Figure 35. Base-centred orthorhombic *Amm2* type for the 1:3 charge ordering ($x = 0.75$). [Reprinted from the *Journal of Magnetism and Magnetic Materials*, Volume 53, page 153, by Z. Jirak, S. Krupicka, Z. Simsa, M. Dlouha and S. Vratislav [192], © 1985, with permission from Elsevier Science.]

magnetic ordering temperature is reached at 100 K. Another interesting result in the $x = 0.1$ sample is that praseodymium ions order below 30–40 K contributing by $0.5\mu_B$ per praseodymium ion to the ferromagnetic component of the moment of the manganese ions. This is in contrast with the result for the end-member where no order of the praseodymium was detected down to 1.5 K [238].

(*b*) $0.2 < x < 0.3$. This is the region of ferromagnetism. The manganese moment reaches $3.75\mu_B$, which is close to the expected spin-only value. The magnetic easy axis is along the (010) direction.

(*c*) $0.3 < x < 0.75$. The charge ordering throughout this range is most fully developed in the $x = 0.5$ compound which is antiferromagnetic of type CE with moments along the (010) direction. Adding holes or electrons in this structure initially has the same effect. It produces a canting between antiferromagnetic layers. On one side, this canting leads over to the ferromagnetic region near $x = 0.3$ where the CE structure is still present in (001) planes with a ferromagnetic component along the 001 direction.There is a transition between antiferromagnetic and canted states when $0.3 < x < 0.4$ [193, 244]. On the other side, the canting leads to the antiferromagnetic C structure for $x = 0.75$. An interesting feature of the $(Pr_{0.3}Ca_{0.7})MnO_3$ compound is the presence of satellite lines in the neutron diffraction pattern which indicates a non-commensurate spiral structure along the (010) axis with period 3.5 nm. It was suggested that the long range interaction causing it to appear is antiferromagnetic superexchange along in-plane diagonals (Mn–O–Mn–O–Mn) which couples manganese neighbours in fourth order [192]. This resembles the situation found in other perovskites such as $SrFeO_3$ [245].

(*d*) $0.75 < x < 1$. This is the two-phase region where the C type coexists with the G-type nearest-neighbour antiferromagnetism of the $x = 1$ end member. Canting is not favoured in G-type structures, where electrons are localized [22].

Even though the magnetic properties of the $(La_{1-x}Ca_x)MnO_3$ and $(Pr_{1-x}Ca_x)MnO_3$ systems are similar, there is an important difference in electronic structure that must be emphasized. A ferromagnetic phase is obtained for $x = 0.3$ in $(La_{1-x}Ca_x)MnO_3$ and for x closer to 0.2 for $(Pr_{1-x}Ca_x)MnO_3$ but the latter does not have the high conductivity associated with ferromagnetism in a cubic or rhombohedral phase. The fact that the transport properties are so different in the two systems (there is no maximum in $R(T)$ curves for $(Pr_{1-x}Ca_x)MnO_3$ for $x \approx 0.2$) reflects the importance of the tolerance factor t' and related structural details such as Mn–O–Mn bond angle for the double-exchange mechanism.

4.2.1.4. *Other systems.* Magnetic structures in other mixed-valence manganites resemble those in either the La–Ca or the Pr–Ca systems. Most of the other results are available for ferromagnets with $x \approx 0.3$ or charge-ordered antiferromagnets with $x \approx 0.5$ [246]. There are more extensive neutron diffraction data on $(La_{1-x}Sr_x)MnO_3$ [189, 191, 247, 248] including compounds with $x \approx 0.125$ [248, 249] and $x = 0.2$ [247] which have a mixed AB-type or canted antiferromagnetic structure. Canted structures are also reported in $(Pr_{1-x}Ba_x)MnO_3$ [250].

$(Gd_{0.67}Ca_{0.33})MnO_3$ has a ferrimagnetic structure with antiparallel gadolinium and manganese sublattices, and a compensation point at 15 K [250].

In some partially substituted compounds, spin-glass-type magnetic structures with random canting can be obtained when ferromagnetic and antiferromagnetic interactions are competing randomly. For example, the Zaragossa group [252, 253] have looked in detail at the $([La_{1-y}Tb_y]_{0.67}Ca_{0.33})MnO_3$ series. The compounds are ferromagnetic metals when $y < 0.25$. When $y > 0.3$, the ground state is an insulator and the magnetic order is of the spin-glass type with $T_f \approx 50$ K. The spin glass seems to be due to the small size of terbium, which influences the balance of ferromagnetic and antiferromagnetic Mn–Mn interactions. There are field-cooling effects in the susceptibility and antiferromagnetic peaks are absent in the neutron diffraction pattern. The critical Mn–O–Mn bond angle separating the ferromagnetic and spin glass states is 157°. A spin glass can also be obtained in compounds with B-site substitutions. Replacing 20% of the manganese in $(La_{0.67}Ca_{0.33})MnO_3$ by copper destroys the ferromagnetic metallic state, leading to a thermally activated conduction with spin-glass order [254, 255], demonstrating again how delocalization is closely related to ferromagnetism. A sufficient amount of aluminium [256, 257] or gallium substitution may be expected to have a similar effect. Iron substitution reduces the magnetization of ferromagnetic compositions drastically, as it introduces strong disordered antiferromagnetic superexchange interactions and again promotes electron localization [258].

A substitution of about 20 at.% Bi for calcium in the other antiferromagnetic end member $CaMnO_3$ also leads to ferromagnetic order, with a large negative magnetoresistance effects around T_C [259, 260]. The system is antiferromagnetic at lower bismuth concentrations [261].

4.2.2. *Curie temperature, magnetization and susceptibility*

4.2.2.1. *Curie temperature*. Various studies have addressed the problem of the variation in Curie temperature in these compounds when changing the 2+ and 3+ cations [185, 262]. Exchange interactions depend on interionic distances and bond angles. Havinga [262] first showed how the strength of the exchange interaction between two Mn^{3+} in octahedral sites varies with the Mn–O–Mn bond angle θ. He deduced the angle from the lattice parameter, assuming a model of stiff octahedra and a fixed Mn–O bond length [262, 263]. The sequence cubic $\rightarrow$ rhombohedral $\rightarrow$ orthorhombic is one of decreasing bond angle, and the net magnetic interaction becomes negative ($\theta_p < 0$) for $\theta < 150$. Bokov *et al.* [264] were the first to investigate the effect of cell distortions on the magnetic properties of the manganites using ternary systems. Those were compounds in which the trivalent cation was partially substituted by a smaller 3+ cation, as in $(Bi_{1-x}La_x)_{0.5}Ca_{0.5}MnO_3$, or in which the divalent cation was substituted, as in $Bi_{0.5}(Ca_{1-x}Ba_x)_{0.5}MnO_3$. The induced distortion sensitively modified the crystallographic and magnetic transition temperatures. Later Hwang *et al.* [185] studied more quantitatively, by neutron scattering, the importance of the Mn–O–Mn bond angle on the magnetic and transport properties of the manganites. Ternary compounds with compositions such as $(La_{0.7-x}Pr_xCa_{0.3})MnO_3$ and $(La_{0.7-x}Y_xCa_{0.3})MnO_3$ allowed a change of tolerance factor and bond angle at constant electron concentration (assuming no change in oxygen stoichiometry). A clear decrease in T_C when the Mn–O–Mn angle decreases from the ideal 180° was measured in these systems and others [188, 265, 266]. The strength of the double exchange (and therefore T_C) depends sensitively upon the orbital overlap between manganese and oxygen. Also, the magnetization of samples with reduced Mn–O–Mn angles is more difficult to saturate. This may be ascribed to the competition between double exchange and superexchange interactions which can lead to canting of the manganese moments. However, the bond angle is only one of the factors influencing the Curie temperature. The range of Mn–O–Mn angles studied has been quite limited ($156.5° < \theta < 168.5°$) and generalization of the correlation of T_C with angle over a large series of cation substitutions is questionable.

With a given alkali cation, there is a clear tendency for T_C to increase with increasing atomic radius (decreasing atomic weight) of the rare earth (figure 36) [267], which is related to the e_g bandwidth [187]. Similarly there is a tendency for T_C to increase with increasing tolerance factor or mean size of the A-site cations and then to saturate [164, 185, 265, 268, 269], (figure 37). This is probably a reflection of increasing Mn–O–Mn bond angle. However, there is no clear trend associating T_C with the atomic weight, size or electronegativity of the alkali ion (figure 36).

For low-T_C samples, typically when $T_C < 100$ K, the magnetic and resistive transitions are found to be hysteretic [113, 185, 267, 269]. This behaviour may be linked with magnetic degrees of freedom associated with noncollinear ferromagnetic order.

Curie temperatures are reduced by nonmagnetic trivalent B-site substitutions such as aluminium, gallium or indium [257, 271], and by iron.

Amorphous $(La_{1-x}Sr_x)MnO_3$, prepared by melt quenching with B_2O_3, is found to have $T_C > 380$ K over a wide range of x [549].

4.2.2.2. *Magnetization*. The low-temperature ferromagnetic moment for the $(La_{1-x}Ca_x)MnO_3$ system was plotted in figure 4. Even at $x = 0.3$, the moment does

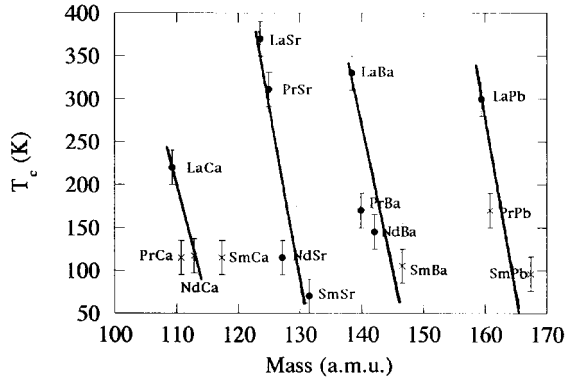

Figure 36. Curie temperature T_C of $(R_{0.7}A_{0.3})MnO_3$ compounds plotted as a function of the average A-site atomic weight [267]. [Reprinted by kind permission of the American Physical Society from page 5763 of *Journal of Applied Physics*, Volume 81, 1997, and the authors, R. M. Thomas, L. Ranno and J. M. D. Coey, © 1997 by the American Physical Society.]

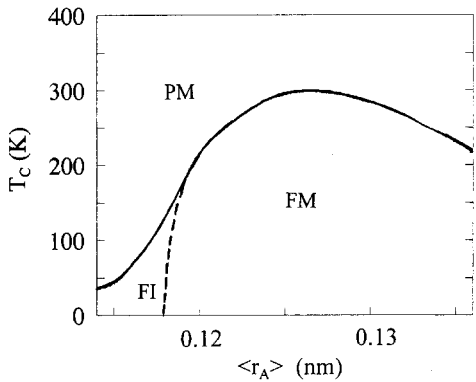

Figure 37. Variation on the Curie temperature T_C of $(R_{0.7}A_{0.3})Mn\}O_3$ compounds as a function of the average A-site atomic radius. The ferromagnetic metal (FM), ferromagnetic insulator (FI) and paramagnetic metal (PM) regions are shown [164, 185, 268]. [Reprinted from page 204 of the *Journal of Solid-state Chemistry*, Volume 120, 1996, [268] by kind permission of the authors and Academic Press.]

not quite reach the spin-only value of $(4-x)\mu_B$ per formula unit. This is due to spin canting in the ferromagnetic state, which was first evidenced by Wollan and Koehler [20]. The magnetization of compounds which are ferromagnetic, but with a spontaneous magnetization considerably less than the spin-only moment, exhibit characteristic differences in field-cooled and zero-field-cooled magnetization, and a coercivity which increases rapidly at low temperatures [272]. Furthermore, there is a high-field slope on the magnetization curve [273] which is far greater than could be explained by Pauli paramagnetism, admitting there are spin-down states at the Fermi level. These effects are typical of magnetic systems with multiple near-degenerate spin configurations (spin-glass behaviour). They can be modelled in terms of magnetically inhomogeneous spin clusters [272]. The moment is also reduced in nonstoichiometric, cation-deficient compositions with

$x \approx 0.3$ [274]. Spin canting around $x = 0.3$ appears to be absent in the $(La_{1-x}Sr_x)MnO_3$ compounds, which behave as good ferromagnets.

The temperature dependence of the sublattice magnetization of $LaMnO_3$ crystals has been followed by neutron diffraction, and the critical exponent β in the expression $M \propto (1 - T/T_C)^{\beta}$ was evaluated as 0.25 [275] or 0.28 [170]. In ferromagnetic $(La_{0.7}Sr_{0.3})MnO_3$ ($T_C = 378.1$ K) the exponent was reported as 0.295 [189] or 0.37 [593]. A value, $\beta = 0.345$, was found for $(La_{0.67}Ca_{0.33})MnO_3$ powder by muon spin relaxation below the critical region [276]. In some other manganites there is evidence for a sharper decline of $M(T)$ near T_C [14], or even a first-order transition [277]. Scaling analyses of the critical behaviour based on magnetization measurements have been reported for $(La_{0.8}Sr_{0.2})MnO_3$ [566] and $(La_{0.7}Sr_{0.3})MnO_3$ [593]. At low temperatures, the magnetization follows a Bloch $T^{3/2}$ law [278].

Ferromagnetic domains have been observed in films of $(La_{0.65}Ca_{0.35})MnO_3$ by magnetic force microscopy. The domains are typically a few microns in size in a film 0.3 μm thick [279]. There is evidence for a reduced moment in thin films (< 50 nm) especially those deposited on MgO [599].

4.2.2.3. *Susceptibility.* Analysis of the Curie–Weiss susceptibility of different manganite compositions has provided information on the strength of the superexchange and double exchange interactions [9, 280]. The susceptibility and magnetization of films of $((La,Y)_{0.67}Ca_{0.33})MnO_3$ and $La_{1-z}MnO_3$ have been interpreted in terms of clusters of the order of ten manganese ions [281]. There is also some evidence for the formation of clusters at a temperature $T_C' > T_C$ in $((La_{0.6}Nd_{0.4})_{0.7}Ca_{0.3})MnO_3$ [276] and in cation-deficient $(La_{0.8}Ca_{0.2})_{1-\delta}MnO_3$ [272]. Magnetization curves in the vicinity of T_C have been fitted to a Langevin function, but a major difficulty with any such analysis is that the applied field increases the local magnetic order and therefore enhances the exchange and increases the size of the magnetic clusters. In $(Sm_{0.65}Sr_{0.35})MnO_3$, there is a field-induced transition in the paramagnetic state from a small-cluster phase (~5Mn) to one with larger clusters [590]. An enhanced Curie–Weiss susceptibility measured in low field in a region of temperature just above T_C might be expected if the carriers are magnetic polarons, but it does not seem to have been systematically observed. In some materials, the susceptibility is enhanced far above T_C [282, 283], but other crystals and films with $x \approx 0.3$ exhibit a good spin-only Curie–Weiss susceptibility right down to T_C. The magnetic polaron, which will have a magnetic moment considerably greater than that of the free ion, might then have a lifetime shorter than the spin–lattice relaxation time. However, more susceptibility measurements on well-characterized material, as well as heat capacity measurements on the same samples in the region of T_C would be useful.

At rf frequencies, the absorption and penetration depth are very sensitive to applied field due to the effect of field on the permeability [550].

4.2.3. *Magnetic resonance and magnetic excitations*

4.2.3.1. *Nuclear magnetic resonance.* A direct probe of charge fluctuations is provided by nuclear magnetic resonance (NMR) measurements on manganese. The ^{55}Mn nucleus with $I = \frac{5}{2}$ and $\mu = 3.468\mu_N$ is 100% abundant. The hyperfine fields for manganese in octahedral coordination in oxides are different for Mn^{4+} and Mn^{3+}. For Mn^{4+} ($3d^3$) the field is isotropic since no orbital moment is associated

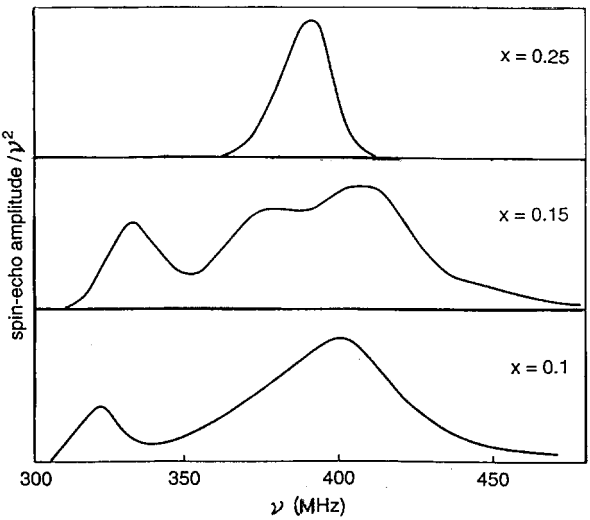

Figure 38. Spin echo ^{55}Mn spectra for $(La_{1-x}Sr_x)MnO_3$ crystals [87] $x = 0.25$ is metallic, $x = 0.15$ and 0.10 are semiconducting. [Reproduced from the *Journal of Physics in Condensed Matter*, Volume 7, page 7020, © 1995, by kind permission of the authors and IOP Publishing Limited.].

with the t_{2g}^3 configuration, and the value is typically 31 T, whereas for Mn^{3+} ($3d^4$) the field is anisotropic on account of the extra e_g electron, and the value is approximately 40 T. The corresponding resonance frequencies are 330 MHz and about 420 MHz respectively.

When charge fluctuations on the manganese are rapid, as in a metal, a single 'motionally narrowed' resonance line appears at a frequency which is a weighted average of those corresponding to the individual electronic configurations. The motional narrowing arises when the charge fluctuations are faster than the resonance frequency of the manganese nucleus, in other words when their lifetime is significantly less than 2.5 ns. On the other hand, when the charge fluctuations are slow or static, then distinct Mn^{3+} and Mn^{4+} resonances appear.

NMR studies have been reported for $(La_{1-x}Pb_x)MnO_3$ [284], $(La_{1-x}Ca_x)MnO_3$ [239, 285, 597] and other ceramics [286, 287] and for $(La_{1-x}Sr_x)MnO_3$ single crystals [87, 288], including oxygen-deficient samples annealed at a very low oxygen pressure [142]. A single narrow ^{55}Mn resonance line is observed at low temperatures in the cubic metallic state at a frequency intermediate between those expected for the Mn^{3+} and Mn^{4+} resonances (figure 38). However, the two ions show distinct resonances in the semiconducting state of compounds with different doping levels. The $Mn^{4+}(t_{2g}^3)$ gives a sharp resonance at about 320 MHz, but the $Mn^{3+}(t_{2g}^3 e_g)$ resonance is broader, possibly because of the anisotropic dipole field created by the e_g electron. Intermediate concentrations, $x \approx 0.2$ where the charge fluctuations are taking place on a nanosecond timescale show more complex spectra. The NMR data therefore provide solid support for the idea of a dynamic Jahn–Teller effect in this concentration range.

There is evidence from NMR that magnetic hyperfine splitting persists on a microsecond time scale above T_C. This is not normally seen in ferromagnets, and it may be taken as evidence for magnetic polarons [287]. Mössbauer spectra on ^{57}Fe-

doped materials in an applied field above T_C have also been interpreted in terms of local ferromagnetic clusters [282, 289].

An independent measurement of the average hyperfine field in $(La_{1-x}Sr_x)MnO_3$ ceramics ($0 \leqslant x \leqslant 0.3$) from low-temperature heat capacity measurements is 36–39 T [290].

Measurements on nuclei of the nonmagnetic A-site ions ^{139}La and ^{81}Y show transferred hyperfine fields in the ferromagnetic state due to the spin-polarized conduction electrons [287, 291, 597].

4.2.3.2. *Ferromagnetic and paramagnetic resonance.* Ferromagnetic resonance (FMR) studies have been conducted on single-crystal spheres of the $(La_{1-x}Pb_x)MnO_3$ series with $0.25 < x < 0.45$ [11, 292], as well as polycrystalline $(La_{0.7}Ca_{0.3})MnO_3$ [293], $(La_{0.67}Ba_{0.33})MnO_3$ [294, 295], $(Nd_{0.7}Sr_{0.3})MnO_3$ [296] and cubic $LaMnO_3$ [296]. Data have also been published on films of $(La_{0.60}Y_{0.07}Ca_{0.33})MnO_3$ [294, 296] and $(La_{0.8}Sr_{0.2})MnO_3$ sandwiched between $YBa_2Cu_3O_7$ layers [296]. These compositions are ferromagnetic and conducting.

In most of these materials, the ferromagnetic linewidth shows an unusual temperature dependence, with a minimum near T_C of a few tens of milliteslas, rising to about 0.2 T at low temperatures. At first this was attributed to intrinsic magnetic inhomogeneity [11], but the effect was subsequently shown to be related to sample size. Small crystals [292], fine dispersed powders [293] and thin films [295, 298] all exhibit narrower lines than large crystals or bulk ceramic samples. The resonance line for thin films is narrow (less than 5 mT) and independent of temperature. These effects appear to be related to the conductivity of the material, and its temperature dependence. The larger samples exhibit an asymmetric line shape with a ferromagnetic antiresonance at low fields [292, 293]. This type of line shape is predicted by the phenomenological Landau–Lifshitz theory [299] when the skin depth is comparable with the sample size. If the main resonance occurs at a field B_r with a particular microwave frequency ω, where $\omega = \gamma B_r$, then the antiresonance in the absence of damping occurs at a field B_a where $(\omega/\gamma)^2 = B_a(\mu_0 M_s + B_r)$. However, a quantitative discrepancy has been found between the peak resistivity measured on bulk samples, and a value at least 20 times smaller inferred from FMR data [293]. The resistivity at microwave frequencies is found to show a negative magnetoresistance effect, analogous to the dc resistivity [296].

From the ferromagnetic resonance frequency, it is possible to deduce the spontaneous magnetization M_s and the anisotropy field H_K. The resonance field is independent of temperature [291, 293] and magnetic anisotropy was found to be negligibly small [293, 294], except in the case of substrate-induced strain [300].

Electron paramagnetic resonance (EPR) has been studied above T_C in a variety of manganite compounds [11, 283, 301–303]. The intensity of the EPR line in the ferromagnetic compositions decreases exponentially with increasing temperature; 20 K above the Curie temperature the signal may be explained by collective precession of clusters of about 30 spins [283]. The temperature dependence of the linewidth is attributed to a one-phonon relaxation process [302, 303].

4.2.3.3. *Spin waves and magnetic excitations.* Spin-wave excitations have been detected by inelastic neutron scattering from single-crystal $LaMnO_3$ [170, 275, 580], $(Nd_{0.5}Pb_{0.5})MnO_3$ [81], $(La_{0.7}Pb_{0.3})MnO_3$ [304] and $(La_{0.7}Sr_{0.3})MnO_3$ [189, 580] and single-crystal and polycrystalline $(La_{1-x}Ca_x)MnO_3$ [305, 306]. The dispersion

relation in antiferromagnetic $LaMnO_3$ was fitted by Moussa *et al.* [170] and Hirota *et al.* [275] with two exchange constants: a ferromagnetic intraplane coupling $J_1 = 9.6\,K$ and an antiferromagnetic interplane coupling $J_2 = -6.8\,K$. Note that the weighted average of the nearest-neighbour interactions is ferromagnetic, 4.1 K. There is an anisotropy gap at the antiferromagnetic wavevector. In $(La_{1-x}Sr_x)MnO_3$ with $0 \leqslant x \leqslant 0.17$, the magnitude of J_2 decreases with increasing x, and the spin wave gap tends to zero as the compound becomes ferromagnetic [580]. On doping with 5 at.% Ca, the compound becomes a canted antiferromagnet with weakened antiferromagnetic coupling, $J_2 = -4.0\,K$ [170]. Local, bound excitations appear, as well as a new, isotropic low-energy branch $E = Dq^2 + \Delta_{sw}$ with $D = 4.6$ MeV Å^2 and $\Delta_{sw} = 11.1\,K$, which cannot be explained in the Heisenberg model. It may be associated with magnetic polarons having a short ferromagnetic correlation length, of about 1 nm.

In the ferromagnetic region, the calcium compound with $x = 0.33$ behaves as an ideal isotropic ferromagnet with $J = 21.8\,K$, showing a gapless dispersion relation $E = Dq^2$ with $D = 170$ meV Å^2 at low temperatures [306]. The strontium crystal with $x = 0.3$ has $J = 24.1\,K$ and $D = 188$ meV Å^2 at 27 K, falling to 114 meV Å^2 at room temperature; the spin-wave stiffness is renormalized with increasing temperature, but it does not go to zero at T_C [189]. The entire dispersion relation for the $(La_{0.7}Pb_{0.3})MnO_3$ crystal could be fitted assuming a single ferromagnetic nearest-neighbour interaction, with $J = 24.1\,K$ and a spin wave gap $\Delta_{sw} = 28\,K$ [304]. The Hund rule coupling J_H has been deduced to be about $12t$ by analysing spin-wave data using the double exchange model [307].

Independent values of D have been derived from the coefficient of the $T^{3/2}$ terms in the low-temperature specific heat or spontaneous magnetization of $(La_{0.7}Sr_{0.3})MnO_3$, and from standing wave resonance on thin films. The value from heat capacity is 130 meV Å^3 [290], but there is no sign of a ferromagnetic spin-wave gap in either the heat capacity or FMR data. The FMR values of D are 160 ± 30 meV A^2 for $(La_{0.67}Ba_{0.33})MnO_3$ at $T \approx 0$ and 90 ± 20 meV Å^2 for $(La_{0.7}Sr_{0.3})MnO_3$ at room temperature [308]. The Bloch $T^{3/2}$ law in the magnetization gives 154 ± 5 meV A^2 [278]. The stiffness is renormalized as a function of temperature, following the normal $T^{5/2}$ law [298].

In the vicinity of T_C a large quasi-elastic central peak appears, which is typical of itinerant ferromagnets. The width is proportional to q^2, and it completely dominates the spectral weight in $(La_{0.67}Ca_{0.33})MnO_3$ as T approaches T_C. Lynn *et al.* [306] attributed this to electron diffusion on the manganese sublattice. The large-q spin waves exhibit broad linewidths due to magnon–electron scattering. From the relative weights of the inelastic (spin wave) and quasi-elastic (spin diffusion) excitations near T_C, it appears that the latter drive the magnetic phase transition in the calcium compound. In their material, the magnetic transition was not a continuous second-order transformation, but there appeared to be a two-phase region below T_C. The quasi-elastic scattering is suppressed by an applied field and it is correlated with the region of greatest magnetoresistance. It extends far above T_C [306]. The diffuse quasi-elastic scattering was also observed by Martin *et al.* [189] and Clausen et al [81], who associated it with magnetic polarons. Lattice polarons were not observed.

4.2.4. *Pressure and magnetovolume effects*

The classical magnetovolume effects are spontaneous and forced (field-induced) volume magnetostriction and linear magnetostriction. Volume magnetostriction is

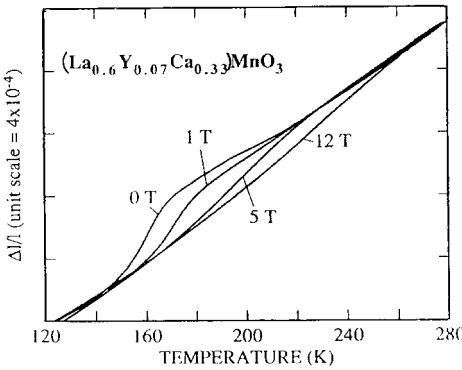

Figure 39. Temperature dependence of the volume magnetostriction of $(La_{0.60}Y_{0.07}Ca_{0.33})$-$MnO_3$ showing anomalous expansion above T_C which can be eliminated by applying a large magnetic field [77]. [Reprinted by kind permission of the American Physical Society from page 3541 of *Physical Review Letters*, Volume 75, 1995, and the authors, M. Ibarra, P. Algarabel, C. Marquina, J. Blasco and J. Garcia, © 1995 by the American Physical Society.]

usually an isotropic effect, unrelated to the direction of magnetization, which has its origin in the volume dependence of the magnetic free energy due to distance-dependent exchange interactions or magnetic moments. The effect is usually manifest around and below the Curie point where the volume strain ω can attain values as high as 1% in certain compounds. When the volume magnetostriction is negative (i.e. the volume increases in the ferromagnetically ordered state), Invar behaviour may be observed if the normal thermal expansion is just cancelled by the temperature-dependent magnetically induced strain over some range of temperature. By contrast, the linear magnetostriction λ is a strain in the direction of magnetization which is accompanied by a strain $-\lambda/2$ of opposite sign in the perpendicular direction. It is a very small effect, responsible for transformer hum; the saturation value λ_s is typically numbered in parts per million.

The volume magnetostriction of $(La_{0.60}Y_{0.07}Ca_{0.33})MnO_3$, measured by Ibarra *et al.* [77] and illustrated in figure 39, is rather unusual. A 0.1% dilation of magnetic origin appears in the semiconducting state, starting well above T_C (150 K), and the effect can be suppressed by applying a magnetic field. Similar effects are observed in $(La_{0.67}Ca_{0.33})MnO_3$ [309] and in compounds with terbium in place of yttrium [79]. A field greater than 10 T, large enough to induce metallic conduction above T_C [98] also serves to eliminate the magnetovolume anomaly [310].

A corollary of the anomalous volume expansion is the effect of pressure on T_C which has been studied for $(La_{0.60}Y_{0.07}Ca_{0.33})MnO_3$ [78] as well as $(La_{1-x}Ca_x)MnO_3$, [311–313], $(Pr_{0.7}Ca_{0.3})MnO_3$ [243, 313] and $(La_{0.75}Sr_{0.25})MnO_3$ in the early work of Patrick [314]. More recently, single crystals of $(La_{1-x}Sr_x)MnO_3$ with $0.15 < x < 0.50$ [86], $(Nd_{0.5}Sr_{0.36}Pb_{0.14})MnO_3$ [315] and $(Nd_{0.62}Pb_{0.30})MnO_3$ [316] have also been invstigated. In every case except oxygen-deficient samples with low T_C, the ferromagnetic state is stabilized by the application of pressure, with $dT_C/dP \approx 10\text{-}30\ K/GPa^{-1}$.

It is remarkable that the effect on T_C of pressure and chemical pressure (achieved by substituting smaller A-site cations) are opposite [267, 313]. However, it can be understood qualitatively since pressure increases the Mn–Mn overlap integral t_0 and

bandwidth W, thereby enhancing T_C ; smaller A-site cations tend to reduce the Mn–O–Mn bond angles, hence diminishing the transfer integral t (equation (1.1)).

The effects of pressure and chemical pressure on the charge ordering which occurs in $(Nd_{1-x}Sr_x)MnO_3$ near $x = 0.5$ and $(Pr_{1-x}Ca_x)MnO_3$ for $0.3 < x < 0.7$ have been thoroughly investigated by Moritomo *et al.* [317]. Pressure suppresses charge order and induces the ferromagnetic metallic state.

4.2.5. *Magnetic-field-induced phase transitions*

Interesting effects of applying a magnetic field are observed in mixed-valence manganites whose composition lies close to an antiferromagnetic–ferromagnetic phase boundary. Referring to the schematic phase diagram given later in figure 51, this may arise when $x \approx 0.15$ or when $x \approx 0.5$, and both cases have been described in the literature. Field-induced transitions may also occur from a canted to a collinear ferromagnetic state, for example $AB \rightarrow B$ (figure 3). These field-induced transitions arise when the ferromagnetic state of magnetization M_1 lies at a very slightly higher in energy than the non-ferromagnetic state of magnetization M_2 so that the former can be stabilized by the energy associated with the magnetic field $-\mu_0 H(M_1 - M_2)$. The transitions are generally first order, exhibiting large hysteresis and they are frequently accompanied by the destruction of a charge-ordered state [318]. The ferromagnetic, charge-disordered state is usually metallic, so remarkable magnetoresistance effects are observed.

In the $(La_{1-x}Sr_x)MnO_3$ system at the low-doping end, the O′–R orthorhombic–rhombohedral phase boundary crosses room temperature at a composition close to that where the magnetic order changes from canted antiferromagnetic to ferromagnetic [249]. The canted antiferromagnetic phase is non-metallic [319] (figure 24). For $x = 0.175$, the structural transition is 285 K, and the magnetic ordering temperature of the O′ phase is 264 K. Asamitsu et al [85, 320] showed that it is then possible to induce the $O' \rightarrow R$ structural phase transition by applying a magnetic field of several teslas. This behaviour was modelled with a Landau expression for the free energy including coupled order parameters M (magnetization) and Q (lattice distortion).

Tomioka and co-workers have described the magnetic field [88, 195, 321] and pressure [321] response of systems with $x \approx 0.5$ which first order ferromagnetically at T_C and then undergo a first-order transition at a lower temperature T_{co} to a charge-ordered antiferromagnetic phase [242]. These temperatures are 265 K and 140 K respectively for $(Pr_{0.5}Sr_{0.5})MnO_3$ [88, 114] and 255 K and 158 K respectively for $(Nd_{0.5}Sr_{0.5})MnO_3$ [195]. Both phases have the O′-orthorhombic structure, but the orthorhombic distortion is greater in the charge-ordered state. Some data as a function of temperature are shown in figure 40. The large hysteresis in temperature or field at the first-order transition in $(Nd_{0.5}Sr_{0.5})MnO_3$ is illustrated in figure 41. The antiferromagnetic ground state vanishes in $(Nd_{1-y}Sm_y)_{0.5}Sr_{0.5}MnO_3$ when $y > 0.8$, but it may be restored by pressure [320]. In $(Pr_{1-y}Y_y)_{0.5}Sr_{0.5}MnO_3$ the ferromagnetic state is suppressed by yttrium substitution but favoured by an applied field [322]. The effects of divalent, trivalent and quadrivalent substitutions for manganese have been investigated [270, 323].

The $(Pr_{1-x}Ca_x)MnO_3$ system differs from $(Pr_{1-x}Sr_x)MnO_3$ insofar as it normally remains semiconducting, with no value of x leading to a colinear ferromagnetic metallic phase in zero field. The strong tendency to charge ordering, extending to $x \approx 0.3$, impedes the formation of a metallic state. Charge ordering and antiferromagnetism occur here at different temperatures for compounds with $0.3 < x < 0.9$

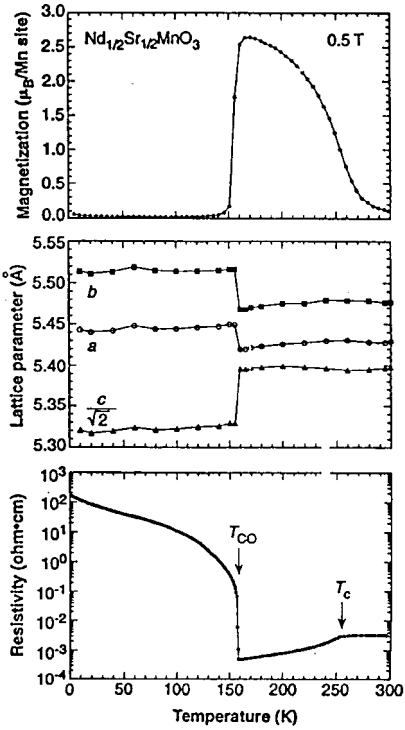

Figure 40. Temperature dependence of the magnetization, lattice parameters and resistivity of $(Nd_{0.5}Sr_{0.5})MnO_3$ [195]. T_C and T_{co} are the ferromagnetic and charge ordering transitions respectively. [Reprinted with permission from page 961 of *Science*, Volume 270, authored by H. Kuwahara, Y. Tomioka, A. Asamitsu, Y. Moritomo and Y. Tokura, © 1995 by the American Association for the Advancement of Science.]

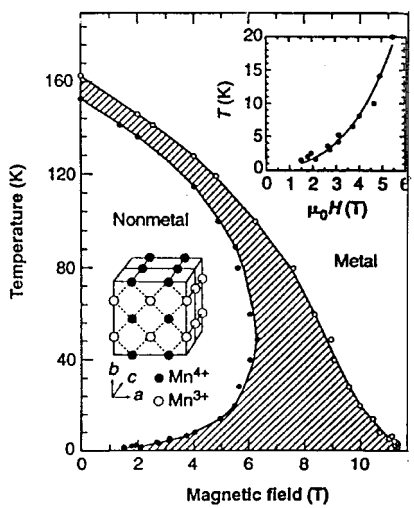

Figure 41. Phase diagram for $(Nd_{0.5}Sr_{0.5})MnO_3$ showing the extent of hysteresis at the first order phase transition [195]. [Reprinted with permission from page 961 of *Science*, Volume 270, authored by H. Kuwahara, Y. Tomioka, A. Asamitsu, Y. Moritomo and Y. Tokura, © 1995 by the American Association for the Advancement of Science.]

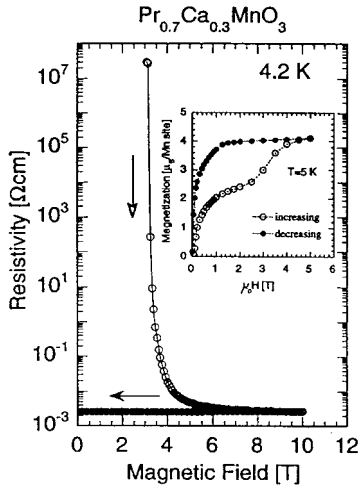

Figure 42. Magnetization curve and resistivity of $(Pr_{0.7}Ca_{0.3})MnO_3$ at 4.2 K [325]. [Reprinted by kind permission of the American Physical Society from page R13 145 of *Physical Review* B, Volume 52, 1995, and the authors, H. Yoshizawa, H. Kawano, Y. Tomioka and Y. Tokura, © 1995 by the American Physical Society.]

(figure 34). Charge localization persists above T_{co} [324], which is in the range 200–250 K, whereas T_N is 130–175 K [90, 325, 326]. When $x \approx 0.3$, there is a transition to a canted antiferromagnetic state with a moment of $1.9\mu_B$ per manganese atom at a lower temperature, $T_{ca} \approx 100$ K. Application of a magnetic field of 4–6 T to $(Pr_{0.7}Ca_{0.3})MnO_3$ at 4.2 K transforms the insulating canted antiferromagnetic state into a metastable ferromagnetic metal, with a change in resistivity of *ten orders of magnitude* (figure 42) [325–327]. Remarkably, it is possible to engender the same transformation by irradiation with X-rays [328] or ultraviolet light [329] (persistent photoconductivity), or by the application of a high voltage [330]. $(Sm_{1-x}Sr_x)MnO_3$ films with $x \approx 0.5$ are similar to $(Pr_{1-x}Ca_x)MnO_3$. There is an antiferromagnetic charge-ordered ground state which can be 'melted' by applying a magnetic field of about 6 T [96].

Canted → collinear transitions with huge hysteresis are also observed for $(La_{0.5}Ca_{0.5})MnO_3$ at 4.2 K [93], for $(Nd_{0.5}Ca_{0.5})MnO_3$ [331] and for $(La_{0.33}Nd_{0.33}Ca_{0.33})MnO_3$ [332]. Most of these magnetic first order transitions lead to very impressive magnetoresistive effects which are presented in section 4.3.

The complex behaviour of the manganites with $x \approx 0.5$ has been summarized by Damay *et al.* [333] in a phase diagram based on average A-site cation size, shown in figure 43. The effect of a magnetic field on the phase transitions is shown by the dotted curve. There is increasing evidence for nanoscale phase segregation in these compunds [596, 597].

4.2.6. *Models*

Goodenough [25] was the first to attempt a comprehensive explanation of the properties of the mixed-valence manganites. He discussed the phase diagram of $(La_{1-x}Ca_x)MnO_3$ in chemical terms, considering the hybridization of manganese orbitals: dsp^2 for Mn^{3+} which forms square coplanar bonds, and d^2sp^3 for Mn^{4+} which forms octahedral bonds to six near neighbours. These ions can form bonds of

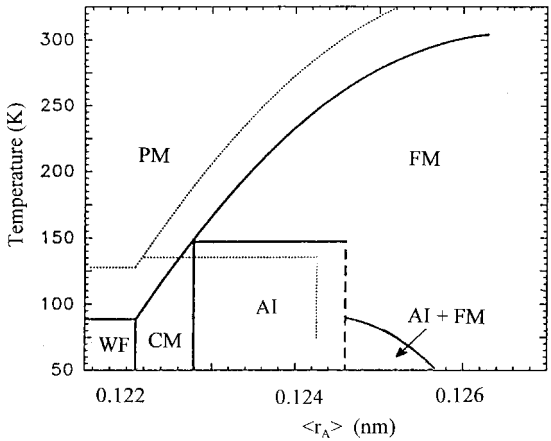

Figure 43. Magnetic phase diagram of $R_{0.5}Sr_{0.5}MnO_3$ compounds as a function of the average A-site cation radius. Of the five regions, three (paramagnetic (PM), charge-ordered antiferromagnet (AI) and weak ferromagnet (WF)) are insulating and two (ferromagnet (FM) and canted anitferromagnet (CM) are metallic [333]. [Reprinted by kind permission of the American Physical Society from page 1372 of *Journal of Applied Physics*, Volume 81, 1997, and the authors, F. Damay, A. Maignan, C. Martin and B. Raveau, © 1997 by the American Physical Society.]

different nature with the surrounding oxygens through which magnetic coupling is mediated.

(1) *Covalent bonds* are formed when one empty manganese orbital points towards an O^{2-} ion. This is a strong short bond which leads to antiferromagnetic superexchange between two manganese atoms forming covalent bonds with a common oxygen atom. Each electron of the bond has the same spin as its corresponding manganese because of the Hund rule coupling. The spins of the two electrons of the oxygen atoms have to be antiparallel because they belong to the same 2p orbital. The resulting coupling between Mn^{4+} ions (or Mn^{3+} in certain cases) is therefore antiferromagnetic.

(2) *Semicovalence* arises when only one out of the two manganese atoms surrounding an O^{2-} has a hybridized orbital available pointing towards the oxygen. In that case, full covalence is not possible since only one side of the O^{2-} orbitals can share an electron with the neighbouring manganese ion. The other bond is ionic, and the oxygen ion is displaced towards the first manganese, with which it forms the covalent bond. One electron is then localized on the oxygen ion to which it confers a magnetic moment that is antiparallel to the spin of the covalent electron (the two electrons sharing the oxygen orbitals have to be antiparallel). Because of the Hund rule, the manganese ion participating in the bond has its moment parallel to the electron shared with the oxygen. On this side of the ionic bond, there is a direct (therefore antiferromagnetic) exchange interaction between the magnetic moment of the anion and that of the neighbouring manganese. The resulting configuration is a ferromagnetic arrangement of the manganese ions with an antiparallel oxygen between them.

(3) *Ionic bonds* are obtained when the empty Mn^{3+} (dsp^2) orbitals point away from the O^{2-} ion. This is a long bond appearing only between two Mn^{3+}. There is no indirect exchange in that case.

(4) *Double exchange* is the last bonding possibility, involving the simultaneous transfer of an electron from the Mn^{3+} to the oxygen and from the O^{2-} to the neighbouring Mn^{4+}. Such hopping is greatest if the spins of the two d shells are parallel, hence the lowest energy of the system at low temperature is obtained for a ferromagnetic arrangement of the two manganese ions. In that case, the configurations Mn^{3+}–O–Mn^{4+} and Mn^{4+}–O–Mn^{3+} are degenerate.

These interactions can account for the observations regarding Mn–Mn coupling [7, 20]: antiferromagnetic between two Mn^{4+} (covalent), ferromagnetic between a Mn^{3+} and a Mn^{4+} (double exchange) and antiferromagnetic (covalent) or ferromagnetic (semicovalent) between Mn^{3+}. With these rules, Goodenough rationalized the crystallographic and magnetic arrangements, associated with the different possible charge orderings. Typical charge-ordered arrangements are obtained for special ratios of Mn^{3+} to Mn^{4+} ions.

(*a*) Pure $CaMnO_3$ (100% Mn^{4+}) contains only Mn^{4+} ions which couple antiferromagnetically. The order is then nearest-neighbour antiferromagnetism (G type) with no lattice distortion.

(*b*) For 75% Mn^{4+}, the arrangement is one of planes of Mn^{4+} alternating with planes containing equal proportions of Mn^{3+} and Mn^{4+}. In these planes, the ordering is purely antiferromagnetic but along chains running in the *c* direction, the coupling is on average ferromagnetic (some Mn^{4+}–Mn^{4+} bonds being mismatched). This is C-type order, where ferromagnetic chains are coupled antiferromagnetically.

(*c*) The 50% Mn^{4+} case is more complex since three possible ordered bond arrangements are electrostatically equivalent. The minimum elastic energy, however, corresponds to a CE-type ordering of semicovalent bonds.

(*d*) At 30% Mn^{4+}, the magnetic order is ferromagnetic with a moment almost equal to the spin only value. This is due to the double exchange between Mn^{3+} and Mn^{4+}. Goodenough explained why the best ferromagnetic phase is not reached at 50% Mn^{4+}. The double-exchange interaction is optimized for a disordered composition which has the largest number of Mn^{3+} ions with one and only one Mn^{4+} near neighbour. The corresponding Mn^{4+} content is 31% . It is interesting to note that, for an ordered lattice, the optimum value would be 25% [25].

(*e*) Pure $LaMnO_3$ (0% Mn^{4+}) is an A-type antiferromagnet where all the bonds in the *c* direction are covalent ($J_2 < 0$), while the in-plane orbital arrangement maximizes the number of ferromagnetic semicovalent bonds ($J_1 > 0$). The magnetic structure is that of ferromagnetic planes coupled antiferromagnetically with the *c* axis shorter than *a* or *b* (the covalent bond is short). Goodenough predicted that the semicovalent bonds would order below a certain temperature to form the O' structure, reducing the elastic energy associated with the different Mn–Mn separations. This semicovalent-bond ordering (orbital ordering) is a cooperative phenomenon that occurs well above the Curie temperature.

Transitions between these different magnetic phases are continuous. They are realized either by inhomogeneous mixing in a two-phase region or by a homogeneous progressive magnetic transition involving canting, as in the low x region. A short summary of the interplay between spin, charge and orbital degrees of freedom in magnetic oxides with reference to the theoretical literature has been written by Khomskii and Sawatzky [32].

Finally, it is worth emphasizing that double exchange is not indispensable for ferromagnetism in manganites, as shown by the example of $(La_{1-x}Ba_x)$-$(Mn_{1-x}Ti_x)MnO_3$ which is ferromagnetic and yet contains no Mn^{4+} [226], or the net ferromagnetic exchange interaction in $LaMnO_3$ (section 4.2.3). Exchange constants have been estimated for the insulating end members by Millis [334], using standard superexchange arguments.

4.2.6.1. *Magnetic properties of the low-doping region:* $0 < x < 0.3$. At low doping levels where some holes are introduced into the Mn^{3+} lattice, deGennes [22] considered a Hamiltonian which takes into account the exchange energy and the kinetic energy of the electronic system, leading to competition between the double exchange and the antiferromagnetic superexchange which may stabilize A_yB_z-type canted antiferromagnetic order. Introducing a possible canting angle θ_0 at zero temperature, between adjacent ferromagnetic planes as a free parameter, deGennes was able to find stable canted configurations. This is because the double exchange energy varies as $\cos(\theta_0/2)$ while the superexchange depends on $\cos\theta_0$. Minimizing the total energy, that is the sum of double exchange and superexchange contributions, deGennes found that θ_0 could be expressed as function of x:

$$\cos\left(\frac{\theta_0}{2}\right) = \frac{bx}{(4|J|S^2)} \tag{4.2}$$

where J is the inter-layer coupling (antiferromagnetic superexchange) and b the out-of-plane overlap integral (double-exchange interaction). Therefore, if $x < 4|J|S^2/b$, canting will exist. For this region of the magnetic phase diagram, the magnetizations of successive planes are inclined at a fixed angle to each other. This leads to three possible degenerate configurations (figure 44). The first corresponds to the angle θ_0 taken in a random direction between plane magnetizations, the second to a situation where every second plane magnetization is parallel, and the third to a helical arrangement. From considerations of terms not included in the original Hamiltonian (anisotropy energies and coupling between next nearest layers), deGennes was able to identify the second of these configurations as being the most stable. The system is therefore canted with θ_0 proportional to the doping x. Predictions of the model are as follows.

(1) The spontaneous magnetization is proportional to the doping x.
(2) The susceptibility is non-zero at high fields.
(3) The magnetic state is canted, consistent with the neutron diffraction data, where the system changes smoothly from antiferromagnetic (type A_y) for the end member to ferromagnetic (type B_z) near concentrations of 30% Mn^{4+}.

deGennes also considered the magnetism at *finite temperatures* and treated the influence of thermal effects on the double exchange carriers in the framework of the molecular field theory. The exact calculation was carried out in the homogeneous case of free Zener carriers. A statistical distribution of molecular field was taken for

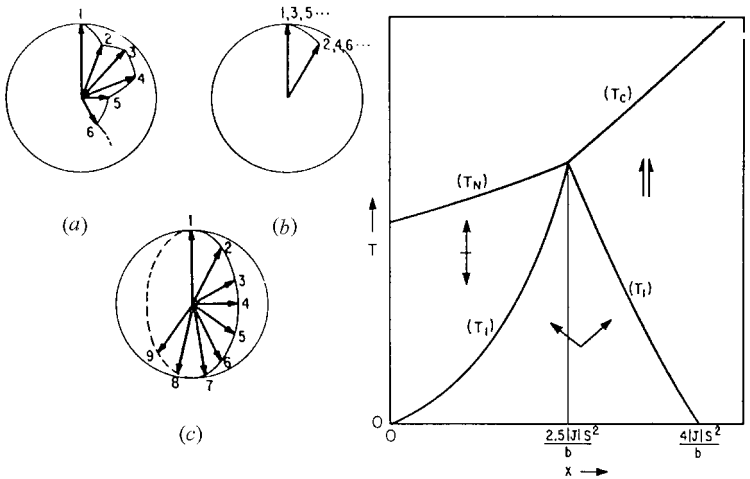

Figure 44. Magnetic phase diagram of mixed-valence manganites, according to deGennes [22]. Of the three possible degenerate magnetic configurations at low doping levels, (*b*) is the most stable. [Reprinted by kind permission of the American Physical Society from page 141 of *Physical Review*, Volume 118, 1960, and the author, P. G. DeGennes, © 1960 by the American Physical Society.]

the spin assembly: $w_n(\mathbf{S}) = \{\lambda/[2\sinh(\lambda)]\}\exp(-\lambda_n \cdot \mathbf{S})$ with n specifying the sublattice to which the spin S belongs, and λ_n being proportional to the molecular field acting on the sublattice n with absolute value λ which is directly linked to the relative magnetization of each sublattice: $m = -1/\lambda + c\tanh(\lambda)$. The distribution function is then introduced into the expression for the free energy: $F = -TS + E_{de} + E_{ex}$, the sum of the entropy, the double exchange energy and the conventional exchange energy, which is minimized with respect to λ and θ, the angle between the two sublattices at non-zero temperatures. At low temperatures, there is always a solution where $\cos\theta$ lies between -1 and $+1$. However, as T increases, the canting angle changes until a critical temperature is reached where the system becomes either purely ferromagnetic or purely antiferromagnetic. The antiferromagnetic arrangement, is obtained when x is small and pure ferromagnetism results at higher doping levels. Two transition points are then observed in all cases: T_1, representing the end of the canted arrangement, and either T_C or T_N depending on x. When θ_0, the angle between the two sublattices in the ground state, is larger than 103°, the canted arrangement becomes antiferromagnetic on raising the temperature above T_1. When θ_0 is smaller than 103°, it becomes ferromagnetic. Some physical anomalies at T_1 in the susceptibility, the specific heat and the electrical conductivity were predicted by deGennes, together with the presence of both ferromagnetic and antiferromagnetic neutron reflections below T_1 [22]. As regards the susceptibility, when the carrier bandwidth is large compared with kT, θ_p and T_C coincide within the molecular-field approximation. The schematic phase diagram is shown in figure 44.

Although this model applies to *homogeneous* systems where the electrons at the Fermi level are delocalized. deGennes also considered the possibility of localized electrons. In this case, the medium around them is locally spin polarized (figure 45). The band magnetic polaron was treated by Kasuya in the spirit of semiconductor theory. For a system consisting of an assembly of these bound states, the salient

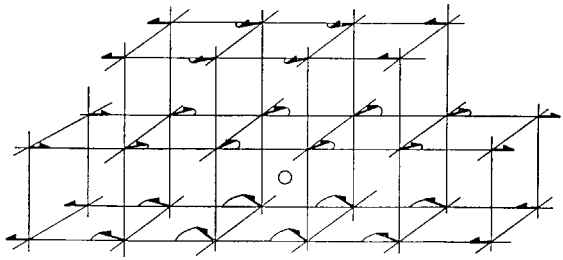

Figure 45. A bound electron polarizes the surrounding ion moments to form a bound magnetic polaron [22]. [Reprinted by kind permission of the American Physical Society from page 141 of *Physical Review*, Volume 118, 1960, and the author, P. G. DeGennes, © 1960 by the American Physical Society.]

features as the temperature is increased should be the same as for the delocalized case [22]. The interlocking of different bound states should prevail up to some temperature T_1 above which the transverse component of the moments exhibits paramagnetic behaviour. The conclusions for free carriers and bound carriers are therefore very similar.

Inoue and Maekawa [335, 336] considered electron correlation effects among the itinerant e_g electrons in the double-exchange Hamiltonian and predicted the existence of spiral states in the low-doping region ($x \approx 0$) and canting in the high doping end ($x \approx 1$). The exchange interaction J was taken as antiferromagnetic for nearest neighbours both in and out of plane, which is inconsistent with all data for the $LaMnO_3$ end member. Hence, their results for the low-doping end of the phase diagram are unrealistic, but stabilization of spiral arrangements by electron–electron interactions remains a possibility for other compositions [192]. The double exchange model in the presence of many itinerant electrons was studied numerically by Zang *et al.* [337], who found it to be locally but not globally ferromagnetically ordered. The model has been extensively studied by Millis *et al.* [338, 339], especially in relation to the transport properties, discussed in the following section.

The conclusion that the presence of any low concentration of Zener electrons in a planar antiferromagnet inevitably leads to canting (e.g. an A_yB_z structure) has been criticized by Mishra *et al.* [340], who suggest that for realistic non-infinite values of the Hund rule coupling $J_H \approx 1$ eV, the canting may be suppressed for certain carrier concentrations. Furthermore, it has been shown by Arovas and Guinea [341] that an inhomogeneous magnetic two-phase region is to be expected in the deGennes model between the ferromagnetic and antiferromagnetic phase fields; the 'canted' phase may actually be composed of finely imbricated nanoscale ferromagnetic and antiferromagnetic domains with different electron concentrations. Phase segregation has also been found in a Kondo lattice model [342, 343] where compositions with average electron density $\langle n \rangle$ around 0.9 per manganese atom ($x \approx 0.1$) spontaneously segregate into antiferromagnetic regions with $\langle n \rangle = 1$ and ferromagnetic regions with $\langle n \rangle = 0.8$. A better awareness of the possibility that magnetic and crystallographic two-phase regions may separate single-phase fields could help to rationalize observations of magnetic and crystallographic inhomogeneity in magnanites [239, 547, 555, 594–597].

Despite the scope for developing the model in conjunction with other interactions, the double-exchange interaction is the principal element needed to account for the itinerant-electron ferromagnetism in mixed-valence manganites.

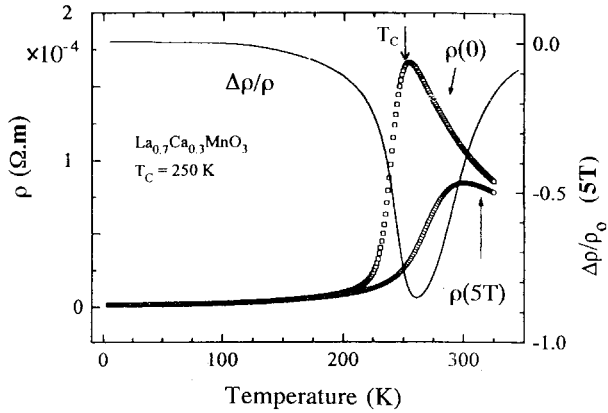

Figure 46. Typical resistivity and magnetoresistance of a mixed-valence manganite showing a metal–insulator transition. Data are for a thin film of $(La_{0.7}Ca_{0.3})MnO_3$ for which $T_C = 250$ K. (From [399].) [Reprinted by kind permission of the American Physical Society from page 860 of *Applied Physics Letters*, Volume 67, 1995, and the authors, M. F. Hundley, M. Hawley, R. H. Heffner, Q. X. Jia, J. J. Neumeier and J. Tesmer, © 1995 by the American Physical Society.]

4.3. *Transport properties*

In the first study of the mixed-valence manganese perovskites, van Santen and Jonker [8] and Jonker [344] reported resistivity measurements on ceramic samples of $(La_{1-x}A_x)MnO_3$ (A = Ba, Ca or Sr) as a function of temperature and composition. Their main result was the striking correlation between the magnitude of the resistivity and the magnetic state of the compounds. Outside the ferromagnetic concentration range, resistivities are high and thermally activated, but a resistance anomaly appears around T_C for the ferromagnetic compositions, where there is a transition from thermally activated to metallic-like conductivity. Representative modern data on a thin film are shown in figure 46.

When Volger [10] discovered the large negative magnetoresistance effect near T_C in 1954 (figure 1), he showed it to be isotropic (independent of the relative orientation of the current and the field) and frequency dependent. He also made the first measurements of Hall effect, thermopower and specific heat. The single-crystal magnetoresistance measurements reported 15 years later by the Canadian group for the $(La_{1-x}Pb_x)MnO_3$ system [12] showed the effect to be quite substantial, with a 20% decrease in resistivity at 310 K in an applied field of 1 T, but these results and those of Volger made little impression on the broader scientific community, who were more aware of the magnetic semiconductors described in section 2, where huge magnetoresistance effects were seen at low temperatures. Twenty more years elapsed before the effect was rediscovered, at a time of intense interest in using magneto-resistance in sensors operating at room temperature. Giant magnetoresistance (GMR) effects in metallic and ferromagnetic structures [345] stimulated research on systems with interfaces between normal and ferromagnetic regions on a nanoscopic scale. Nowadays, GMR effects of order 10% are reproducibly achieved under low (around 5 mT) in-plane applied fields in spin valve structures at room temperature, far below the Curie point.

The largest magnetoresistance for the manganites usually appears near T_C which can be above room temperature for some compositions (e.g. La–Na or La–K with

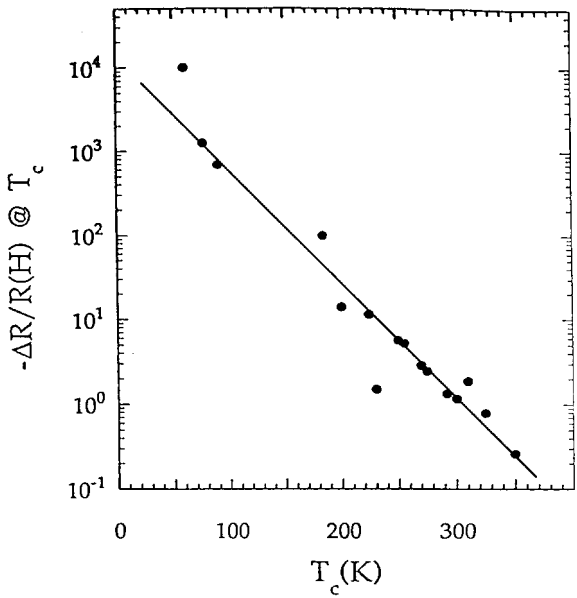

Figure 47. Variation in the high-field CMR effect (5–12 T) in mixed–valence manganites at their Curie temperatures as a function of T_C. [Reprinted by kind permission of the American Physical Society from page 295 of *Physical Review Letters*, Volume 76, 1996, [316] and the authors, K. Khazeni, Y. X. Jia, V. H. Crespi, M. L. Cohen and A. Zettl, © 1996 by the American Physical Society.]

$x \approx 0.15$ [109, 346, 347]; La–Ba, La–Pb or La–Sr with $x \approx 0.3$). The resistivity peak temperature T_m almost coincides with T_C for crystals with $x \approx 0.3$. The isotropic negative magnetoresistive effect requires an applied field well in excess of 1 T, to approach saturation, as illustrated for the thin film of $(La_{0.7}Ca_{0.3})MnO_3$ in figure 46. The saturation magnetoresistance in the vicinity of T_C is bounded by the drop in resistivity below T_C, which depends in turn on T_C itself [103, 316], as shown in figure 47. The field-induced change in resistivity is comparable with the high-field resistivity when the Curie point is close to ambient temperature, but it can be several orders of magnitude greater when T_C lies at low temperature. The correlation is shown in figure 48, where $\rho(T_m)/\rho_0$ is plotted against $1000/T_m$. The resistivity of any particular sample depends essentially on its magnetization.

A different type of magnetoresistance effect is the anisotropic magnetoresistance which depends on the relative orientation of the current and magnetization, changing sign four times as the magnetization rotates in the plane of a thin film. It is a small effect ($\approx -0.2\%$) related to the orbital moment, which has been observed at low fields in films of tetragonal $(La_{0.7}Ca_{0.3})MnO_3$ [129, 563].

4.3.1. *Resistivity and magnetoresistance*

4.3.1.1. *Variations with doping level.* The end member $LaMnO_3$ is a semiconductor, with reported values of the activation energy ranging from 0.10 to 0.36 eV [348]. The sample-dependent bandgap is small compared with the energy of the charge-transfer excitation measured optically (about 1 eV) [205] or the bandgap measured by photoelectron spectroscopy (about 1.3 eV) [75] but it is comparable to the

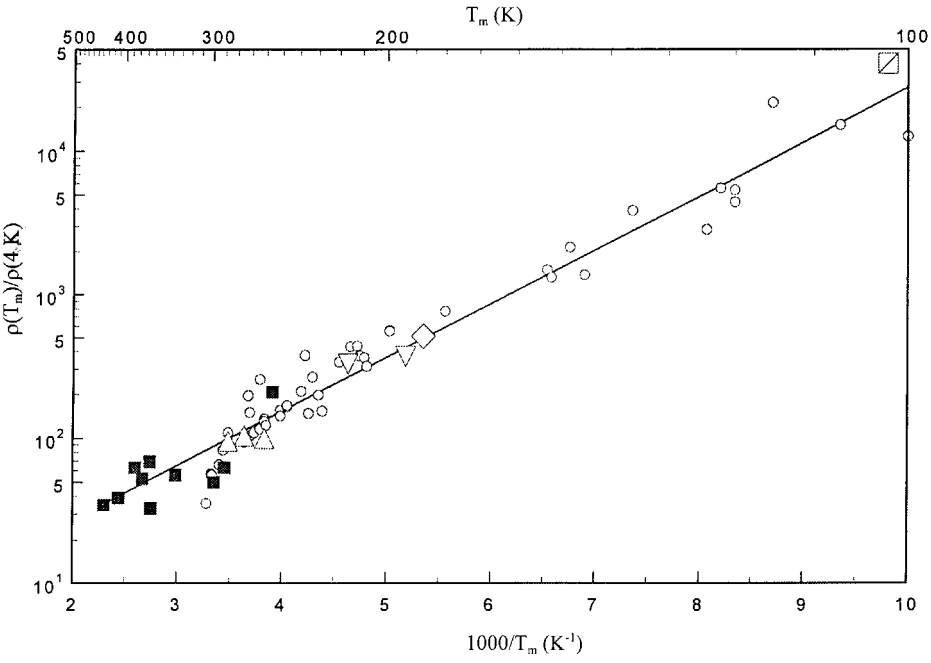

Figure 48. Variation in the logarithm of the resistivity ratio ρ_m/ρ_0 in thin films of mixed-valence manganites as a function of $1000/T_m$: (○) $(La_{0.7}Ca_{0.3})MnO_3$; (■), $(La_{0.8}Sr_{0.2})MnO_3$; (▽), (△), (◇), (⊠), (La, Pr, Ca, Sr)MnO_3. (By courtesy of K. Steenbeck.)

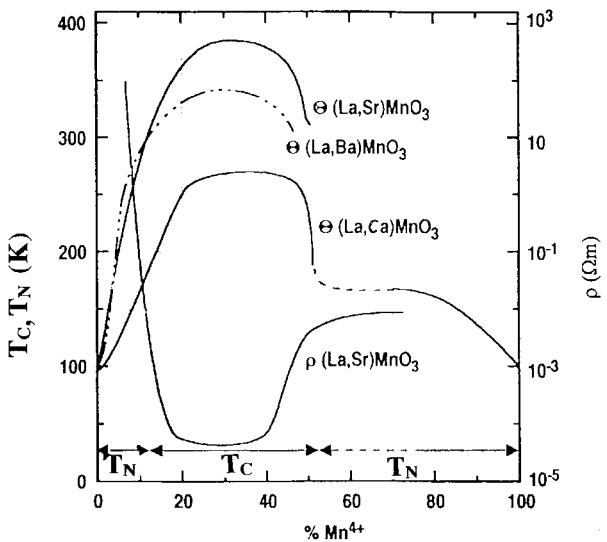

Figure 49. Magnetic ordering temperatures and resistivities as a function of Mn^{4+} content or x (schematic). [Reprinted from the *Journal of Magnetism and Magnetic Materials*, Volume 151, R. von Helmholt, J. Wecker, K. Samwer and K. Bärner, page 411, © 1995 [546] with permission from Elsevier Science.]

calculated indirect gap (figure 31). The variations probably reflect doping of the material by defects and non-stoichiometry, and localization of the resulting carriers.

Figure 49 sketches the variation in resistivity and magnetic ordering temperatures for some lanthanum manganites as a function of the proportion of Mn^{4+}, which is varied by cation doping (or cation deficiency). The correlation of the two phenomena is the basis for Zener's double-exchange model. For antiferromagnetic phases, the Zener bandwidth is zero and the insulating character dominates the transport. As the material becomes ferromagnetic, the conduction electrons hop from one manganese atom to another with spin memory. The ferromagnetic interaction is therefore associated with high electronic mobilities and low resistivities. Electronic transport follows the magnetic transitions, with very high resistivities for the $x = 0$ end member, minimum resistivity obtained for $x = 0.3$ and higher resistivities for the other antiferromagnetic structures at $x > 0.5$. The number of conduction holes can be taken as the number of Mn^{4+} introduced at low doping (small x) and the resistivity might be expected to follow this number. Instead, it is found experimentally that the conduction changes rather rapidly at a threshold corresponding to a hole concentration of $x \approx 0.15$, which suggests that localization must play an important role in the transport properties at low doping levels. Charge ordering, even on a local scale, also promotes localization; in the $(La_{1-x}Sr_x)MnO_3$ system, for example, charge ordering occurs around $x = 0.125$ [191]. The electrical resistivity of a crystal with $x = 0.15$ is anisotropic, being a factor of 2 to 5 lower for the current in plane rather than along the c axis [349].

4.3.1.2. *Ferromagnetic state*. The ferromagnetic state in compounds with $x \approx 0.3$ is metallic in the sense that the resistivity is almost temperature independent, with a slight positive temperature coefficient. Experimental evidence for metallic behaviour comes from power-law dependences of R at temperatures above about 50 K where T^2 [84, 122, 556, 592] or $T^{2.5}$ [309] increases have been reported. These could be ascribed to correlation effects in a degenerate electron gas [350], but there may also be a contribution from spin-wave scattering. In fact, the coefficient of the T^2 term derived from the measurements of Urushibara on single crystals, which is a measure of the correlation strength, is comparable with values for other highly correlated electron metals such as $CeAl_3$ and $CeCu_2Si_2$ [351]. However, only in a few compounds such as $(La_{0.7}Sr_{0.3})MnO_3$ does the magnitude of the residual resistivity have the value expected of a metal, $\rho_0 < 1.5 \times 10^{-6}\,\Omega\,m$, applying the criterion that the mean free path should exceed the interatomic spacing [352]. There is a body of experimental evidence from low T measurements that this compound is a half-metallic ferromagnet, including spin-resolved photoemission spectra, Andreev reflection measurements at 2 K [567], tunnelling spectroscopy [212] and spin polarized transport [447], with predominantly $\uparrow$ electrons present at E_F. In other compounds, the residual resistivity can be up to *ten orders of magnitude* greater (as shown in figure 50), making them extremely peculiar metals. The T^2 variation is suppressed below 10–20 K [556] and, in some cases, a slight upturn in ρ is reported [10, 121, 316, 353] which can be eliminated by applied field or pressure.

The resistivity in the 'bad' metallic state is unusually sensitive to pressure, with variations in ρ_0 of one order of magnitude per gigapascal [315, 353]. It is also dependent on the substrate and preparation conditions for thin films which may distort the lattice [354, 355] and depends critically on the grain size [2, 356, 357] and grain-boundary angle [358]. A variation in ρ_0 from 3×10^{-6} to $2 \times 10^{-3}\,\Omega\,m$ for

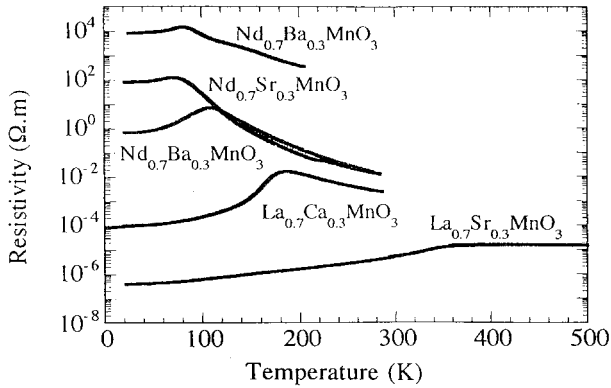

Figure 50. Resistivity as a function of temperature for films of mixed-valence manganites with $x = 0.3$. [Reprinted by kind permission of the American Physical Society from page 3910 of *Physical Review Letters*, Volume 75, 1995, [359] and the authors, J. M. D. Coey, M. Viret, L. Ramo and K. Ounadjela, © 1995 by the American Physical Society.]

$(La_{0.67}Ca_{0.33})MnO_3$ has been attributed by Gupta *et al.* [357] to spin-dependent scattering at grain boundaries as the crystallite size decreases from bulk to 3 μm. Resistivities as high as $8 \times 10^3\ \Omega$ m are attributed by Coey *et al.* [359] to intrinsic magnetic barriers between misaligned ferromagnetic regions which are in the nanometre size range. Large reductions in ρ_0 are associated with increases in reduced magnetization [186], and it is likely that canted Mn^{4+} spins in the low temperature ferromagnetic state are the origin of the lack of magnetic saturation [360]. Very direct evidence of spin-dependent scattering in the ferromagnetic metallic state has been provided by the resistive behaviour of bilayers and heterostructures described in section 4.3.3.

There is also evidence for a highly-resistive surface layer associated with a reduced magnetization in films less than 50 nm thick [598, 599, 601]. Quantized conductance with steps of $2e^2/h$ has been observed in point contacts between manganite crystals [578].

4.3.1.3. *Temperature-induced transitions.* Magnetic transitions are commonly observed by varying the temperature. In mixed-valence manganites these can be of three types: Curie and Néel points and transitions to a canted state. A schematic magnetic phase diagram is shown in figure 51.

Néel points (x–x′ in figure 51) are generally not accompanied by major resistivity changes and, in any case, activated behaviour persists through the transition to the antiferromagnetic state.

At the Curie point, where ferromagnetic order sets in for compounds with x around 0.3, the resistivities present large anomalies with associated CMR (w–w′ in figure 51). These are the 'type I' transitions of the Caen group [361]. A typical curve was shown in figure 46 where a high maximum is obtained near T_C. Electric and magnetic transitions are close to one another but may not be completely superimposed. The peak in the resistivity, especially of poorly crystallized ceramics lies at a temperature T_m somewhat below T_C [268, 362], but in crystals these temperatures almost coincide [363]. An interesting property is that they are both pressure and magnetic field dependent, with increases of order $30\ K\ GPa^{-1}$ and $10\ K\ T^{-1}$ respectively.

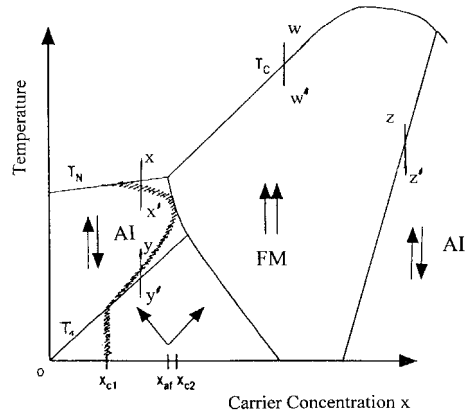

Figure 51. Schematic magnetic phase diagram of $(La_{1-x}A_x)MnO_3$. [Modified from the *Journal of Magnetism and Magnetic Materials*, Volume 151, R. von Helmholt, J. Wecker, K. Samwer and K. Bärner, page 411 © 1995 [546] with permission from Elsevier Science.]

The metal–insulator transition in manganites is atypical in that it is the low-temperature phase which is metallic, and the high-temperature phase which is insulating, rather than the reverse. This is due to the magnetic nature of the transition; the fact that the double-exchange sets in just below T_C drives the material metallic. As an external field is applied, the magnetic order is enhanced and the resistivity decreases. The field is most effective near T_C where the magnetic susceptibility is a maximum. The transition in compounds which show their resistivity peak at low temperatures, $T_m < 100$ K, tends to exhibit thermal hysteresis [113, 185, 267, 270, 278, 364]. This was taken as evidence of a first-order transition between the ferromagnetic metal and paramagnetic insulator states related to a double-well potential for the Mn–O bond [277]. However, the bond lengths measured as a function of temperature were found to vary rapidly but continuously near T_C [190], and another view is that the hysteresis is magnetic rather than structural in origin [267, 365], linked to the presence of degenerate canted ferromagnetic structures. Effects in the resistivity analogous to magnetic viscosity support the latter interpretation [270].

Large resistance changes can also occur at a temperature where the compounds undergo a transition from an antiferromagnetic (or ferromagnetic) to canted state (the temperature T_1 in deGennes' [22] model; y–y′ in figure 51). The cell parameters were found to vary much more at T_1 than at T_C or T_N. The T_1 transitions are also strongly hysteretic. First-order effects associated with these magnetic structure changes are comparable with the crystallographic changes induced by an applied field discussed in section 4.2.5 [85].

Resistance changes in the opposite sense accompany the re-entrant antiferromagnetic transition near $x = 0.5$ (z–z′ in figure 51), as discussed in section 4.2.5. These are the 'type II' transitions of the Caen group [361]. They are also very pressure sensitive and, in certain cases, can be triggered by applied pressures of the order of 0.5 GPa [321]. Under pressure, the resistivity becomes strongly hysteretic thereby emphasizing the first-order character of the transition.

4.3.1.4. *Magnetoresistance*†. Numerous papers present magnetoresistance measurements at the w–w′ transition in different manganese oxide compounds. A large effect is essentially linked to the presence of an adequate amount of Mn^{4+}, around 30% , which can be introduced by cation substitution or cation deficiency [184]. The effect is inhibited by charge order. It increases as the resistivity ρ_m in the localized state just above T_C increases (figures 47 and 48), but the residual resistivity ρ_0 is usually a lower bound on the minimum resistivity that can be achieved.

Large applied fields are needed to achieve CMR effects in bulk and thin-film crystals. Kusters *et al.* [80] decreased the resistance of their $(Nd_{0.5}Pb_{0.5})MnO_3$ crystal by two orders of magnitude near $T_C = 180$ K by applying an 11 T field. von Helmholt *et al.* [15] reported large effects at room temperature in oriented $(La_{0.67}Ba_{0.33})MnO_3$ films grown by PLD on $SrTiO_3$ substrates, followed by post-annealing treatments at 900°C in order to raise T_C above 300 K. The resistive transition becomes sharper and the magnetoresistance ratio defined as $R(0)/R(H)$ at room temperature reached 2.5 at $\mu_0 H = 6$ T. The effect can be much larger in compounds having a lower Curie temperature as illustrated in figure 47. Jin *et al.* [1] at Bell laboratories grew $(La_{0.67}Ca_{0.33})MnO_3$ thin films by pulsed laser deposition on $LaAlO_3$ substrates which showed an $R(0)/R(H)$ of 5.6 at 200 K in an applied field $\mu_0 H = 6$ T. Here a suitable post-annealing treatment (900°C under an oxygen pressure of 3 atm for $\frac{1}{2}$h) reduces the transition temperature and greatly enhances the magnetoresistance ratio to 'colossal' values of order 10 000 at 110 K and 6 T [366]. It is reported that there is also an optimum film thickness of about 100 nm [98] for the magnetoresistive effect, possibly related to strain. The magnitude of the magnetoresistance effect is increased by substituting some yttrium for lanthanum, but the Curie temperature is decreased [164, 185, 289, 367, 368]. Again, the effect is optimized by appropriate annealing [369]. At constant doping, the decrease in Curie temperature when a heavier rare earth is substituted for lanthanum depends on the rare earth cation radius [188]. The high-field magnetoresistance changes sign and becomes positive above $2T_C$ [164].

A comprehensive study of the influence of deposition conditions and post-annealing treatments on the magnetoresistance was reported by the Maryland group [95, 101]. Thin films of $(La_{0.67}Ba_{0.33})MnO_3$ and $(Nd_{0.7}Sr_{0.3})MnO_3$ were synthesized by PLD in a 40 Pa N_2O atmosphere at temperatures ranging from 615 to 815°C. The films grown at lower temperatures exhibited better crystallographic quality. The temperature at which the resistivity of the films reaches its maximum is found to decrease with increasing deposition temperature, and the resistance of that maximum is pushed to higher values. For the post-anneal, both temperature and time of the treatment tend to increase the temperature of the maximum and lower the peak resistivity. For the lower Curie temperatures, $R(0)/R(H)$ of order 100 can be reproducibly achieved in 8 T by the post-deposition treatments. The largest negative magnetoresistance effects are correlated with substrate-induced lattice distortion [355, 370]. Reducing the oxygen content in $(La_{0.67}Ba_{0.33})MnO_{3-\delta'}$ extends the temperature range in which the large magnetoresistive effect is observed, and eventually makes the compound insulating when $\delta' = 0.2$ [274]. Defects induced

† Different definitions of the magnetoresistance ratio appear in the literature, including $[R(0) - R(H)]/R(0)$, $[R(0) - R(H)]R(H)$ and $R(0)/R(H)$. The first lies between 0 and 1, while the others take very large values. The third definition has the advantage that it can be plotted on a logarithmic scale.

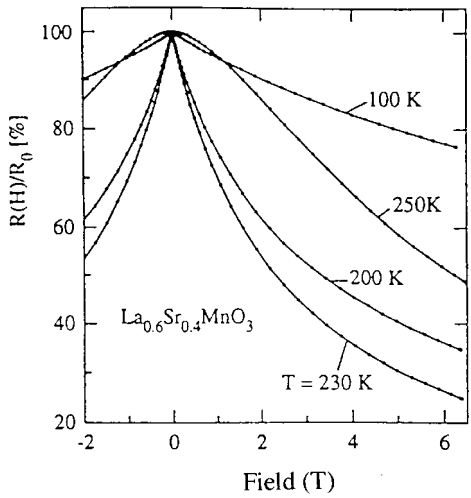

Figure 52. Magnetic field effect in $(La_{0.7}Ca_{0.3})MnO_3$ thin films at different temperatures above and below $T_C = 240$ K. [Reprinted by kind permission of the American Physical Society from page 2331 of *Physical Review Letters*, Volume 71, 1993, [15] and the authors, R. von Helmholt, J. Wecker, B. Holzapfel, L. Schultz and K. Samwer, © 1993 by the American Physical Society.]

by irradiation with Ar^+ ions have a similar effect [151]. Prolonged annealing of $(La_{1-x}Sr_x)MnO_3$ first decreases and then increases the resistivity [371].

The decrease in resistivity with applied magnetic fields appears to be different above and below T_C. Figure 52 shows a representative set of $R(H)$ curves at different T. Above T_C, the magnetoresistive effect is not very large in small fields, and the curves are bell shaped initially with $\Delta\rho \propto H^2$ [82, 365, 372] or $\Delta\rho \propto M^2$ [263]. In the vicinity of T_C, the resistivity drops rather quickly at low fields and saturates at higher fields but, at low temperatures, the effect is again small. Just below T_C, $\Delta\rho$ varies roughly as H^2 [372], but others report that the resistivity is nearly linear in H [373] or that conductivity is linear in H^2 [374]. In fact, what seems to be qualitatively different behaviour may just reflect the effect of the magnetization. In the paramagnetic state, $M \propto H$, and hence $\Delta\rho \propto H^2$. On the critical isotherm, $M \propto H^{1/\delta}$ where $\delta \approx 3$-5, and hence $\Delta\rho \propto H^{2/\delta}$. Below T_C, M depends nonlinearly on H; an exponential variation $\Delta\rho \propto \exp(-H/H^0)$ has been reported [375]. A single scaling function $\Delta\rho \propto \exp[-(M/M^0)^2]$ can reproduce the field and temperature dependence both above and below T_C [376]. The field dependence may best be rationalized in terms of a normal resistor in series with a magnetoconductor, which varies as H^2 above T_C and as $|H|$ below T_C [377].

Size effects are important in fine-grained polycrystals. The high-field CMR is independent of grain size [378], but there is a low-field magnetoresistance at all temperatures below T_C in polycrystalline material which is absent in single crystals (figure 53). The low-field effect is distinctly different from CMR. It increases with decreasing grain size and grows rapidly at low temperatures. The effect, which has been observed in polycrystalline ceramics [2, 357, 379, 380] and thin films [106, 377, 381], is attributed to spin-dependent grain-boundary scattering. The boundaries are about 1 nm wide. The grain-boundary scattering has been isolated in elegant model experiments on manganite strips on a bicrystal substrate [382, 383,

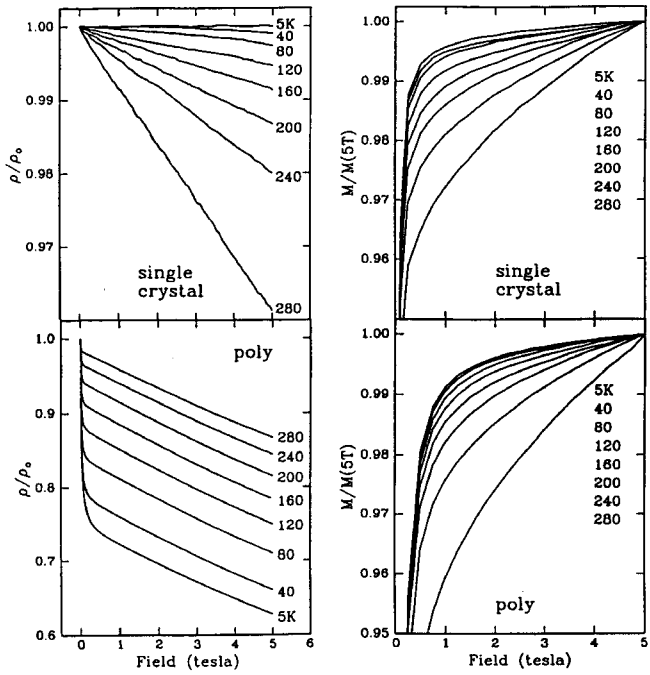

Figure 53. Comparison of the negative magnetoresistance of single-crystal and polycrystalline $(La_{1-x}Sr_x)MnO_3$. [Reprinted by kind permission of the American Physical Society from page 2041 of *Physical Review Letters*, Volume 77, 1996, [2] and the authors, H. Y. Hwang, S. W. Cheong, N. P. Ong and B. Batlogg, © 1996 by the American Physical Society.]

572]. Domain wall scattering varies as δ_w^{-3}, where δ_w is the wall width, hence the narrow 'domain walls' that occur at grain boundaries may be much more efficient at scattering electrons than the wide Bloch walls that occur in the bulk [383]. Unlike the high-field colossal magnetoresistance which is an intrinsic property, usually greatest near T_C, the low-field response reflects the micromagnetic state of the sample and peaks at the coercive field. The effect can be seen most directly in pressed powder compacts of manganites (figure 54) [385, 600] and other half-metallic ferromagnets [386, 387], where the resistance is entirely due to interparticle contacts. Powder magnetoresistance is associated with the degree of alignment of the magnetization of the grains or particles, but it may be sensitive to paramagnetic or quenched spin disorder at grain boundaries [357, 379, 388]. Surface spin disorder can arise because absent bonds weaken the exchange interactions of atoms in the interface, or alter the balance of ferromagnetic and antiferromagnetic interactions. A different explanation of the low-field magnetoresistance of tetragonal $(La_{0.6}Ca_{0.3})MnO_3$ films in terms of domains has been given by O'Donnell *et al.* [130]. Gibbs *et al.* [564] interpret a voltage-dependence of the low-field magnetoresistance of $(La_{0.7}Ca_{0.3})MnO_3$ in terms of surface spin disorder [565]. Whatever the explanation, the low-field effect could be more significant for applications than the intrinsic colossal magnetoresistance, but the effects reported at room temperature so far are very small [106]. A linear negative magnetoresistance of order 1% per tesla is observed in high fields in many granular manganite systems (figure 53). It has been discussed phenomenologically by Evetts *et al.* [572] in terms of an interface layer with reduced magnetization.

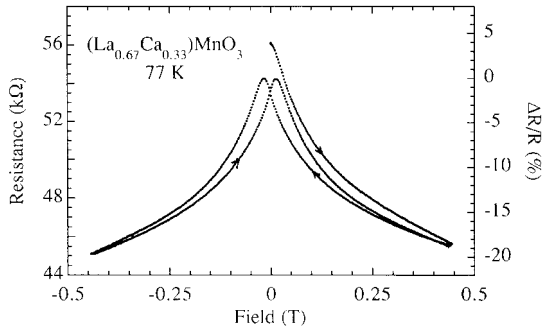

Figure 54. Magnetoresistance of a $(La_{0.67}Ca_{0.33})MnO_3$ powder compact at 77 K. The initial magnetization curve is shown, together with the hysteresis which arises from the magnetic hysteresis of the ferromagnetic powder. [Reprinted from page 1519 of *Philosophical Transactions of the Royal Society of London* A, Volume 356, 1998, [385], authored by J. M. D. Coey, with kind permission of the author and The Royal Society.]

Most magnetoresistance measurements have been made on thin films with the field H applied in the film plane; so there is no demagnetizing effect. Nevertheless, it is important to understand which of the magnetic vectors B, H or M produces the magnetoresistance phenomenon. Insofar as conduction is by spin-polarized electrons, the important quantity appears to be the magnitude of the magnetization $|M_{av}|$ averaged over the spin diffusion length λ_s, which is expected to be a multiple of the mean free path λ, probably a few tens of interatomic spacings. Well above T_C,where the magnetization follows a Brillouin function which is linear in field at low fields. $|M_{av}| \approx M$ ($=0$ in zero field). Magnetization varies very quickly around T_C, where small fields have a large effect (high magnetic susceptibility). Below T_C in the multidomain ferromagnetic state $|M_{av}| \approx M_s$, since the domain size is much greater than λ_s and the domain wall width is also likely to be greater than λ_s. At temperatures well below T_C, the spontaneous magnetization in compounds with $x \approx 0.3$ is close to the saturation value and the field effect on the magnetization at the scale of the spin diffusion length is minimal, the saturation of M being only due to domain wall motion. However, the magnetization is sharply inhomogeneous near grain boundaries in a ferromagnetic polycrystal, and there $|M_{av}|$ can be much less than M_s for those electrons crossing from one grain to the next.

The largest magnetoresistive effects seem to accompany first order transitions (see section 4.2.5). Neutron studies presented earlier [5] established that the $(Pr_{1-x}Ca_x)MnO_3$ system has charge-ordered phases over the entire composition range. The Czech group noted the absence of the cubic structure normally associated with ferromagnetism in these systems together with the absence of a fall in resistivity below T_C. Low-temperature measurements have shown the existence of a first order transition between a state of high thermally-activated resistivity and metallic-like behaviour in $(Pr_{0.70}Ca_{0.26}Sr_{0.04})MnO_3$ [389], $(Nd_{0.7}Ca_{0.2}Sr_{0.1})MnO_3$ [390], $(Pr_{0.58}La_{0.12}Ca_{0.30})MnO_3$ [391], $(Pr_{0.7}Ca_{0.3})MnO_3$ [326], $(Pr_{1-x}Ca_x)MnO_3$ [90] and $(Nd_{0.7}Sr_{0.3})MnO_3$ [101], the latter in thin film form being most probably oxygen non-stoichiometric. Huge resistance ratios are related to cation size [390, 392]. In fact, a good recipe for making compounds with a first-order transition triggered by a magnetic field consists of making an atomic mixture of two compounds, one of which presents charge ordering down to low temperature with activated resistivity

over the entire range (for instance $(Pr_{0.7}Ca_{0.3})MnO_3$), and the other behaving "normally" with a resistivity maximum near T_C (for instance $(Pr_{0.7}Sr_{0.3})MnO_3$ or $(La_{0.7}Ca_{0.3})MnO_3$). A judicious choice of the proportion of each leads to a compound with borderline behaviour in the thermally activated regime where application of a strong magnetic field may induce a phase transition. Such effects are generally hysteretic and the removal of the applied field does not necessarily restore the initial state unless the temperature is increased again (see figure 41). At a first-order irreversible transition from a semiconducting state, the resistivity of $(Pr_{0.70}Ca_{0.26}Sr_{0.04})MnO_3$, for example, was reduced by an impressive 11 orders of magnitude in 4 T at 30 K [389]. It is possible to tip the balance between charge-ordered and metallic ground states by oxgen isotope exchange [557]. High-resolution electron microscopy reveals that some of these compounds are inhomogeneous on a microscopic scale [393], and there is evidence of those segregation [559].

Large magnetic field effects on the resistance are also observed for compounds undergoing low-temperature magnetic transitions involving re-entrant antiferromagnetism or canting (T_1) transitions z–z′ or y–y′ in figure 51. $(La_{0.5}Ca_{0.5})MnO_3$ orders first as a canted ferromagnet, and at lower temperatures as an antiferromagnetic insulator, with huge magnetoresistance around the z–z′ transition [394]. $(R_{0.5}Sr_{0.5})MnO_3$ shows a transition from ferromagnetic or paramagnetic metal to paramagnetic insulator when R = Sm [96, 395, 396], but there are two magnetic transitions when R = Pr [114] or Nd [197, 246] and the antiferromagnetic ground state may be charge ordered (see figures 40 and 43). The Tsukuba group have studied the ferromagnetic → antiferromgnetic transition in $(Nd_{1-x}Sr_x)MnO_3$ and $(Sm_{1-x}Sr_x)MnO_3$ near $x = 0.5$ [397] and in $((Nd, Sm)_{0.5}Sr_{0.5})MnO_3$ single crystals [321]. The transition is accompanied by charge ordering, cell distortion and re-entrant thermally activated conduction. It is so strongly hysteretic that it can be completely suppressed by applied fields. In the case of the $[(Nd_{0.25}Sm_{0.75})_{0.5}Sr_{0.5}]$-$MnO_3$, a relatively low field (1 T) was enough to wipe out the re-entrant behaviour and to generate a six-order-of-magnitude resistivity decrease. At 4 K there is a similar irreversible field-induced transition from a canted semiconducting state to a metastable ferromagnetic metallic state, where the resistivity of $(Pr_{0.6}Ca_{0.4})MnO_3$ changes by more than 12 orders of magnitude [173]. Caignaert *et al.* [159] showed that the passage to a canted state through an antiferromagnetic state greatly enhances the magnitude of the magnetoresistive effect at the transition. The effect of many B-site substitutions on the magnetoresistance at transitions occurring in manganites with $x \approx 0.5$ has been reported by the Caen group [271, 323, 333, 396].

Another interesting observation concerns the variation in the magnetic transition temperature T_1 between the antiferromagnetic and canted states (y–y′ in figure 51) with applied fields. Application of a large magnetic field can greatly shift T_1 to extend the conducting temperature range while affecting the paramagnetic Curie temperature very little. The Caen group reported a shift from 75 K to 130 K in a 5 T field, while the paramagnetic Curie temperature remained constant at 170 K in their $(Pr_{0.70}Sr_{0.05}Ca_{0.25})MnO_3$ sample [398]. In other magnetic compounds of the same series, the cell parameters were found to vary at T_C so as to minimize the distortion of the octahedron. This effect is more important in compounds which do not present an intermediate magnetic structure (only one magnetic ordering temperature in figure 51) [159] and is almost invisible when the activated behaviour survives at low temperatures. This is consistent with the fact that the Jahn–Teller effect becomes dynamic for the conventional manganites below T_C as electrons become more mobile.

4.3.1.5. *Paramagnetic state*. As in the case of the high-temperature superconductors, the physical properties of the manganites in the region above the transition temperature are anomalous. Transport above T_C is still a matter of controversy as numerous groups have reported different behaviour. Data on compounds with $x \approx 0.3$ were first fitted with a purely activated law

$$\rho = \rho_\infty \exp\left(\frac{E_0}{kT}\right) \tag{4.3}$$

where the gap E_0 is typically 0.1 eV [80, 374, 399]. There is also evidence for a

$$\rho \propto T \exp\left(\frac{E_0}{kT}\right) \tag{4.4}$$

behaviour over an extended temperature range [122, 354, 370, 591]. Others find that Mott's variable range hopping (VRH) expression

$$\rho = \rho_0 \exp\left[\left(\frac{T_0}{T}\right)^{1/4}\right] \tag{4.5}$$

is appropriate [82, 232, 254, 309, 359, 400, 401]. The simple activation law (4.4) could indicate the opening of a gap at the Fermi level above T_C. Photoemission data support the view that a small bandgap appears at T_C in $(La_{0.7}Ca_{0.3})MnO_3$ [213, 402] and $(La_{0.7}Sr_{0.3})MnO_3$ [553] (although the manganite surface probed in photoemission is unrepresentative of the bulk [403]), and there is evidence from tunnelling spectroscopy for a change in the density of states below and above T_C [404]. However, it is difficult to justify a gap over a range of Mn^{4+} concentrations from $x = 0.2$ to $x = 0.4$ in the absence of any change in structure. Moreover, Hundley *et al.* [399] could not interpret their activated behaviour as excitation to extended states, since the measured mobility was so small that a mean free path could not be defined. Others who found $\rho = \rho_\infty \exp(E_0/kT)$ activated behaviour did not have Hall or other transport results to identify the form of transport [374, 405].

A common view is that the carriers form small dielectric polarons (see figure 57 later) [80, 406, 407, 591]. There is some direct evidence of small polaron formation in the distribution of Mn–O bond lengths contained in the pair distribution function of $(La_{1-x}Ca_x)MnO_3$ with $x = 0.12$ [408]. The hopping motion of polarons leads to a resistivity of the form $\rho = (kT/ne^2D)\exp(E_0/kT)$ where n is the carrier density and D is the polaron diffusion constant. Here, there may be contributions to E_0 of magnetic, elastic (Jahn–Teller) or coulombic origin. Park *et al.* [213] suggested that strong polaron effects lead to a charge fluctuation energy of about 1.5 eV above T_C, but that the Jahn–Teller effect is less significant than the normal small-polaron contribution. Good agreement with data was reported for the simple form $\rho \propto T \exp(E_0/kT)$, with $E_0 = c + E_{trap}$, where E_{trap} is the trapping energy [122, 409]. Another related form of polaron conduction, in which the pre-factor is also dependent on the state of magnetization, was used to extract the lattice polaron trapping energy of about 0.35 eV [354]. Remarkably, this value remained constant for a variety of films having different magnetic and transport properties. Perhaps the most extended high-temperature measurements on single crystals and thin films of the calcium- and strontium-doped lanthanum manganites are those of Snyder *et al.* [123]. Their resistivity data, shown in Figure 55, follow the small-polaron hopping law very well. These workers showed that at least part of the hopping energy must

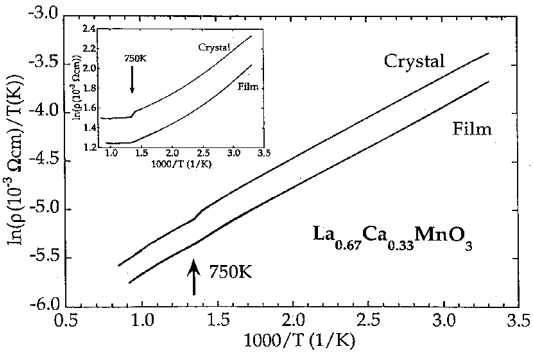

Figure 55. High temperature resistivity of $(La_{0.67}Ca_{0.33})MnO_3$ film and crystal in zero field plotted according to (4.4) or (4.3) (insert). [Reprinted by kind permission of the American Physical Society from page 14434 of *Physical Review* B, Volume 53, 1996, [122] and the authors, G. J. Snyder, R. Hiskes, S. Di Cariolis, M. R. Beesley and T. H. Geballe, © 1996 by the American Physical Society.]

come from lattice distortions, as can be seen as the abrupt change from temperature independent to activated transport near the 750 K structural transition in the inset of figure 55. The thermopower, discussed in the next section, favours polaron hopping in the paramagnetic state.

Another plausible view is that the presence of magnetic disorder above T_C together with the intrinsic variations in the Coulomb potential due to the presence of A^{3+} and A^{2+} ions in the lattice leads to the formation of a *mobility edge* [50]. At high temperatures, carriers will be excited from the Fermi energy E_F to the mobility edge $E\mu$, giving an activated conductivity. At lower temperatures it may be possible to discern a nearest-neighbour hopping process with a lower activation energy, which transforms into uncorrelated VRH, $\ln \rho \propto T^{-1/4}$, when the available phonon energy is so small as to make the longer-range hops necessary to find a site sufficiently close in energy for hopping to occur. This view is not incompatible with small dielectric-polaron formation since VRH of small polarons also leads to $\ln \rho \propto T^{-1/4}$ [410]. For highly correlated electron systems a small gap appears at E_F and the hopping law is then $\ln \rho \propto T^{-1/2}$ at temperatures below the correlation gap [411]. Experimental evidence for VRH behaviour is presented in figure 56 in a range of ferromagnetic manganites with $x \approx 0.3$ above T_C. Resistivity data there can usually be fitted with a power law between $\frac{1}{2}$ and $\frac{1}{4}$. There is also evidence of VRH behaviour when $x \approx 0.5$ [114].

An important question in the manganites is the relative weight of the magnetic and Coulomb random potentials in the establishment of a mobility edge. The fluctuating Coulomb potential may be caused by substitution or vacancies on A or B sites. For instance, the electron occupancy corresponding to 30% Mn^{4+} can be achieved in three ways, namely by divalent cation substitution with $x = 0.3$, by lanthanum deficiency with $z = 0.077$ or by non-stoichiometry with $\delta = 0.048$ (see section 3.4). All three are ferromagnets, but only the first two are metals. Activated conduction is measured down to the lowest temperatures in ferromagnetic $(LaMn)_{0.95}O_3$ [156, 175]. This demonstrates that the Coulomb random potential due to the B-site (manganese) vacancies is well able to produce localization even in the absence of a random magnetic potential. In cation-deficient $La_{1-z}MnO_3$, where

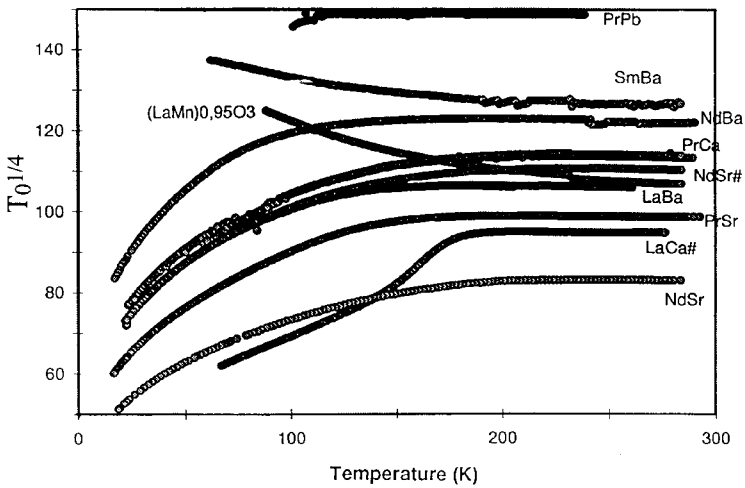

Figure 56. Plot of the parameter $T_0^{1/4}$ against temperature showing VRH behaviour above T_C in a range of $x = 0.3$ compounds: (#) thin films [232]. [Reprinted by kind permission of the American Physical Society from page 8067 of *Physical Review* B, Volume 55, 1997, [232] and the authors, M. Viret, L. Ranno and J. M. D. Coey, © 1997 by the American Physical Society.]

there are only A-site vacancies, the carriers are localized when $z < 0.05$, whether in the antiferromagnetic phase ($z < 0.03$) or in the ferromagnetic phase ($0.03 < z < 0.05$) [280]. However, the ferromagnet with $z > 0.05$ is a metal [184]. Therefore, for similar Mn^{3+} to Mn^{4+} ratios [102, 412], B-site vacancies localize the e_g electrons more effectively than do A-site vacancies. In the substituted lanthanum compounds with A site disorder $(La_{1-x}A_x^{2+})MnO_3$, the random potential variations ΔV due to divalent and trivalent A-site ions are insufficient to produce localization in the ferromagnetic state when $x = 0.3$. This indicates that the ratio of ΔV to the occupied σ^* bandwidth W is less than the critical value for 'diagonal' or Anderson localization. However, when a smaller rare earth, such as praseodymium or samarium replaces lanthanum, a ferromagnetic insulating state is often found. This may be associated with a decreased Mn–O–Mn bond angle which reduces the transfer integral and bandwidth, hence tipping $\Delta V/W$ above the value necessary for localization [351].

We have seen that the manganites with $x \approx 0.3$ which are ferromagnetic metals below T_C generally exhibit activated conduction above T_C. Setting aside some minor changes in lattice parameters at T_C, the metal–non-metal transition must evidently be magnetically driven. It is very likely that the carriers polarize their immediate environment creating short-range correlations. The large effective mass and small activation energy of the carriers indicate polaron formation. We have discussed the possibility that these polarons are normal dielectric small polarons where the electron bears with it a dilatation of the MnO_6 octahedron. Other possibilities are Jahn–Teller polarons where the electron carries with it an axial distortion of the MnO_6 octahedron, and magnetic polarons where there is a ferromagnetic polarization of the surrounding manganese core spins (figure 57). The influence of an applied field on the resistivity and thermal expansion above T_C indicates that the polarons have magnetic character [15, 80, 265, 309, 400]. Although small-angle neutron scat-

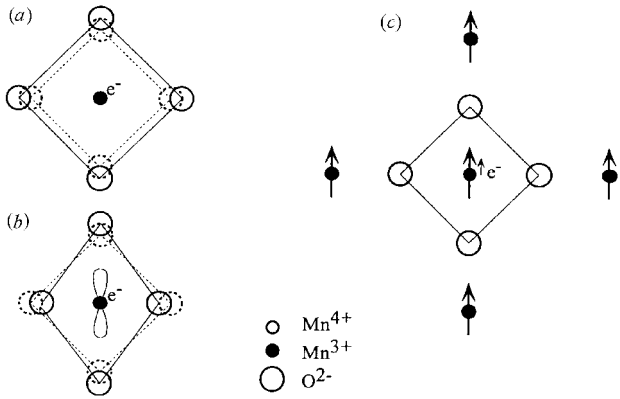

Figure 57. Schematic picture of (*a*) a small dielectric polaron, (*b*) a Jahn–Teller polaron and (*c*) a magnetic (spin) polaron.

tering [306, 309, 400, 413] confirms the presence of nanometre-scale magnetic coherence and fluctuating short-range order in the vicinity of T_C which persists up to about $1.3T_C$, spin-polarized neutron measurements did not support the existence of magnetic polarons with a well defined size, at least in a $(La_{0.75}Sr_{0.25})MnO_3$ crystal [413], where there is magnetic coherence similar to that encountered in the critical region of iron or nickel. Viret *et al.* introduced a spin pair correlation function of a form consistent with magnetic exchange interactions that extend beyond nearest neighbours. As regards the dynamics of the magnetic fluctuations, muon spin relaxation indicates unusual spin dynamics below T_C [276]; NMR shows that two neighbouring moments remain parallel for more than 10^{-5} s [287]. More direct evidence of spin correlations on the scale of 1 nm at T_C has been deduced from analysis of the quasi-elastic neutron peak in the calcium compounds [306]. In the strontium crystal, a picture of slowly fluctuating moments where ferromagnetic interactions are mediated by Zener electron hopping seems preferable to one of fast-moving spin polarons with a definite size. Nevertheless, it is likely that spin polarons exist in the calcium compounds, especially at low doping of the antiferromagnetic end member [305]. These ferromagnetic polarons will overlap as the carrier concentration increases, leading to the state of strong magnetic coherence above T_C in the ferromagnetic concentration range.

4.3.1.6. *The Jahn–Teller effect*. When Jahn–Teller polarons are frozen, the Jahn–Teller distortion becomes cooperative as in the O′ structure of compounds with small values of x. The more conducting rhombohedral compounds with $x \approx 0.3$ have equal Mn–O bond lengths imposed by symmetry, but dynamically-fluctuating local distortions may still stabilize the Jahn–Teller polarons [174]. Both static and dynamic distortions have been evidenced by neutron diffraction.

The Jahn–Teller polaron can form in a solid when the Jahn–Teller stabilization energy δ_{JT} is comparable with the conduction electron bandwidth W. Unlike the dielectric polaron where a charge polarisation decorates the carriers and a local isotropic distortion increases their effective mass, the Jahn–Teller polaron carries with it an anisotropic local distortion which removes the degeneracy of the electronic ground state. Some evidence for the Jahn–Teller polaron is seen in the temperature-

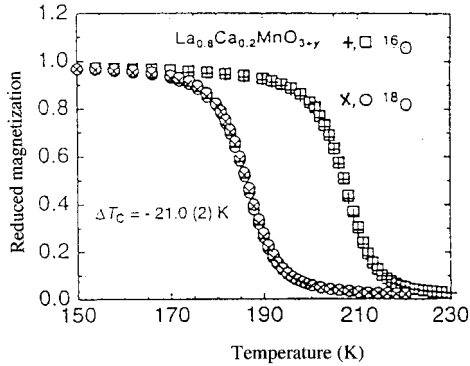

Figure 58. Temperature dependence of the magnetization of $(La_{0.8}Ca_{0.2})MnO_3$ samples made with different oxygen isotopes. [Reprinted with permission from *Nature*, Volume 381, page 676, [6], © 1996 Macmillan Magazines Ltd, and the authors, G. Zhao, K. Conder, H. Keller and K. A. Müller.]

dependence of the lattice parameters of orthorhombic samples with $x \approx 0.3$. As these manganites with $x \approx 0.3$ are cooled towards T_C, the ratio $c/2^{1/2}a$ in the orthorhombic cell decreases sharply [159, 187, 190, 319] reflecting an increasing deformation of the MnO_6 octahedron in the basal plane which splits the e_g band. The greater the distortion, the more localized are the charge carriers. This deformation disappears in the metallic state, below T_C. The dynamic Jahn–Teller effect has been detected through the variation of the Debye–Waller factor for samples with $x \approx 0.3$ in the vicinity of T_C [190, 413, 415] and in measurements of the optical conductivity [416, 583]. Ion channeling experiments also seem to provide direct evidence for a dynamic Jahn–Teller distortion around T_C [417]. Neutron Pair Distribution Function analysis [571] has shown the presence of local Jahn–Teller distortions above and below the magnetic ordering temperature for $(La_{1-x}Sr_x)MnO_3$ with $0 < x < 0.4$. Local distortions exist even in the metallic phase. The holes are shared among three Mn states at low temperatures, but they are localized on a single site in the paramagnetic state. Other pair distribution function measurements have been interpreted in terms of dielectric polarons above T_c [408].

More dramatic evidence for polarons, which are probably the Jahn–Teller variety, is the isotope effect on the Curie temperature discovered in $(La_{0.8}Ca_{0.2})MnO_3$ by Zhao *et al.* [6] (figure 58). T_C is 21 K higher in samples made with ^{16}O than in those made with ^{18}O. An isotope effect on the EPR signal is also associated with a larger exchange integral in ^{16}O than in ^{18}O samples [418].

The composition with $x = 0.2$ is one where the dynamic Jahn–Teller effect for Mn^{4+} is most pronounced [285]. No such isotope effect is found in the ferromagnetic perovskite $SrRuO_3$, where there is no strong Jahn–Teller ion. The effective polaron bandwidth W_{eff} depends on the characteristic frequency ω of the optical phonons involved:

$$W_{\text{eff}} = W \exp\left(-\frac{\gamma \delta_{\text{JT}}}{\hbar\omega}\right) \tag{4.6}$$

where W is the bare bandwidth, δ_{JT} is the Jahn–Teller stabilization energy which is about 0.5 eV [185, 203, 338] and γ is a parameter depending on δ_{JT}/W, which is in the range 0–1 [6]. Another estimate of δ_{JT} is 0.35 eV [354]. The phonon frequency varies

as $M^{-1/2}$, where M is the isotope mass. Hence a significant reduction in W_{eff} is expected on passing from ^{16}O to ^{18}O. This translates into a reduction in Curie temperature since $T_C \propto W_{\text{eff}}$ in the limit where the Hund rule coupling $J_H \gg W_{\text{eff}}$ [21, 174]. Kresin and Wolf [548] relate this effect to the Franck–Condon factor, and hence to the oxygen mass. In some cases a metal–insulator transition is induced by replacing ^{16}O by ^{18}O [557, 559].

The absence of polaron conduction and CMR effects in mixed-valence cobalt perovskites [561] is indirect evidence in favour of Jahn–Teller polarons in manganites, since neither low-spin nor high-spin Co^{4+} is a strong Jahn–Teller ion.

4.3.2. *Other transport properties*

4.3.2.1. *Hall effect.* In contrast with normal metals and semiconductors, the Hall resistivity of magnetic materials, contains an additional term which depends on the magnetization:

$$\rho_{xy} = R_0 B + \mu_0 R_E M, \tag{4.7}$$

where the normal Hall coefficient R_0 is $-1/ne$ and the extraordinary Hall coefficient R_E depends on asymmetric electron scattering due to spin-orbit coupling. R_E may be positive, negative or even zero in special cases. In ferromagnets, the second term is frequently, but not necessarily, more than an order of magnitude larger than the ordinary Hall effect [419]. Any real measurement also includes a term which is due to the extrinsic *IR* drop because the voltage contacts do not lie on an equipotential. If a simple one-carrier model is assumed, the Hall mobility $\mu_H = R_0/\rho$ may be deduced from measured values of R_0 and the normal resistivity $\rho = \rho_{xx}$.

The sign of the Hall carriers in the ferromagnetic state of mixed-valence manganites should depend critically on the Jahn–Teller splitting of the e_g band [420]. If this band is fully split, the expected carrier concentration is x holes ($x < 0.5$) whereas, if it is unsplit, the carrier concentration should be $1 - x$ electrons. However, holes in the oxygen 2p band may also contribute to the Hall signal.

The manganites are awkward materials for Hall effect measurements. One experimental problem arises because it may be difficult to achieve magnetic saturation. Even far below T_C, the magnetization curve of most manganites shows a high-field slope which means that the second term in equation (4.7) mimics the first term. Another problem arises when the magnetoresistance is large; any imbalance in the Hall leads produces a ρ_{xx} signal which may mask the Hall contribution and it is necessary to separate the odd and even parts.

Volger [10], in his first measurements of the Hall effect in ceramics of $(La_{1-x}Sr_x)MnO_3$ [10], obtained a very low value for the mobility in the paramagnetic state. The Hall coefficient is negative and the deduced electron concentration contradicts thermopower measurements (see below). In the ferromagnetic state, Volger reported that the extraordinary Hall effect is small and negative and superimposed on the immeasurably small normal part. An upper limit obtained for the mobility is only $10^{-5}\,m^2\,V^{-1}\,s^{-1}$, the real value being 'probably even considerably less'. 30 years later, Tanaka *et al.* [421] reported Hall effect measurements on polycrystalline $(La_{0.8}Ca_{0.2})MnO_3$. Because of the smallness of the signals only an upper limit on the mobility could be estimated as $7 \times 10^{-6}\,m^2\,V^{-1}\,s^{-1}$ at 300 K. Since the mean free path λ equals $v_F m\mu/e$ where v_F is the Fermi velocity (equal to about $10^6\,m\,s^{-1}$), this leads to a λ of less than a tenth of a nanometer, inconsistent with band transport. A similar mobility was measured

in a crystal of $(Nd_{0.5}Pb_{0.5})MnO_3$ near T_C [80], and a carrier concentration of $5 \times 10^{26}\,m^{-3}$ below 100 K was deduced. Liu *et al.* [363] reported successful Hall effect measurements on their single crystals of $La_{0.65}(PbCa)_{0.35}MnO_3$ at 5 K where the resistivities were in the microhm metre range. The inferred electron density is typically metallic with $n_H \approx 10^{29}\,m^{-3}$. This result is consistent with the density of states deduced from low-temperature heat capacity measurements which lead to a metallic density of states for a range of polycrystalline samples [359].

Low temperature data have also been reported for thin films of $(La_{0.67}Ca_{0.33})MnO_3$ and $(La_{0.67}Sr_{0.33})MnO_3$ [122]. At first, no extraordinary Hall effect was observed in either of these films, or in gadolinium-doped $(La_{0.67}Ca_{0.33})MnO_3$ [422]. This is reminiscent of the behaviour of the europium chalcogenides [423, 424], and may reflect the fact that no orbital angular momentum is associated with the $^4A_{2g}$ state of the Mn^{4+} ion. Subsequently, an extraordinary Hall effect was seen in measurements near T_C on the calcium compound [377]. Values of 0.9 holes per manganese atom and 2.1 holes per manganese atom were deduced from R_0 by Snyder *et al.* [122, 373] for the calcium and strontium compounds respectively. These values, together with the low-temperature resistivity, lead to a reasonable mean free path of about 8 nm, although the number of holes is too large with respect to the doping level indicated by the formulae. In another report [425], the apparent hole concentration for the calcium compound is more than an order of magnitude less and temperature dependent, increasing below T_C. The Hall effect was also measured on $(La_{0.7}Ba_{0.3})MnO_3$ [426] and $(La_{0.33}Ca_{0.67})MnO_3$ [591] thin films over the entire range of temperatures. The latter data are interpreted in terms of small polaron theory. In the former case, the extraordinary part of the Hall voltage is positive and clearly visible at low fields (figure 59). The normal part of the Hall effect is negative, but electron densities of the order of 6 electrons per manganese atom were inferred from the high-field slopes. This obviously unphysical result may arise from the linear high-field slope of the magnetization curve which leads to an underestimate of the normal Hall coefficient. There is a difference in the sign of R_0 in these $x = 0.3$ films

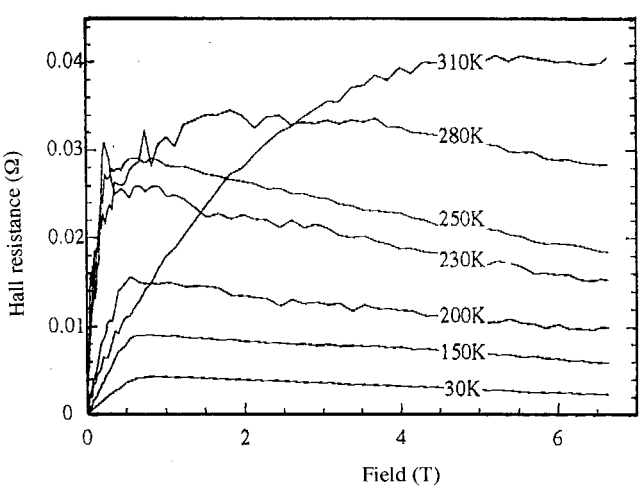

Figure 59. Hall resistance in a $(La_{0.67}Ba_{0.33})MnO_3$ film at different temperatures. The extraordinary Hall effect is visible at low fields, and the normal (high-field) Hall voltage is negative [426]. [Reprinted by kind permission of R. von Helmholt.]

with barium, and those with strontium or calcium [122, 425]. In gadolinium-doped $(La_{0.67}Ca_{0.33})MnO_3$, R_0 is also negative, and it is thermally activated above $2T_C$ with an activation energy of 0.9 eV. This is evidence for small-polaron conduction in the paramagnetic state [422].

An extraordinary Hall effect is measured in both the antiferromagnetic and the ferromagnetic phases of $(Pr_{0.5}Ca_{0.5})MnO_3$. The normal term corresponds to 0.8 holes per formula, with a mobility of $5 \times 10^{-6}\ m^2\ V^{-1}\ s^{-1}$ [427].

4.3.2.2. *Thermoelectric power.* Measurement of the electric field induced by a temperature gradient across a sample provides complementary information to the resistivity. The Seebeck coefficient S is defined as $\Delta V/\Delta T$, the thermoelectric voltage per degree of temperature difference. Because no current flows, the thermopower does not depend on the connectivity of conducting regions, and the thermopowers of individual grains are additive. There have been many measurements of the thermopower of samples with $x \approx 0.3$ which exhibit a metal–insulator transition [10, 401, 421, 428–435]. These data, on ceramics, thin films and single crystals, are not very consistent and results are sensitive to details of sample preparation and composition [433]. Thermopower has also been reported for $(LaMn)_{1-\delta}MnO_3$ as a function of δ [175, 236]. There are calculations as a function of U_{dd} and δ_{JT} [436].

The Seebeck coefficient of a metal in the free-electron model is

$$S = \frac{k}{|e|}\left(\frac{kT}{E_F}\right) = 87\frac{kT}{E_F}\ \mu V\ K^{-1}. \tag{4.8}$$

For example, the value at 100 K when the Fermi energy E_F is 1 eV is about 1 $\mu V\ K^{-1}$. Several groups have independently measured samples which show a very small thermopower in the metallic state below T_C ($S < 2\ \mu V\ K^{-1}$), with no evident temperature dependence [400, 421, 428, 431, 437, 438]. Zhou *et al.* interpreted this as evidence of condensation of the conduction electrons below T_C into a novel extended vibronic state where the quasiparticles are electrons coupled to the dynamic Jahn–Teller distortions, which exhibit no dispersion. However, the data below T_C on some $(La_{1-x}Sr_x)MnO_3$ single crystals [429] and $(La_{0.67}Ca_{0.33})MnO_3$ thin films [401] exhibit a different behaviour, which might be construed as a superposition of metallic, ferromagnetic [439] and phonon drag terms.

Tanaka *et al.* [421] published data obtained on oxygen-controlled $[(La_{0.8}Ca_{0.2})Mn]_{1-\delta}O_3$ polycrystalline samples with $0 < \delta < 0.2$. Positive or near-zero thermopower was measured for all samples over the entire temperature range, indicating that mobile carriers are mainly holes. The two regimes visible in the resistivity against temperature curves are reflected in the thermopower. Below T_C, the effect is nearly zero and independent of T or else proportional to T in samples showing metallic resistivity. For non-metallic cation-deficient samples with $\delta > 0.01$, whose resistivities are activated over the entire range of temperatures, and for the metallic samples above T_C, S varies roughly as $1/T$.

When the resistivity is thermally activated, the thermopower may also be expected to show semiconducting-like behaviour. The Seebeck coefficient for a semiconductor is

$$S = -\frac{k}{|e|}\left(\frac{\Delta}{kT} + B\right) = -87\left(\frac{\Delta}{kT} + B\right)\ \mu V\ K^{-1} \tag{4.9}$$

where Δ is an activation energy, positive for electrons or negative for holes, and B is a constant of order ln 2 which is related to the entropy of the carriers. It is sometimes written as $\ln[2(1-c)/c]$ where c is the number of carriers per site; the factor 2 is due to spin degeneracy. Thermopower varying as $1/T$ has generally been observed above T_C. The activation energy Δ inferred from the $1/T$ variation is a factor of three to ten smaller than that deduced from resistivity measurements [401, 432], which is characteristic of a hopping conduction process [437, 440]. The thermopower of $(La_{1-y}Y_y)_{0.67}Ca_{0.33}MnO_3$ depends sensitively on the e_g bandwidth [434]. There is often a broad peak near T_C in samples showing a metal–insulator transition which is attributed by Mahendiran *et al.* [184] to a coupling of holes and spins, analogous to phonon drag. In many cases, the thermopower changes sign from positive below T_C to negative well above T_C. The zero crossing may be explained by the opposite signs of the hole contribution and the entropy term B in equation (4.9). However, no evidence has been found of a $T^{-1/2}$ variation predicted by Mott and Davies [50] for VRH in the range where a $\log\rho$ against $T^{-1/4}$ law fits the resistivity data [401]. There is a strong magnetic field dependence of S in the vicinity of T_C which demonstrates that the carriers are magnetic in character. When a large positive anomaly is observed around T_C, the thermopower is reduced by the field (giant magnetothermopower) [401, 432, 441]. At higher temperatures, when the thermopower has become negative, the effect of the field is to reduce its absolute value [429]. Well above T_C the magnetic field has little effect on S, and it is thought that the transport there is due to hopping of dielectric polarons [441]. A typical curve of S against T is shown in figure 60.

The pressure dependence of S has been measured by Zhou and co-workers [277, 431] who found that the large positive bump above T_C is reduced in magnitude as the Curie temperature is increased by pressure.

Thermopower measurements were carried out across the entire composition range by Volger [10] for $(La_{1-x}Sr_x)MnO_3$, by the Bangalore group for $(La_{1-x}Ca_x)MnO_3$ [184] and by the Czech group [192] for the $(Pr_{1-x}Ca_x)MnO_3$ series. The praseodymium compounds show no ferromagnetic metal phase, and

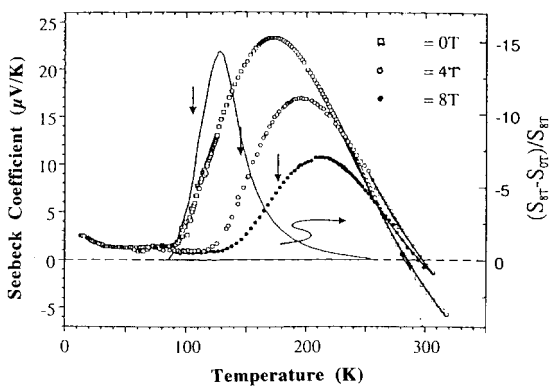

Figure 60. Typical thermopower measurement as a function of temperature for a $(La_{0.67}Ca_{0.33})MnO_3$ thin film, (——) $\Delta S/S(H)$. [Reprinted by kind permission of the American Physical Society from page 1576 of *Applied Physics Review Letters*, Volume 68, 1996, [401], and the authors, M. Jaime, M. B. Salamon, K. Pettit, M. Rubinstein, R. E. Treece, J. S. Horwitz and D. B. Chrisey, © 1996 by the American Physical Society.]

therefore no metal–insulator transition. The behaviour of the thermopower is not greatly changed at the magnetic phase transitions, in contrast with what happens at the crystallographic transitions. Jirak *et al.* [192] concluded that, in the low-doping regime, $x < 0.3$, their compounds show p-type activated behaviour. The $x = 0.4$ sample was p type above the Néel point (170 K) and n type below. For all higher doping levels the conduction is essentially n type. The Seebeck coefficient for $(Nd_{0.5}(Sr,Pb)_{0.5}MnO_3$ is negative for $T > 100$ K [432]. Likewise those of $(La_{1-x}Ca_x)MnO_3$ and $(La_{1-x}Sr_x)MnO_3$ become negative when $x > 0.25$ [185, 438, 442]. The p-type conduction at low doping levels is consistent with Jahn–Teller splitting of the e_g band. The sign of $S(T)$ at $x = 0.3$ depends on cation size [443]. The thermopower in the small-polaron regime above T_C is smaller than expected from the nominal Mn^{3+} to Mn^{4+} ratio [438]. Cation-deficient $(LaMn)_{1-\delta}O_3$ shows a positive thermopower at all temperatures, indicating that the holes produced by cation doping are different in nature to those produced by cation deficiency [433, 442].

4.3.3. *Heterostructures*

Sandwich structures and superlattices have been prepared from the ferromagnetic manganites with non-magnetic spacer layers, that may be insulating, metallic or superconducting.

In superlattices of $(La_{0.67}Ca_{0.33})MnO_3$ and the ferromagnetic metallic oxide $SrRuO_3$ ($T_C = 162$ K), enhancement of the magnetoresistance effect in the ferromagnetic state at low temperatures in the superlattice compared with the pure film is ascribed to spin-dependent scattering at the interfaces [444].

Tunnel spin valves, sandwich structures where an insulating barrier separates two ferromagnetic layers, are appropriate systems for an enhanced magnetoresistive response since small applied fields can modify the magnetic configuration. The barrier decouples the ferromagnetic electrodes so that their relative orientation can easily be changed. Trilayers can be fabricated for current perpendicular to the plane geometry using conventional ultraviolet lithography. In tunnel junctions with fully polarized electrodes, electron tunnelling (supposedly without spin flip) is classically forbidden when the electrodes have antiparallel magnetization. The IBM group first reported magnetoresistive effects in excess of 80% in $(La_{0.7}Sr_{0.3})MnO_3/SrTiO_3/(La_{0.7}Sr_{0.3})MnO_3$ or $(La_{0.7}Ca_{0.3})MnO_3/SrTiO_3/(La_{0.7}Ca_{0.3})MnO_3$ trilayers at 4.2 K [445, 446]. A similar structure where a $SrTiO_3$ layer 3 nm thick separates manganite layers 25 and 33 nm thick has been measured by Viret *et al.* [447]. Charge carriers were forced to tunnel between a $(La_{0.7}Sr_{0.3})MnO_3$ bottom stripe into a 6 μm side $(La_{0.7}Sr_{0.3})MnO_3$ square through the insulator 3 nm thick. Figure 61 shows a magnetoresistance curve at 4.2 K where the nominal resistance is multiplied by 5.5 when the top square flips into the antiparallel configuration. This magnetoresistive effect at such low fields (of the order of 10 mT) is the highest yet reported in any magnetoresistive system. Effects of this magnitude demonstrate the high degree of spin polarization of electrons at the Fermi level in mixed-valence manganites. A quantitative estimate of the spin polarization can be made using the relation [69] $(S_{\uparrow\uparrow} - S_{\uparrow\downarrow})/(S_{\uparrow\uparrow} + S_{\uparrow\downarrow}) = (1 - 2a)^2$, where $S_{\uparrow\uparrow}$ and $S_{\uparrow\downarrow}$ are the conductances in the parallel and antiparallel states, and a is the proportion of spin-up carriers. A 450% magnetoresistive effect gives $a = 0.91$ and a polarization of $P = 83\%$. This is much higher than in any of the 3d metals or alloys, where the largest polarization of tunnelling electrons is 40%, for iron [69]. A high degree of spin polarization ($P > 80\%$) has also been inferred for $(La_{0.67}Ca_{0.3})MnO_3$ and $(La_{0.7}Sr_{0.3})MnO_3$ by

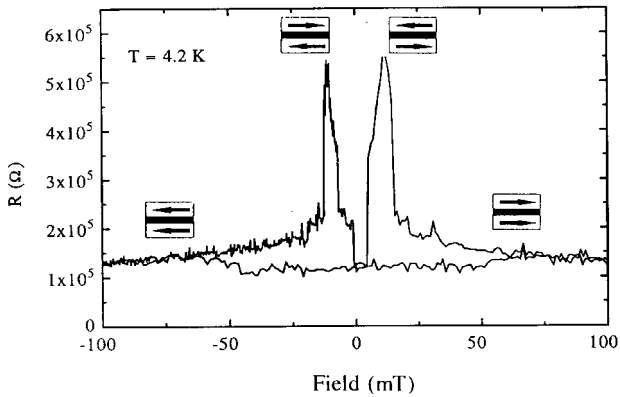

Figure 61. Magnetoresistance ratio for a sandwich structure of two $(La_{0.67}Sr_{0.33})MnO_3$ films separated by a 3 nm layer of $SrTiO_3$. The applied field switches the magnetization of the two magnetic layers. [Reprinted from page 545 of *Europhysics Letters*, Volume 39, 1997, [447] by kind permission of EDP Sciences.]

several other techniques [212, 447, 567]. There is evidence from spin-resolved photoemission and magnetic circular dichroism that the magnetization of the surface layer falls much more rapidly than the bulk [587].

Positive or negative magnetoresistance is reported in tunnel junctions where one of the manganite electrodes is replaced by Fe_3O_4 [602].

The magnetoresistance of tunnel spin valves falls dramatically as the temperature is raised. This was explained by the presence of an oxygen-deficient layer at the $SrTiO_3$–$(La_{0.7}Sr_{0.3})MnO_3$ interface which has a lower Curie temperature than the bulk of the $(La_{0.7}Sr_{0.3})MnO_3$ and induces spin flipping which decreases the magnetoresistive effects. A similar problem has been identified in fine-grained polycrystalline ceramics [379]. It appears crucial to be able to control the magnetization of the interface layer in order to achieve a large effect at room temperature. The effect is also sensitive to the bias used to measure the resistance as the I–V curves are nonlinear [573, 447, 581]. The differential conductance is actually maximum at a bias of ± 1.7 V, which is comparable to the width of the e_g band [581].

Owing to the similarities between the crystal structure of high-temperature superconductors and the manganites, it is possible to make heterostructures involving layers of these two families. A group at Hitachi laboratories first produced these structures [111], and studied the I–V curves and electronic transport between two superconducting layers separated by a manganite barrier [111, 448]. They argued that supercurrents were able to tunnel through up to 500 nm of ferromagnetic manganite. The I–V curves showing tunnelling-like behaviour were reproduced by others who demonstrated (by Faraday rotation measurements) that the $(La_{0.7}Ca_{0.3})MnO_3$ layer remained ferromagnetic [449], and reported Shapiro-like steps under microwave illumination [110]. However, this does not constitute evidence for tunnelling through the full layer. It is possible that the measurements can be explained by a proximity effect with a very resistive interface between the superconductor and the manganite due to interdiffusion of copper and manganese, and no novel tunnelling effect is required. More recently, $YBa_2Cu_3O_7/(La_{0.7}Ca_{0.3})MnO_3/YBa_2Cu_3O_7$ trilayers were successfully prepared for current-perpendicular-to-plane measurements by post-deposition lithography [450]. The resulting devices exhibit no

supercurrents, and the electrical conduction could be well described by the Glazman–Matveev [451] model for inelastic quasiparticle tunnelling via localized states.

Other structures have been studied in the current-in-plane configuration [112, 115]. The Hitachi group reported on the magnetoresistive effects of trilayer structures in which a thin (500 Å) $YBa_2Cu_3O_7$ layer is sandwiched between two thicker (1500 Å) $(La_{0.7}Ca_{0.3})MnO_3$ layers. The negative magnetoresistance measured at 77 K was reported to be enhanced compared with that of a single layer. It seems likely that the oxygen stoichiometry of both $YBa_2Cu_3O_7$ and $(La_{0.7}Ca_{0.3})MnO_3$ is changed when synthesized in heterostructures. A shift in Curie temperatures of the manganite layer may generate the change in magnetoresistive effect.

Jakob *et al.* [115] and Xiong et al [452] prepared $YBa_2Cu_3O_7/(La_{0.7}Ba_{0.3})MnO_3/YBa_2Cu_3O_7$ superlattices with thicknesses ranging from 2 to 10 nm by a sputtering technique. Although the superconducting transition temperature of the $YBa_2Cu_3O_7$ was reduced in the as-deposited structures from 89 to 40 K, they were able to show that superconductivity and magnetism coexist, confined to their respective layers. The magnetoresistance and superconductivity phenomena behave independently, and the influence of the direction of an applied field (going from in plane to out of plane) provided the evidence for decoupling of the superconducting and magnetic layers. This result is incompatible with supercurrent tunnelling through the manganite layers.

A trilayer device involving an underlayer of $(La_{0.67}Sr_{0.33})MnO_3$ with an ultrathin layer of La_2CuO_4 and a top layer of superconducting $DyBa_2Cu_3O_7$ ($T_{sc} = 71$ K) suggests that the critical current of the superconductor is greatly reduced when a current flows in the ferromagnetic underlayer [453] (figure 62). This is attributed to pair breaking caused by spin-polarized carriers injected into $DyBa_2Cu_3O_7$. Fast switching devices might be based on this phenomenon, but the magnetic and heating effects of the injection current have to be carefully distinguished.

To conclude, it has been demonstrated that epitaxial structures of high-T_C superconductors and manganites can be grown. The current-in-plane measurements evidence the decoupling of superconductivity and magnetism. The interesting

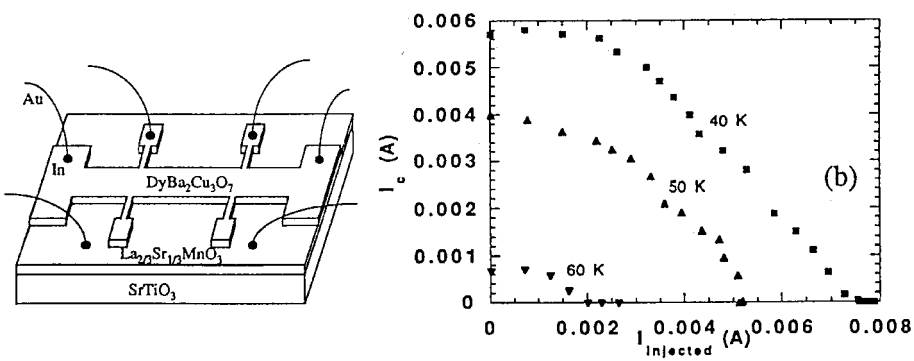

Figure 62. Ferromagnetic/superconductor device and observed variation in the critical current of the $DyBa_2Cu_3O_7$ as a function of the current injected from the $(La_{0.7}Sr_{0.3})MnO_3$ layer. [Reprinted by kind permission of the American Physical Society from page 1134 of *Physical Review Letters*, Volume 78, 1992, [453], and the authors, V. A. Vas'ko, V. A. Larkin, P. A. Kraus, K. R. Nikolaev, D. E. Grupp, C. A. Nordman and A. M. Goldman, © 1992 by the American Physical Society.]

potential interplay between the two effects will be better seen in precise current-out-of-plane experiments where spin-polarized electrons are made to traverse superconducting regions, or Cooper pairs forced into magnetic surroundings. The main experimental difficulty in achieving synthesis of thin good-quality sandwich layers resides in the quality of the interfaces. Most groups find that the barrier layers exhibit very high resistivities probably owing to poor interface quality associated with interdiffusion of copper and manganese which would prevent charge carriers from crossing the structures unscathed.

A current out-of-plane heterostructure designed by Gibbs and Gehring to change the magnetization, and hence the resistance, of a manganite layer by injection of spin-polarized carriers has the layer of $(La_{0.7}\ Ca_{0.3})MnO_3$ sandwiched between two layers of nickel or permalloy [564, 565]. Again interface scattering is the dominant effect.

Hysteretic resistance changes of 100% have been reported in a field-effect transistor (FET) structure with a manganite channel and a ferroelectric gate electrode [577].

4.3.4. *Models*

Spin disorder scattering has been repeatedly invoked to explain the transport properties of GMR systems. The first models were developed in the late 1950s and 1960s by deGennes and Friedel [36], Kasuya [439], van Peski-Tinbergen and Dekker [454] and Fisher and Langer [37]. These early calculations deal with spin scattering of conduction electrons in ferromagnetic metals and degenerate semiconductors. Resistivity anomalies are expected at the Curie point because of the onset of magnetic order. Friedel and deGennes have considered the effects of long-range order on the scattering near the critical point. Above T_C, the magnetic scattering is constant and temperature independent. They deduced, however, that the resistivity should present a singularity at the Curie temperature with a smooth decrease in scattering below T_C. Fisher and Langer argued that short-range fluctuations make the dominant contribution to the temperature-dependent part of the resistivity, so that the singularity should be in the derivative of the resistivity at T_C (which is expected to follow the heat capacity). These theories apply to ferromagnetic metals where the densities of conduction electrons with up and down spins are comparable ($N^{\uparrow} \approx N^{\downarrow}$). However, for double-exchange materials, Searle and Wang [12] pointed out that this approximation is invalid. In fact, $(N^{\uparrow} - N^{\downarrow})/(N^{\uparrow} + N^{\downarrow})$ is of order $\Delta E/E_F$ where ΔE is the energy difference of spin up and spin down electrons and E_F is the Fermi level. In the double-exchange case, we have $\Delta E/E_F > 1$. In most conventional models, the scattering by spin disorder enters the expression of the conductivity via the scattering cross section. To calculate it, theories use the Born approximation or take $\Delta E/E_F$ as an expansion parameter, both of which require $\Delta E/E_F \ll 1$. Kasuya's [439] expression, however, was used successfully in lightly doped EuO [455], although $\Delta E/E_F \gg 1$, and the results were confirmed independently by later work [46].

Searle and Wang [12] constructed a simple model from the molecular-field approach considering a strong coupling between the manganese cores and the conduction-electron spins. They consider two kinds of possible excitation: the first consists in flipping one manganese spin along with the spin of any Zener electron located at the site (because of the Hund coupling). This effectively removes that electron from those contributing to the global double-exchange interaction since it

can no longer hop from its site to the others (its spin is no longer parallel to that of the other manganese cores). The second is the spin flip of a manganese core alone which does not remove an electron from the double-exchange interaction. Hence, electrons can be separated into two groups: those contributing to the double-exchange interaction and those which do not. Zener [3] derived the expression for the decrease in energy due to the double-exchange interaction:

$$\Delta E_{\mathrm{DE}} = -K\langle S_{\mathrm{d}z}\rangle\langle s_z\rangle + \tfrac{1}{2}\gamma\langle s_z\rangle^2, \tag{4.10}$$

where K represents the decrease in energy due to long-range spin correlation (due to the Hund coupling), γ the increase in the average kinetic energy associated with the increasing bandwidth and $\langle S_{\mathrm{d}z}\rangle$ and $\langle s_z\rangle$ the macroscopic averages of spin polarizations associated with Mn^{4+} cores and Zener electron spins respectively. It is then possible to write the total energy density of the electron system as a function of the average spin polarizations associated with the manganese cores and the double-exchange electrons, which can be expressed as a function of the applied field using a molecular-field expression. The scattering probabilities of the electrons are then calculated following Zener's assumptions that an electron can only travel between two manganese sites if they have parallel spins. The scattering probabilities ($P^{\uparrow}$ and $P^{\downarrow}$ respectively for up electrons and down electrons) can then be expressed as a function of the average spin polarization ($\langle s_z\rangle$, with z the quantization axis given by the external field) of the electrons in a very simple manner:

$$P^{\uparrow} = \tfrac{1}{2} - \langle s_z\rangle,\ P^{\downarrow} = \tfrac{1}{2} + \langle s_z\rangle, \tag{4.11}$$

and $\langle s_z\rangle$ is proportional to $\langle S_{\mathrm{d}z}\rangle$. It may be evaluated by using the reduced magnetization, $M(T)/M(0)$. Conductivities of up and down bands are inversely proportional to the scattering probabilities and the expression for the total conductivity obtained by Searle and Wang is

$$\sigma_t = \sigma^{\uparrow} + \sigma^{\downarrow} = \frac{1}{C}\left(\frac{N^{\downarrow}}{1 + M(T)/M(0)} + \frac{N^{\uparrow}}{1 - M(T)/M(0)}\right) \tag{4.12}$$

with C an adjustable parameter. Expressing the up and down electron populations as functions of the scattering probabilities, and hence the normalized magnetization, one gets

$$\sigma_t = \frac{N}{C}\frac{1 + [M(T)/M(0)]^2}{1 - [M(T)/M(0)]^2} \tag{4.13}$$

with N the total carrier density. Figure 63 compares the result of fits from different models to the resistivity curve obtained by the Canadian group in their single crystals of $(La, Pb)MnO_3$. The model gives a fairly good fit to their data.

Kubo and Ohata [456] obtained essentially the same result from a more rigorous approach starting from the double exchange Hamiltonian (also known as the s–d model or Kondo lattice Hamiltonian, although the s–S coupling here is positive, whereas in the Kondo effect it is negative)

$$H = -t_{\mathrm{eff}} \sum_{\langle ij\rangle\sigma} c^{\dagger}_{i\sigma} c_{j\sigma} - J_{\mathrm{H}} \sum_i \mathbf{S}_i \cdot \mathbf{s}_i. \tag{4.14}$$

They detailed the resulting conductivity further by calculating that the resistivity should vary as $T^{9/2}$ at low temperature in the spin-wave approximation. Although, as already indicated in section 4.3.12, temperature exponents of the order of 2 were

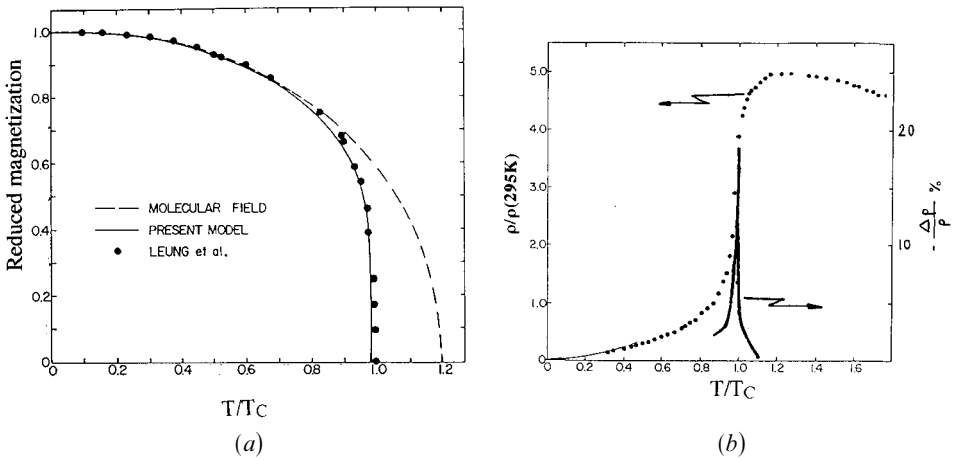

Figure 63. (*a*) Reduced magnetization of $(La_{0.69}Pb_{0.31})MnO_3$ crystal as a function of temperature: (●), experimental data; (——), based on model of Searle and Wang [12]; (- - -), result of the standard molecular field approximation. (*b*) Normalized resistivity and magnetoresistance in 1 T as a function of T/T_C: (●), experimental data; (——), solid line is based on the model of Searle and Wang [12]. [Reprinted from page 2023 of *Canadian Journal of Physics*, Volume 48, by C. W. Searle and S. T. Wang, © 1970 [12], by kind permission of NRC Research Press].

measured at low temperature, $T^{9/2}$ corrections have been seen by Snyder *et al.* [122]. Furukawa [457] included a term $-\mu\sum_{j\sigma} n_\sigma$ where μ is the chemical potential, and pointed out that large shifts of μ ($\approx 0.1\,W$) are to be expected as a function of temperature and magnetization.

It is noticeable that the extremely steep slope of the $R(T)$ curve just below T_C (figure 46) cannot be accounted for by the above models. Consequently, several groups have developed other models to account for the temperature and magnetic field dependences of the resistivity, and have proposed scaling relationships between ρ and M. [232, 375, 399, 458, 459]. Pierre *et al.* [460] proposed an exchange-induced band crossing model, like EuO (figure 11). Zhang [420] considered a spin-polaron model with clustering where the transfer integral is treated as a perturbation. Another approach is a qualitative percolation model based on transport of Ising-like spins on a resistor network [461]. The work of Hundley *et al.* [399], based on the observation that transport occurs by hopping above T_C, resulted in the following empirical relationship:

$$\rho(H, T) = \rho_m \exp\left(\frac{-M(H, T)}{M_0}\right), \tag{4.15}$$

where ρ_m and M_0 are fitting parameters. Although, in general, ρ_m is linear in T for hopping processes near 250 K, Hundley *et al.* were able to fit data over a wide temperature range using $\rho_m = 21\,m\Omega\,cm$ and $\mu_0 M_0 = 0.20\,T$ (figure 4.64). This suggested a direct link between resistivity and the state of magnetization of the sample. Furthermore, the relationship is exponential, leading to a picture in which the binding energy of the carrier is magnetization dependent. Nonetheless, quantitative agreement depends on the fitting parameters (M_s is one third of the experimental magnetization) and their interpretation is unclear. Dionne [459] proposed a similar model where the thermally-activated hopping energy depends on magnetiza-

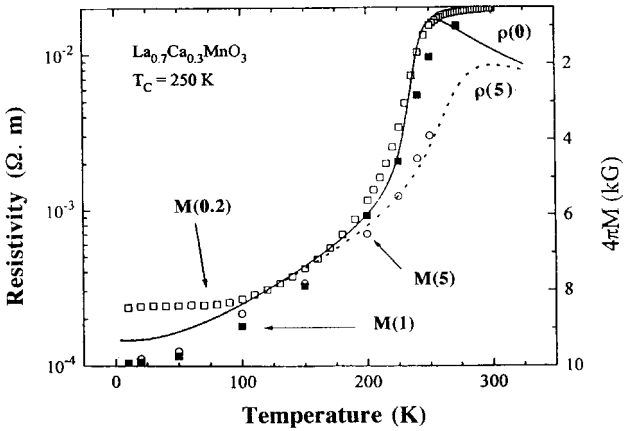

Figure 64. Resistivity data on $(La_{0.7}Ca_{0.3})MnO_3$ at different temperatures and applied fields scaled in terms of the magnetization. [Reprinted by kind permission of the American Physical Society from page 860 of *Applied Physics Letters*, Volume 67, 1995, [399] and the authors, M. F. Hundley, M. Hawley, R. H. Heffner, Q. X. Jia, J. J. Neumeier and J. Tesmer, © 1995 by the American Physical Society.]

tion [458]. Another form of phenomenology incorporates a two-current model [462, 463], where the conductivity of one channel is purely dependent on magnetic order, and the other is due to excitation of carriers across a gap E_0. The form chosen [463], namely

$$\sigma = a\alpha\left(\frac{M}{M_s}\right)^2 + \beta \exp\frac{-E_0}{kT} \tag{4.16}$$

where α, β and E_0 are fitting parameters mimics the observed transport reasonably well. At low temperatures, the first term is large and short circuits the sample. At T_C, the magnetization becomes zero, and only the second term remains. Snyder *et al.* [377] suggested that the magnetoresistance above and below T_C are best fitted by a resistance in series with a magnetoconductor giving the empirical expression

$$\rho = \rho_\infty + \frac{1}{\sigma_0 + F(H)} \tag{4.17}$$

where $F(H) \approx |H|$ for $T < T_C$ and $F(H) \approx H^2$ for $T > T_C$.

Several attempts have been made to incorporate both magnetic and lattice effects within one theoretical framework. Apart from any shortcomings in fitting the data to a magnetic term alone, there is experimental evidence from near-edge X-ray absorption [414] and ion channelling [417] for local lattice distortions, especially above T_C, in calcium- or barium-doped $LaMnO_3$. Furthermore, a more rigorous quantitative calculation by Millis *et al.* [338] based on the double-exchange Hamiltonian (equation (4.14)) was unable to give the correct order of magnitude for the Curie temperature and could not account for the experimental resistivity behaviour. Their main results for electrical transport were as follows.

(1) ρ only has a derivative discontinuity at T_C in the model while the resistivity peak is found around $T_C/2$.

(2) Below T_C, there are two terms in the expression for the resistivity: the amplitude of the spin fluctuations and an additional term proportional to M^2. Their effect is opposite and, at least near T_C, the latter dominates and makes the resistivity increase with increasing applied field.
(3) The calculated resistivity above T_C (about 1.5 mΩ cm) is far too small.

These observations are a consequence of the approximations made. If the Hund rule coupling J_H, is much greater than t, the average hopping energy (proportional to the bandwidth), local fluctuations of $\mathbf{S}_i \cdot \mathbf{S}_j$ scatter electrons. This is the case for the results of Millis *et al.* When $J_H \ll t$, fluctuations in $\mathbf{S}_i$ are most important and lead to the Fisher–Langer [37] predictions which yield decreasing resistivity with decreasing temperature. Since $J_H > t$ in manganites (table 5), Millis *et al.* are critical of any mean-field approach, including those of Searle and Wang [12] and Furukawa [464, 465]. They also point out that their result differs from the work of Kubo and Ohata [456] because of their inclusion of the $\mathbf{S}_i \cdot \mathbf{S}_j$ fluctuations. Millis *et al.* [338] argue that the magnetic fluctuations do not significantly reduce the electron bandwidth in the double exchange model, so that a Fermi liquid picture of weakly scattered bandlike electrons follows. Their calculation demonstrates that double exchange alone cannot account quantitatively for the properties of the manganites, and they suggest that a complementary mechanism, namely the Jahn–Teller distortion, should be included in a description of the motion of the e_g charge carriers. Millis and colleagues [174, 466] have also calculated the effects of combining Jahn–Teller distortions with magnetic interactions to obtain the resistivity and magnetic transition temperature. Qualitative agreement with experimental data is obtained. In addition, they have examined in detail the Fermi-liquid-to-polaron cross-over [339, 467], which was alluded to in the original work [338] to explain the low value for the conductivity.

Röder and co-workers [468, 469] have also studied a model which includes Jahn–Teller coupling in the double-exchange model. This model does not account for the resistivity in detail but finds that the charge is dressed by both lattice distortion and local magnetic order. Röder and co-workers showed that, for $T \ll T_C$, the polarons are very large, extending over many lattice sites and, consequently, overlap one another to form bands as envisaged by Zhou *et al.* [431]. For $T \approx T_C$, the carrier becomes self-trapped by the lattice distortion with spin polarization around the position of the hole. A similar conclusion has been drawn by Lee and Min [470]. This picture is very similar to the bound magnetic polaron of Kasuya and Yanase [39], except that the trapping potential is the substitutional impurity; for $T > T_C$, in the dilute limit, the polaron is a localized charge surrounded by a near-neighbour spin cloud.

An argument that the Jahn–Teller effect is inessential has been advanced by Varma [231] who points out that similar insulator–metal transitions occur in mixed-valence $Tm(Se_xTe_{1-x})$ compounds where no Jahn–Teller distortion exists. He explained the insulating state by carrier localization due to magnetic disorder, which creates non-diagonal disorder in the hopping matrix elements t_{ij} connecting near-neighbour sites where the spins are randomly distributed and slowly fluctuating. The result is a band where at least one half of the states are localized. If the carrier is localized, it will also tend to form a spin polaron whose motion in the presence of an electric field will be governed by the slow spin fluctuations. With increasing magnetic order, near and below T_C, these localization effects become smaller. Similarly, an

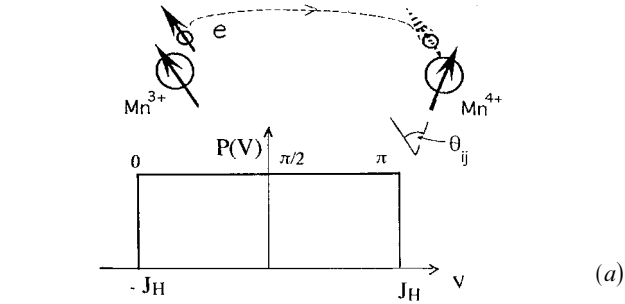

(a)

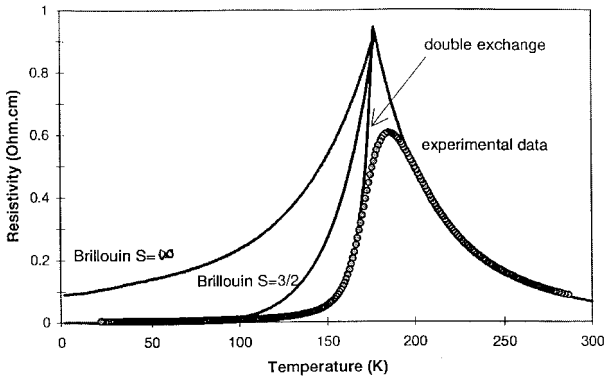

(b)

Figure 65. (*a*) The spin-dependent potential distribution $P(V)$ experienced by a hopping Zener electron in the paramagnetic state [232]. (*b*) Resistivity of a $La_{0.70}Ca_{0.3}MnO_3$ film fitted with the magnetic localization model equation (4.18) with different expressions for the magnetization. [Reprinted by kind permission of the American Physical Society from page 8067 of *Physical Review* B, Volume 55, 1997, and the authors, M. Viret, L. Ranno and J. M. D. Coey, © 1997 by the American Physical Society.]

applied magnetic field decreases the magnetic disorder and increases the localization length, thereby decreasing the resistivity.

The magnetic character of the metal–insulator transition and the VRH behaviour observed above T_C (figure 56) advocate a theory that combines these elements. The problem here is that localization lengths $1/\alpha$, inferred from T_0 using the expression $kT_0 = 18\alpha^3/N(E)$ appropriate for Anderson localization in doped semiconductors where $N(E)$ is the density of states, are of order 0.05 nm which is clearly unphysical [359]. The Dublin group [232, 471] developed the idea of carrier localization by magnetic rather than charge disorder to explain the transport properties over the entire range of temperature and field. The metal–insulator transition is ascribed to a modification of the spin-dependent exchange potential $-J_H\mathbf{s}\cdot\mathbf{S}$ associated with the onset of magnetic order at T_C. Here J_H is the on-site Hund rule exchange coupling of an e_g electron with $s = \frac{1}{2}$ to the t_{2g} ion core with $S = \frac{3}{2}$. Since $J_H \approx 1$ eV, there is a band of states of width $U_m \approx 2$ eV (equation (1.2)) into which the electron may hop (figure 65) and the e_g electrons may be localized by the random spin-dependent potential above T_C, where conduction is by VRH. When a magnetic field is applied to the manganite or when there is an internal molecular field, the random distribution of spin directions is narrowed, and the average magnetic potential decreases. Over the whole temperature range, the resistivity is expected to vary as [232]

$$\ln\left(\frac{\rho}{\rho_\infty}\right) = \left(\frac{T_0[1-(M/M_s)^2]}{T}\right)^{1/4} \tag{4.18}$$

where M/M_s is the reduced magnetization. Also, considering that the number of available sites for the hopping electron may be limited by the Jahn–Teller distortions and other factors, the parameter T_0 is different from Mott's original value, given above; the expression becomes $kT_0 = 171\alpha^3 U_m v$, where v is the cell volume. Taking $U_m = 2\,\text{eV}$, the corresponding localization lengths are typically in the range 0.4 nm, the average hopping range at room temperature is 1.5 nm and the hopping energy at room temperature is $\Delta E = 0.1\,\text{eV}$. These values are physically plausible since the localization length exceeds the ionic radius of Mn^{3+} and the hopping distances are three to four times the Mn–Mn separation. Moreover, the resistivity and magnetoresistance curves are well reproduced by the above modified VRH formula (equation 4.18) [232], as shown in figure 65. The potential associated with the on-site Hund's rule interaction seen by hopping electron is non-diagonal for simple tunnelling. However, the effect of some non-magnetic random diagonal potential can be enhanced by this off-diagonal contribution, leading to a magnetically-driven Anderson metal–insulator transition near T_C [584, 585].

Nagaev [27, 472] has developed a theory where the resistivity peak and magnetoresistance are explained by considering localization and scattering from an exchange potential that is caused by a difference in the local magnetization close to a divalent impurity and far from it.

An alternative to considering the effects of magnetization on the localization length is to construct an electronic density of states for the e_g band (figure 66) where the density of states itself is greatly modified at T_C. For simplicity we assume that the e_g band is unsplit by the Jahn–Teller effect and can accommodate two electrons. The exchange splitting remains in the paramagnetic state, since the local moment persists. A decrease in bandwidth with increasing temperature reflects the effect of magnetic order on t or W. For $T \ll T_C$, localized states are due only to Coulombic disorder, due to A-site substitution, and possible Jahn–Teller distortions. Since the total number of states remains the same, the area under the curve has to be conserved. The Fermi level E_F which, in the metallic regime, is within the extended states above the mobility edge $E\mu$ that separates the localized from the extended states, can find itself in the localized region of the density of states (shown shaded) as magnetic disorder increases. At very high temperatures, the bandwidth reduction is greatest because the bandwidth is $6t\cos(\theta/2)$ in the double-exchange model and the magnetic disorder includes even nearest neighbours. Most (possibly all) states are localized because of a

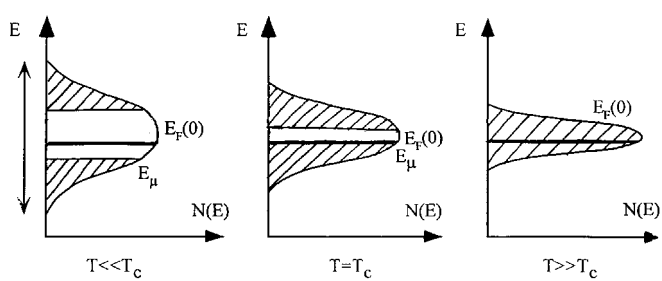

Figure 66. Band picture for manganites with $x \approx 0.3$ as a function of temperature.

combination of the influence of Coulombic disorder on the mobility edge and magnetic disorder on the bandwidth. Anomalies in the density of states due to possible correlation effects have been neglected, since no unequivocal evidence for a $T^{-1/2}$ dependence for ln ρ has been found so far.

It remains a challenge to clarify and modify these pictures. Very likely both magnetic and charge disorder, and lattice distortion effects, play some role in the transport above T_C. It is a question of relative magnitude. Evidence for Jahn–Teller and lattice polaronic effects in the electronic transport has been presented, but magnetic interactions clearly dominate the potential near T_C. The respective roles of the two lattice effects, the magnetic and Coulombic disorder in the localization process in the different regimes of carrier concentration and temperature, needs to be better understood.

4.4. *Thermal properties*

4.4.1. *Heat capacity*. The heat capacity of several ferromagnetic manganite compositions with $x \approx 0.3$ has been measured at low temperature [290, 359, 473]. There are also low temperature data on $(La_{1-x}Sr_x)MnO_3$ [290] for $0 \leqslant x \leqslant 0.3$, and on nonstoichiometric $LaMnO_3$ [233], as well as data on $(La_{1-x}Ca_x)MnO_3$ for $T > 50$ K [474] and $(La_{0.8}Ca_{0.2})MnO_3$ for $T > 100$ K [475]. By fitting low-temperature data on $x = 0.3$ compositions of a nonmagnetic rare-earth to just an electronic and a lattice term, that is

$$C = \gamma T + \beta T^3, \tag{4.19}$$

Coey and co-workers [232] deduced $\gamma = 5\text{-}8$ mJ mol^{-1} K^{-2}, which corresponds to a density of carriers at the Fermi level $N(E_F) = 3\gamma/(\pi k_B)^2$ of about 4×10^{28} m^{-3} eV^{-1}. This is a relatively high value for a metal, but the value of γ is uncorrelated with the residual resistivity ρ_0 which varies by several orders of magnitude in these compounds. With 0.7 electrons per formula (1.2×10^{28} m^{-3}), the width of the e_g band is estimated as 0.9 eV. Debye temperatures are in the range 330–400 K [290, 359] . Including extra terms in T^{-2} and $T^{3/2}$ to take account of the hyperfine and spin-wave contributions improves the fit to the data [290] and reduces γ to 3.3 mJ mol^{-1} K^{-2}, leading to a broader e_g bandwidth (about 1.6 eV).

In compounds of magnetic rare earths, the low-temperature specific heat is dominated by single-ion excitations of the rare earth. The overall crystal-field splitting of the lowest J multiplet is about 100 K for praseodymium or neodymium [199, 200] (figure 25) and the crystal-field levels are further split by the exchange field acting at the rare earth site.

The low-temperature heat capacity of the stoichiometric $LaMnO_3$ end member has been fitted with T^{-2}, T^3 and T^2 terms, with the lattter being ascribed to two-dimensional ferromagnetic magnons in the A-type magnetic structure [290]. A comparison of two cation-deficient $(LaMn)_{1-\delta}O_3$ samples, one ferromagnetic and the other antiferromagnetic, shows an unexpectedly large heat capacity at low temperature in both cases, namely $\gamma > 20$ mJ mol^{-1} K^{-2}, which has been ascribed to a high density of localized states below the mobility edge [233].

Heat capacity anomalies have been observed in the vicinity of the Curie temperature for the $(La_{1-x}Ca_x)MnO_3$ system [474, 475], where a typical lambda anomaly is observed for $x = 0.33$. The associated entropy of $0.4R$ ln 2 per mole is attributed to the spin disorder entropy less a contribution due to charge localization above T_C [474]. The magnetic entropy change in an applied field ΔS_m has been

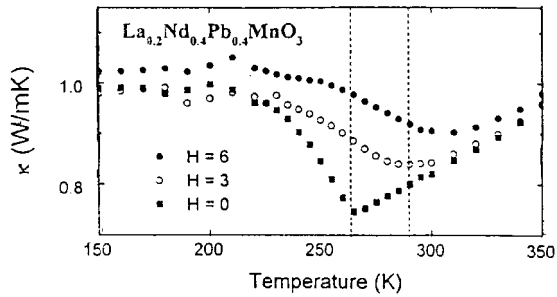

Figure 67. Variation in the thermal conductivity of $(La_{0.2}Nd_{0.4}Pb_{0.4})MnO_3$. [Reprinted by kind permission of the American Physical Society from page 3947 of *Physical Review Letters*, Volume 78, 1992, [479], and the authors, D. W. Visser, A. P. Ramirez and M. A. Subramanian, © 1992 by the American Physical Society.]

inferred from the magnetization curves using the thermodynamic relation $\Delta S_m = \int_0^H (dM/dT)_H \, dH$ [476–478]. Heat capacity anomalies appear at the two phase transitions in samples with $x \geqslant 0.5$ [474], one of which is associated with charge order, and also at the $O \rightarrow O'$ structural transition [122].

4.4.2. *Thermal conductivity*

Like the resistivity, the thermal conductivity κ exhibits an anomaly in the vicinity of T_C which can be modified in an applied field [479] (figure 67). It increases by 30% in 6 T at 265 K. An unusual positive temperature coefficient $dk/dT > 0$ above T_C is associated with scattering from large dynamic lattice distortions accompanying charge transport near T_C in the insulating phase. Thermal diffusivity (related to κ by $D_T = \kappa/CV\rho$) has been measured in $(La_{0.67}Ca_{0.33})MnO_3$ [430], where there is a broad dip near T_C related to κ and the magnetic part of the specific heat.

The importance of anharmonic lattice vibrations is evident in the Debye–Waller factor, which rapidly decreases with increasing temperature [415]. The effective Grüneisen parameter is of order 20–80, instead of the usual value of around two.

4.5. *Optical properties*

Systematic investigations of the optical absorption and optical conductivity of RMO_3 perovskites have covered frequencies from infrared to ultraviolet [202, 205, 558, 583]. Arima and Tokura [205] showed how the main absorption edge due to $2p(O) \rightarrow 3d(Mn)$ charge transfer in $LaMO_3$ falls from 6 eV for M = Sc to zero for M = Ni ($LaNiO_3$ is a metal) (figure 68).

There is some dispute as to where the charge transfer absorption sets in for $RMnO_3$. A common view is to associate the absorption edge at 3.1 eV with this transition, and to assign the weaker absorption feature at about 1.7 eV to the dipole forbidden $^5E_g \rightarrow {}^5T_{2g}$ transition of the Mn^{3+} ion [92, 202, 480], which may be split by the Jahn–Teller effect [92]. This crystal-field transition corresponds to promotion of a t_{2g} electron into a vacant e_g orbital. However, Arima and Tokura argue that the stability of the $S = \frac{5}{2}$ final state ($3d^5\underline{L}$) depresses the onset of the $2p(O) \rightarrow 3d(Mn)$ charge transfer to about 1 eV, and the strong increase of conductivity above 3 eV is then associated with promoting a spin down oxygen electron to form an $S = \frac{3}{2}$, $t_{2g}^4 e_g$ or $t_{2g}^3 e_g^2$ excited state which lies higher in energy by $\frac{5}{2}J_H - \Delta_{cf}$ or $\frac{5}{2}J_H$ respectively,

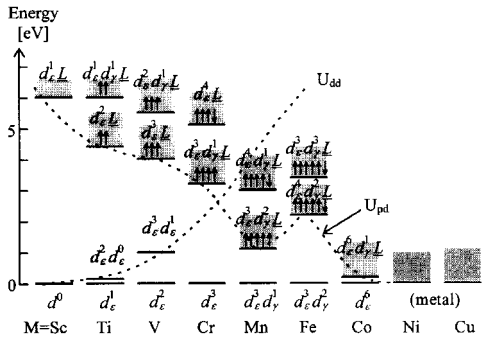

Figure 68. Excited energy levels of the $LaMO_3$ perovskite series (M= 3d metal) deduced from optical absorption [205]. [Reprinted with permission from the *Journal of the Physical Society of Japan*, Volume 64, page 2492.]

where J_H is the Hund rule coupling for an electron to the $S = 2$ ion core and Δ_{cf} is the crystal-field splitting.

Measurements of the optical properties of the mixed-valence manganites have been limited to a few compositions. Optical conductivity of $(La_{0.67}Ba_{0.33})MnO_3$ in the range 150–4000 cm^{-1} has been deduced from room-temperature optical reflectivity spectra [480]. A broad peak around 1000 cm^{-1} (0.13 eV) was associated with polaron transport. Extrapolation of the far-infrared reflectivity gives a zero-frequency optical resistivity of 1.4 μΩ m for $(La_{0.7}Ca_{0.3})MnO_3$ samples prepared in different ways, which is lower than any of their measured dc resistivities. The dc conductivity of manganites is very sensitive to polycrystalline grain structure, whereas the high-frequency optical measurement reflects the intrinsic property of the material. Extensive reflectivity measurements on single crystals of ferromagnetic $(La_{0.825}Sr_{0.175})MnO_3$ as a function of wavelength and temperature were reported by Okimoto *et al.* [204]. These data, expressed as optical conductivity and shown in figure 69, and those of Kaplan *et al.* [416] on thin films of $(Nd_{0.7}Sr_{0.3})MnO_3$ show very similar structure in the region of 1.5 and 3 eV to that reported in absorption [92, 480]. On sweeping through the Curie point and insulator–metal transition which occurs at 280 K, they found a considerable shift of spectral weight from the 1.5 eV and higher-energy structure to lower energies. The shift in spectral weight towards low frequencies resembles that observed on passing from $SmNiO_3$ (a semiconductor) to $NdNiO_3$ (a metal) [205]. The difference between the electronic structures of these adjacent compounds is attributed to the influence of the Mn–O–Mn bond angle on the bandwidth W. The low-frequency conductivity increases markedly in $(La_{0.825}Sr_{0.175})MnO_3$ at low temperatures (figure 69), and Okimoto *et al.* interpreted their data as an increase in the Drude-like free-carrier optical conductivity with decreasing temperature, consistent with the dc transport measurements although the extrapolated zero-frequency conductivity exceeds the dc value. Applying a sum rule, they found that the effective number n_{eff} of electrons deduced from the optical conductivity rises spectacularly with decreasing temperature from essentially zero at 280 K. The quantity n_{eff} depends sensitively on the reduced magnetization, varying roughly as $(M/M_s)^8$.

Okimoto *et al.* [204] viewed the structure at 1.5 eV as an $e_g^{\uparrow} \rightarrow e_g^{\downarrow}$ spin-flip transition, the energy difference being essentially the Hund rule exchange energy

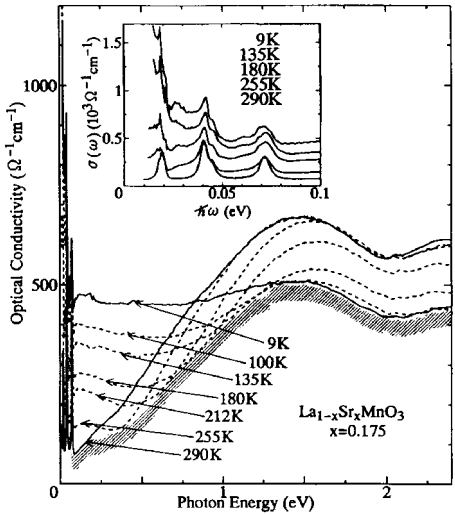

Figure 69. Optical conductivity spectra of $(La_{0.825}Sr_{0.175})MnO_3$ ($T_C = 238$ K) at various temperatures. The shaded part of the curve represents the temperature-independent part of the spectrum, deduced from the envelope of the various curves. The far infrared spectrum showing optical phonon excitations is shown in the inset. [Reprinted by kind permission of the American Physical Society from page 109 of *Physical Review Letters*, Volume 55, 1995, [204] and the authors, Y. Okimoto, T. Katsufuji, T. Ishikawa, A. Urushibara, T. Arima and Y. Tokura, © 1995 by the American Physical Society.]

J_H due to the coupling of the e_g electron to the localized $t_{2g}^{\uparrow}$ ($S = \frac{3}{2}$) spin manifold. Their estimate of J_H led them to conclude that the difference in the spectra in the high-temperature semiconducting state compared with the low-temperature metallic state is due to a shift from transitions out of a narrow, nearly filled $e_g^{\uparrow}$ band to an empty $e_g^{\downarrow}$ band while, at lower temperatures, the $e_g^{\uparrow}$ band broadens owing to the increase in bandwidth provided by the double-exchange mechanism (figure 66), and a greater fraction of the optical conductivity is now produced by excitations within the $e_g^{\uparrow}$ subband, thereby robbing the spin-flip transitions of much of their strength. This results in a decrease in the structure at 1.5 eV and the observed increase in the low-temperature conductivity.

Kaplan *et al.* [416] also studied the magnetic-field dependence of the optical conductivity in thin films of $(Nd_{0.7}Sr_{0.3})MnO_3$. Their optical transmission data are shown in figure 70. Their zero-field data resemble those in figure 69, except that the peak is now in the neighbourhood of 1.0 eV and it increases in intensity with decreasing temperature, with a sharp drop at lower energies. The increase in low-frequency conductivity with decreasing temperatures is as expected for the insulator–metal transition. Data on the variation in conductivity as a function of temperature in zero field or at constant temperature in an applied field unequivocally demonstrate that the variation in spectra and therefore the optical conductivity depend only on the state of magnetization of the system, produced either by exchange forces as the material is lowered through T_C or by the externally applied magnetic field. The assignment by Kaplan *et al.* of the conductivity peak near 1 eV stems from their observation that this peak shifts to a lower energy and increases in spectral weight as

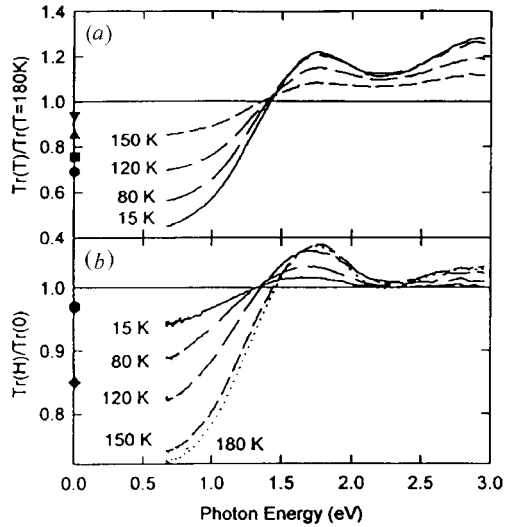

Figure 70. Optical transmittance ratios for a thin film of $(Nd_{0.7}Sr_{0.3})MnO_3$ ($T_C \approx 150\,K$); (*a*) ratio of optical transmittance at several temperatures to that at 180 K in zero field; (*b*) ratio of transmittance in 8.9 T to that in zero field at several temperatures. [Reprinted by kind permission of the American Physical Society from page 2081 of *Physical Review Letters*, Volume 77, 1996, [416], and the authors, S. G. Kaplan, M. Quijada, H. D. Drew, D. B. Tanner, G. C. Xiong, R. Ramesh, C. Kwon and T. Venkatesan, © 1996 by the American Physical Society.]

the temperature is lowered. Furthermore the low-frequency response which they obtained is not Drude-like in that it does not vary as $1/\omega$, implying that the shifting peak dominates the response. They argued that the transition cannot be due to an $e_g^{\uparrow} \rightarrow e_g^{\downarrow}$ spin flip since that would not produce a temperature- and field-dependent energy shift. Furthermore, they ruled out a $2p \rightarrow e_g$ charge transfer on the grounds that this should be magnetization independent as electrons of both spins participate in the oxygen 2p band. They assigned the transition as a $d \rightarrow d$ charge transfer from an occupied $Mn^{3+}e_g^{\uparrow}$ state to an unoccupied $Mn^{4+}e_g$ level. The energy difference for the hop arises from the Jahn–Teller distortion at the occupied site, convoluted by magnetic polaron and band effects. The peak does not disappear below T_C because the Jahn–Teller distortion is not coupled directly to magnetism, but the energy of the peak decreases because the extra binding energy of the occupied state is due to magnetic trapping and disappears with increasing magnetic order. Optical conductivity has also been reported for the $(La_{1-x}Ca_x)MnO_3$ series by Kim *et al.* [582, 583]. For $x = 0.3$, they find a sharp Drude peak, and a broad mid-infrared absorption which they associate with a lattice polaron. They also find the $d \rightarrow d$ charge transfer and an intra-atomic $t_{2g} \rightarrow e_g$ transition for Mn^{3+}.

Three phonon modes are optically active in the infrared, at about 200, 400 and 600 cm^{-1}. These correspond to an M–O stretching mode, an M–O–M bending mode and an A-site mode. The bending mode is split in the O′ structure of $LaMnO_3$. There are numerous Raman-active modes [277, 482] including a broad band at 650 cm^{-1} (0.085 eV), possibly associated with magnetic, electronic or Jahn–Teller excitations, and another mode at 2100 cm^{-1} which could be a plasmon or a single-particle electronic excitation [483]. The influence of substrate-induced lattice distortion on

the infrared phonon mode was measured in thin films of $(La_{0.7}Ca_{0.3})MnO_3$ [484]. Raman and infrared spectra are available for $NdAlO_3$ [485], and there are some infrared data for $CaMnO_3$ [486].

Finally, we mention the phenomenon of an optically induced phase transition in $(Pr_{0.7}Ca_{0.3})MnO_3$ from an insulating charge-ordered canted antiferromagnetic state to a conducting ferromagnetic state [329].

4.5.1. *Magneto-optics*

The earliest optical characterization of mixed-valence manganites was aimed at evaluating the materials for magneto-optic recording. There have been studies of magneto-optic Kerr effect [480, 487, 551] and Faraday effect [92, 117] as a function of wavelength. The magneto-optic activity is greatest in the vicinity of the absorptions near 1.8 and 3 eV, associated with intra-atomic $d \rightarrow d$ transitions and $2p(O) \rightarrow 3d(Mn)$ charge transfer respectively [92, 480], indicating that spin-polarized Mn d levels are involved in both of these transitions. The Kerr rotation reaches a maximum value of 0.2° at 3.2 eV, in $(La_{0.7}Sr_{0.3})MnO_3$ [487], whereas the Faraday effect exceeds $40\,000^\circ\,cm^{-1}$ in $(La_{0.7}Ca_{0.3})MnO_3$ at the same energy [92]. Thin $(La_{0.8}Sr_{0.2})MnO_3$ films deposited by sputtering on $GdGa_5O_{12}$ substrates and post-annealed exhibit perpendicular anisotropy [117], and they may be of interest for Curie point recording using the Kerr effect.

4.5.2. *X-ray absorption spectroscopy and magnetic circular dichroism*

The advent of intense synchrotron sources has opened new possibilities for the study of electronic structure in the solid state. X-ray absorption spectroscopy is a powerful tool for investigating the local electronic structure of the atoms forming a compound. The use of circularly polarized X-rays can provide information about the spin character of the electronic levels; X-ray magnetic circular dichroism (MCD) spectra are obtained by taking the difference between spectra obtained with the sample magnetization parallel and antiparallel to the incoming, circularly polarized photon.

Interpretation of the spectral structure is a general problem in MCD measurements, and peak assignment for mixed valence manganites is a matter of controversy. However, measurements of the oxygen K-edge and manganese K-edge dichroism in manganites lead to several very interesting conclusions [167, 402, 488]. X-ray absorption spectroscopy and MCD measurements recorded at 30 K by Pellegrin *et al.* [488] on $(La_{1-x}Sr_x)MnO_3$ single crystals with $x = 0.15$, $x = 0.18$ and $x = 0.40$ show very similar features indicating that the local symmetry of the manganese ions is retained when crossing the insulator–metal boundary. This implies that a local Jahn–Teller distortion is still present in the metallic compositions. The MCD spectra reveal a surprising feature, namely that the $t_{2g}^{\downarrow}$ level of the Mn^{4+} ion lies lower in energy than the $e_g^{\uparrow}$ level. Of course, this is not the case for Mn^{3+} since numerous measurements have shown that the d^4 ion is high-spin. This $t_{2g}^{\downarrow}/e_g^{\uparrow}$ level inversion is at least 0.6 eV, which requires that both the crystal-field splitting Δ_{cf} and the Jahn–Teller splitting δ_{JT} be large; the latter was estimated as 1 eV by the Groningen group. Doped holes are also found to have a strong oxygen 2p character along with a high degree of spin polarization parallel to the manganese 3d levels, leading to the suggestion that $LaMnO_3$ should be regarded as a charge transfer insulator [488]. The orbital contribution to the manganese magnetic moment has

also been estimated using sum rules. It is found to be $-0.055\mu_B$, opposite to the spin, as expected for a 3d shell that is less than half filled.

Subias *et al.* [167] reported manganese K-edge measurements for $(La_{1-x}Ca_x)MnO_3$ as a function of temperature and composition. The X-ray absorption near-edge structure changed very little on varying x or on going through T_C, indicating that the electronic state of the Mn atom remains unaltered. In fact, the most important local changes in the electronic structure take place in the paramagnetic state, at temperatures above T_C. The effect of an applied magnetic field above T_C was also shown to be similar to decreasing the temperature. These results support a picture where ferromagnetic correlations already exist above T_C and where reducing T and applying a magnetic field have the same effect of enhancing these correlations. Furthermore, Subias *et al.* [167] found a quantitative discrepancy on comparing the first 10 eV of the absorption spectra with expected intensities for a weighted sum of $LaMnO_3$ and $CaMnO_3$ signals which was interpreted as evidence for the existence of an intermediate oxidation state for the manganese. Since the interaction time for the photoelectric process is extremely short (about 10^{-19} s), fluctuations on a slower time scale should lead to a weighted sum. The dichroic spectra were interpreted as showing that a unique type of manganese is present in these mixed-valence compounds.

The evidence from X-ray absorption measurements that the local symmetry is unaffected by changes in resistivity regime suggests that local electronic configurations on a very short time scale are the same in either the insulating or the conducting states. Correlations on a length scale longer than that probed in the measurements are therefore the key element for understanding the microscopic origin of the transport properties of the manganites.

5. Related compounds

There are different manganese oxides with structures related to perovskite and other ferromagnetic perovskites which it is useful to discuss briefly in the present context.

5.1. *Other manganese oxides*

A series of layer structures (the Ruddlesden–Popper phases) can be derived from perovskite, in a way that is familiar from high-temperature superconductors. By introducing an NaCl-type AO block after every n (MnO_2) sheets, the general formula becomes

$$A_{n+1}Mn_nO_{3n+1}.$$

Here the $n = \infty$ limit corresponds to the perovskite $AMnO_3$ (figure 71).

The $n = 1$ member has the K_2NiF_4 structure. An example is the manganite $(LaSr)MnO_4$ which contains only Mn^{3+} ions and is an antiferromagnet with $T_N = 110$ K [489] whereas Sr_2MnO_4 which contains only Mn^{4+} ions is an antiferromagnet with $T_N = 170$ K [490]. Mixed manganese valence can therefore be obtained in the $(La_{1-x}Sr_{1+x})MnO_4$ solid solutions without changing the two-dimensional MnO_2 sheets. The d_{z^2} orbitals are oriented perpendicular to the sheets; so there is little overlap and much less itineracy than in the perovskites. The system remains semiconducting for all values of x. Unlike the quasicubic manganites, no ferromagnetic order is found in the range $0.25 < x < 0.75$ [491], but the magnetic order of the spin glass type was observed with $T_f \approx 20$ K [489]. The susceptibility shows a Curie–

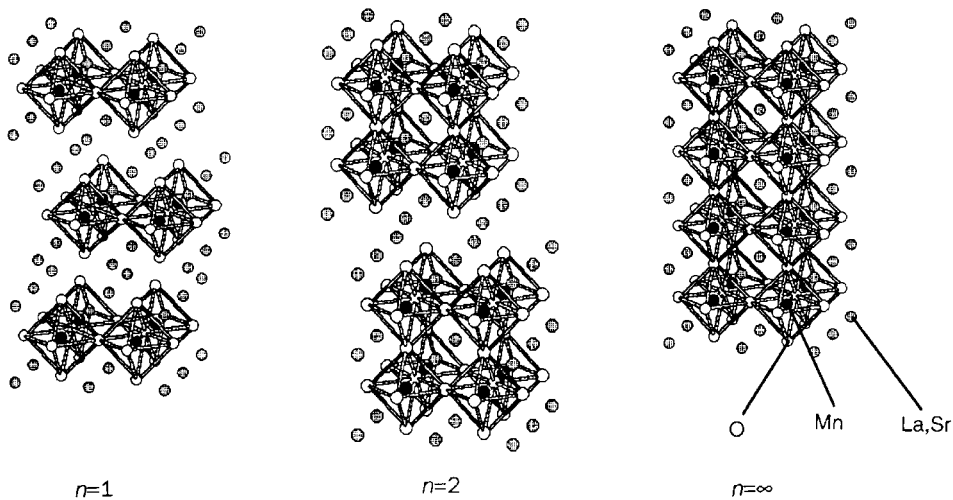

Figure 71. Crystal structure of the $n = 1$, $n = 2$ and $n = \infty$ members of the $A_{n+1}Mn_nO_{3n+1}$ series. [Reprinted with permission from *Nature*, Volume 380, page 141, [494], © 1996 Macmillan Magazines Ltd, and the authors, Y. Morimoto, A. Asamitsu, H. Kuwahara and Y. Tokura.]

Weiss behaviour with a positive value of θ which is greatest when $x \approx 0.4$, which is also the concentration where the thermally activated conductivity is greatest. Resistivity is much greater along the *c*-axis than in the *a–b* plane. Charge ordering occurs below 220 K when $x = 0.5$: $(LaSr_3)Mn_2O_8$. The charge ordering is three dimensional, but only one manganese site in *four* is occupied by the extra electrons [492]. This would indicate that the Mn^{3+} has disproportionated into Mn^{4+} and Mn^{2+}, so that the charge-ordered state may be considered as a background of t_{2g}^3 ion cores with spin-triplet bipolarons ($t_{2g}^3e_g^2$) localized on every fourth lattice site. Another study [493], however, found charge order consisting of Mn^{3+} and Mn^{4+} cations alternating along (110) directions, and antiferromagnetic order below 110 K.

The $n = 2$ member has composition $A_3Mn_2O_7$. Crystals with A = $(La_{0.6}Sr_{0.4})$ and A = $(La_{0.47}Ca_{0.53})$ have been studied by Moritomo *et al.* [494] and Kimura *et al.* [495] respectively. These materials are ferromagnetic metals, but the three-dimensional Curie temperature is much lower than for the corresponding $n = \infty$ perovskite (T_C = 126 K compared with 360 K for $(La_{0.6}Sr_{0.4})MnO_3$). The CMR effect is analogous to that in perovskites with similar Curie temperatures except that the resistivity is quite anisotropic, being two to three orders of magnitude less in-plane than it is along the *c* axis (figure 72). The low-field magnetoresistance effect is observed at low temperatures in polycrystalline and thin film samples [496]. A broad peak in the in-plane resistivity near 300 K suggests that the double MnO_2 sheets order ferromagnetically there, but are only weakly coupled in the c-direction. The material can be regarded as a natural multilayer where spin-polarized electrons tunnel through the AO insulating layer separating the ferromagnetic sheets. Long-lived antiferromagnetic fluctuations persist well above T_C [497], which may enhance magnetic localization. A structural refinement based on neutron powder diffraction has revealed that $(Sr_2{-}_xNd_x)Mn_2O_7$ with $x = 0$ or 0.1 are two-phase systems, with only one phase showing long-range magnetic order [498].

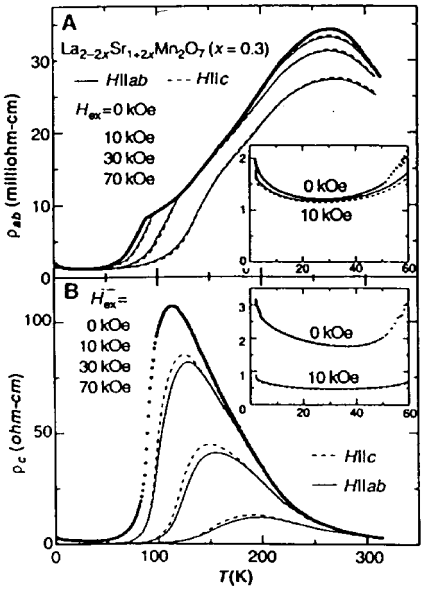

Figure 72. Temperature dependence of the resistivity of a $(La_{1.4}Sr_{1.6})Mn_2O_7$ crystal measured (A) perpendicular to the c axis and (B) parallel to the c axis, showing highly anisotropic conductivity with peaks at the two- and three-dimensional ordering temperature, and a large field effect on the three-dimensional ordering temperature. [Reprinted with permission from *Nature*, Volume 380, page 141, [494]. © 1996 Macmillan Magazines Ltd, and the authors, Y. Morimoto, A. Asamitsu, H. Kuwahara and Y. Tokura.]

The $n = 1$, 2, 3 and ∞ phases with A = Ca (Mn^{4+}) all order antiferromagnetically with T_N in the range 110–120 K [179].

The pyrochlore manganites $R_2Mn_2O_7$ where R is a heavy rare earth, scandium, yttrium, thallium or indium have a large cubic cell containing eight formula units. The Mn^{4+} ions are octahedrally coordinated, and the MnO_6 units form a lattice of corner-sharing tetrahedra. Since the Mn^{4+}-O–Mn^{4+} interaction is negative, this is a highly frustrated magnetic structure, in which noncollinear or random spin freezing might be expected at sufficiently low temperatures. In fact some pyrochlores (R = Tl or In) are ferromagnets with T_C around 130 K [499, 500], and a ferromagnetic moment slightly in excess of that expected for Mn^{4+} [500]. This is explained by Raju *et al.* [500] in terms of oxygen deficiency, which introduces some Mn^{3+} and permits double exchange leading to dominant ferromagnetic interaction. The pyrochlores are therefore electron-doped d^3 compounds, in contrast with the mixed-valence perovskites with $x \approx 0.3$, which are hole-doped d^4 compounds, provided that the degeneracy of the e_g states is lifted by the Jahn–Teller distortion. The Hall coefficient corresponds to only 0.005 electrons per formula unit [501]. Chemical doping is achieved by substituting Sn^{4+} for La^{3+} [502]. There is a sharp fall in resistivity below T_C in $Tl_2Mn_2O_7$ and the low-temperature state is metallic with a residual resistivity of order $10^{-4}\,\Omega$ m. The high-temperature state also seems to be metallic since $d\rho/dT > 0$. A large negative magnetoresistance effect has been observed in the vicinity of T_C and the resistance change is found to scale as $(M/M_s)^2$ for $M/M_s < 0.1$ [500] (figure 73). Subramanian *et al.* [503, 504] and Shimakawa *et al.*

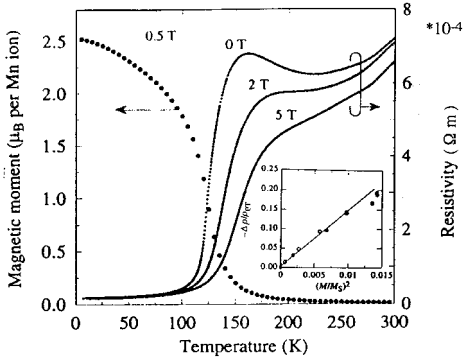

Figure 73. Magnetization and resistivity of $Tl_2Mn_2O_7$. The inset shows the variation in the magnetoresistance above T_C with $(M/M_S)^2$. [Reprinted with permission from *Nature*, Volume 379, page 53, [501], © 1996 Macmillan Magazines Ltd, and the authors, Y. Shimakawa, Y. Kubo and T. Manako.]

[505] discounted double exchange and attributed the ferromagnetic state to Mn^{4+}–Mn^{4+} superexchange. They considered the negative magnetoresistance to be due to unusually large scattering from spin fluctuations [37]. $Tl_2Mn_2O_7$ may be a material where 2p holes are mainly responsible for the exchange and magnetoresistance. The magnetoresistance effect is greatly enhanced in $(Tl_{2-x}In_x)Mn_2O_7$ mixed oxides which exhibit a miscibility gap between $x = 0.4$ and $x = 1.7$ [506]. This may be related to intergranular transport.

5.2. *Other perovskites*

The manganites are not the only mixed-valence perovskite oxides to exhibit ferromagnetism, negative magnetoresistance effects or a metal–insulator transition. The analogous ferromagnetic cobalt compounds were first investigated by Jonker and van Santen [507]. More recent systematic investigations of $ACoO_3$ and A_2CoO_4 with a mixture of lanthanum and calcium, barium or strontium cations on A sites show negative magnetoresistance in excess of 5% , with the larger effects for the barium-containing compounds [508, 509]. The negative magnetoresistance is greatest in the vicinity of the metal–insulator transition, which occurs around $x \approx 0.2$ in $(La_{1-x}Sr_x)CoO_3$, where the resistance change again scales with the square of the magnetization [510]. The effect changes sign and becomes small and positive for $x > 0.5$ [511]. The cobalt ions are in a diamagnetic low-spin state, t_{2g}^6 in $LaCoO_3$ below 90 K, but paramagnetic cobalt with a net spin is stabilized at higher temperatures, or by divalent substitution [512, 513]. These ions can order ferromagnetically, as in the mixed-valence manganites. $(La_{0.5}Sr_{0.5})CoO_3$ is a tetragonal ferromagnet [514]. A giant extraordinary Hall effect (section 4.3.5) in $(La_{0.5}Ca_{0.5})CoO_3$ which exceeds that of iron by two orders of magnitude is associated with the coexistence of high- and low-spin cobalt [509]. There is also exceptionally large magnetostriction ($\lambda \approx 10^{-3}$) [560]. A spin state transition occurs in $(La_{2-x}Sr_x)CoO_4$ at $x \approx 0.7$ [515]. Cobalt substitution in $LaMnO_3$ induces ferromagnetism, since the cobalt becomes divalent and creates Mn^{3+}–Mn^{4+} double-exchange pairs [516]. The $Sr(Fe_{1-x}Co_x)O_3$ compounds are magnetically inhomogeneous [516].

The end-member nickel oxides $RNiO_3$ are a very interesting set of compounds. They crystallize in the O-type $GdFeO_3$ structure (figure 21). When R is a small cation such as yttrium or lutetium, they are charge-transfer insulators with a small gap. Compounds with large cations such as lanthanum are metals, and intermediate cases such as praseodymium, neodymium or samarium, exhibit an insulator–metal transition as a function of temperature, at 135 K, 200 K and 400 K respectively. In common with most other transition-metal oxides, it is the low-temperature phase which is the insulator. The high-temperature metallic phase is stabilized by applying pressure; $dT_{MI}/dP = -42\,K\,GPa^{-1}$ [518]. (The mixed-valence manganites are exceptional in exhibiting a metal–insulator transition where the ground state is a ferromagnetic metal.) The Ni^{3+} in $RNiO_3$ is in a low-spin state $t_{2g}^6e_g^1$ and orders antiferromagnetically, except in $LaNiO_3$, which is a Pauli paramagnet [519]. The properties of the nickel perovskites have been explained in terms of the Ni–O–Ni bond angle, which varies from 151.7° for R = Ho to 165.2° for R = La [520]. When the tolerance factor approaches unity, the d band broadens as the bond straightens out, and the charge-transfer gap $U_{pd} - W$ tends to zero [206].

The K_2NiF_4 structure compounds such as La_2NiO_4 are insulators where the Ni^{2+} ($t_{2g}^6e_g^2$) orders antiferromagnetically. Doping with strontium introduces Ni^{3+} which forms an ordered array of small polarons in the lattice [521]. Charge-ordering transitions are found in $La_{2-x}Sr_xNiO_4$ for $x = 0.33$ and $x = 0.5$ below 235 K and 340 K respectively [522].

The rare-earth orthoferrites $RFeO_3$ are antiferromagnetic insulators, with a superexchange interaction which depends on bond angle. On doping with divalent A site cations there may be a tendency for Fe^{4+} to disproportionate into Fe^{3+} ($t_{2g}^3e_g^2$) and Fe^{5+} (t_{2g}^3) [522]. An alternative view which finds support in soft X-ray absorption spectroscopy is that the iron remains predominantly d^5 ($t_{2g}^3e_g^2$), with the holes located on the oxygen ligands [210]. $SrFeO_3$ has a spiral spin structure with $T_N = 135$ K [523]. The double perovskite Sr_2MoFeO_6 is a half-metallic ferromagnet with a Curie temperature of 430 K [588]. Compounds with iron and rhenium have T_C as high as 538 K [589].

The ruthenium perovskites $ARuO_3$ with A = Ca or Sr have an orthorhombic structure with $a \approx c/2^{1/2} > b$. $SrRuO_3$ is a ferromagnetic metal with $T_C = 165$ K. The paramagnetic susceptibility suggests that the ruthenium is in a low-spin state t_{2g}^4; $S = 1$. The d band therefore has π^* character, as in CrO_2, which is also a ferromagnetic metal, with t_{2g}^2 ions and $T_C = 396$ K. Like CrO_2 [525], there is a resistivity anomaly at T_C in $SrRuO_3$, but $d\rho/dT$ remains positive for $T > T_C$, and negative magnetoresistance effects of order 10% in 10 T are found near T_C [526]. There is a large electronic specific heat: for $SrRuO_3$ $\gamma = 29\,mJ\,mol^{-1}\,K^{-2}$. The narrow π^* bandwidth is sensitive to the size of the A cation, which controls the Ru–O–Ru bond angle. $CaRuO_3$ is an enhanced Pauli paramagnet [527]. Sr_2RuO_4 is a superconductor with $T_{sc} = 0.9$ K [528], whereas $Sr_3Ru_2O_7$ is a metallic ferromagnet with $T_C = 105$ K [529] and $Ca_3Ru_2O_7$ is an antiferromagnet with $T_N = 56$ K [530].

Although the ferromagnetism in the ruthenates and CrO_2 appears to have a different origin from that in manganites, namely direct overlap of t_{2g} orbitals rather than double exchange involving e_g electrons, there is a similar sensitivity of the electronic ground state to cation size and crystal structure. On the basis of LSDA + U calculations, it has been proposed that CrO_2 can also be regarded as a half-metallic double exchange oxide, with one of the t_{2g} (d_{xy}) electrons tightly localized and the other, Zener electron, in a half-filled π^* band [531].

6. Applications

Mixed-valence manganites have potential for applications based on their chemical and physical properties. Briefly, the chemical applications include catalysis, such as catalysts for automobile exhausts, oxygen sensors and solid electrolytes in fuel cells. The catalytic activity is associated with the Mn^{3+}–Mn^{4+} mixed valence [532], and the possibility of forming oxygen vacancies in the solid. Both cation vacancies and alkali ion substitution increase the catalytic activity [180]. $LaMnO_3$ with monovalent (sodium, potassium or rubidium) substitution has been used for the reduction and decomposition of NO. The oxide with divalent substitution, calcium, strontium or lead, has been used for NO reduction [533], CO oxidation [534, 535] and NH_3 oxidation [536].

Applications exhibiting the physical properties of manganites have been reviewed by Venkatesan *et al.* [575]. Physical properties that may be exploited include the temperature dependence of resistivity and the magnetoresistance. The rapid variation in resistivity in the vicinity of T_C, with relative changes as high as 10–20% K^{-1} suggest uses as a bolometer [576]. The ability to modify the composition of the perovskite oxides so as to place the Curie temperature anywhere in the range from 50 to 400 K and thereby to tune the temperature variation in the resistivity gives flexibility. Drawbacks are the temperature-dependent sensitivity with the highest values available only in a narrow range near T_C. Furthermore, the maximum sensitivity falls rapidly as T_C increases; also when T_C is low (less than 100 K), the resistivity shows thermal hysteresis.

Prospects are brighter for exploiting the magnetoresistance. Potential applications include magnetic sensors, magnetoresistive read heads and magnetoresistive random access memory. In ferromagnetic compositions with $x \approx 0.3$, the maximum high-field magnetoresistance is associated with the resistivity peak near T_C. One method to broaden the magnetoresistive temperature response is to use material with a canted ferromagnetic structure having a composition with $0.4 < x < 0.5$ [93, 184] or $x \approx 0.1$ [551].

A direct application of magnetoresistance is to use the materials as magnetic field sensors. The isotropy of the magnetoresistance means that a spherical crystal with a demagnetizing factor $N = \frac{1}{3}$ may be used to sense the magnitude of a magnetic field regardless of its direction [537]. Other shapes, such as films or cylinders, may be used to measure the field in a particular direction or plane but the appropriate demagnetizing factor should be taken into account. A simple prototype position sensor based on a thin film with permanent magnet bias has been developed [136]. It is based on $(La_{0.67}Ca_{0.33})MnO_3$ which is sprayed or screen printed onto a ceramic substrate and fired at 1400°C. A Wheatstone bridge configuration is used to improve sensitivity and to compensate for thermal drift. Sensitivity is about 10% T^{-1}. Changes of position may be detected with great accuracy (≈nm) using a manganite film moving in a field gradient $> 10^2\,T\,m^{-1}$ produced by permanent mangets [574]. Another sensor application is a magnetoresistive microphone [366]. When the manganite sensor is presented to the field B directly it is possible to detect the relatively large fields, of order 1 T, which are required to modify significantly the ferromagnetic order and thereby to induce magnetoresistance. However, the sensitivity $(1/\rho)\,(d\rho/dB_0)$ can be enhanced by flux concentration using a soft anhysteretic ferrite to guide the flux to a small cross section occupied by the manganite sensor [538]. The magnetoresistive response can be amplified a thousand-fold in a limited field range (figure 74). Segments of $YBa_2Cu_3O_7$ have

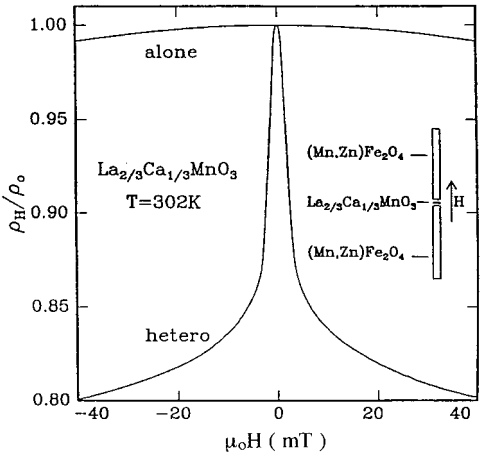

Figure 74. Resistivity as a function of applied field at room temperature for a thin $(La_{0.67}Ca_{0.33})MnO_3$ film with and without flux concentration using long rods of Mn–Zn ferrite. [Reprinted by kind permission of the American Physical Society from p. 3494 of *Applied Physics Letters*, Volume 68, 1996, [538], and the authors, H. Y. Hwang, S.-W. Cheong and B. Batlogg, © 1996 by the American Physical Society.]

also been used to enhance the flux below the superconducting transition temperature $T_{sc} = 90\,K$ [539]. A way of greatly enhancing the field sensitivity is to operate at microwave [296] or radio frequency ($\approx 10\,MHz$) with the ferromagnetic manganite in the coil of an LC circuit. Here it is the field-dependence of the permeability which is detected [550].

A promising approach to achieving a good low-field magnetoresistive response is to focus on the micromagnetic structure rather than to depend on the applied field to modify the intrinsic magnetic structure within each domain, in other words to exploit the low-field magnetoresistance rather than the CMR. Here, the low-field response is favoured by a high density of grain boundaries [357, 379, 382, 538, 540], and in tunnel spin valve structures [445–447]. A first step towards miniaturizing the tunnel spin valve is the current-perpendicular-to-plane sandwich device consisting of a pillar composed of two layers of ferromagnetic manganite separated by a $SrTiO_3$ spacer layer which has been constructed by Sun *et al.* [446], (figure 75). The 5 nm $SrTiO_3$ layer has the effect of exchange decoupling the two ferromagnetic layers, and a 50% change in resistance is observed according to whether the magnetization of the two manganite layers is parallel or antiparallel. The switching field for the device was 16 $kA\,m^{-1}$ (200 Oe) at 125 K. Besides showing the potential for generating large resistivity changes in low fields with manganite heterostructures, this prototype device demonstrates how it is possible to use films of ferromagnetic manganites as electronic spin polarizers and analysers. A problem here is that the low-field magnetoresistance, whether in spin-polarized tunnel junctions, polycrystalline ceramics or powder compacts is strongly temperature and voltage dependent in all circumstances where it has been observed to date. Huge effects are seen at cryogenic temperatures, but the effect at room temperature does not exceed 1% . Read heads, for example, have to be able to operate up to 100°C, which is uncomfortably close to the maximum Curie temperature in strontium-doped manganites.

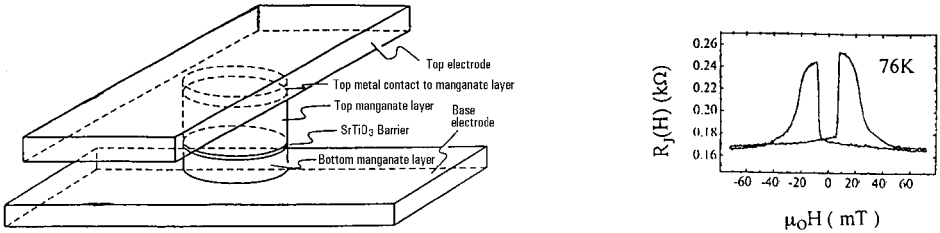

Figure 75. A three-layer spin switch composed of a 7 μm pillar, showing a large change in resistivity as the relative orientation of the magnetization of the ferromagnetic manganite layers is changed. [Reprinted by kind permission of the American Physical Society from page 3266 of *Applied Physics Letters*, Volume 69, 1996, [446], and the authors, J. Z. Sun, W. J. Gallagher, P. R. Duncombe, L. Krusin-Elbaum, R. A. Altman, A. Gupta, Y. Lu, G. Q. Gong and G. Xiao, © 1996 by the American Physical Society.]

The ferromagnetic metallic manganites have an almost completely spin-polarized 3d band. They are therefore a potential source of spin-polarized electrons for a variety of spin electronic devices. The problem here is how best to inject these electrons across the manganite interface at room temperature while still retaining their spin polarization. Compatibility with existing silicon-based structures may need to be addressed. Three-terminal devices based on manganite/superconductor heterostructures operating at liquid-nitrogen temperature [453] may open new perspectives in high-speed electronics. It has been suggested that manganite/superconductor layer structures could be useful for ultrasonic wave amplification, thermal switching and thermocouple infrared detection [481]. Field effect transistor structures with a manganite channel and a ferroelectric dielectric layer have potential for non-volatile memory [577].

An issue which needs to be considered further is noise in manganite devices. There are reports of exceptionally large $1/f$ noise [541–543] or thermal noise in the vicinity of T_C. The huge $1/f$ noise has a non-Gaussian character associated with magnetic inhomogeneities [543]. An implication is that there may be problems exploiting the low-field magnetoresistance effect in low-frequency applications, but the $1/f$ noise need not be a problem in high-frequency applications such as read heads.

The field dependence of the microwave absorption [296, 544] may find applications in microwave devices operating at room temperature.

Changes in entropy of magnetic origin comparable with those seen in gadolinium can be induced in a modest applied field close to room temperature [476–478]. The ability to tune the Curie temperature chemically and to smear the transition, together with their chemical stability and low cost, make the mixed-valence manganites interesting magnetocaloric working substances for an Ericsson-cycle magnetic refrigerator with a wide working span.

Finally, the suggestion of X-ray, ultraviolet- or electric-field-induced ferromagnetism associated with the elimination of the charge-ordered state in $(Pr_{0.7}Ca_{0.3})MnO_3$ opens new possibilities of patterning small ferromagnetic structures [328–330].

7. Conclusions

The flood of interest in the mixed-valence manganites which was triggered by von Helmholt's and Chahara's reports of large negative magnetoresistance in thin films of barium- and calcium-substituted $LaMnO_3$ prepared by pulsed laser deposition [15, 16] owes much to the high-temperature superconductor boom which preceded it. The expertise was available and resources were in place to prepare films, ceramics and crystals of this type of oxide and to characterize the crystallographic, electronic and magnetic properties thoroughly with a wide range of techniques. Papers are now appearing at the rate of 200 per year. Unlike high-T_{sc} compounds, where the materials were new, the mixed-valence manganites had been studied for almost 50 years and there was an extensive repository of knowledge of their properties. The physical and chemical content of some of the early papers is remarkable and contrasts with some more recent contributions where many researchers make light work. Many of the physical concepts needed to analyse the experimental data were available at the time of the 1970 review by Goodenough and Longho [17], while others relating to highly correlated electron transport in narrow bands have been refined by consideration of metal–insulator transitions in 3d oxides [352] and the difficult problem of high-T_{sc} superconductivity.

The electronic phase diagrams have proved to be very rich, with competing tendencies to electron localization, charge and orbital order, and different types of magnetic order. Phases with completely different properties can be very close in energy—hence the spectacular phase transitions as a function of temperature, pressure or magnetic field. More surprises may be expected, and potentially useful phenomena uncovered as understanding of the physical and chemical principles involved are brought together. There is great scope in perovskite chemistry for multiplying results such as those surveyed in this review by different ionic substitutions. On the other hand, the chemistry can be used to tune the structure and doping level to achieve desired combinations of properties, or to engineer transitions between near-degenerate magnetic and electronic states. The maximum Curie temperatures available in mixed-valence manganites (about 100°C) are low for purposes such as magnetic read heads, but there now seems to be little prospect of significantly enhancing them: most possible chemical substitutions have been tried.

Unlike the high-T_{sc} problem, the physical issues raised by the mixed-valence manganites, namely localization, phase separation, charge and orbital ordering, double exchange, superexchange and polaron formation, are essentially soluble. The physics is complex but the principles are in place. A consensus may be expected to emerge when the essential features of the physical phenomena are laid out clearly, and the magnitudes of the interactions involved are established. This review will be a guide in that direction.

What is needed now? For further studies of intrinsic physical properties, more single crystals of different compositions are required. The phase diagrams such as those in figures 23, 24 and 34 need to be completed and more chemical systems added; more sophisticated structural characterization should lead to an understanding of electronic two-phase regions where Coulomb interactions impose a very short length scale on phase segregation and there is a tendency to charge ordering. Statistical descriptions of the local structure on different time scales may need to be developed. In the area of thin films and heterostructures, an important task is to uncover the role of the grain boundary in polycrystalline films and ceramics and to understand the contributions of intrinsic and/or interface effects to the temperature

dependence of the low-field magnetoresistance. Generally, the temperature range for useful magnetoresistive effects needs to be extended, perhaps with the double perovskites. Then, a knowledge of the exact degree of spin polarization of the conduction electrons in different materials together with an understanding of spin flip processes in barriers and interfaces [603] and proper characterization and control of the interfaces in heterostructures will be essential to achieve effective spin injection in layered or planar devices. Changes in the electronic structure induced by photons, electric field or other means which are long lived (hysteretic phase transitions) need to be explored and controlled, especially in thin films, for potential storage applications.

There is much work to be done, but it is sufficiently challenging and potentially rewarding in terms of interesting physics and novel magnetoelectronic devices that the subject of mixed-valence manganites and related compounds will probably flourish for at least another decade. The manganite research has directed the attention of the community more generally towards half-metallic ferromagnetic oxides, where near-perfect spin polarization opens prospects for novel devices based on magnetic control of the electron stream.

Acknowledgments

The authors are grateful to many colleagues who have read the manuscript, or parts of it, and who have offered their comments and criticism, especially F. Ott, K. O'Donnell, J. Cullen, L. Ranno, J. P. Contour, A. Barry, J. Versluijs, R.-M. Thomas, R. Borges, T. T. M. Palstra, G. A. Gehring and J. Fontuberta. D. I. S. Coey helped to prepare the bibliography.

This work formed part of the activity of the Oxide Spin Electronics Network, a Training and Mobility of Researchers network supported by the European Commission. It was also partly supported by the Office of Naval Research through Grants ONR N00014-96-1-0767 and 97-1-0166.

References

[1] Jin, S., Tiefel, T. H., McCormack, M., Fastnacht, R. A., Ramesh, R., and Chen, L. H., 1994, *Science*, **264,** 413.
[2] Hwang, H. Y., Cheong, S. W., Ong, N. P., and Batlogg, B., 1996, *Phys. Rev. Lett.*, **77,** 2041.
[3] Zener, C., 1951, *Phys. Rev.*, **81,** 440.
[4] Zener, C., 1951, *Phys. Rev.*, **82,** 403.
[5] Pollert, E., Krupicka, S., and Kuzwicova, E., 1982, *J. Phys. Chem. Solids*, **43,** 1137.
[6] Zhao, G., Conder, K., Keller, H., and Müller, K. A., 1996, *Nature*, **381,** 676.
[7] Jonker, G., and van Santen, J., 1950, *Physica*, **16,** 337.
[8] von Santen, J. H., and Jonker, G. H., 1950, *Physica*, **16,** 599.
[9] Jonker, G. H., 1956, *Physica*, **22,** 707.
[10] Volger, J., 1954, *Physica*, **20,** 49.
[11] Searle, C. W., and Wang, S. T., 1969, *Can. J. Phys.*, **47,** 2703.
[12] Searle, C. W., and Wang, S. T., 1970, *Can. J. Phys.*, **48,** 2023.
[13] Morrish, A. H., Evans, B. J., Eaton, J. A., and Leung, L. K., 1969, *Can. J. Phys.*, **47,** 2691.
[14] Leung, L. K., Morrish, A. H., and Searle, C. W., 1969, *Can. J. Phys.*, **47,** 2697.
[15] von Helmholt, R., Wecker, J., Holzapfel, B., Schultz, L., and Samwer, K., 1993, *Phys. Rev. Lett.*, **71,** 2331.

[16] Chahara, K., Ohno, T., Kasai, M., and Kozono, Y., 1993, *Appl. Phys. Lett.*, **63,** 1990.
[17] Goodenough, J. B., and Longho, J., 1970, Landholdt–Börnstein, group III, Vol. 4a (Berlin: Springer).
[18] Verwey, E. J. W., and de Boer, J. H., 1936, *Recl Trav. chim. Pays-Bas Belg.*, **55,** 531.
[19] Verwey, E. J. W., 1935, *Z. Phys.*, **91,** 65.
[20] Wollan, E. O., and Koehler, W. C., 1955, *Phys. Rev.*, **100,** 545.
[21] Anderson, P. W., and Hasegawa, H., 1955, *Phys. Rev.*, **100,** 675.
[22] deGennes, P. G., 1960, *Phys. Rev.*, **118,** 141.
[23] Cullen, J. R., and Callan, E., 1973, *Phys. Rev.*, **7,** 397.
[24] Kanamori, J., 1959, *J. Phys. Chem. Solids*, **10,** 87.
[25] Goodenough, J. B., 1955, *Phys. Rev.*, **100,** 564.
[26] Edmonds, A. R., 1960, *Angular Momentum in Quantum Mechanics* (Princeton University Press).
[27] Nagaev, E. L., 1996, *Phys. Usp.*, **39,** 781.
[28] Ramirez, A. P., 1997, *J. Phys.: condens. Matter*, **9,** 8171.
[29] Methfessel, S., and Mattis, D. C., 1968, *Handbuch der Physik*, Vol. 18 (Berlin: Springer), p. 389.
[30] McGuire, T. R., Argyle, B. E., Shater, M. W., and Smart, J. S., 1962, *Appl. Phys. Lett.*, **1,** 17.
[31] Passell, L., Dietrich, O. W., and Als-Nielsen, J., 1976, *Phys. Rev.* B, **14,** 4897.
[32] Khomskii, D. I., and Sawatzky, G. A., 1997, *Solid St. Commun.*, **102,** 87.
[33] Kasuya, T., 1970, *IBM J. Res. Dev.*, **14,** 214.
[34] Holtzberg, F., McGuire, T. R., Methfessel, S., and Suits, J. C., 1964, *Phys. Rev. Lett.*, **13,** 18.
[35] von Molnár, S., and Methfessel, S., 1967, *J. Appl. Phys.*, **38,** 959.
[36] deGennes, P. G., and Friedel, J., 1958, *J. Phys. Chem. Solids*, **4,** 71.
[37] Fisher, M., and Langer, J., 1968, *Phys. Rev. Lett.*, **20,** 665.
[38] von Molnár, S., and Kasuya, T., 1968, *Phy. Rev. Lett.*, **21,** 1757.
[39] Kasuya, T., and Yanase, A., 1968, *Rev. mod. Phys.*, **40,** 684.
[40] Kasuya, T., Yanase, A., and Takeda, T., 1970, *Solid St. Commun.*, **8,** 1543.
[41] Kasuya, T., 1970, *Proceedings of the Tenth International Conference on the Physics of Semiconductors*, p. 243.
[42] Nagaev, E. L., 1974, *Phys. Stat. sol.* (b), **65,** 11.
[43] Nagaev, E. L., 1992, *J. of Magn. magn. Mater.*, **110,** 39.
[44] Oliver, M. R., Dimmock, J. O., and Reed, T. B., 1970, *IBM J. Res. Dev.*, **14,** 276.
[45] Oliver, M. R., Dimmock, J. O., McWhorter, A. L., and Reed, T. B., 1972, *Phys. Rev.* B, **5,** 1078.
[46] Penney, T., Shater, M. W., and Torrance, J. B., 1972, *Phys. Rev.* B, **5,** 3669.
[47] Shapira, Y., Foner, S., Aggarwal, R. L., and Reed, T. B., 1973, *Phys. Rev.* B, **8,** 2316.
[48] Kasuya, T., 1970, *Solid St. Commun.*, **8,** 1635.
[49] von Molnár, S., and Kasuya, T., 1970, *Proceedings of the Tenth International Conference on the Physics of Semiconductors*, p. 233.
[50] Mott, N. F., and Davies, E., 1971, *Electronic Processes in Noncrystalline Materials* (Oxford University Press).
[51] Cutler, M., and Mott, N. F., 1969, *Phys. Rev.*, **181,** 1336.
[52] von Molnár, S., and Holtzberg, F., 1973, *AIP Conf. Proc.*, **10,** 1259.
[53] Penney, T., Holtzberg, F., Tao, L. J., and von Molnár, S., 1974, *AIP Conf. Proc.*, **18,** 908.
[54] Mott, N. F., 1967, *Adv. Phys.*, **16,** 49.
[55] von Molnár, S., Briggs, A., Flouquet, J., and Remenyi, G., 1983, *Phys. Rev. Lett.*, **51,** 706.
[56] Washburn, S., Webb, R. A., von Molnár, S., Holtzberg, F., Flouquet, J., and Remenyi, G., 1984, *Phys. Rev.* B, **30,** 6224.
[57] Zachariasen, W. H., 1949, *Acta crystallogr.*, **2,** 57.
[58] Anderson, P. W., 1958, *Phys. Rev.*, **109,** 1492.

[59] Kamijo, A., Takase, A., Isikawa, Y., Kunrii, S., Suzuki, T., and Kasuya, T., 1980, *J. Phys., Paris*, **41,** C5, 189.
[60] von Molnár, S., and Penney, T., 1985, *Localization and Metal Insulator Transitions*, edited by H. Fritzche and D. Adler (New York: Plenum).
[61] Slater, J. C., 1937, *J. Appl. Phys.*, **8,** 385.
[62] Pauling, L., 1938, *Phys. Rev.*, **54,** 899.
[63] Busch, G., and Wachter, P., 1968, *Z. angew. Phys.*, **26,** 1.
[64] Esaki, L., Stiles, P. J., and von Molnár, S., 1967, *Phys. Rev. Lett.*, **19,** 852.
[65] von Molnár, S., 1970, *IBM J. Res. Dev.*, **14,** 269.
[66] Baum, G., Kisker, E., Mahan, A. H., Raith, W., and Reihl, B., 1977, *Appl. Phys.*, **14,** 149.
[67] Hao, X., Moodera, J. S., and Meservey, R., 1990, *Phys. Rev.* B, **42,** 8235.
[68] Moodera, J. S., Meservey, R., and Hao, X., 1993, *Phys. Rev. Lett.*, **70,** 853.
[69] Meservey, R., and Tedrow, P. M., 1994, *Phys. Rep.*, **238,** 173.
[70] Johnson, M., 1993, *Phys. Rev. Lett.*, **70,** 2142.
[71] Landauer, R., and Hall, J. J., 1968, *Science*, **160,** 736.
[72] Landauer, R., 1970, *Phys. Today*, **23,** 22.
[73] Valenzuela, R., 1994, *Magnetic Ceramics* (London: Cambridge University Press).
[74] Schiffer, P., Ramirez, A. P., Bao, W., and Cheong, S.-W., 1995, *Phys. Rev. Lett.*, **75,** 3336.
[75] Chainani, A., Mathew, M., and Sarma, D. D., 1993, *Phys. Rev.* B, **47,** 15397.
[76] Hervieu, M., Mahesh, R., Rangavittal, N., and Rao, C. N. R., 1995, *Eur. J. solid st. inorg. Chem.*, **32,** 79.
[77] Ibarra, M., Algarabel, P., Marquina, C., Blasco J., and Garcia, J., 1995, *Phys. Rev. Lett.*, **75,** 3541.
[78] Arnold, Z., Kamenev, K., Ibarra, M., Algarabel, P., Marquina, C., Blasco, J., and Garcia, J., 1995, *Appl. Phys. Lett.*, **67,** 2875.
[79] DeTeresa, J., Blasco, J., Ibarra, M., Garcia, J., Marquina, C., Algarabel, P., and del Moral, A., 1995, *Solid St. Commun.*, **96,** 627.
[80] Kusters, R. M., Singleton, J., Keen, D. A., McGreevy, R., and Hayes, W., 1989, *Physica* B, **155,** 362.
[81] Clausen, K. N., Hayes, W., Keen, D. A., Kusters, R. M., McGreevy, R. L., and Singleton, J., 1989, *J. Phys.: condens. Matter*, **1,** 2721.
[82] Jia, Y. X., Lu, L., Khazeni, K., Crespi, V. H., Zettl, A., and Cohen, M. L., 1995, *Phys. Rev.* B, **52,** 9147.
[83] Revcolevschi, A., and Dhalenne, G., 1993, *Adv. Mater.*, **5,** 657.
[84] Urushibara, A., Moritomo, Y., Arima, T., Asamitsu, A., Kido, G., and Tokura, Y., 1995, *Phys. Rev.* B, **51,** 14103.
[85] Asamitsu, A., Moritomo, Y., Tomioka, Y., Arima, T., and Tokura, Y., 1995, *Nature*, **373,** 407.
[86] Moritomo, Y., Asamitsu, A., and Tokura, Y., 1995, *Phys. Rev.* B, **51,** 16491.
[87] Anane, A., Dupas, C., Dang, K. L., Renard, J. P., Veillet, P., Guevara, A. M. D. L., Millot, F., Pinsard, L., and Revcolevschi, A., 1995, *J. Phys.: condens. Matter*, **7,** 7015.
[88] Tomioka, Y., Asamitsu, A., Moritomo, Y., Kuwahara, H., and Tokura, Y., 1995, *Phys. Rev. Lett.*, **74,** 5108.
[89] Tomioka, Y., Asamitsu, A., Moritomo, Y., and Tokura, Y., 1995, *J. phys. Soc. Japan*, **64,** 3626.
[90] Lees, M. R., Barratt, J., Balakrishnan, G., and Paul, D. M., 1995, *Phys. Rev.* B, **52,** 14303.
[91] Alvarado, S. F., Eib, W., Munz, P., Siegmann, H. C., Campagna, M., and Remeika, J. P., 1976, *Phys. Rev.* B, **13,** 4918.
[92] Lawler, J. F., Lunney, J. G., and Coey, J. M. D., 1994, *Appl. Phys. Lett.*, **65,** 3017.
[93] Lawler, J. F., Coey, J. M. D., Lunney, J. G., and Skumryev, V., 1996, *J. Phys.: condens. Matter*, **8,** 10737.
[94] von Helmholt, R., Wecker, J., Samwer, K., Haupt, L., and Bärner, K., 1994, *J. appl. Phys.*, **76,** 6925.

[95] Ju, H. L., Kwon, C., Li, Q., Greene, E. L., and Venkatesan, T., 1994, *Appl. Phys. Lett.*, **65,** 2108.
[96] Kasai, M., Kuwahara, H., Tomioka, Y., and Tokura, Y., 1996, *J. appl. Phys.*, **80,** 6894.
[97] McCormack, M., Jin, S., Tiefel, T. H., Fleming, R. M., Phillips, J. M., and Ramesh, R., 1994, *Appl. Phys. Lett.*, **64,** 3045.
[98] Jin, S., Tiefel, T. H., McCormack, M., O'Brien, H. M., Chen, L. H., Ramesh, R., and Schurig, D., 1995, *Appl. Phys. Lett.*, **67,** 557.
[99] Xiong, G. C., Li, Q., Ju, H. L., Greene, R. L., and Venkatesan, T., 1995, *Appl. Phys. Lett.*, **66,** 1689.
[100] Satyalakshmi, K., Manoharan, S. S., Hegde, M., Prasad, V., and Subramanyam, S., 1995, *J. Appl. Phys.*, **78,** 6861.
[101] Xiong, G., Li, Q., Ju, H., Bhagat, S., *et al.*, 1995, *Appl. Phys. Lett.*, **67,** 3031.
[102] Gupta, A., McGuire, T., Duncombe, P., Rupp, M., *et al.*, 1995, *Appl. Phys. Lett.*, **67,** 3494.
[103] Hundley, M. F., Neumeier, J. J., Heffner, R. H., Jia, Q. X., Wu, X. D., and Thompson, J. D., 1996, *J. Appl. Phys.*, **79,** 4535.
[104] Kung, P. J., Fenner, D. B., Potrepka, D. M., and Budnick, J. I., 1996, *Appl. Phys. Lett.*, **69,** 427.
[105] Srinivasan, G., Babu, V. S., and Seeha, M. S., 1995, *Appl. Phys. Lett.*, **67,** 2090.
[106] Gu, J. Y., Kwon, C., Robson, M. C., Trajanovic, Z., Gosh, K., and Sharma, P., 1997, *Appl. Phys. Lett.*, **70,** 1763.
[107] Zhang, W., Boyd, I. W., Elliot, M., and Herrenden-Harkerand, W., 1996, *Appl. Phys. Lett.*, **69,** 1154.
[108] Zhang, W., Boyd, I. W., Elliot, M., and Herrenden-Harkerand, W., 1996, *Appl. Phys. Lett.*, **69,** 3599.
[109] Sahana, M., Singh, R. N., Shivakumara, C., Vasanthacharya, N. Y., *et al.*, 1997, *Appl. Phys. Lett.*, **70,** 2909.
[110] Kishino, S., Kuroda, H., Shibutani, T., and Niu, H., 1994, *Appl. Phys. Lett.*, **65,** 781.
[111] Kasai, M., Ohno, T., Kanke, Y., Kozono, Y., Hanazono, M., and Sugita, Y., 1990, *Jap. J. Appl. Phys.*, **29,** L2219.
[112] Chahara, K., Ohno, T., Kasai, M., Kanke, Y., and Kozono, Y., 1993, *Appl. Phys. Lett.*, **62,** 780.
[113] Singh, S. K., Palmer, S., Paul, D. M., and Lees, M. R., 1996, *Appl. Phys. Lett.*, **69,** 263.
[114] Wagner, P. H., Metlushko, V., Trappeniers, L., Vantomme, A., Vanacken, J., Kido, V., Moshchalkov, V. V., and Bruynseraede, Y., 1992, *Phys. Rev.* B, **55,** 3699.
[115] Jakob, G., Moshchalkov, V. V., and Bruynseraede, Y., 1995, *Appl. Phys. Lett.*, **66,** 2564.
[116] Zeng, X. T., and Wong, H. K., 1995, *Appl. Phys. Lett.*, **166,** 3371.
[117] Cho, J., Gomi M., and Abe, M., 1990, *Jap. J. Appl. Phys.*, **29,** 1686.
[118] Li, Y. Q., Zhang, J., Pombrik, S., diMascio, D., Stevens, W., Yan, Y. F., and Ong, N. P., 1995, *J. Mater. Res.*, **10,** 2116.
[119] Dahmen, K.-H., and Carris, M. W., 1992, *J. Alloys Componds*, **251,** 270.
[120] Dahmen, K.-H., and Carris, M. W., 1992, *Chem. Vapour Deposition*, **3,** 27.
[121] Heremans, J. J., Carris, M., Watts, S., Dahmen, K.-H., and von Molnár, S., 1992, *J. Appl. Phys.*, **81,** 4967.
[122] Snyder, G. J., Hiskes, R., DiCarolis, S., Beasley, M. R., and Geballe, T. H., 1996, *Phys. Rev.* B, **53,** 14434.
[123] Snyder, G. J., Beasley, M. R., and Geballe, T. H., 1995, *Mater. Res. Symp. Proc.*, **401,** 541.
[124] Worledge, D. C., Snyder, G. J., Beasley, M. R., Geballe, T. H., Hiskes, R., and DiCarolis, S., 1996, *J. Appl. Phys* **80,** 5158.
[125] Eckstein, J. N., Bozovic, I., Rzchowski, M. S., O'Donnell, J., Hinaus, B. M., and Onellion, M., 1996, *Epitaxial Oxide Thin Films* (Pittsburgh, Pennsylvania: Materials Research Society), p. 467.

[126] Achutharaman, V. S., Kraus, P. A., Vas'ko, V. A., Nordman, C. A., and Goldman, A. M., 1995, *Appl. Phys. Lett.*, **67,** 1019.
[127] Vas'ko, V. A., Nordman, C. A., Kraus, P. A., Achutharaman, V. S., Ruosi, A. R., and Goldman, A. M., 1996, *Appl. Phys. Lett.*, **68,** 2571.
[128] Bozovic, I., and Eckstein, J. N., 1997, *Appl. Surf. Sci.*, **113–114,** 189.
[129] Eckstein, J., Bozovic, I., O'Donnell, J., Onellion, M., and Rzchowski, M., 1996, *Appl. Phys. Lett.*, **69,** 1312.
[130] O'Donnell, J., Onellion, M., Rzchowski, M. S., Eckstein, J. N., and Bozovic, I., 1997, *Phys. Rev.* B, **55,** 5873.
[131] Matsumoto, Y., Sasaki, T., and Hombo, J., 1991, *J. electrochem. Soc.*, **158,** 1259.
[132] Sasaki, T., Matsumoto, Y., Hombo, J., and Ogawa, Y., 1991, *J. solid-st. Chem.*, **91,** 61.
[133] Sasaki, T., Morikawa, T., Hombo, J., and Matsumoto, Y., 1990, *Denki Kogaku*, **58,** 567.
[134] Sasaki, T., Matsumoto, Y., Hombo, J., and Nagata, M., 1993, *J. solid-st. Chem.*, **105,** 255.
[135] Itoh, M., Shimura, T., Hayashi, T., and Inaguma, Y., 1996, *Solid St. Commun.*, **97,** 179.
[136] Balcells, L., Enrich, R., Mora, J., Calleja, A., Fontcuberta, J., and Obradors, X., 1996, *Appl. Phys. Lett.*, **69,** 1486.
[137] Tamura, S., and Yamamoto, A., 1980, *J. Mater. Sci.*, **15,** 2120.
[138] Pauthenet, R., and Veyret, C., 1970, *J. Phys.*, Paris, IV, **31,** 65.
[139] Huang, Q. A., Santoro, A., Lynn, J. W., Erwin, R. W., Borchers, J. A., Peng, J. L., and Greene, R. L., 1997, *Phys. Rev.* B, **55,** 14987.
[140] Kuo, J. H., Andersen, H., and Sparlin, D., 1989, *J. solid-st. Chem.*, **83,** 52.
[141] Tofield, B. C., and Scott, W. R., 1974, *J. solid-st. Chem.*, **10,** 183.
[142] deLéon-Guevara, A. M., Berthet, P., Berthon, J., Millot, F., Revcolevschi, A., Anane, A., Dupas, C., Dang, K. L., Renard, J. P., and Veillet, P., 1997, *Phys. Rev.* B, **56,** 6031.
[143] Roosmalen, J. A. M. V., and Cordfunke, E. H. P., 1991, *J. solid-st Chem.*, **93,** 212.
[144] Cherry, M., Islam, M. S., and Catlow, C., 1995, *J. solid-st. Chem.*, **118,** 125.
[145] Yasuda, I., and Hishinuma, M., 1996, *J. solid-st. Chem.*, **123,** 382.
[146] Cherry, M., Islam, M. S., Gale, J., and Catlow, C., 1995, *J. phys. Chem.*, **99,** 14914.
[147] Kamata, K., Nakajima, T., Hayashi, T., and Nakajima, T., 1988, *Mater. Res. Bull.*, **13,** 49.
[148] Abbattista, F., and Borlera, M. L., 1981, *Ceram. Int.*, **7,** 137.
[149] Caignaert, V., Nyuyen, N., Hervieu, M., and Raveau, B., 1985, *Mater. Res. Bull.*, **20,** 479.
[150] Patil, S. I., Shreekala, R., Lanke, U., Bhagwat, A., and Ogale, S. B., 1996, *Nucl. Instrum. Meth.* B, **114,** 42.
[151] Chen, C. H., Talyansky, V., Kwon, C., Rajeswari, M., Sharma, P., and Ramesh, R., 1996, *Appl. Phys. Lett.*, **69,** 3089.
[152] Roosmalen, J. A. M. V., Cordfunke, E. H. P., Helmholdt, R. B., and Zandbergen, H. W., 1994, *J. solid-st. Chem.*, **110,** 100.
[153] Roosmalen, J. A. M. V., van Vlaanderen, P., Cordfunke, E. H. P., Ijdo, W. L., and Ijdo, D. J. W., 1995, *J. solid-st. Chem.*, **114,** 516.
[154] Matsumoto, G., *J. phys. Soc. Japan*, **29,** 606.
[155] Goodenough, J. B., 1997, *Proceedings of Materials Research Society Meeting*, Boston, Massachusetts, 1997 (Pittsburgh, Pennsylvania: Materials Research Society).
[156] Ranno, L., Viret, M., Mari, A., Thomas, R. M., and Coey, J. M. D., 1996, *J. Phys: condens. Matter*, **8,** L33.
[157] Harwood, G., 1955, *Proc. phys. Soc.* B, **65,** 586.
[158] McGuire, T. R., Gupta, A., Duncombe, P. R., Rupp, M., Sun, J. Z., Laibowitz, R. B., Gallagher W. J., and Xiao, G., 1996, *J. appl. Phys.*, **79,** 4549.
[159] Caignaert, V., Suard, E., Maignan, A., Simon, C., and Raveau, B., 1996, *J. Magn. magn. Mater.*, **153,** L260.
[160] Roosmalen, J. A. M. V., and Cordfunke, E. H. P, 1994, *J. solid-st. Chem.*, **110,** 106.

[161] Goldschmidt, V., 1958, *Geochemistry* (Oxford University Press).
[162] Shannon, R. D., and Prewitt, C. T., 1976, *Acta crystallogr.* A, **32,** 785.
[163] Licci, F., Turilli, G., and Ferro, P., 1996, *J. Magn. magn. Mater.*, **164,** L268.
[164] Mahendiran, R., Mahesh, R., Raychaudhuri, A. K., and Rao, C. N. R., 1996, *Phys. Rev.* B, **53,** 12160.
[165] Wang, Z. L., Jin, J. S., Jiang, Y. D., and Zhang, J., 1997, *Appl. Phys. Lett.*, **70,** 3362.
[166] Liu, R., Wu, J. B., Chang, C. Y., Lin, J. G., Hwang, C. Y., Chen, J. M., and Liu, R. G., 1996, *J. solid-st. Chem.*, **125,** 112.
[167] Subias, G., Garcia, J., Proietti, M. G., and Blasco, J., 1997, *Phys. Rev.* B, **56,** 8183.
[168] Saitoh, T., Bocquet, A. E., Mizokawa, T., Namatame, H., Fujimori, A., Abbate, Y., Takeda, Y., and Takano, M., 1995, *Phys. Rev.* B, **51,** 13942.
[169] Goodenough, J. B., 1996, *Magnetism and the Chemical Bond* (New York: Wiley–Interscience).
[170] Moussa, F., Hennion, M., Rodriguez-Carvajal, J., Moudden, H., and Revcolevschi, A., 1996, *Phys. Rev.* B, **54,** 15149.
[171] Wold, A., and Arnott, R. J., 1959, *J. Phys. Chem. Solids*, **9,** 176.
[172] Goodenough, J. B., 1971, *Prog. Solid st. Chem.*, **5,** 185.
[173] Lees, M. R., Barratt, J., Balakrishnan, G., and Paul, D. M., 1996, *J. Phys.: condens. Mater*, **8,** 2967.
[174] Millis, A. J., Shraiman, B. I., and Mueller, R., 1996, *Phys. Rev. Lett.*, **77,** 175.
[175] Töpfer, J., and Goodenough, J. B., 1997, *J. solid-st. Chem.*, **130,** 117.
[176] Cheetham, A. K., Rao, C. N. R., and Vogt, T., 1996, *J. solid-st. Chem.*, **126,** 337.
[177] Maignan, A., Michel, C., Hervieu, M., and Raveau, B., 1992, *Solid St. Commun.*, **101,** 277.
[178] Yakel, H. L., 1955, *Acta crystallogr.*, **8,** 394.
[179] MacChesney, J. B., Williams, H. J., Potter, J. F., and Sherwood, R. C., 1967, *Phys. Rev.*, **164,** 779.
[180] Voorhoeve, R. J. H., Remeika, J. P., Trimble, L., Cooper, A., Disalvo, F., and Gallagher, P., 1975, *J. solid-st. Chem.*, **14,** 395.
[181] Islam, M. S., Cherry, M., and Winch, L., 1996, *J. Chem. Soc., Faraday Trans.*, **92,** 479.
[182] Mitchell, J., Argyriou, D., Potter, C., Hinks, D., Jorgensen, J., and Bader, S., 1966, *Phys. Rev.* B, **54,** 6172.
[183] Itoh, M., Nishi, K., Yu, J. D., and Inaguma, Y., 1997, *Phys. Rev.* B, **55,** 14408.
[184] Mahendiran, R., Mahesh, R., Rangavittal, N., Tewari, S., Raychauduri, A., Ramakrishnan, T., and Rao, C., 1996, *Phys. Rev.* B, **53,** 3348.
[185] Hwang, H. Y., Cheong, S. W., Radaelli, P. G., Marezio, M., and Batlogg, B., 1995, *Phys. Rev. Lett.*, **75,** 914.
[186] Garcia-Munoz, J. L., Fontcuberta, J., Martinez, B., Seffar, A., Pinol, S., and Obradors, X., 1997, *Phys. Rev.* B, **55,** R668.
[187] Garcia-Munoz, J. L., Fontcuberta, J., Suaaidi, M., and Obradors, X., 1996, *J. Phys.: condens. Matter*, **8,** L787.
[188] Sharma, N., Nigam, A. K., Pinto, R., Venkataramani, N., Prasad, S., Chandra, G., and Pai, S. P., 1997, *J. Magn. magn. Mater.*, **166,** 65.
[189] Martin, M., Shirane, G., Endoh, Y., Hirota, K., Morimoto, Y., and Tokura, Y., 1996, *Phys. Rev.* B, **53,** 14285.
[190] Radaelli, P. G., Marezio, M., Hwang, H. Y., Cheong, S.-W., and Batlogg, B., 1996, *Phys. Rev.* B, **54,** 8992.
[191] Yamada, Y., Hino, O., Nohdo, S., Kanao, R., Inami, T., and Katano, S., 1996, *Phys. Rev. Lett.*, **77,** 904.
[192] Jirak, Z., Krupicka, S., Simsa, Z., Dlouha, M., and Vratislav, S., 1985, *J. Magn. magn. Mater.*, **53,** 153.
[193] Tomioka, Y., Asamitsu, A., Kuwahara, H., Moritomo, Y., and Tokura, Y., 1996, *Phys. Rev.* B, **53,** R1689.
[194] Chen, C. H., and Cheong, S. W., 1996, *Phys. Rev. Lett.*, **76,** 4042.

[195] Kuwahara, H., Tomioka, Y., Asamitsu, A., Moritomo, Y., and Tokura, Y., 1995, *Science*, **270,** 961.
[196] Caignaert, V., Milange, F., Hervieu, M., Suard, E., and Raveau, B., 1996, *Solid St. Commun.*, **99,** 173.
[197] Laffez, P., van Tendeloo, G., Millange, F., Caignaert, V., Hervieu, M., and Raveau, B., 1996, *Mater. Res. Bull.*, **31,** 905.
[198] Podlesnyak, A., Rosenkranz, S., Fauth, F., Marti, W., Scheel, H., and Furrer, A., 1994, *J. Phys.: condens. Matter*, **6,** 4099.
[199] Podlesnyak, A., Rosenkranz, S., Fauth, F., Marti, W., Furrer, A., Mirmelstein, A., and Scheel, H., 1993, *J. Phys.: condens. Matter*, **5,** 8973.
[200] Bartolome, F., Kuzmin, M. D., Merino, R., and Bartolome, J., 1994, *IEEE Trans. Magn.*, **30,** 960.
[201] Radwanski, R. J., (unpublished).
[202] Rao, G. S., Rao, C., and Ferraro, J., 1970, *Appl. Spectrosc.*, **24,** 436.
[203] Burns, R. G., 1992, *Mineralogical Applications of Crystal Field Theory*, second edition (London: Cambridge University Press).
[204] Okimoto, Y., Katsufuji, T., Ishikawa, T., Urushibara, A., Arima, T., and Tokura, Y., 1995, *Phys. Rev. Lett.*, **75,** 109.
[205] Arima, T., and Tokura, Y., 1995, *J. phys. Soc. Japan*, **64,** 2488.
[206] Sarma, D., Shanthi, N., Barman, S., Hamada N., Sawada, H., and Terakura, K., 1995, *Phys. Rev. Lett.*, **75,** 1126.
[207] Zaanen, J., Sawatzky, G. A., and Allen, J. W., 1985, *Phys. Rev. Lett.*, **55,** 418.
[208] Zaanen, J., and Sawatzky, G. A., 1990, *J. solid-st. Chem.*, **88,** 8.
[209] Abbate, M., de Groot, F. M. F., Fuggle, J. C., Fujimori, A., Strebel, O., Lopez, F., Domke, M., Kaindl, G., Sawatzky, G. A., Takano, M., Takeda, Y., Eisaki, H., and Uchida, S., 1992, *Phys. Rev.* B, **46,** 4511.
[210] Sherman, D., 1984, *Am. Mineral.*, **69,** 788.
[211] Ju, H. L., Sohn, H.-C., and Krishnan, K. M., 1992, *Phys. Rev. Lett.*, **79,** 3230.
[212] Wei, J. Y. T., Yeh, N. C., and Vasquez, R. P., 1997, *Phys. Rev. Lett.*, **79,** 5150.
[213] Park, J.-H., Chen, C. T., Cheong, S.-W., Bao, W., Meigs, G., Chakarian, V., and Idzerda, Y. U., 1996, *Phys. Rev. Lett.*, **76,** 4215.
[214] Bocquet, A. E., Mizokawa, T., Saitoh, T., and Namatame, H., 1992, *Phys. Rev.* B, **46,** 3771.
[215] Pickett, W. E., and Singh, D. J., 1995, *Europhys. Lett.*, **32,** 759.
[216] Pickett, W. E., and Singh, D. J., 1996, *Phys. Rev.* B, **53,** 1146.
[217] Satpathy, S., Popovic, Z. S., and Vukajlovic, F. R., 1996, *Phys. Rev. Lett.*, **76,** 960.
[218] Satpathy, S. Popovic, Z. S., and Vukajlovic, F. R., 1996, *Jap. J. Appl. Phys.*, **79,** 4555.
[219] Solovyev, I., Hamada, N., and Terakura, K., 1996, *Phys. Rev. Lett.*, **76,** 4825.
[220] Hamada, N., Sawada, H., and Terakura, K., 1995, *Spectroscopy of Mott Insulators and Correlated metals,* edited by A. Fujimori and Y. Tokura (Berlin: Springer).
[221] Boer, P., van Leuken, H., de Groot, R. A., Rojo, T., *et al.*, 1997, *Solid St. Commun.*, **102,** 621.
[222] Mizokawa, T., and Fujimori, A., 1995, *Phys. Rev. Lett.*, **51,** 12880.
[223] Mizokawa, T., and Fujimori, A., 1996, *Phys. Rev.* B, **54,** 5368.
[224] Tobola, J., Kaprzyk, S., and Pierre, J., 1997, *Acta Phys. Polonica* A, **92,** 461.
[225] Solovyev, I., Hamada, N., and Terakura, K., 1996, *Phys. Rev.* B, **53,** 7158.
[226] Elemans, J. B. A. A., van Laar, K. R., van der Veen, K. R., and Loopstra, B. O., 1971, *J. solid-st. Chem.*, **3,** 238.
[227] Shi, F., Ding, M., and Lin, T., 1995, *Solid St. Commun.*, **96,** 931.
[228] Mazzaferro, J., Balseiro, C. A., and Alascio, B., 1985, *J. Phys. Chem. Solids*, **46,** 1339.
[229] Allub, R., and Alascio, B., 1996, *Solid St. Commun.*, **99,** 613.
[230] Allub, R., and Alascio, B., 1997, *Phys. Rev.* B, **55,** 14113.
[231] Varma, C. M., 1996, *Phys. Rev.* B, **54,** 7328.
[232] Viret, M., Ranno, L., and Coey, J. M. D., 1997, *Phys. Rev.* B, **55,** 8067.
[233] Ranno, L., Viret, M., and Coey, J. M. D. (unpublished).

[234] Dzyaloshinsky, I., 1958, *J. Phys. Chem. Solids*, **4,** 241.
[235] Moriya, T., 1960, *Phys. Rev.*, **120,** 91.
[236] Töpfer, J., Doumerc, J., and Grenier, J.-C., 1996, *J. Mater. Chem.*, **6,** 1511.
[237] Arulraj, A., Mahesh, R., Subbanna, G. N., Mahendiran, R., Raychaudhuri, A. K., and Rao, R., 1996, *J. solid-st. Chem.*, **127,** 87.
[238] Quezel-Ambrunaz, S., 1968, *Bull. Soc. Fr. Mineral. et de Crystallogr.*, **91,** 339.
[239] Allodi, G., Renzi, R. D., Guidi, G., Licci, F., and Pieper, M. W., 1997, *Phys. Rev.* B, **56,** 6036.
[240] Radaelli, P. G., Cox, D. E., Marezio, M., Cheong, S.-W., Schiffer, P. E., and Ramirez, A. P., 1995, *Phys. Rev. Lett.*, **75,** 4488.
[241] Jirak, Z., Krupicka, S., Nekvasil, V., Pollert, E., Villeneuve, G., and Zounova, F., 1980, *J. Magn. magn. Mater.*, **15–18,** 519.
[242] Knizek, K., Jirak, Z., Pollert, E., and Zounova, F., 1992, *J. solid-st. Chem.*, **100,** 292.
[243] Jirak, Z., 1997, *J. Appl. Phys.*, **81,** 4675.
[244] Yoshizawa, H., Kajimoto, R., Kawano, H., Toimioka, T., and Tokura, Y., 1997, *Phys. Rev.* B, **55,** 2729.
[245] Takeda, T., Yamaguchi, Y., and Watanabe, H., 1972, *J. phys. Soc. Japan*, **33,** 967.
[246] Kawano, H., Kajimoto, R., Yoshizawa, H., Tomioka, Y., Kuwaara, H., and Tokura, Y., 1997, *Phys. Rev. Lett.*, **78,** 4253.
[247] Geissinger, E., Braunstein, R., Ladizinsky, E., Haupt, L., Schunemann, J., Baerner, K., Sondermann, U., and Andresen, A., 1991, *Solid St. Commun.*, **78,** 503.
[248] Kawano, H., Kajimoto, R., Kubota, M., and Yoshizawa, H., 1991, *Phys. Rev.* B, **53,** 2202.
[249] Kawano, H., Kajimoto, R., Kubota, M., and Yoshizawa, H., 1996, *Phys. Rev.* B, **53,** 14 709.
[250] Jirak, Z., and Pollert, E., 1990, *Eur. J. solid st. Inorg. Chem.*, **27,** 421.
[251] Snyder, G. J., Booth, C. H., Bridges, F., Hiskes, R., DiCarolis, S., Beasley, M. R., and Geballe, T. H., 1997, *Phys. Rev.* B, **55,** 6453.
[252] DeTeresa, J. M., Ibarra, M. R., Garcia, J., Blasco, J., Ritter, C., Algarabel, P. A., Marguina, C., and delMoral, A., 1996, *Phys. Rev. Lett.*, **76,** 3392.
[253] Blasco, J., Garcia, J., de Teresa, J. M., Ibarra, M. R., Algrabel, P. A., and Marquina, C., 1996, *J. Phys.: condens. Matter*, **8,** 7427.
[254] von Helmholt, R., Haupt, L., Bärner, K., and Sondermann, U., 1992, *Solid St. Commun.*, **82,** 693.
[255] Haupt, L., von Helmholt, R., Sondermann, U., and Bärner, K., 1992, *Phys. Lett.* A, **165,** 473.
[256] Martin, C., Maignan, A., and Raveau, B., 1996, *J. Mater. Chem.*, **6,** 1245.
[257] Blasco, J., Garcia, J., de Teresa, J. M., Ibarra, M. R., Perez, J., Algarabel, P. A., Marquina, C., and Ritter, C., 1997, *Phys. Rev.* B, **55,** 8905.
[258] Leung, L. K., Morrish, A. H., and Evans, B. J., 1976, *Phys. Rev.* B, **13,** 4069.
[259] Bokov, V. A., Grigoryan, N. A., and Bryzhina, M. V., 1967, *Phys. Stat., sol.*, **20,** 745.
[260] Chiba, H., Kikuchi, M., Kusaba, K., Muraoka, Y., and Syono, Y., 1996, *Solid St. Commun.*, **99,** 499.
[261] Bao, W., Axe, J. D., Chen, C. H., and Cheong, S.-W., 1997, *Phys. Rev. Lett.*, **78,** 543.
[262] Havinga, E. E., 1966, *Philips Res. Rep.*, **21,** 432.
[263] Fontcuberta, J., Martinez, B., Seffar, A., Piñol, S., Garcia-Muñoz, J. L., and Obradors, X., 1996, *Phys. Rev. Lett.*, **76,** 1122.
[264] Bokov, V. A., Grigoryan, N. A., Bryzhina, M. V., and Tikhonov, V. V., 1968, *Phys. Stat. sol.*, **28,** 835.
[265] Fontcuberta, J., Martinez, B., Seffar, A., Piñol, S., Garcia-Muñoz, J. L., and Obradors, X., 1996, *Europhys. Lett.*, **34,** 379.
[266] Sun, J. R., Rao, G. H., Liang, J. K., and Zhou, W. Y., 1996, *Appl. Phys.* A, **69,** 3926.
[267] Thomas, R. M., Ranno, L., and Coey, J. M. D., 1997, *J. appl. Phys.*, **81,** 5763.

[268] Mahesh, R., Mahendiran, R., Raychaudhuri, A. K., and Rao, C. N. R., 1996, *J. solid-st. Chem.*, **120,** 204.
[269] Maignan, A., Simon, C., Caignaert, V., and Raveau, B., 1996, *Z. Phys.* B, **99,** 305.
[270] von Helmholt, R., Wecker, J., Lorenz, T., and Samwer, K., 1995, *Appl. Phys. Lett.*, **67,** 2093.
[271] Maignan, A., Martin, C., and Raveau, B., 1997, *Z. Phys.* B, **102,** 19.
[272] Ju, H. L., and Sohn, H., 1992, *J. Magn. Magn. Mater.*, **167,** 200.
[273] de Brion, S., Chouteau, G., and Lejay, P., (unpublished).
[274] Ju, H. L., Gopalakrishnan, J., Peng, J. L., Li, Q., *et al.*., 1995, *Phys. Rev.* B, **51,** 6143.
[275] Hirota, K., Kaneko, N., Nishizawa, A., and Endoh, Y., 1996, *J. phys. Soc. Japan*, **65,** 3736.
[276] Heffner, R. H., Le, L. P., Hundley, M. F., Neumeier, J. J., Luke, G. M., Kojima, K., Nachumi, B., Uemura, Y. J., MacLaughlin, D. E., and Cheong, S. W., 1996, *Phys. Rev. Lett.*, **77,** 1869.
[277] Archibald, W., Zhou, J.-S., and Goodenough, J. B., 1996, *Phys. Rev.* B, **53,** 14445.
[278] Smolyaninova, V. N., Hamilton, J. J., Greene, R. L., Mukovskii, Y. N., *et al.*, 1997, *Phys. Rev.* B, **55,** 5640.
[279] Lu, Q., Chen, C. C., and de Lozanne, A., 1997, *Science*, **276,** 2006.
[280] Lotgering, F., 1970, *Philips Res. Rep.*, **25,** 8.
[281] Sun, J. Z., Krusin-Elbaum, L., Gupta, A., Xiao, G., and Parkin, S., 1996, *Appl. Phys. Lett.*, **69,** 1002.
[282] Fontcuberta, J., Martinez, B., Seffar, A., Piñol, S., Garcia-Muñoz, J. L., and Obradors, X., 1996, *J. Appl. Phys.*, **79,** 5182.
[283] Oseroff, S. B., Torikachvili, M., Singley, J., Ali, S., Cheong, S. W., and Schultz, S., 1996, *Phys. Rev.* B, **53,** 6521.
[284] Leung, L. K., and Morrish, A. H., 1977, *Phys. Rev.* B, **15,** 2485.
[285] Matsumoto, G., 1970, *J. phys. Soc. Japan*, **29,** 615.
[286] Matsumoto, G., and Iida, S., 1966, *J. phys. Soc. Japan*, **21,** 2734.
[287] Kapuzta, Cz., Reidel, P. C., Tomka, G. J., Kocemba, W., Ibarra, M. R., De Teresa, J. M., Viret, M., and Coey, J. M. D. (unpublished).
[288] Anane, A., Dupas, C., LeDang, K., Renard, J. P., Veillet, P., Pinsard, L., and Revcolevschi, A., 1996, *Appl. Phys. Lett.*, **69,** 1160.
[289] Fontcuberta, J., Martinez, B., Garcia-Munoz, J. L., Seffar, A., Piñol, S., Roig, A., Molins, E., and Obradors, X., 1996, *Solid St. Commun.*, **97,** 1033.
[290] Woodfield, B. F., Wilson, M. L., and Byers, J. M., 1997, *Phys. Rev. Lett.*, **78,** 3201.
[291] Gubkin, M. K., Khimich, T. A., Kleparskaya, E. V., Perekalina, T. M., *et al.*, 1996, *J. Magn. magn. Mater.*, **154,** 351.
[292] Wang, S., and Searle, C. W., 1970, *Can. J. Phys.*, **49,** 387.
[293] Ramachandran, J. S., Bhagat, S. M., Peng, J. L., and Rubenstein, M., 1995, *Solid St. Commun.*, **96,** 127.
[294] Lofland, S., Bhagat, S., Ju, H., Xiong, G., Venkatesan, T., and Greene, R., 1995, *Phys. Rev.* B, **52,** 15058.
[295] Robson, M. C., Kwon, C., Kim, K. C., Sharma, R. P., Venkatesan, T., Ramesh, R., Lofland, S. E., Dominguez, M., Tyagi, S. D., and Bhagat, S. M., 1996, *J. appl. Phys.*, **80,** 2334.
[296] Dominguez, M., Bhagat, S., Lofland, S., Ramachandran, J., Xiong, G., Ju, H., Venkatesan, T., and Greene, R., 1995, *Europhys. Lett.*, **32,** 349.
[297] Ohno, T., Kasai, M., Kanke, Y., Kozono, Y., and Hanazono, M., 1992, *Solid St. Commun.*, **81,** 993.
[298] Lofland, S. E., Bhagat, S. M., Kwon, C., Robson, M. C., Sharma, R., Ramesh, R., and Venkatesan, T., 1995, *Phys. Lett.* A, **209,** 246.
[299] Morrish, A. H., 1965, *The Physical Principles of Magnetism* (New York: Wiley).
[300] Kwon, C., Kim, K. C., Robson, M. C., Lofland, S. E., Bhagat, S. M., Venkatesan, T., Ramesh, R., and Gomez, R. D., 1997, *J. Magn. magn. Mater.*, **172,** 229.

[301] Lofland, S. E., Bhagat, S. M., Ju, H., Xiong, G., Venkatesan, T., and Greene, R., 1996, *J. appl. Phys.*, **79,** 5166.
[302] Seehra, M. S., Ibrahim, M. M., Babu, V. S., and Srinivasan, G., 1996, *J. Phys.: condens. Matter*, **8,** 11 283.
[303] Rettori, C., Rao, D., Singley, J., Kidwell, D., Oseroff, S. B., Causa, M. T., Neumier, J. J., McClellan, K. J., Cheong, S.-W., and Schultz, S., 1997, *Phys. Rev.* B, **55,** 3083.
[304] Perring, T. G., Aeppli, G., Hayden, S. M., Carter, S. A., Remeika, J. P., and Cheong, S. W., 1996, *Phys. Rev. Lett.*, **77,** 711.
[305] Hennion, M., Moussa, F., Rodriguez-Carvajal, J., Pinsard, L., and Revcolevschi, A., 1997, *Phys. Rev.* B, **56,** R497.
[306] Lynn, J., Erwin, R., Borchers, J., Huang, Q., and Santoro, A., 1996, *Phys. Rev. Lett.*, **76,** 4046.
[307] Furukawa, N., 1996, *J. phys. Soc. Japan*, **65,** 1174.
[308] Lofland, S. E., and Bhagat, S. M., 1995, *Phys. Lett.* A, **209,** 246.
[309] DeTeresa, J. M., Ibarra, M. R., Blasco, J., Garcia, J., Marquina, C., Algarabel, P., Arnold, Z., Kamenez, K., Ritter, C., and von Helmholt, R., 1996, *Phys. Rev.* B, **54,** 1187.
[310] DeTeresa, J. M., Blasco, J., Ibarra, M. R., Garcia, J., Marquina, C., and Algarabel, P., 1996, *J. appl. Phys.*, **79,** 1.
[311] Tamura, S., 1983, *J. Magn. magn. Mater.*, **31–34,** 805.
[312] Neumeier, J. J., Hundley, M. F., Thompson, J. D., and Heffner, R. H., 1995, *Phys. Rev.,* B, **52,** R7006.
[313] Hwang, H., Palstra, T. T. M., Cheong, S.-W., and Batlogg, B., 1995, *Phys. Rev.* B, **52,** 15 046.
[314] Patrick, L., 1954, *Phys. Rev.*, **93,** 384.
[315] Khazeni, K., Jia, Y. X., Crespi, V. H., Lu, L., Zettl, A., and Cohen, M. L., 1996, *J. Phys.: condens. Matter*, **8,** 7723.
[316] Khazeni, K., Jia, Y. X., Crespi, V. H., Cohen, M. L., and Zettl, A., 1996, *Phys. Rev. Lett.*, **76,** 295.
[317] Moritomo, Y., Kuwahara, H., Tomika, Y., and Tokura, Y., 1997, *Phys. Rev.* B, **55,** 7549.
[318] Tokura, Y., Tomioka, Y., Kuwahara, H., Asamitsu, A., Moritomo, Y., and Kasai, M., 1996, *Physica* C, **263,** 544.
[319] Argyriou, D. N., Mitchell, J. F., Potter, C. D., Hinks, D. G., Jorgensen, J. D., and Bader, S. D., 1996, *Phys. Rev. Lett.*, **76,** 3826.
[320] Asamitsu, A., Moritomo, Y., Kumai, R., Tomioka, Y., and Tokura, Y., 1996, *Phys. Rev.* B, **54,** 1716.
[321] Tokura, Y., Kuwahara, H., Moritomo, Y., Tomioka, Y., and Asamitsu, A., 1996, *Phys. Rev. Lett.*, **76,** 3184.
[322] Wolfman, J., Maignan, A., Simon, C., and Raveau, B., 1996, *J. Magn. magn. Mater.*, **159,** L299.
[323] Maignan, A., and Raveau, B., 1997, *Z. Phys.* B, **102,** 299.
[324] de Teresa, J. M., Ibarra, M. R., Marquina, C., Algarabel, P. A., 1996, *Phys. Rev.* B, **54,** R12 689.
[325] Yoshizawa, H., Kawano, H., Tomioka, Y., and Tokura, Y., 1995, *Phys. Rev.* B, **52,** R13 145.
[326] Barratt, J., Lees, M. R., Balakrishnan, G., and Paul, D. M., 1996, *Appl. Phys. Lett.*, **68,** 424.
[327] Yoshizawa, H., Kawano, H., Tomioka, Y., and Tokura, Y., 1996, *J. Phys. Soc. Japan*, **65,** 1043.
[328] Kiryuklin, V., Casa, D., Hill, J. P., Keimer, B., Vigilante, A., Tomioka, Y., and Tokura, Y., 1992, *Nature*, **384,** 813.
[329] Miyano, K., Tanaka, T., Tomioka, Y., and Tokura, Y., 1997, *Phys. Rev. Lett.*, **78,** 4257.
[330] Asamitsu, A., Tomioka, Y., Kuwahara, H., and Tokura, Y., 1997, *Nature*, **388,** 50.

[331] Mahendiran, R., Mahesh, R., Gundakaram, R., Raychaudhuri, A., *et al.*, 1996, *J. Phys.: condens. Matter*, **8,** L455.
[332] Rao, G. H., Sun, R. J., Liang, J. K., Zhou, W. Y., and Cheng, X. R., 1996, *Appl. Phys. Lett.*, **69,** 424.
[333] Damay, F., Maignan, A., Martin, C., and Raveau, B., 1997, *J. appl. Physics.*, **81,** 1372.
[334] Millis, A. J., 1997, *Phys. Rev.* B, **55,** 6405.
[335] Inoue, J., and Maekawa, S., 1995, *Phys. Rev. Lett.*, **74,** 3407.
[336] Inoue, J., and Maekawa, S., 1995, *Mater. Sci. Eng.*, **B31,** 193.
[337] Zang, J., Röder, H., Bishop, A. R., Trugman, S. A., 1997, *J. Phys.: condensed. Matter,* **9,** L157.
[338] Millis, A. J., Littlewood, P. B., and Shraiman, B. I., 1995, *Phys. Rev. Lett.*, **74,** 5144.
[339] Millis, A. J., Mueller, R., and Shraiman, B., 1996, *Phys. Rev.* B, **54,** 5389.
[340] Mishra, S., Satpathy, S., Aryasetiawan, F., and Gunnarson, O., 1997, *Phys. Rev.* B, **55,** 2725.
[341] Arovas, D., and Guinea, F., 1998, *Phys. Rev.* B, **58,** to be published.
[342] Yunoki, S., Hu, J., Malvezzi, A. L., Moreo, A., Furukawa, N., and Dagotto, E., 1998, *Phys. Rev. Lett.*, **80,** 845.
[343] Dagotto, E., Yunoki, S., Malvezzi, A. L., Moreo, A., Hu, J., Capponi, S., Poilblanc, D., and Furukana, N., 1998, *Phys. Rev.* B, to be published.
[344] Jonker, G. H., 1954, *Physica*, **20,** 1118.
[345] Baibich, M., Broto, J.-M., Fert, A., Nguyen van Dau, F., Petroff, F., Etienne, P., Creuzet, G., Fredrich, A., and Chazelas, J., 1988, *Phys. Rev. Lett.*, **61,** 2472.
[346] Imura, M., Takahashi, T., Takamura, H., Tanaka, T., Sugimoto, S., Homma, M., and Okada, M., 1996, *Mater. Trans. Japan Inst. Metals,* **37,** 1219.
[347] Imura, M., Takamura, H., Tanaka, T., Homma, M., and Okada, M., 1996, *J. Ceram. Soc. Japan*, **104,** 151.
[348] Jonker, G. H., 1966, *J. appl. Phys.*, **37,** 1424.
[349] Anane, A., Dupas, C., LeDang, K., Renard, J., Veillet, P., Guevara, A. M. D. L., Millot, F., Pinsard, L., Revcolevschi, A., and Jansen, A. G. M., 1997, *J. Magn. magn. Mater.*, **165,** 377.
[350] Ashcroft, N. W., and Mermin, N. D., 1976, *Solid State Physics* (New York: Holt, Rinehart and Winston).
[351] Stewart, G. R., Fisk, Z., and Williams, J. O., 1984, *Phys. Rev.* B, **28,** 172.
[352] Mott, N. F., 1985, *Metal–Insulator Transitions*, second edition (London: Taylor & Francis).
[353] Zhou, J.-S., Archibald, W., and Goodenough, J. B., 1998, *Phys. Rev.* B, **57,** R2017.
[354] Yeh, N.-C., Vasquez, R., Beam, D., Fu, C.-C., Huynh, H., and Beach, G., 1996, *J. Phys.: condens. Matter*, **9,** 3713.
[355] Yeh, N.-C., Vasquez, R. P., Wei, J. Y. T., Fu, C. C., Beach, G., Huynh, J., Samilov, A. V., Boris, A. V., Kovaleva, N. N., and Bazhenov, A. Z., 1997, *Proceedings of Materials Research Society Meeting*, San Francisco, California 1997 (Pittsburgh Pennsylvania: Materials Research Society), p. 145.
[356] Sánchez, R. D., Rivas, J., Vasquez, C., Lopez-Quintela, A., Causa, M. T., Tovar, M., and Oseroff, S., 1996, *Appl. Phys. Lett.*, **68,** 134.
[357] Gupta, A., Gong, G. Q., Xiao, G., Duncombe, P. R., Lecoeur, P., Trouilloud, P., Wang, Y. Y., Dravid, V. P., and Sun, J. Z., 1996, *Phys. Rev.* B, **54,** R15629.
[358] Kim, K. H., Gu, J. Y., Choi, H. S., Eom, D. J., Jung, J. H., and Noh, J., 1997, *Phys. Rev.* B, **55,** 4023.
[359] Coey, J. M. D., Viret, M., Ranno, L., and Ounadjela, K., 1995, *Phys. Rev. Lett.*, **75,** 3910.
[360] Kaplan, S. G., Quijada, M., Drew, H. D., Tanner, D. B., Xiong, G. V., Ramesh, R., Kwon, C., and Venkatesan, T., 1996, *Phys. Rev. Lett.*, **77,** 2081.
[361] Wolfman, J., Simon, C., Hervieu, M., Maignan, A., and Raveau, B., 1996, *J. solid-state Chem.*, **123,** 413.

[362] Mahendiran, R., Mahesh, R., Raychaudhuri, A. K., and Rao, C. N. R., 1996, *Solid St. Commun.*, **99,** 149.
[363] Liu, J. Z., Chang, I. C., Irons, S., Klavins, P., Shelton, R. N., Song K., and Wasserman, S. R, 1995, *Appl. Phys. Lett.*, **66,** 3218.
[364] Kasai, M., Kuwahara, H., Moritomo, Y., Tomioka, Y., and Tokura, Y., 1996, *Jap. J. appl. Phys.*, **15,** L489.
[365] Canedy, C. L., Ibsen, K. B., Xiao, G., Sun, J. Z., Gupta, A., and Gallagher, W. J., 1996, *J. appl. Phys.*, **79,** 4546.
[366] Jin, S., 1996, *Mater. Trans. Japan Inst. Metals*, **37,** 888.
[367] Jin, S., O'Bryan, H., Tiefel, T., McCormack, M., and Rhodes, W., 1994, *Appl. Phys. Lett.*, **66,** 382.
[368] Nossov, A., Pierre, J., Vassiliev, V., and Ustinov, V., 1996, *Solid St. Commun.*, **101,** 361.
[369] Nossov, A., Pierre, J., Vassiliev, V., and Ustinov, V., 1996, *J. Phys.: condens. Matter*, **8,** 8513.
[370] Yeh, N.-C., Fu, C. C., Wei, J. Y. T., Vasquez, R. P., *et al.*, 1997, *J. appl. Phys.*, **81,** 97.
[371] Sengoku, N., and Ogawa, K., 1996, *Jap. J. appl. Phys.*, **35,** 5432.
[372] Sharma, N., Nigam, A. K., Pinto, R., Venkataramani, N., Prasad, S., Chandra, G., and Pai, S. P., 1996, *J. Magn. magn. Mater.*, **154,** 296.
[373] Li, K., Liu, L., Sun, J., Xu, X. J., Rang, J., Cao, X. W., Zhu, J. S., and Zhang, Y. H., 1996, *J. Phys.* D, **29,** 14.
[374] Xiong, G. C., Bhagat, S., Li, Q., Dominguez, M., Ju, H., Greene, R., and Venkatesan, T., 1996, *Solid St. Commun.*, **97,** 599.
[375] Martinez, B., Fontcuberta, J., Seffar, A., Garcia-Munoz, J. L., Piñol, S., and Obradors, X., 1996, *Phys. Rev.* B, **54,** 10001.
[376] O'Donnell, J., Onellion, M., Rzchowski, M. S., Eckstein, J. N., and Bozovic, I., 1996, *Phys. Rev.* B, **54,** R6841.
[377] Snyder, G. J., Beasley, M. R., Geballe, T. H., Hiskes, R., and DiCarolis, S., 1996, *Appl. Phys. Lett.*, **69,** 4254.
[378] Mahesh, R., Mahendiran, R., Raychaudhuri, A. K., and Rao, C. N. R., 1996, *Appl. Phys. Lett.*, **68,** 2291.
[379] Balcells, L., Fontcuberta, J., Martinez, B., and Obradors, X., 1998, *J. Phys.: condens. Matter*, **10,** 1889.
[380] Ju, H. L., and Sohn, H., 1997, *Solid St. Commun.*, **102,** 463.
[381] Shreekala, R., Rajeshwari, M., Ghosh, K., Goyal, A., Gu, J. Y., Kwon, C., Trajanovic, Z., Boettcher, T., Green, R. L., Ramesh, R., and Venkatesan, T., 1997, *Appl. Phys. Lett.*, **71,** 282.
[382] Mathur, N., Burnell, G., Isaac, S. P., Jackson, T. J., Teo, B. S., MacManus-Driscoll, J. L., Cohen, L. F., Evetts, J. E., and Blamire, M. G., 1997, *Nature,* **387,** 266.
[383] Steenbeck, K., Eich, T., Kirsch, K., O'Donnell, K., and Steinbeiss, E., 1997, *Appl. Phys. Lett.*, **71,** 968.
[384] Gehring, G. A., and Coombes, D. J., 1998, *J. Magn. magn. Mater.*, **177,** 873.
[385] Coey, J. M. D., 1998, *Phil. Trans. roy. Soc.* A, **356,** 1519.
[386] Coey, J. M. D., Berkowitz, A. E., Balcells, L., Putris, F. F., and Barry, A., 1998, *Phys. Rev. Lett.*, **80,** 3815.
[387] Coey, J. M. D., Berkowitz, A. E., Balcells, L., Putris, F. F., and Parker, F. T., 1998, *Appl. Phys. Lett.*, **72,** 734.
[388] Balcells, L., Fontcuberta, J., Martinez, B., and Obradors, X., 1998, *J. Phys.: condens. Matter*, **10,** 1883.
[389] Maignan, A., Simon, C., Caignaert, V., and Raveau, B., 1995, *Solid St. Commun.*, **96,** 623.
[390] Millange, F., Maignan, A., Caignaert, V., Simon, C., and Raveau, B., 1996, *Z. Phys.* B, **101,** 169.
[391] Maignan, A., Simon, C., Caignaert, V., and Raveau, B., 1995, *C. r. hebd. Seanc. Acad. Sci., Paris, II,* **321,** 297.

[392] Kuwahara, H., Tomioka, Y., Moritomo, Y., Asamitsu, A., Kasai, M., Kumai, R., and Tokura, Y., 1996, *Science*, **272,** 80.
[393] Hervieu, M., Tendeloo, G. V., Caignaert, V., Maignan, A., and Raveau, B., 1996, *Phys. Rev.* B, **53,** 14274.
[394] Gong, G. C., Canedy, C. L., Xiao, G., Sun, J. Z., Gupta, A., and Gallagher, W. J., 1996, *J. appl. Phys.*, **79,** 4538.
[395] Damay, F., Nguyen, N., Maignan, A., Hervieu, M., and Raveau, B., 1996, *Solid St. Commun.*, **98,** 997.
[396] Damay, F., Maignan, A., Nguyen, N., and Raveau, B., 1996, *J. solid-st. Chem.*, **124,** 385.
[397] Tomioka, Y., Kuwahara, H., Asamitsu, A., Kasai, M., and Tokura, Y., 1997, *Appl. Phys. Lett.*, **70,** 3609.
[398] Maignan, A., Simon, C., Caignaert, V., and Raveau, B., 1996, *J. Magn. magn. Mater.*, **152,** L5.
[399] Hundley, M. F., Hawley, M., Heffner, R. H., Jia, Q. X., Neumeier, J. J., and Tesmer, J., 1995, *Appl. Phys. Lett.*, **67,** 860.
[400] de Teresa, J. M., Ibarra, M. R., Algarabel, P. A., Ritter, C., Marqina, C., Blasco, J., Garcia, C., Moral, A. D., and Arnold, Z., 1992, *Nature*, **386,** 256.
[401] Jaime, M., Salamon, M. B., Pettit, K., Rubinstein, M., Treece, R. E., Horwitz, J. S., and Chrisey, D. B., 1996, *Appl. Phys. Lett.*, **68,** 1576.
[402] Park, J.-H., Chen, C. T., Cheong, S.-W., Bao, W., Meigs, G., Chakarian, V., and Idzerda, Y. U., 1996, *J. appl. Phys.*, **79,** 4558.
[403] Choi, J., Liou, S.-H., Dowben, P. A., Zhang, J., and Plummer, E. W., 1998, *J. Appl. Phys.*, **81,** to be published.
[404] Biswas, A., and Raychaudhuri, A. K., 1996, *J. Phys.: condens. Matter*, **8,** L739.
[405] Troyanchuck, I. O., 1992, *Soviet Phys. JETP*, **75,** 132.
[406] Gerthsen, P., and Härdtl, K. H., 1962, *Z. Naturf.* (a), **17,** 514.
[407] Heikes, R. R., Miller, R. C., and Mazelsky, R., 1962, *Physica*, **30,** 1600.
[408] Billinge, S. J. L., DiFrancesco, R. G., Kwei, G. H., Neumeier, J. J., and Thompson, J. D., 1996, *Phys. Rev. Lett.*, **77,** 715.
[409] Dionne, G. F., 1996, Massachusetts Institute of Technology Technical Report.
[410] Triberis, G. P., and Friedman, L. R., 1985, *J. Phys.* C, **18,** 2281.
[411] Shklovskii, B. I., and Efros, A. L., 1984, *Electronic Properties of Doped Semiconductors* (Berlin: Springer).
[412] Manoharan, S. S., Kumar, D., Hedge, M. S., Satyalakshmi, K. M., Prasad, V., and Subramanyam, S. V., 1995, *J. solid-st. Chem.*, **117,** 420.
[413] Viret, M., Glättli, H., Fermon, C., deLeon-Guevara, A. M., and Revcolevschi, A., 1998, *Europhys. Lett.*, **42,** 301.
[414] Tyson, T. A., deLeon, J. M., Conradson, S. O., Bishop, A. R., Neumeier, J. J., Röder, H., and Zang, J., 1996, *Phys. Rev.* B, **53,** 13985.
[415] Dai, P., Zhang, J., Mook, H. A., Liou, S.-H., *et al.*, 1996, *Phys. Rev.* B, **54,** R3694.
[416] Kaplan, S. G., Quijada, M., Drew, H. D., Tanner, D. B., Xiong, G. C., Ramesh, R., Kwon, C., and Venkatesan, T., 1996, *Phys. Rev. Lett.*, **77,** 2081.
[417] Sharma, R. P., Xiong, G. C., Kwon, C., Ramesh, R., Greene, R. L., and Vankatesan, T., 1996, *Phys. Rev.* B, **54,** 10014.
[418] Shengelaya, A., Zhao, G. M., Keller, H., and Muller, K. A., 1996, *Phys. Rev. Lett.*, **77,** 5296.
[419] Campbell, I., and Fert, A., 1982, *Ferromagnetic Materials*, Volume 3, edited by E. P. Wahlford (Amsterdam: North-Holland).
[420] Zhang, S., 1996, *J. appl. Phys.*, **79,** 4542.
[421] Tanaka, J., Umehara, M., Tamura, S., Tsukioka, M., Ehara, S., 1982, *J. phys. Soc. Japan*, **512,** 1236.
[422] Jaime, M., Hardner, H. T., Salamon, M. B., Rubinstein, M., Dorsey, P., and Emin, D., 1997, *Phys. Rev. Lett.*, **78,** 951.
[423] Shapira, Y., Foner, S., and Oliveira, N., 1972, *Phys. Rev.* B, **6,** 2647.
[424] Stankiewicz, J., von Molnár, S., and Holtzberg, F., 1986, *J. Magn. magn. Mater.*, **54–57**, 1217.
[425] Nunez-Regueiro, J., Gupta, D., and Kadin, A., 1996, *J. appl. Phys.*, **79,** 5179.

[426] von Helmholt, R., 1995, PhD Thesis, Erlangen.
[427] Wagner, P., Mazilu, D., Trappeniers, L., Moshchalkov, V. V., and Bruynserade, Y., 1997, *Phys. Rev.* B, **55,** R14721.
[428] Hejtmanek, J., Jirak, Z., Sedmidubsky, D., Maignan, A., Simon, C., Caignaert, V., Martin, C., and Raveau, B., 1996, *Phys. Rev.* B, **54,** 11974.
[429] Asamitsu, A., Moritomo, Y., and Tokura, Y., 1996, *Phys. Rev.* B, **53,** R2952.
[430] Liebe, J., Kraus, E., Haupt, L., Mandal, P., and Barner, K., 1996, *Appl. Phys. Lett.*, **68,** 2343.
[431] Zhou, J.-S., Archibald, W., and Goodenough, J. B., 1996, *Nature*, **381,** 770.
[432] Crespi, V. H., Lu, L., Jia, Y. X., Khazeni, K., Zettl, A., and Cohen, M. L., 1996, *Phys. Rev.* B, **53,** 14303.
[433] Mahendiran, R., Tiwary, S., Raychaudhuri, A., Mahesh, R., and Rao, C. N. R., 1996, *Phys. Rev.* B, **54,** R9604.
[434] Fontcuberta, J., Seffar, A., Granados, X., Garcia-Munoz, J. I., Obradors, X., and Piñol, S., 1996, *Appl. Phys. Lett.*, **68,** 2288.
[435] Fisher, B., Patlagan, I., and Reisner, G. M., 1996, *Phys. Rev.* B, **54,** 9359.
[436] Marsh, D. B., and Harris, P. E., 1996, *Phys. Rev.* B, **54,** 16602.
[437] Palstra, T. T. M., Ramirez, S. P., Cheong, S.-W., Zagarszi, B. R., Schiffer, P., and Zagnen, J., 1997, *Phys. Rev.* B, **56,** 5104.
[438] Hundley, M. F., and Neumeier, J. J., 1997, *Phys. Rev.* B, 11511.
[439] Kasuya, T., 1959, *Prog. Theor. Phys.*, **22,** 227.
[440] Emin, D., 1975, *Phys. Rev. Lett.*, **35,** 882.
[441] Jaime, M., Salamon, M. B., Rubinstein, M., Treece, R., Horwitz, J., and Chrisey, D. B., 1996, *Phys. Rev.* B, **54,** 11914.
[442] Mahendiran, R., Tiwary, S., and Raychaudhuri, A., 1996, *Solid St. Commun.*, **98,** 701.
[443] Hejtmanek, J., Jirak, Z., Sedmidubsky, D., Maignan, A., Simon, C., Caignaert, V., Martin, C., and Raveau, B., 1996, *Phys. Rev.* B, **54,** 11947.
[444] Gong, G. Q., Gupta, A., Xiao, G., Lecoeur, P., and McGuire, T. R., 1996, *Phys. Rev.* B, **54,** R3742.
[445] Lu, Y., Li, X. W., Gong, G. Q., Xiao, G., Gupta, A., Lecoeur, P., Sun, J. Z., Wang, Y. Y., and Dravid, V. P., 1996, *Phys. Rev.* B, **54,** R8357.
[446] Sun, J. Z., Gallagher, W. J., Duncombe, P. R., Krusin-Elbaum, L., Altman, R. A., Gupta, A., Lu, Y., Gong, G. Q., and Xiao, G., 1996, *Appl. Phys. Lett.*, **69,** 3266.
[447] Viret, M., Drouet, M., Contour, J. P., Nassar, J., Fermon, C., and Fert, A., 1997, *Europhys. Lett.*, **39,** 545.
[448] Kozono, Y., Kasai, M., Kanke, Y., Ohno, T., Hanazono, M., and Sugita, Y., 1991, *Physica* C, **185–189,** 1919.
[449] Lawler, J. F., Lunney, J. G., and Coey, J. M. D., 1994, *Physica* C, **235–240,** 737.
[450] Bari, M. A., Cabeza, O., Capogna, L., Woodall, P., Muirhead, C. M., and Blamire, M. G., 1997, *IEEE Trans. Appl. Supercond.*, **7,** 2304.
[451] Glazman, L. I., and Matveev, K. A., 1988, *Soviet Phys. JETP*, **67,** 1276.
[452] Xiong, G. C., Li, Q., Ju, H. L., Greene, R. L., and Venkatesan, T., 1995, *IEEE Trans. Appl. Sufercon.*, **5,** 1643.
[453] Vas'ko, V. A., Larkin, V. A., Kraus, P. A., Nikolaev, K. R., Grupp, D. E., Nordman, C. A., and Goldman, A. M., 1992, *Phys. Rev. Lett.*, **78,** 1134.
[454] Peski-Tinbergen, T. V., and Dekker, A. J., 1963, *Physica*, **29,** 917.
[455] von Molnár, S., and Shafer, M. W., 1970, *J. appl. Phys.*, **41,** 1093.
[456] Kubo, K., and Ohata, N., 1972, *J. phys. Soc. Japan*, **33,** 21.
[457] Furukawa, N., 1997, *J. phys. Soc. Japan*, **66,** 2523.
[458] Tokura, Y., Urushibara, A., Moritomo, Y., Arima, T., Asamitsu, A., Kido, G., and Furukawa, N., 1994, *J. phys. Soc. Japan*, **63,** 3931.
[459] Dionne, G. F., 1996, *J. appl. Phys.*, **79,** 5172.
[460] Pierre, J., Robaut, F., Misat, S., Strobel, P., Nossov, A., Ustinov, V., and Vassiliev, V., 1996, *Physica* B, **225,** 214.
[461] Bastiansen, P. J. M., and Knops, H. J. F., 1998, *Comp. Mater. Sci.*, **10,** 225.

[462] Sun, J. Z., Krusin-Elbaum, L., Parkin, S. S. P., and Xiao, G., 1995, *Appl. Phys. Lett.*, **67,** 2726.
[463] Nunez-Regueiro, J., and Kadin, A., 1996, *Appl. Phys. Lett.*, **68,** 2747.
[464] Furukawa, N., 1994, *J. phys. Soc. Japan*, **63,** 3214.
[465] Furukawa, N., 1995, *J. phys. Soc. Japan*, **64,** 2734.
[466] Millis, A. J., 1996, *Phys. Rev.* B, **53,** 8434.
[467] Millis, A. J., Mueller, R., and Shraiman, B., 1996, *Phys. Rev.* B, **54,** 5389.
[468] Röder, H., Zang, J., and Bishop, A. R., 1996, *Phys. Rev. Lett.*, **76,** 1356.
[469] Zang, J., Bishop, A. R., and Röder, H., 1996, *Phys. Rev.* B, **53,** R8840.
[470] Lee, J. D., and Min, B. I., 1996, *Phys. Rev.* B, **55,** 12454.
[471] Viret, M., Ranno, L., and Coey, J. M. D., 1997, *J. appl. Phys.*, **81,** 4964.
[472] Nagaev, E. L., 1996, *Phys. Rev.* B, **54,** 16608.
[473] Hamilton, J. J., Keating, E. L., Ju, H. L., Raychaudhuri, A. K., Smolyaninova, N. V., and Greene, R. L., 1996, *Phys. Rev.* B, **54,** 14926.
[474] Ramirez, A. P., Schiffer, P., Cheong, S.-W., Bao, W., Palstra, T. T. M., Gammel, P. L., Bishop, D. J., and Zegarski, B., 1996, *Phys. Rev. Lett.*, **76,** 3188.
[475] Tanaka, J., and Mitsuhashi, T., 1984, *J. phys. Soc. Japan*, **53,** 24.
[476] Zhang, X. X., Tejada, J., Xin, Y., Sun, G. F., Wong, K. W., and Bohigas, X., 1996, *Appl. Phys. Lett.*, **69,** 3596.
[477] Guo, Z. B., Du, Y. W., Zhu, J. S., Huang, H., Ding, W. P., and Feng, D., 1997, *Phys. Rev. Lett.*, **78,** 1142.
[478] Guo, Z. B., Zhang, J. R., Huang, H., Ding, W. P., and Du, Y. W., 1992, *Appl. Phys. Lett.*, **70,** 904.
[479] Visser, D. W., Ramirez, A. P., and Subramanian, M. A., 1992, *Phys. Rev. Lett.*, **78,** 3947.
[480] Fumagalli, P., Spaeth, C., Guntherodt, G., and von Helmholt, R., 1995, *IEEE Trans. Magn.*, **31,** 3277.
[481] Tang, Y., Shaltout, I., Braunstein, R., von Helmholt, R., Haupt, H., and Bärner, K., 1994, *Phys. Stat. sol.* (b), **182,** 509.
[482] Haupt, L., Schuenemann, J.-W., Baerner, K., Sondermann, U., Rager, B., Abdelouhab, R. M., Braunstein, R., and Dong, S., 1989, *Solid St. Commun.*, **72,** 1093.
[483] Gupta, R., Sood, A. K., Mahesh, R., and Rao, C. N. R., 1996, *Phys. Rev.* B, **54,** 14899.
[484] Boris, A. V., Kovaleva, N. N., Bazhenov, A. V., Samoilov, A. V., Yeh, N. C., and Vasquez, R. P., 1997, *J. appl. Phys.*, **81,** 5756.
[485] Alain, P., and Piriou, B., 1971, *Phys. Stat. sol.* (b), **43,** 669.
[486] Henning, O., and Strobel, U., 1967, *Wissenschaftliche Z. Hochschule Architektur Bauwesen Weimar*, **14,** 645.
[487] Popma, T. J. A., and Kamminga, M. G. J., 1975, *Solid St. Commun.*, **17,** 1073.
[488] Pellegrin, E., Tjeng, L. H., de Groot, F. M. F., Hesper, R., Flipse, C. F. J., O'Mahony, J. D., Moritomo, Y., Tokura, Y., Chen, C. T., and Sawatzky, G. A., 1997, *J. Electron Spectron.*, **86,** 115.
[489] Moritomo, Y., Tomioka, Y., Asamitsu, A., Tokura, Y., and Matsui, Y., 1995, *Phys. Rev.* B, **51,** 3297.
[490] Boloux, J. C., Soubeyroux, J. L., LeFlem, G., and Hagenmuller, P., 1981, *J. solid-st. Chem.*, **38,** 34.
[491] Rao, C. N. R., Ganguly, P., Singh, K. K., and Ram, R. A. M., 1988, *J. solid-st. Chem.*, **72,** 14.
[492] Bao, W., Carter, S. A., Chen, C. H., Cheong, S.-W., Battlog, B., and Fisk, Z., 1993, *Phys. Rev.* B, **47,** 15397.
[493] Sternlieb, B. J., Jill, J. P., Wildgruber, U. C., Luke, G. M., Nachumi, B., Morjmoto, Y., and Tokura, Y., 1996, *Phys. Rev. Lett.*, **76,** 2169.
[494] Moritomo, Y., Asamitsu, A., Kuwahara, H., and Tokura, Y., 1996, *Nature*, **380,** 141.
[495] Kimura, T., Tomioka, Y., Kuwahata, H., Asamitsu, A., Tomura, M., and Tokura, Y., 1996, *Science*, **274,** 1698.
[496] Asano, H., Hayakawa, J., and Matsui, M., 1997, *Appl. Phys. Lett.*, **70,** 2303.

[497] Perring, T. G., Aeppli, G., Moritomo, Y., and Tokura, Y., 1997, *Phys. Rev. Lett.*, **78,** 3197.
[498] Battle, P. D., Green, M. A., Laskey, N. S., Milburn, J. E., Radaelli, P. G., Rosseinsky, M. J., Sullivan, S. P., and Vente, J. F., 1996, *Phys. Rev.* B, **54,** 15967.
[499] Troyanchuk, I., and Derkachenko, V., 1988, *Soviet Phys. solid St.*, **30,** 2003.
[500] Raju, N. P., Greedan, J. E., and Subramanian, M. A., 1994, *Phys. Rev.* B, **49,** 1086.
[501] Shimakawa, Y., Kubo, Y., and Manako, T., 1996, *Nature*, **379,** 53.
[502] Dai, S., Li, Z. W., Morrish, A. H., Zhou, X. Z., Zhao, J. G., and Xiong, X. M., 1997, *Phys. Rev.* B, **55,** 14125.
[503] Subramanian, M. A., Toby, B. H., Ramirez, A. P., Marshall, W. J., Sleight, A. W., and Kwei, G. H., 1996, *Science*, **273**, 81.
[504] Kwei, G. H., Booth, C. H., Bridges, F., and Subramanian, M. A., 1997, *Phys. Rev.* B, **55,** R688.
[505] Shimakawa, Y., Kubo, Y., Manako, T., Sushko, Y. V., Argyriou, D. N., and Jorgensen, J. D., 1997, *Phys. Rev.* B, **55,** 6399.
[506] Cheong, S.-W., Hwang, H., Batlogg, B., and Rupp, L. R., 1996, *Solid St. Commun.*, **98,** 165.
[507] Jonker, G., and van Santen, J., 1953, *Physica*, **19,** 120.
[508] Briceno, G., Xiang, X.-D., Chang, H., Sun, X., and Schultz, P. G., 1995, *Science*, **270,** 273.
[509] Samoilov, A. V., Yeh, N. C., and Vasquez, R. P., 1997, *Epitaxial Oxide Thin Films*, MRS Symposium III, p. 247.
[510] Yamaguchi, S., Taniguchi, H., Takagi, H., Arima, T., and Tokura, Y., 1995, *J. phys. Soc. Japan*, **64,** 1885.
[511] Mahendiran, R., Raychaudhuri, A. K., Chainani, A., and Sarma, D. D., 1995, *J. Phys.: condens. Matter*, **7,** L561.
[512] Ganguly, P., Kumar, P. S. A., Santhosh, P. N., and Mulla, I. S., 1994, *J. Phys.: condens. Matter*, **6,** 533.
[513] Mahendiran, R., and Raychaudhuri, A. K., 1996, *Phys. Rev.* B, **54,** 16044.
[514] Wang, Z. L., and Zhang, J., 1996, *Phys. Rev.* B, **54,** 1153.
[515] Moritomo, Y., Higashi, K., Matsuda, K., and Nakamura, A., 1997, *Phys. Rev.* B, **55,** R14725.
[516] Park, J. H., Cheong, S. W., and Chen, C. T., 1992, *Phys. Rev.* B, **55,** 11072.
[517] Takeda, T., Watanabe, T., Komura, S., and Fujii, H., 1987, *J. Phys. Soc. Japan*, **56,** 731.
[518] Obradors, X., Paulius, L. M., Maple, M. B., Torrance, J. B., Nazzal, A. I., Fontcuberta, J., and Granados, X., 1993, *Phys. Rev.* B, **47,** 12353.
[519] Garcia-Mũnoz, J. L., Rodriguez-Carvajal, J., Lacorre, P., and Torrance, J. B., 1992, *Phys. Rev.* B, **46,** 4414.
[520] Torrance, J. B., Lacorre, P., Nazzal, A., Ansaldo, E., and Niedermayer, C., 1992, *Phys. Rev.* B, **45,** 8209.
[521] Chen, C., Cheong, S., and Cooper, A., 1993, *Phys. Rev. Lett.*, **71,** 2461.
[522] Cheong, S.-W., Hwang, H., Chen, C., Batlogg, B., Rupp, L., and Carter, S., 1994, *Phys. Rev.* B, **49,** 7088.
[523] Battle, P. D., Gibb, T. C., and Lightfoot, P., 1990, *J. solid-st. Chem.*, **84,** 271.
[524] Takeda, T., Komura, S., and Fujii, H., 1983, *J. Magn. magn. Mater.*, **31–34,** 797.
[525] Ranno, L., Barry, A., and Coey, J. M. D., 1997, *J. appl. Phys.*, **81,** 5774.
[526] Shepard, M., McCall, S., Cao, G., and Crow, J. E., 1992, *J. appl. Phys.*, **81,** 4978.
[527] Cao, G., McCall, S., Shepard, M., and Crow, J. E., 1992, *Phys. Rev.* B, **56,** 321.
[528] Maeno, Y., Hashimoto, H., Yoshida, K., Nishizaki, S., Fujita, T., Bednorz, J. G., and Lichtenberg, F., 1994, *Nature*, **372,** 532.
[529] Cao, G., McCall, S., and Crow, J. E., 1997, *Phys. Rev.* B, **55,** R672.
[530] Cao, G., McCall, S., Crow, J. E., and Guertin, R. P., 1996, *Phys. Rev. Lett.*, **78,** 1751.
[531] Korotin, M. A., Anisimov, V. I., Khomskii, D. I., and Sawatzky, G. A, 1998, *Phys. Rev. Lett.*, **80,** 4305.
[532] Pedersen, L. A., and Libby, W. F., 1972, *Science*, **176,** 1355.

[533] VOORHOEVE, R. J. H., REMEIKA, J. P., and JOHNSON, D. W., 1973, *Science*, **177,** 62.
[534] PARRAVANO, J., 1953, *J. Am. chem. Soc.*, **75,** 1497.
[535] VOORHOEVE, R. J. H., REMEIKA, J. P., FREELAND, P. E., and MATTHIAS, B. T., 1972, *Science*, **177,** 353.
[536] VRIELAND, E. G., 1974, *J. Catal.*, **32,** 415.
[537] RANNO, L., VIRET, M., VALENTIN, F., MCCAULEY, J., and COEY, J. M. D., 1996, *J. Magn. magn. Mater.*, **157/158,** 291.
[538] HWANG, H. Y., CHEONG, S.-W., and BATLOGG, B., 1996, *Appl. Phys. Lett.*, **68,** 3494.
[539] DONG, Z. W., BOETTCHER, T., CHEN, C. M., TAKEUCHI, I., RAJESWARI, M., SHARMA, R. P., and VENKANTESAN, T., 1996, *Appl. Phys. Lett.*, **69,** 3432.
[540] O'DONNELL, J., ONELLION, M., RZCHOWSKI, M. S., ECKSTEIN, J. N., and BOZOVIC, I., 1997, *Phys. Rev.* B, **55,** 5873.
[541] RAJESWARI, M., GOYAL, A., RAYCHAUDHURI, A. K., ROBSON, M. C., XIONG, G. C., KWON, C., RAMESHR, R., GREENE, L., VENKATESAN, T., and LAKEOU, S., 1996, *Appl. Phys. Lett.*, **69,** 851.
[542] ALERS, G. B., RAMIREZ, A. P., and JIN, S., 1996, *Appl. Phys. Lett.*, **68,** 3644.
[543] HARDNER, H. T., WEISSMAN, M. B., JAIME, M., TREECE, R. E., DORSEY, P. C., HORWITZ, J. S., and CHRISEY, D. B., 1997, *Appl. Phys. Lett.*, **81,** 272.
[544] TYAGI, S., LOFLAND, S., DOMINGUEZ, M., and BHAGAT, S., 1996, *Appl. Phys. Lett.*, **68,** 2893.
[545] HEREMANS, J. J., WATTS, S., WIRTH, S., YU, X., and VON MOLNAR, S., 1998, *J. appl. Phys.*, **83,** 7055.
[546] VON HELMHOLT, R., WECKER, J., SAMWER, K., and BÄRNER, K., 1995, *J. Magn. magn. Mater.*, **151,** 411.
[547] VON MOLNÁR, S., and COEY, J. M. D., 1998, *Current Opinion in Solid St. and Mater. Sci.*, **3,** 171.
[548] KRESIN, V. Z., and WOLF, S. A., 1997, *Philos. Mag.* B, **76,** 241.
[549] INOMATA, K., HASHIMOTO, S., and NAKAMURA, S., 1988, *J. Appl. Phys*, **27,** L883.
[550] OWENS F. J., 1994, *J. Appl Phys.*, **82,** 3054.
[551] KRINCHIK, F. S., GANSHINA, E. A., and TRIFONOV, A. YU., 1991, *Soviet Phys. Solid. St.*, **33,** 907.
[552] MAHENDIRAN, R., MAHESH, R., RAYCHAUDHURI, A. K., and RAO, C. N. R., 1995, *J. Phys D.; Appl. Phys.*, **25,** 1743.
[553] PARK, J. H., VESCOVO, E., KIM, H. J., RAMESH, R., and VENKATESAN, T., 1998, *Nature*, **392,** 794.
[554] MORI, S., CHEN, C. H., and CHEONG, S. W., 1998, *Nature*, **392,** 473.
[555] AROVAS, D. P., and GUINEA, F., 1998, *Phys. Rev.* B, **58,** 9150.
[556] JAIME, M., LIN, P., SALAMON, M. B., and HAN, P. D., 1998, *Phys. Rev.* B, **58,** R5901.
[557] BABUSHKINA, N. A., BELOVA, L. M., GORBENKO, O. YU., KAUL, A. R., BOSAK, A. A., OZHOGIN, V. I., and KUGEL, K. I., 1998, *Nature*, **391,** 159.
[558] JUNG, J. H., KIM, K. H., EOM, D. J., NOH, T. W., CHOI, E. J., YU, J., KWON, Y. S., and CHUNG, Y., 1997, *Phys. Rev.* B, **55,** 15489.
[559] IBARRA, M. R., ZHAO, G. M., DETERESA, J. M., GARCIA-LANDA, B., ARNOLD, Z., MARQUINA, C., ALGARABEL, P. A., KELLER, H., and RITTER, C., 1998, *Phys. Rev.* B, **57,** 7446.
[560] IBARRA, M. R., MAHENDIRAN, R., MARQUINA, C., GARCIA-LANDA, B., and BLASCO, J., 1998, *Phys. Rev.* B. **57,** R3217.
[561] MAHENDIRAN, R., and RAYCHAUDHURI, A. K., 1996 *Phys. Rev.* B, **54,** 16044.
[562] FINKMAN, E., COHEN, E., and VAN UITERT, L. G., 1972, *Phys. Rev.* B, **7,** 2899.
[563] ZIESE, M., and SENA, S. P., 1998, *J. Phys. condens. mater.*, **10,** 2727.
[564] GIBBS, M. R. J., ZIESE, M., GEHRING, G. A., BLYTHE, H. J., COOMBES, D. J., SENA, S. P., and SHEARWOOD, C., 1998, *Philos. Trans. roy. Soc.* A, **356,** 1681.
[565] ZIESE, M., SENA, S., SHEARWOOD, C., BLYTHE, H. J., GIBBS, M. R. J., and GEHRING, G. A., 1998, *Phys. Rev.* B, **57,** 2963.
[566] MOHAN, CH-V., SEEGER, M., KRONMÜLLER, H., MURUGARAJ, P., and MAIER, J., 1998, *J. Magn. magn. Mater*, **183,** 348.

[567] Soulen, D. J., Byers, J. M., Osofsky, M. S., Nadgorny, B., Ambrose, T., Cheng, S. F., Boussard, P. R., Tanaka, C., Moodera, J. S., Barry, A., and Coey, J. M. D., 1998, *Science*, **282,** 85.
[568] Anane, A., 1998, PhD thesis, Université de Paris XI.
[569] Skumryev, V., Ott, F., Coey, J. M. D., Anane, A., Regnard, J. P., and Revcolevschi, A., 1998, *Europ. Phys. J.* B (in press).
[570] Hennion, M., Moussa, F., Biotteau, G., Rodriguez-Carvajal, J., Pinsard, L., and Revcolevschi, A., 1998, *Phys. Rev. Lett.*, **81,** 1957.
[571] Louca, D., Egami, T., Brosha, E. L., Röder, H., and Bishop, A. R., 1997, 1998, *Phys. Rev.* B, **56,** R8475.
[572] Evetts, J. E., Blamire, M G., Mathur, N., Isaac, S. P., Teo, B. S., Cohen, L. F., and MacManus-Driscoll, J. L., 1998, *Philos. Trans. roy. Soc.* A, **356,** 1593.
[573] Sun, J. Z., 1998, *Philos. Trans. roy. Soc.* A, **356,** 1693.
[574] Steenbeck, K., and Steinbeiss, E., 1988 (unpublished).
[575] Venkatesan, T., Rajeswari, M., Dong, Z. W., Ogale, S. B., and Ramesh, R., 1998, *Philos. Trans. roy. Soc.* A, **356,** 1661.
[576] Goyal, A., Rajeswari, M., Shreekala, R., Lofland, R., Bhagat, S. M., Boettcher, T., Kwon, C., Ramesh, R., and Venkatesan, T., 1997, *Appl. Phys. Lett.*, **71,** 2535.
[577] Mathews, S., Ramesh, R., Venkatesan, T., and Benedetto, J., 1998, *Science,* **276,** 238.
[578] Ott, F., Barberan, S., Lunney, J., Coey, J. M. D., and Revcolevschi, A., 1998, *Phys. Rev.* B, **58,** 4656.
[579] Troyanchuk, O., 1992, *Sov. Phys. JETP*, **75,** 132.
[580] Moudden, A. H., Vasilu-Doloc, L., Pinsard, L., and Revcolevschi, A., 1998, *Physica* B, **241–243,** 276.
[581] Viret, M., Nassar, J., Drouet, M., Contour, J. P., Fermon, C., and Fert, A., 1999, *J. Magn. magn. Mater.* (in press).
[582] Kim, K. H., Jung, J. H., and Noh, T. W., 1998, *Phys. Rev. Lett.*, **81,** 1517.
[583] Kim, K. H., Jung, J. H., Noh, T. W., Choi, E. J., and Yu, J., 1998, *Phys. Rev.* B, **57,** R11 043.
[584] Sheng, L., Xing, D. Y., Sheng, D. N., and Ting, C. S., 1997, *Phys. Rev. Lett.*, **79,** 1710.
[585] Sheng, L., Xing, D. Y., Sheng, D. N., and Ting, C. S., 1997, *Phys. Rev.* B, **56,** R7053.
[586] Rodrigez-Carvajal, J., Hennion, M., Moussa, F., Pinsard, L., and Revcolevschi, A., 1997, *Physica* B, **234–236**, 848.
[587] Park, J. H., Vescovo, E., Kim, H. J., Kwon, C., Ramesh, R., and Venkatesan, T., 1998, *Phys. Rev. Lett.*, **81,** 1953.
[588] Kobayashi, K. I., Kimura, T., Sawada, H., Tekura, K., and Tokura, Y., 1998, *Nature*, **395,** 677.
[589] Longho, J., and Ward, R., 1961, *Inorg. Chem.*, **83,** 2816.
[590] Borges, R. P., Ott, F., Skumriev, V., Coey, J. M. D., Arnaudas, J. I., and Ranno, L. (unpublished).
[591] Jakob, G., Westerburg, W., Martin, F., and Adrian, H., 1988, *Phys. Rev.* B, **58,** 14966.
[592] Okuda, T., Asamitsu, A., Tomioka, Y., Kimura, T., Taguchi, Y., and Tokura, Y., 1998, *Phys. Rev. Lett.*, **81,** 3203.
[593] Ghosh, K., Lobb, C. J., Greene, R. L., Karabashev, S. G., Shulyatev, D. A., Aresenov, A. A., and Mukovskii, Y., 1998, *Phys. Rev. Lett.*, **81,** 4740.
[594] Yunoki, S., Hu, J., Malvezzi, A. L., Moreo, A., Furukawa, N., and Dagotto, E., 1998, *Phys. Rev. Lett.*, **80,** 845.
[595] Dagotto, E., Yunoki, S., Hu, J., Malvezzi, A. L., Moreo, A. Hu, J., Capponi, D., Poilblanc, D., and Furukawa, N., 1998, *Phys. Rev.* B, **57**.
[596] Mori, S., Chen, C. H.,, and Cheong, S. W., 1998, *Phys. Rev. Lett.*, **81,** 3972.
[597] Allodi, G., De Renzi, R., Licci, F., and Pieper, M. W., 1998, *Phys. Rev. Lett.*, **81,** 4736.
[598] Sun, J. Z., Abraham, D. W., Rao, R. A., and Eom, C. B. (unpublished).

[599] HARZHEIM, G., SCHUBERT, J., BECKERS, L., ZANDER, W., MEERTENS, D., OSTHÖVER, C., and BUCHAL, C., 1988, *Mater. Sci. Eng.* B, **56,** 147.
[600] COEY, J. M. D., 1999, *J. Appl. Phys.* (in press).
[601] BORGES, R. P., HASCH, W., LUNNEY, J. G., and COEY, J. M. D. (unpublished).
[602] OGALE, S. B., GHOSH, K., PAI, S. P., ROBSON, M., LI, E., LIN, I., GREENE, R. L., RAMESH, R., VENKATESAN, T., and JOHNSON, M., 1998, *Mater. Sci. Eng.* B, **56,** 134.
[603] GUINEA, F., 1998, *Phys. Rev.* B, **58,** 9212.